Mechanistic Study of Scale Inhibitors Retention in Carbonate Formations for Application in Squeeze Treatment

The Thesis by

Khosro Jarrahian

Submitted for Degree

Doctor of Philosophy in Petroleum Engineering

School of Energy, Geoscience, Infrastructure and Society (EGIS)

Institute of GeoEnergy Engineering (IGE)

Heriot-Watt University

Edinburgh, United Kingdom

June 2020

Abstract

The development of effective scale-inhibitor (SI) squeeze treatments remains a challenge for carbonate reservoirs because of their chemical reactivity with the SI. This interaction frequently results in the precipitation of a SI/Ca complex which may either contribute to extending the squeeze lifetime, or alternatively, it may induce formation damage. Thus, the SI – carbonate interaction may be a benefit or a problem.

The work in this PhD takes a systematic approach to understanding the retention mechanisms of SI in carbonate formations. Factor are considered such as, the detailed carbonate-formation mineralogy, the type of SI and reservoir conditions. Static bulk adsorption/ compatibility experiments, described as "apparent adsorption" (Γ_{app}) tests, have been performed to evaluate the region where different retention mechanisms may apply; viz. pure adsorption (Γ) and coupled adsorption/precipitation (Γ/Π) of different SI species onto the carbonate mineral from brine solutions.

Apparent adsorption and compatibility (no mineral) experiments were conducted for five SIs at various conditions: initial pH values, mineralogical compositions (calcite, limestone, and dolomite), and temperatures. The SI species used in this study included a phosphonate (di-ethylene tetra-amine penta (DETPMP)), a phosphate ester (polyhydric alcohol phosphate ester (PAPE)), and three polymeric SIs (polyphosphino carboxylic acid (PPCA), P-functionalized copolymer (PFC), and sulfonated polyacrylic acid copolymer (VS-Co)). All precipitates were studied using environmental scanning electron microscopy/energy dispersive X-ray (ESEM/EDX) and particle-size analysis (PSA).

The main conclusions from these coupled Γ/Π experiments are as follows:

- ✓ For all SI-carbonate mineral systems under virtually all pH and T conditions, clear regions of pure adsorption (Γ) and coupled adsorption/precipitation (Γ/Π) were clearly observed with the region of Γ/Π being dominant in almost all cases (except for VS-CO – see below).

- ✓ For the polymeric SIs (PPCA, PFC, and VS-Co), the highest retention (apparent adsorption) levels were observed at *low pH* for all carbonate substrates. This was

because of the increase in divalent cations calcium and magnesium (Ca^{2+} and Mg^{2+}) available from rock dissolution forming SI–M^{2+} complexes which then precipitate. For DETPMP and PAPE SIs, the retention level was greatest at ***higher pH*** values, because the SI functional groups were more dissociated and, hence, available for complexation with M^{2+} ions. Thus, the polymer precipitation (phase separation; Π) was mainly affected by the concentration of Ca^{2+} in solution, and the phosphonate and phosphate ester were main affected by the final pH, where the higher the final pH levels led to further dissociation of the SI and more precipitation.

✓ The polymeric VS-Co species was rather exceptional in that it predominantly showed pure adsorption with only a low amount of precipitation ($\Gamma_{app} \sim 1.2$ mg/g) in contact with the dolomite substrate. This is because of the presence of sulfonate groups (low pK_a) which have much weaker binding with the Ca^{2+}.

✓ For polymeric inhibitors, the retention level (Γ_{app}) was highest on calcite (highest relative calcium content), followed by limestone and dolomite. DETPMP and PAPE SIs showed the highest retention levels on dolomite (higher final solution pH and more SI dissociated), followed by limestone and calcite.

✓ For all SI species, higher retention (more precipitation, Π) was observed at elevated temperatures. At lower temperatures, an extended region of pure adsorption was observed for all SIs.

The information presented in this study will be helpful in SI product selection on the basis of mineralogy and reservoir conditions. As a consequence, longer squeeze lifetimes and improved efficiency of SI deployment in carbonate reservoirs can be achieved. In addition, this study provides valuable data for developing and validating models of the SI/carbonate/Ca/Mg system that can be incorporated into squeeze design simulations.

Dedication

I dedicate the thesis to my wonderful mother for her endless support and sacrifices and the soul of my beloved father

Acknowledgments

I would love to dedicate this work to the stars of my life, to my family! To my lovely mother who has sacrificed her life to us, my beloved father soul. Their sacrifice for providing me with all necessities and education during the early years is immeasurable. All assistance and concern from my brothers and sisters, is highly appreciated. I wish they were here and could celebrate this moment with me. I would also like to express my gratitude to my supervisors, Professor Ken Sorbie and Mr. Mike Singleton, for their invaluable guidance, motivation and support during the course of my PhD. I would not have been able to complete this research, and I would not have made it through my PhD degree without them. Giving me the opportunity to work under their supervision, to me, was a lot more than the opportunity itself; this was also a pivotal turning point in my life – I cannot begin to comprehend what my life would be without it. Thank you for their trust, diligence and commitment to my success.

I am also thankful to the following companies for sponsorship of the Flow Assurance and Scale Team (FAST) at Heriot-Watt University: ADNOC, Baker Hughes, Energi Simulation, Halliburton Multi-Chem, Nalco Champion, Petronas, Repsol Sinopec, Schlumberger MI-Swaco, Shell, Equinor, Petrobras, Total and Wintershall.

My sincere gratitude goes to my colleagues and friends in the Flow Assurance and Scale Team (FAST). I would like to thank Prof. Eric Mackay for his greatest sources of support over the past few years not only on a professional level, but also on a personal level. Thank you for always being so generous with your attention and time, for building my confidence and for being invested in my success. I am grateful to Dr. Lorraine Boak for her guidance in the laboratory especially with ICP and the knowledge she shared throughout the years at Heriot-Watt University. She played my mum's role away from home, a great mentor and an incredible friend. She was always there to listen too, and I value her friendship. I would like to thank Dr. Alexander Graham for being my go to person to ask just about anything, for supporting me on a personal level and for training me how to work with ESEM-EDX machine; He always tried to assist me how to properly develop my peer-reviewed journal articles. I would not have published these papers without his support. Cutting me some slack when I was under pressure was also extremely important in enabling me to do this work without feeling overly stressed. He was a real friend of mine. Thank you for everything.

Furthermore, I would like to thank Katherine McIver for helping me in the lab at the beginning of this PhD and also sharing her knowledge when I started this work; Wendy McEwan for analysing my samples and explaining the results; Thomas McGravie and Tom Clark for assisting me with maintenance, repairs and technical support throughout this PhD. Special thanks to Heather O'Hara for all the help and guidance – nothing can happen without you.

I would also like to thank my friends in FAST. Thank you all; Alsu Valiakhmetova for being a fantastic friend and a great source of support; Mohamed Arab for his great friendship and assistance; Duarte Silva for being one of the most wonderful souls I had the pleasure of meeting and befriending; Giulia Ness for her remarkable support and friendship; Xu Wang, Bader Al-Harbi and Yaser Alduailej for their friendship. Without you all, doing this PhD would have been a very difficult and lonely task. Thank you for being the music in the background.

Additionally, I would like to acknowledge Dr. Jim Buckman in providing the ESEM/EDX machine and allow me to use it; Special thanks to Dr. Nicholas Odling from School of Geoscience in the University of Edinburgh for allowing me to use their facility to crush my carbonate samples.

A huge thank you goes to Masoud Ghaderi-Zefreh. You have been a wonderful flatmate and close friend, a source of wisdom and inspiration, a feeling of joy and contentment, and an invaluable asset in my support network and my life. A very special thank you goes to Saleh Goodarzian, Pejman Ahamdi, Edris Joonaki, Aliakbar Hassanpour, and Mehrdad Vasheghani-Farahani. You made finishing this work very fun and exciting. Thank you for being there for me always and ever, for inspiring hope and optimism, and for making everything pink! I am very fortunate to have you in my life as both, a very close friend and a reliable source of support.

I am grateful to Prof. Stuart Clarke from the University of Cambridge and Dr. Helen Lewis of Institute of GeoEnergy Engineering, Heriot-Watt University for agreeing to examine this thesis. Their time invested in reading and evaluation of this thesis was invaluable.

Finally, to all the friends cheering for me from all corners of the world, thank you. In particular, I would like to mention Farhad Moghadam (thank you for being an exceptional friend despite how busy you are), Saleh Hojjati (your friendship is life – I am so glad I met you), Nasir Rajabi, Ehsan Nikjoo, Vahid Azari, Hamid Rafiee, Omid Norouzi, Ramin Moghadasi, Banin Seiedi,

Table of Contents

Table of Figures

12

13

Table of Tables

Nomenclature

SI	Scale Inhibitor
MIC	Minimum Inhibitor Concentration
K_{sp}	Equilibrium Solubility Product
m/V	Mass Volume ratio
α,β	Freundlich Constant
φ	Fraction of the precipitation
ppm	Parts per Million
C	Concentration
C_0	Initial concentration
C_f	Final concentration
pH	Negative logarithm of the solution hydrogen ion activity
HEDP	Hexamethylenediamine Tetramethylene Phosphonic Acid
OMTHP	Octa-Methylene-Tetramine Hexa (Methylene Phosphonic Acid)
DETPMP	Diethylenetriamine Penta (Methylene Phosphonic Acid)
PPCA	Polyphosphino Carboxylic Acid
PFC	P-functionalized co-polymer
VS-Co	Sulfonated Polyacrylic Acid Copolymer
PAPE	Polyhydric Alcohol Phosphate Ester
$\Gamma(C)$	Adsorption isotherm
Γ	Pure adsorption
Π	Precipitation
Γ_{app}	Apparent adsorption
$[Ca^{2+}]$	Calcium concentration

$[Mg^{2+}]$	Magnesium concentration
M^{2+}	Divalent cation
SI_Ca_n	Calcium inhibitor complex precipitation
$C_{1,0}$	Initial Ca^{2+} concentration
$C_{2,0}$	Initial DETPMP concentration
$C_{1,f}$	Final Ca^{2+} concentration
$C_{2,f}$	Final DETPMP concentration
m	Initial mass of carbonate substrate (before SI_Ca_n precipitation forms),
m'	Final mass of carbonate substrate (after SI_Ca_n precipitation forms)
$f_{Ca,1}$	the mass fraction of Ca^{2+} in the carbonate substrate (before SI_Ca_n precipitation forms)
$f_{Ca,2}$	the mass fraction of Ca^{2+} in the SI_Ca_n precipitation complex
Mw	Molecular Weight
NSSW	NorthSea Sea Water
ICP-OES	Inductively Coupled Plasma - Optical Emission Spectroscopy
ESEM	Environmental Scanning Electron Microscopy
EDX	Energy-dispersive X-ray spectroscopy

List of Publications

Jarrahian. K, Sorbie. K.S, Singleton. M, Boak. L and Graham. A, *"The Effect of pH and Mineralogy on the Retention of Polymeric Scale Inhibitors on Carbonate Rocks for Application in Squeeze Treatments"; SPE Production & Operations, 2019, 34(02);* https://doi.org/10.2118/189519-PA

Jarrahian. K, Boak. L, Graham. A, Singleton. M and Sorbie. K.S, "*Experimental Investigation of the Interaction between a Phosphate Ester Scale Inhibitor and Carbonate Rocks for Application in Squeeze Treatments"; Energy & Fuels, 2019, 33(05);* https://doi.org/10.1021/acs.energyfuels.9b00382

Jarrahian. K, Sorbie. K.S, Singleton. M, Boak. L and Graham. A, *"Building a Fundamental Understanding of Scale-Inhibitor Retention in Carbonate Formations"; SPE Production & Operations, 2020, 35(01);* https://doi.org/10.2118/193635-PA

Jarrahian. K and Sorbie. K.S, *"Mechanistic Investigation of Adsorption Behavior of Two Scale Inhibitors on Carbonate Formations for Application in Squeeze Treatments"; Energy & Fuels (ACS publisher), 2020, 34(04*); https://doi.org/10.1021/acs.energyfuels.0c00326

Jarrahian. K, Sorbie. K.S, Singleton. M and Boak. L, *"Surface Chemistry of Phosphonate Scale Inhibitor Retention Mechanisms in Carbonate Reservoirs"; Crystal Growth & Design (ACS publisher), 2020, 20(08);* https://doi.org/10.1021/acs.cgd.0c00570

Silva. D, **Jarrahian. K**, Sorbie. K.S and Mackay. E, *"Thermodynamic Modelling of the Precipitation Chemistry of Phosphonate Scale Inhibitors and Divalent Cations (Ca and Mg): Application to Precipitation Squeeze Treatments",* Chemistry in the Oil Industry Symposium, Organised by RSC, Manchester, UK, November 2019

Jarrahian. K, Sorbie. K.S, Singleton. M and Boak. L, *"Mechanistic Study of Interaction between Polymeric and Phosphate Ester Scale Inhibitors and Carbonate Rocks for Scale Inhibitor Squeeze Treatment",* 2017 Oilfield Chemistry Symposium, Geilo, Norway, March 2017

Jarrahian. K, Sorbie. K.S, Singleton. M and Boak. L, *"Experimental Study of Retention Mechanism of Two Different Types of Scale Inhibitors in Carbonate Formations",* 2016 Annual Meeting AIChE, San Francisco, CA, USA, November 2016

1. CHAPTER 1: INTRODUCTION

1.1. What is "scale"?

Scale formation is the deposition of sparingly soluble inorganic salts from aqueous solutions[1]. It is caused by a change in the saturation equilibrium when there is variation in temperature, pressure, or change in the solution chemistry [2]. Oilfield scale will only occur when free-water is produced [3]. Oilfield scaling is a common problem in the oil and gas industry. Problems with scale cost the industry millions of dollars in damage and lost production [4]. Mineral scale deposition can occur once water has broken through into the producer wells and the type and severity of the scale depends on the water chemistry of the injected and formation brines and the physical conditions (temperature and pressure)[5]. Seawater, as the main source for injection water, has high concentrations of anions such as SO_4^{-2}, while formation waters are usually rich in cations such as Ca^{2+}, Ba^{2+} and Sr^{2+}. Mixing these incompatible or chemically different waters leads to precipitation of minerals such as $CaSO_4$, $BaSO_4$ and $SrSO_4$ during water flooding processes [6–9]. Precipitation of minerals occurs when the concentration of solute exceeds its solubility under specific thermodynamic conditions. In addition, the release of carbon dioxide during reservoir depletion and the drawdown of production wells also contributes to the formation of carbonate scale[10]. The effect scale formation on the production depends on the location. Scale in the near wellbore can cause severe formation damage. It can block the fluid flow by clogging the pores, leading to reduced production rates. If the scale is formed in the production tubing the flowing area is reduced, resulting to a reduction in the production rate. Scale in the topside facilities may lead to accumulation of scale in the surface facilities, insufficient separation, and poor water quality. This can result in significant production losses[11].

1.2. Mechanism of Scale Formation

In general, scales start to form at supersaturated conditions through nucleation, crystal growth and agglomeration processes[11,12]. Firstly, the small mineral nanocrystals must grow from the solution. An unstable cluster of the atoms at which the deposition of solid takes place is developed. This process is called nucleation, as illustrated in Figure 1.1 and Figure 1.2 . The nuclei are ion clusters, ion pairs and crystal lattice particles. At the condition where the crystal nuclei flow together with the solution in the system and not deposited onto the surface, homogeneous nucleation takes place[13]. If the nuclei come from the foreign particles, then the

nucleation is categorized as heterogeneous nucleation. It usually causes by the high degree of turbulence which leads to more scale precipitation.
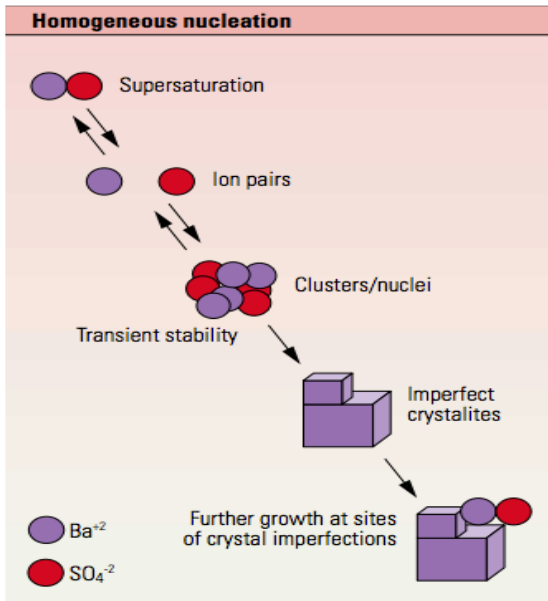
Figure 1.1. Homogeneous Nucleation[14]
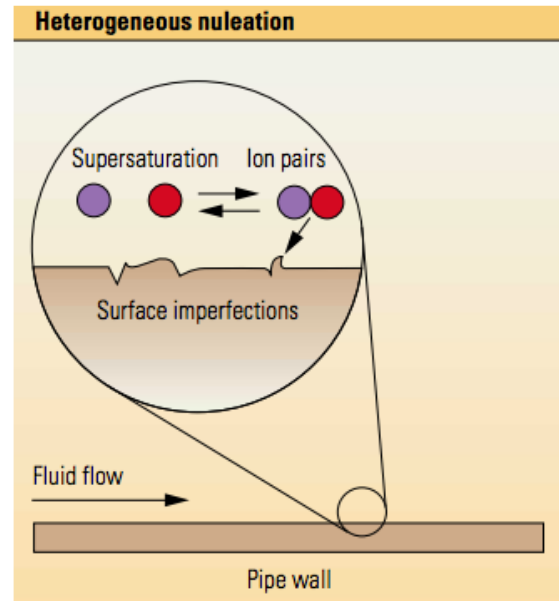
Figure 1.2. Heterogeneous Nucleation[11]

1.3. Various Types of Scale

Several types of scale form in oil fields. The most common scales are as follows[1]:

- Calcium carbonate (calcite and aragonite)
- Sulphate salts of calcium (gypsum), strontium (celesite), and barium (barite)
- Sulphide scales of Iron (II), zinc, and lead (II)
- Sodium chloride (halite)

1.3.1. Carbonate scale

When pressure drops, CO_2 comes out of the produced water and causes water pH and saturation index of carbonate minerals to increase and thus precipitation occurs. The governing equations for calcium carbonate precipitation are as follows:

$$HCO_3^-(aq) + H^+(aq) \rightleftharpoons H_2CO_3(aq) \rightleftharpoons CO_2(g) + H_2O(l) \tag{1.1}$$

$$2HCO_3^-(aq) + Ca^{2+}(aq) \rightleftharpoons CaCO_3(s) + CO_2(g) + H_2O(l) \tag{1.2}$$
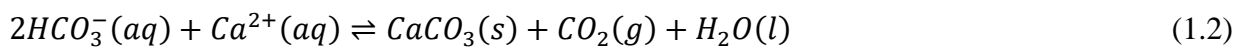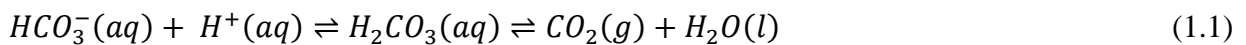
Since CO_2 is released from the water as a result of pressure reduction (in chokes and separators), the above reaction (reaction 1.2) proceeds to the right and thus calcium carbonate precipitates. Calcium carbonate will not deposit in the well when there is a high CO_2 content and low pH. As the pressure drops, the scaling will escalate upstream further into the producing well[3]. Figure 1.3 shows a thick scale layer of calcium carbonate in a production tubing[1].

Figure 1.3. Calcium carbonate scales[1]

1.3.2. Sulphate Scale

Unlike carbonate scales which can be treated by acidization, the sulphate scales of barium and strontium are very insoluble and difficult to remove. This type of scale is usually a problem in seawater-flooded reservoirs. Sulphate scales form by the mixing of sulphate ions and group (II) metal ions, except magnesium. The sulphate scale formation causes severe formation damage and flow assurance issues. These reactions are:

$$Ba^{2+}(aq) + SO_4^{2-}(aq) \rightarrow BaSO_4(s)$$
$$Sr^{2+}(aq) + SO_4^{2-}(aq) \rightarrow SrSO_4(s) \tag{1.3}$$
$$Ca^{2+}(aq) + SO_4^{2-}(aq) \rightarrow CaSO_4(s)$$
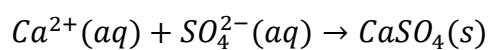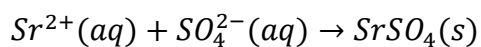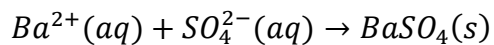
As you go down group (II) in the periodic table, the solubility of the sulphates decreases. Consequently, barium sulphate is the least soluble and hardest to control. Sulphate scaling, is usually formed when formation water is mixed with injected seawater. This causes precipitation of sulphate scales. It is the high concentration of sulphate ions in the seawater mixing with group (II) metal ions in the formation water that lead to scale formation[3].

1.3.3. Sulphide Scale

Sulphide scales are less common but can still cause serious problems. This type of scale is formed mainly by the interaction between hydrogen sulphide and iron, zinc or lead. The most common among them is iron sulphide, mainly from the corrosion of steel in producing wells. In oil wells, the bulk of hydrogen sulphide comes from the activity of sulphate-reducing bacteria, SRBs, on the sulphate ions in the injected seawater. The SRBs reduce sulphate ions to hydrogen sulphide (H_2S), which is in equilibrium as follows:

$$H_2S + H_2O \rightleftharpoons H_3O^+ + HS^- \tag{1.4}$$
$$HS^- + H_2O \rightleftharpoons H_3O^+ + S^{2-} \tag{1.5}$$

Iron (II) ions are formed mainly by corrosion of steel either in the injector or producing wells. They can react with the sulphide ions and form iron sulphide scale[3].

$$Fe^{2+}(aq) + S^{2-}(aq) \rightarrow FeS(s) \tag{1.6}$$

1.3.4. Halite Scale

Halite (NaCl) has been considered a non-conventional scale but with the recent upsurge in deep-water, high pressure, high temperature, gas condensate fields there has been more coverage of this type of scale in the literature[15,16]. Halite precipitation is unsurprisingly more often a challenge in high salinity wells and can plug downhole production tubulars, topside process equipment and pumps. Deep, high temperature wells are particularly susceptible to halite deposition as they can be prone to a greater degree of cooling, one of the major drivers for deposition. Unlike conventional carbonate and sulphate scales, for halite scale the driving force for precipitation is small yet the concentration of ions is huge[17].

Halite scaling is also a self-scaling process. The drivers are falling temperature and evaporation. Halite solubility in water decreases with decreasing temperature, favouring halite dropout during the production of high total dissolved solids (TDS) brines to the surface. Evaporative loss of liquid water is generally the result of gas breakout from under saturated condensate and oil wells, as well as the expansion of gas in gas wells. This increase in water vapour can leave behind insufficient liquid water to maintain halite solubility in the coproduced brine phase. Halite self-scaling is found with both high-temperature and low-temperature wells (e.g., with 125 and 350°F bottom hole temperature (BHT) gas/gas condensate wells).

The most common method of countering the deposition of halite scale is the injection of fresh or less saline water, via batch treatments to the affected zones or via continuous injection upstream of the deposition zones. This is a very valid approach that is both cost effective and efficient. However, this is not always the most practical solution as the large volumes of fresh water required may not be available, nor may it be possible to introduce the water in the required volume to the affected zones. In these instances, sub-stoichiometric chemical halite inhibitors are a valid alternative[18].

1.4.   Location of Scale Deposition

As mentioned above, scale is deposited along the water path wherever the injected brine comingles with formation water or under physical changes like pressure or temperature. The scales can be precipitated along the injection well, wellbore, reservoir or surface equipment as presented in Figure 1.4 & Table 1.1..
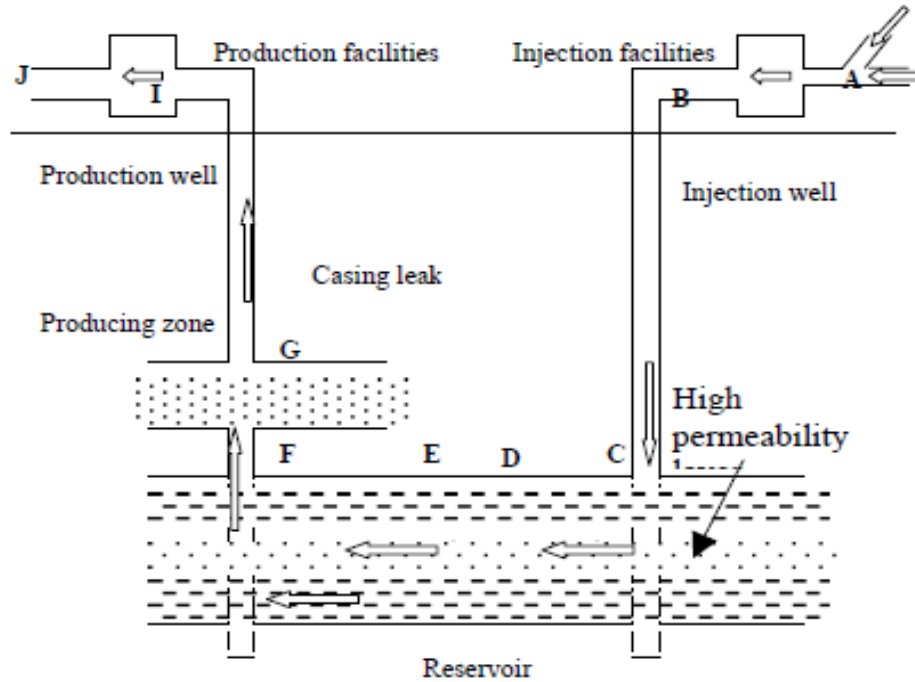
Figure 1.4. Location of Scale Deposition[3]

Table 1.1. Potential Scale Deposition[19]

Location	Scale Formation Mechanism
A to B	Mixing of Brine
B to C	Increasing Pressure and Temperature
C to D	Decreasing Pressure
C to F	Reaction with Rock by Cation Exchange, dissolution, etc.
D to F	Mixing of Injection Water and Formation Water
E to J	Decreasing Pressure and temperature. Release CO_2 and water evaporation
F	Breakthrough of Mixed water (Sea Water+ Formation Water)
A to B	Mixing of Brine

1.4.1. Reservoir Matrix

Scale deposition in the subsurface is a critical issue especially in pore throats which impact on porosity and permeability reduction, see Figure 1.5. Carbonate scales and sulphate scales that are deposited in the near wellbore can block the perforation interval and reduce well productivity. However, scales precipitated deep in the reservoir would not be a severe problem since they are not accumulated locally[20]. The more scale dropped out deep in the reservoir, the lower the scale potential will be at near or in the wellbore, depending on the mixing process and how depleted the scaling ions are when they reach the production well. For example, if $BaSO_4$ is precipitated out deep in the reservoir, it will reduce Ba^{2+} ion concentration and reduce scale potential at the wellbore.
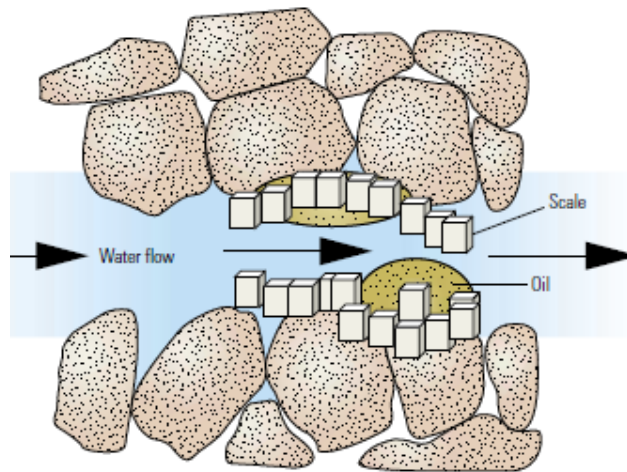
Figure 1.5. Scale deposition in the Matrix Reservoir[11]

1.4.2. Producer and Injector Wells

Deposition of scale in the tubing will reduce the internal diameter of the pipe, see Figure 1.6. It will reduce flow area and increase flow resistance inside the tubing. The carbonate and sulphate scale deposited near and at the wellbore will block down-hole equipment including perforation intervals, gas lift mandrels, nipples, etc., and the result is production losses are observed. Deposition is also possible in production equipment or surface pipelines. An example of a severe problem due to this type of deposition was reported in the Miller field. Production declined dramatically from 30,000 Barrels of Fluid per Day (BFPD) to 0 (BFPD) within 24 hours. It was investigated and found that there was a reduction up to 40% of flow area in the tubing due to

scale build up[3]. Injection wells have the potential for scale deposition through auto scaling processes due to a change in temperature and pressure along the wellbore. At the initial stage of injection, scale is possible around wellbore due to contacting of injection water with formation water or completion water, as seen in Figure 1.7.
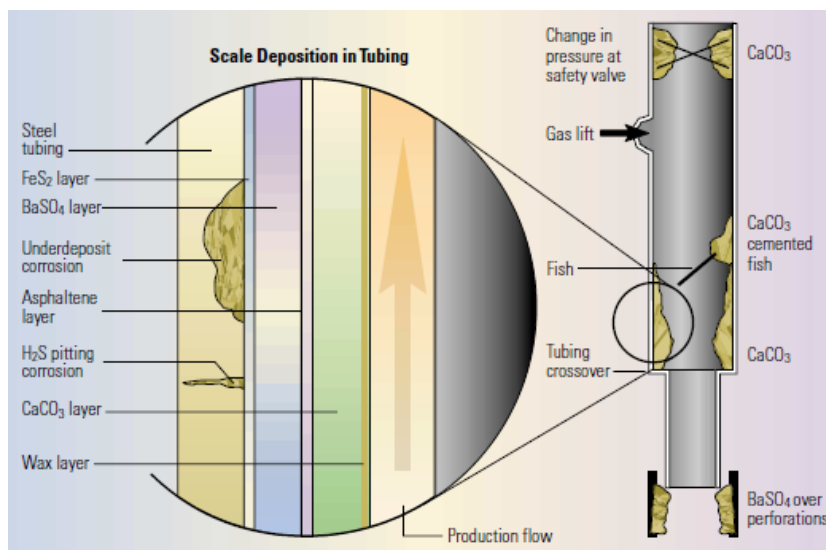
Figure 1.6. Scale deposition in the wellbore[3]
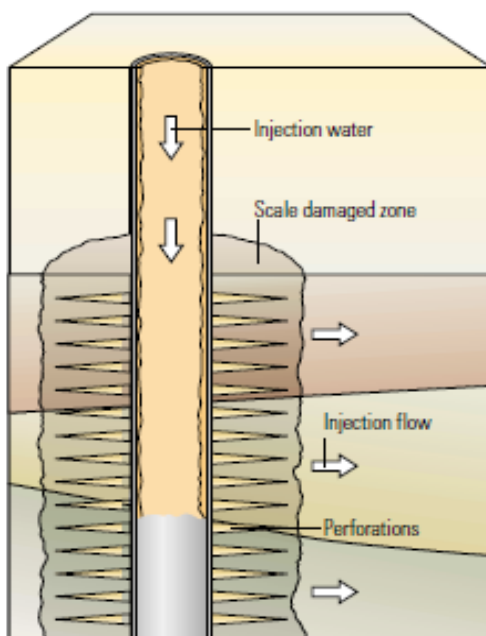
Figure 1.7. Scale Deposition in the Injection Well[3]

1.5. Detection methods of Scale Deposition

1.5.1. Visual Inspection

Visual inspection is the easiest, quickset and cheapest investigation and the first step to identify the presence of scale. The sample can be taken from surface equipment, for instance, separator, pump, choke, etc. The sample can be analysed in a laboratory by microscopic investigation in terms of colour, size hardness and odour.

1.5.2. Core analysis

A lot of laboratory study had been conducted using core analysis to observe scale deposition. A core sample is taken from a reservoir and investigated in a laboratory. The core is dried and cut into sections. Scanning Electron Microscopy (SEM) is used to study crystal habit, scale size, morphology and scale distribution in the core[21].

1.5.3. Gamma Ray and Calliper Logs

Gamma Ray and Calliper Logs are run down through tubing to detect scale deposition along the wellbore. As seen in Figure 1.8, a Calliper Log is run to measure decreasing tubing inner diameter as an indication of scale deposition. In addition, a Gamma Ray Log is run to detect radioactive radium Ra226. It is usually present together with scale especially barium sulphate, $BaSO_4$.
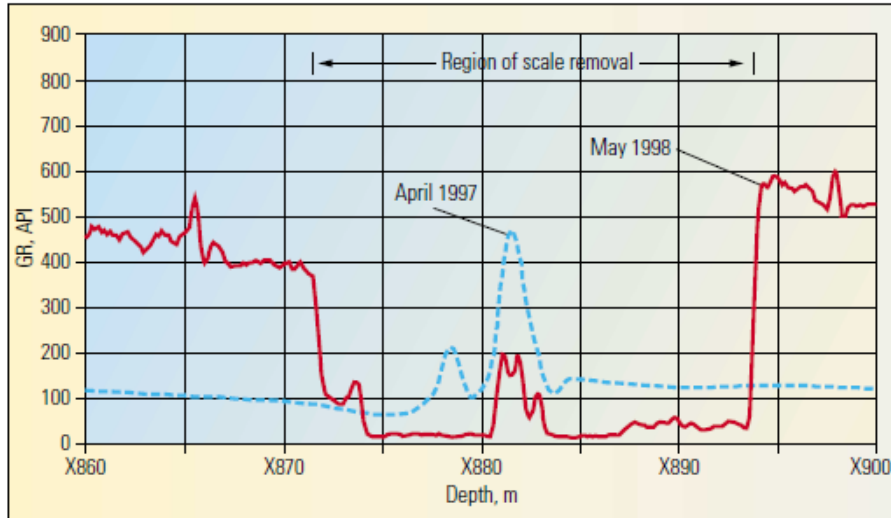
Figure 1.8. Gamma Ray Log to identify scale deposition in the wellbore[11]

Blue dash line represents Gamma Ray log run in April 1997 before a scaling removal job. While the red line represents a Gamma Ray log run in 1998 after a scale removal job. The focused interval depth is X872m to X894m. As seen in Figure 1.8, there was a peak API (American Petroleum Institute) value (blue dash line) within the depth of interest, indicating scale deposition over a range of depths. After the removal job in May 1998, the Gamma Ray log was run again into the wellbore. It was observed that there was a significant reduction of API indicating the success of the scale removal job[11].

1.5.4. Produced Water

Scale detection can be identified by the study of produced water, especially if it coincides with decreasing production rate. A water sample is taken from the well and one conducts water chemical analysis. The potential for scale deposition is indicated by a reduction in scaling ion concentration, such as Ca^{2+}, Mg^{2+} and Ba^{2+} in the produced water, especially after injected water reaches producer wells[22].

1.6. Scale Prevention and Removal

Scale prevention has become more important due to most of operated fields which have already entered secondary or tertiary recovery. The use of water injection or water based Enhanced Oil

Recovery (EOR) to improve oil recovery becomes crucial due to the incompatibility between injected water and formation water. The scale deposition in the field will cause high production loss and costly treatments[3,11].

1.6.1. Scale Prevention

Through the concept of nucleation and crystal growth discussed earlier, the scale inhibitors (SIs) are designed to stop the development of nucleation; scale growth and adherence to the surface thus potentially reduce the rate of scale formation[9]. Once the solid has been precipitated, the removal scales job operation should not damage the reservoir, wellbore or other equipment. With physical prevention, there are some methods that are practically applied including the selection of injected fluid, water treatment before injection, pH control and some other physical methods[23] such as Nuclear Magnetic Resonance (NMR), micro electrolysis, electrostatic, high pressure-high frequency and anti-bond polymer methods. However, these techniques are rather inefficient.

The formation of scales may also be mitigated by chemical treatments. Injecting diluted sea water which has low ion concentration could minimize the formation of scales since it reduces the active scaling ions in the solution. Moreover, scales can also be inhibited by adding SIs, ion exchange, chemical treatment, dilution to lower the solubility limit, etc. Especially for sulphate scales, the sequestering and chelating ions (Ca^{2+}, Sr^{2+} and Ba^{2+}) are possibly applied[24].

1.6.2. Scale Inhibitor

Scale inhibitors (SIs) are chemicals used to prevent the formation of scale. An inhibitor is defined as "Any chemical agent that reduces the rate of formation of a fouling scale". SIs are water-soluble chemicals that prevent or retard the nucleation and/or crystal growth of inorganic scales, causing deformation of the normal crystal growth pattern and block the formation of larger crystals[1]. A good SI should be:

- *Efficient:* it must be able to inhibit the scale in question, irrespective of the mechanisms operating.
- *Stable:* it must be stable under high temperatures

- *Compatible:* it must not interfere with the action of other oilfield chemicals, nor be affected itself by them. It must be compatible with the chemical injection system under operating conditions.
- *Threshold inhibition***:** these species must inhibit scale formation at very low concentrations, typically between 1-20 ppm active inhibitor concentrations. This level is also referred as a minimum inhibitor concentration (MIC).

- *Long squeeze lifetime:* these must show long return profiles from the reservoir, typically between 3-12 months at levels higher than the required threshold concentration level.

The SI must interact either with the anions or the cations in solution, to successfully bind to the scale particle. These interactions are often necessary to hold the inhibitor tightly on the scale surface, to prevent the molecules with similar functional groups to interact with the lattice ions on the crystal surface[1].

1.7.   Properties of Scale Inhibitors

The ion composition, pH, salinity and temperature from field to field varies considerably [25]. For example, the water properties in the central North Sea tend to have a high barium content with a pH range from 4.4 to 7.5. However, the typical water found in the Southern North Sea has high salinity with high sulphate content. Thus, the chemical SI should have characteristics which can withstand the in-situ environment. The chemical inhibitors have to be stable in brine rich in divalent ions, stable in the presence of another chemical, stable at pressure and temperature, and have a good balance for adsorption-desorption, low toxicity, high biodegradability at a reasonable cost[7].

1.8.   Techniques of Scale Inhibitor Deployment

The chemical Sis are placed into reservoir formations to mitigate scale depositions in the production zone. There are two techniques that are used in the field implementations, (I) hydraulic fracturing and (II) squeeze inhibitor.

1.8.1. Hydraulic Fracturing

It is often possible to place the chemical inhibitor along with a hydraulic fracturing treatment, see Figure 1.9. The inhibitor together with proppant fracture fluid are injected down to the wellbore. Water soluble Polyphosphates have been used in this way and have been effective to minimize calcite and sulphate scales in the reservoir matrix [26]. However, this technique is expensive and needs proper fracturing design.
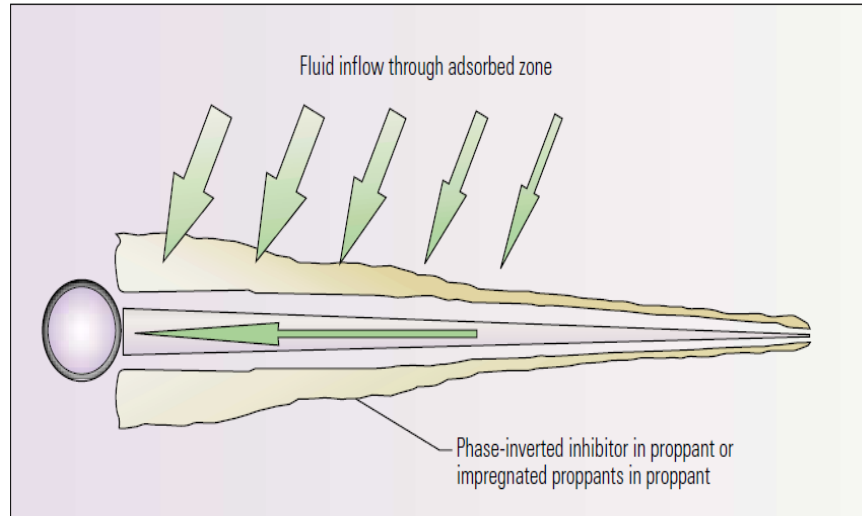
Figure 1.9. Hydraulic Fracturing Inhibition Treatment[11]

1.8.2. Continuous Scale Inhibitor Injection

The continuous injection scale treatment method is a technique in which the inhibitor is pumped down tubing from the surface and enters the production stream at a depth where scaling is not yet occurring. Chemicals must be injected continuously. The treating string usually has a surface pump, a metering device, a connection to the wellhead, and an entry to the flow stream. The objective of the treatment is to prevent scaling of downhole equipment and stop precipitation on the formation face near the wellbore. Liquid solutions of SIs are typically applied in this method, and the equipment is installed by the well service company. The liquid SIs are usually diluted to achieve good distribution of the inhibitor in the brine stream and to avoid precipitation caused by concentrated inhibitor contacting the brine. Continuous treatment allows the most efficient application of chemical inhibitor because only the effective dosage required is actually pumped down the treating string. The most undesirable features of continuous injection are (1) the

continual need for personnel to refill chemical pumps at specified times and (2) the risk that the pump can fail and allow scale to build up, which can result in expensive remedial operations.

1.8.3. Scale Inhibitor Squeeze Treatments

Squeeze treatment is a method to place the chemical inhibitor in the reservoir by pumping down through the wellbore. The chemical solution will penetrate to the near wellbore and further into formation, see Figure 1.10. This method starts with pre-flush stage by injecting brine. It is then continued by the squeezing stage where the SI chemical is injected and pushed further into the formation. The chemical will be adsorbed onto the surface rock. It prevents the scale formation. Later, the over-flush stage is started, and the well is shut in for a period of time. The chemical will be produced afterwards together with reservoir fluid[7,26,27]. This method will be repeated until the concentration of the SIs is no longer effective. Compared to the hydraulic fracturing and continuous injection methods, the squeeze inhibition method is inexpensive[28].
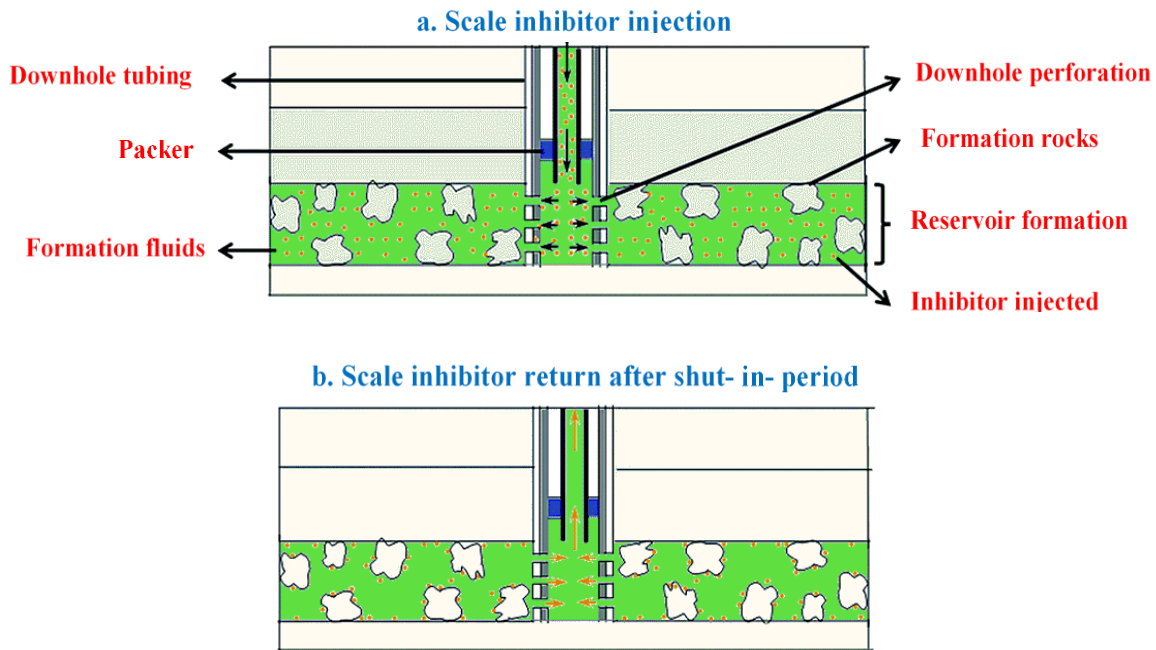
Figure 1.10. Schematic of the field SI squeeze operation. (a) The process of injecting inhibitor into formation; (b) the process of returning inhibitor after the shut-in period[27]

Here we explain a squeeze treatment in detail. A squeeze treatment is where a SI is injected or ″squeezed″ into the near-well rock formation. Once the chemical has been placed in the rock formation, it interacts with the formation (either through adsorption or precipitation). During subsequent oil and water production, the inhibitor returns into the produced waters by

desorption/re-dissolution at low concentrations (threshold levels) over long periods of time, known as the squeeze lifetime. The basic field squeeze strategy is as follows:

- **Preflush:** The preflush stage is normally injected to condition the formation, with typically a mutual solvent being deployed to improve inhibitor retention and well clean-up times.
- **Main Treatment (Inhibitor Injection):** This stage contains the SI injection, normally at a concentration in the range of 2.5% to 20%.
- **Overflush:** The overflush stage, usually a brine, is deployed to displace the chemical slug deeper into the reservoir and thus expose the chemical to a greater surface area of rock to achieve a higher level of retention.
- **Shut-in:** the shut-in or soak period (generally between 6 and 24 hrs) is the time allowed for the inhibitor to adsorb or precipitate on the formation.
- **Back Production:** The well is brought back on production.

Squeeze treatments are not completely trouble free. Major problems can arise if an unsuitable SI chemical is placed downhole. If the reservoir conditions are unsuitable for the applied chemical, problems associated with the formation of pseudo scales and emulsions can arise[29], such as near wellbore plugging[30]. Pseudo scales are formed by temperature-dependant interactions between ions such as Mg^{2+} and Ca^{2+}, present in the field brine and applied inhibitor solution. Precipitation will occur if the critical concentration range of these ions and the added inhibitor solution is reached. It has also been suggested that the interaction of certain low pH phosphonate species with calcium carbonate scale, involves the dissolution of calcite, followed, by the secondary precipitation of calcium phosphonate[31]. Emulsions are caused by surfactant-type inhibitors, e.g. phosphate-ester SIs or low pH phosphonates, and can block pore throats in a similar way to mineral scale, resulting in a decline in productivity[10].

The success of the treatment is defined by squeeze lifetime which is specified in terms of how long the SI is back produced at a concentration greater than the 'MIC'. Often the squeeze lifetime is described in terms of the volume of produced water that scale formation is protected by [SI] $\geq$ MIC[32,33]. The squeeze lifetime in turn depends to a large degree on which mechanism the SI is 'retained' within the porous medium, i.e. by adsorption or precipitation. Besides the interaction mechanism of the inhibitor with the formation (adsorption/precipitation), the lifetime of the

squeeze depends upon a number of other physical and chemical parameters of the reservoir such as the surface chemistry of the formation (quartz or clays), the wettability of the rock surface, the pH of the aqueous media contacting the formation, the formation temperature and pressure etc. and some of these factors are discussed in detail later in this section in the light of their relevance to the research topic of this thesis.

1.9. Types of Scale Inhibitor

A list of the most common classes of SIs is as follows[1]:

- Polyphosphates
- Phosphates
- Small, non-polymeric phosphonates and aminophosphonates
- Polyphosphates
- Polycarboxylates
- Phosphino polycarboxyate polymers
- Polysulphonates

Some of these inhibitors widely used in the oilfield industry are explained in detail below:

1.9.1. Phosphonate Scale Inhibitors

Phosphonate SIs (e.g., DETPMP- penta phosphonate shown in Figure 1.11) forms a class of high performing inhibitors which mainly work through a crystal growth inhibition mechanism. However, it is known that phosphonates tend to have a lower "cut off" temperature. This means phosphonate performs quite poorly at low temperature and work best above a 'switch on' temperature[34]. The primary bonding mechanism for the phosphonate group is the ionic interaction between the PO_3^{2-} group and the Ba^{2+} ions of the crystal growth sites[33,35]. This is supported by the fact that the optimum pH for SI performance is reached when the pKa value (The pKa is the negative base -10 logarithm of the acid dissociation constant (Ka) of a solution. The smaller the value of pKa, the stronger the acid) for $PO_3H^- \rightleftharpoons PO_3^{2-} + H^+$ is exceeded[35–37]. Phosphonate-based SIs has several advantages in squeeze treatments. One disadvantage with these SIs is that they are poorly biodegradable. There have been several attempt to make environmentally friendly, biodegradable, SIs but rarely phosphonate-based[38].
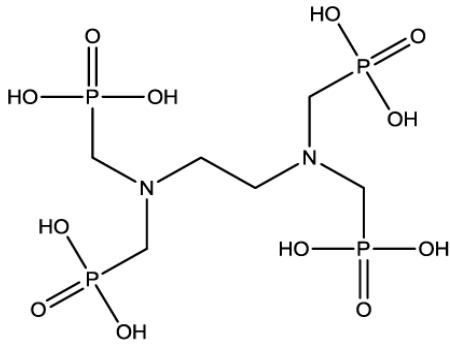
Ethylene Diamine Tetra (Methylene Phosphonic Acid)- EDTMP   Diethylene Triamine Penta (Methylene Phosphonic Acid) - DETPMP
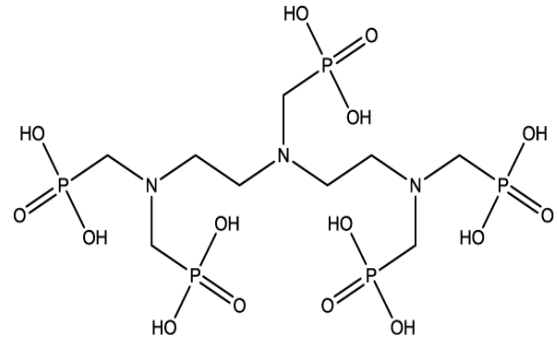
Figure 1.11. Common oilfield SIs containing phosphonate groups[36]

1.9.2. Polymeric Scale Inhibitors

Polymeric SIs (e.g. PPCA- Polyphosphino Carboxylic Acid and VS-Co- sulfonated polyacrylic acid copolymer shown in Figure 1.12) are widely used in the oil and gas field because of their enhanced thermal stability and better environmental compatibility. However, the squeeze efficiency of such threshold inhibitors is typically poor in conventional squeeze treatment[39]. These types of SI work mainly by nucleation inhibition, although as noted above, they also show some (poorer) crystal growth retardation. A practical observation supporting this is that the inhibition efficiency (IE) of most polymers is high at early times in these tests but tends to be lower at 24 hours (where crystal growth mechanisms are more dominant[33,40]. It is well documented that PPCA, as a common example of polymeric SI, is principally a nucleation inhibitor, which is effective over longer residence times although it is gradually consumed with in the growing crystal lattice. Similarly, this is also true for polyvinyl sulphonate (PVS), polymeric SI that has the least crystal growth inhibition properties. PVS is generally in a highly dissociated state (due to the low pKa of the sulphonate groups) with weak metal binding, which means that it plays a less effective role in the crystal growth mechanism. It is known that sulphonate groups do not bind to Ca^{2+} or Mg^{2+} cations because these functional groups have very low Ka values[33,41].
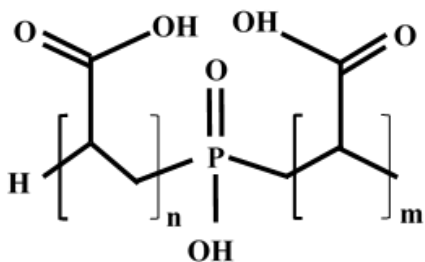
Phosphino PolyCarboxylic Acid (PPCA)   sulfonated polyacrylic acid copolymer (VS-Co)
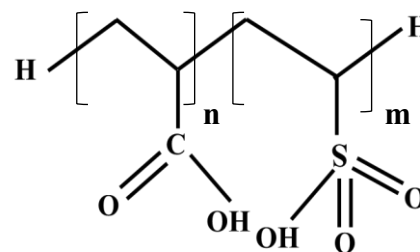
Figure 1.12. Chemical Structure of Polymeric Scale Inhibitors[42]

Carboxylated species, particularly polycarboxylates such as PPCA and maleic acid ter polymer (MAT- a green SI) are generally regarded as having crystal growth inhibition properties in-between those of sulphonated polymers (such as PVS) and conventional phosphonate SIs. These differences can be explained on the basis of the binding constants of the functional groups sulphonate, carboxylate and phosphonate with Ca^{2+} cations. At any selected pH and temperature, Ca^{2+} and Mg^{2+} bond strongest to phosphonate groups (large binding constants, like those quoted for DETPMP above), followed by carboxylate (moderate binding constants), followed by sulphonate (much weaker binding constants). The performances of the polycarboxylate inhibitors in terms of IE (Inhibition Efficiency) can be unsatisfied due to the many bonds between the inhibitor and the surface with a polymeric species. Thus, both dissociated and un-dissociated acid groups can co-ordinate to the surface. It follows that co-polymers such as sulfonated polyacrylic acid copolymer (VS-Co) will operate via both nucleation inhibition and crystal growth inhibition mechanisms.

Polymeric SIs are less sensitive compared with phosphonate SIs to temperature. Similarly, PPCA and non-polymeric, mono-phosphonated, carboxylated species such as 2-Hydroxy Phosphonoacetic Acid (HPAA) and 2-Phosphonobutane 1, 2, 4-tricarboxylic acid (PBTC) also have crystal growth inhibition qualities, although probably not as good as highly phosphonated species. For this reason, selected phosphonated and/or carboxylated SIs can be used synergistically to improve their crystal growth inhibition properties[34].

1.9.3. Phosphate Ester Scale Inhibitors

Phosphate esters are derivatives of phosphoric acid and alcohols (Figure 1.13). They are sensitive to acidic conditions and temperature changes. These inhibitors undergo hydrolysis (break apart into several components) at elevated temperatures and in low-pH (acidic) conditions. For that reason, they are used in wells with Bottom Hole Temperatures (BHTs) below 150°F. They can withstand temperatures of 180°F (82°C) - 200°F (93°C) for a few hours. Within these temperature limitations, phosphate esters are generally very effective calcium carbonate ($CaCO_3$) and calcium sulphate ($CaSO_4$) inhibitors. Except in acid environments (pH<5.5), they also provide excellent control of strontium sulphate ($SrSO_4$) and barium sulphate ($BaSO_4$) precipitation. In general, phosphate esters are soluble in and compatible with high-calcium brines[1,3].

Polyhydric alcohol phosphate ester (PAPE)   Diester Phosphate Ester (PE)
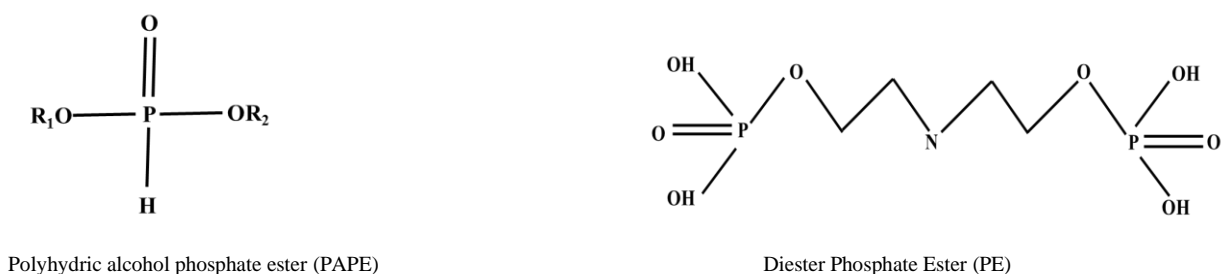
Figure 1.13. Chemical Structure of Phosphate Ester Scale Inhibitors[3]

As phosphate esters show excellent inhibition efficiency at lower temperatures, these SIs may be applied in reservoirs with $T < 80°C$ as squeeze treatments and in topside facilities where fluids are cooler. The excellent inhibition efficiency combined with the higher degree of biodegradation leads this family to be considered excellent environmental SIs[43].

1.10. How Scale Inhibitors are Retained in Oil Reservoirs

It is well known that the two main retention mechanisms that have been found to occur in a formation are adsorption (Γ) and precipitation (Π), as shown schematically in Figure 1.14. These two mechanisms have already been mentioned above but they are now discussed in more detail below.
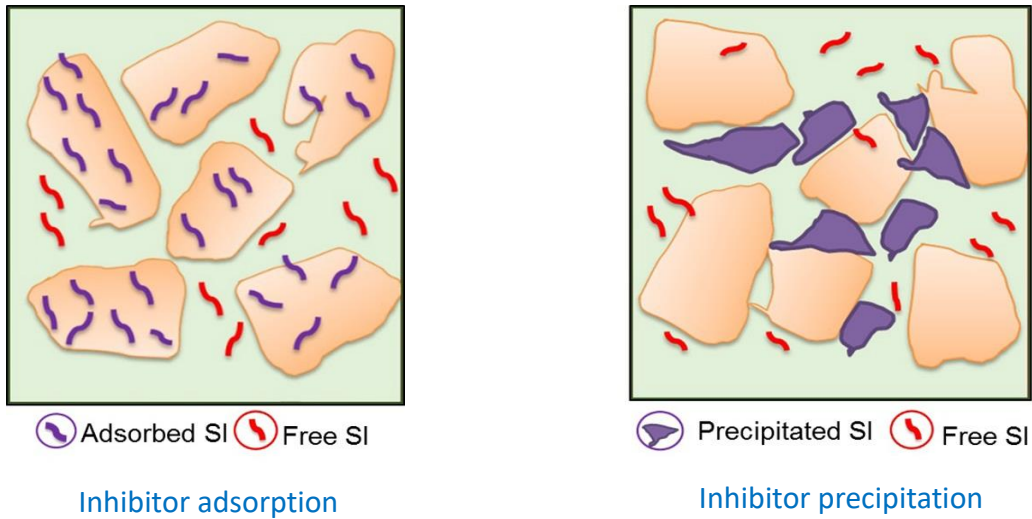
Figure 1.14. Two main mechanisms of scale inhibitor retention in porous media[44]

1.10.1. Adsorption Mechanism

Adsorption of SI occurs through electrostatic and van der Waals interactions between the inhibitor and formation minerals and this is generally described by an adsorption isotherm, $\Gamma(C)$, which describes the amount of SI adsorption (in units of mg/g of rock for example) as a function of the SI concentration, $[SI] = C$[42].

1.10.2. Adsorption of Scale Inhibitors on Sandstone Formations

Adsorption is the common mechanism by which SI is physically or chemically retained on to the rock mineral surface within the porous medium[10]. This process predominantly occurs within sandstone formations, especially in the presence of divalent cations (such as $[Ca^{2+}]$, $[Mg^{2+}]$, $[Fe^{2+}]$ etc.). The process is affected by the surface charge properties of the formation and nature of the inhibitor molecule used[45]. Generally, as the pH increases the degree of dissociation of both the inhibitor molecule and the rock surface increases, this makes the rock substrate more negatively charged, and the divalent cations are then adsorbed on to the negatively charged rock surface making it less negative and slightly more positive, it is this positive site that attracts and lead to the adsorption of an anionic inhibitor molecule[45]. This phenomenon of adsorption is illustrated by the following chemical equations (1.7-1.9), where a silanol ($SiOH$) surface is used as an example:

$$SiOH + H_2O \rightleftharpoons SiO^- + H_3O^+ \qquad (1.7)$$

The equation (1) represents how a quartz (silanol) surface dissociates to form a negatively charged surface which then adsorbs divalent cations, such as calcium, within the porous medium according to the following chemical equation;

$$SiO^- + Ca^{2+} \rightleftharpoons SiOCa^+ \qquad (1.8)$$

Adsorbing this positively charged ion will alter (reverse) the ionic characteristics of the formation surface making it slightly positive; this will then facilitate the amount at which a negatively charged anionic inhibitor molecule would be adsorbed on to the positively charged rock site[46].

$$SiOCa^+ + R - CO_2^- \rightleftharpoons SiOCa^+O_2C - R \qquad (1.9)$$

It is this change in surface charge and the degree of dissociation of the SI molecules (also pH dependant), that controls the mechanism by which the SI adsorbs onto the sandstone substrate. At low pH values the hydrogen boding mechanism is dominant, whilst at higher pH values the cation bridging mechanism predominates (see below).

1.10.3. H bonding

The silica surface is neutrally charged at lower pH values and is covered by a monomer of hydrogen-bonded water molecules[47]. Associated SI molecules are polar in nature and will displace the water molecules from the surface, leading to a high level of adsorption[32,48–50]. As the solution pH increases, the degree of dissociation of both the SI and the silica surface increases resulting in a decrease in adsorption due to the repulsion of the negatively charged ions formed. This decrease in the level of adsorption in only observed in distilled water where there are no divalent cations, particularly Ca^{2+} and Mg^{2+} [48,51], or a system in which the SI concentration is low[51].

1.10.4. Cation Bridging

In brine systems, the electrostatic repulsion described above is not observed. This is due to the presence of metal cations, including Ca^{2+}, which adsorbs onto the negatively charged silica

surface, leading to an occurrence charge reversal. The inhibitor anions in solution are then adsorbed onto this positively charged surface through the cation bridges[32,49–51].

$$SiOCa^+ + A^- \rightleftharpoons SiOCa^+A^- \tag{1.10}$$

1.10.5. Adsorption of Scale Inhibitors on Carbonate Formations

In contrary to sandstone adsorption, it was found that the retention mechanism of SI on to a carbonate formation can be a more complex process. This is because the carbonate rock itself is a very reactive substrate which can react with the inhibitor molecule, therefore complicating the adsorption process[52]. Interfacial phenomena at carbonate/water interfaces are controlled by the electrical-double-layer (EDL) forces. Therefore, it is necessary to understand the behaviour of the ions' interactions with the rock surface. Charged species are transferred across any solid/liquid interface until it reaches equilibrium. The interface can be visualized as a semi-permeable membrane that allows the common charged species between solid and solution to pass through. These species are called potential-determining ions. As a result of the relative motion between the charged dispersed phase and the bulk liquid, the EDL is sheared. The potential, at this shear plane, is commonly called electrokinetic or zeta potential (ζ). Various methods are applied to measure the potential at the shear plane. However, the most commonly used technique is the electrophoresis method[53].

Calcite, when dissolved in water, produces the following species,
$H_2CO_3, HCO_3^-, CO_3^{-2}, Ca^{2+}, CaHCO_3^+, CaOH^+, Ca(OH)_2(aq)$ and $CaCO_3(aq)$ via the following reactions:

$$CaCO_3(s) \rightleftharpoons CaCO_3(aq) \tag{1.11}$$

$$CaCO_3(aq) \rightleftharpoons Ca^{2+} + CO_3^{2-} \tag{1.12}$$

$$CO_3^{-2} + H_2O \rightleftharpoons HCO_3^- + OH^- \tag{1.13}$$

$$HCO_3^- + H_2O \rightleftharpoons H_2CO_3 + OH^- \tag{1.14}$$

$$H_2CO_3 \rightleftharpoons CO_2 + H_2O \tag{1.15}$$

$$CaHCO_3^+ \rightleftharpoons H^+ + CaCO_3(aq) \tag{1.16}$$

$$Ca^{2+} + OH^- \rightleftharpoons CaOH^+ \tag{1.17}$$

$$CaOH^+ + OH^- \rightleftharpoons Ca(OH)_2(aq) \tag{1.18}$$

$$Ca(OH)_2(aq) \rightleftharpoons Ca(OH)_2(s) \tag{1.19}$$

Examination of the proceeding equations shows that, when calcite approaches equilibrium with water at high pH values, an excess of the negative HCO_3^- and CO_3^{-2} species will exist, whereas at low pH values, an excess of the positive $Ca^{2+}, CaHCO_3^+$ and $CaOH^+$ species will occur. These ionic species may be produced at the solid/solution interface or may form in solution and subsequently adsorb on the mineral in amounts proportional to their concentrations in solution. The net result will be in either case: a positive charge on the surface at low pH or a negative charge at high pH. Isoelectric point, or point of zero charge, represents zero ζ at a certain pH value. Carbonate particles carry positive charges in high-salinity brines[54,55].

To understand the SI adsorption behaviour in carbonate systems, the likely mechanisms occurring are shown schematically in Figure 1.15 . When the SI first contacted the carbonate formation, it dissolved the rock, increasing the solution pH. This increase in solution pH then causes the inhibitor to become more dissociated. All SIs are a weak polyacid (e.g., H_nA), which dissociates as follows[42]:

$$H_nA \rightleftharpoons H_{n-1}A^- + H^+ \rightleftharpoons H_{n-2}A^{-2} + 2H^+ \rightleftharpoons H_{n-3}A^{-3} + 3H^+ \rightleftharpoons \cdots \rightleftharpoons A^{n-} + nH^+$$

Low pH

High pH
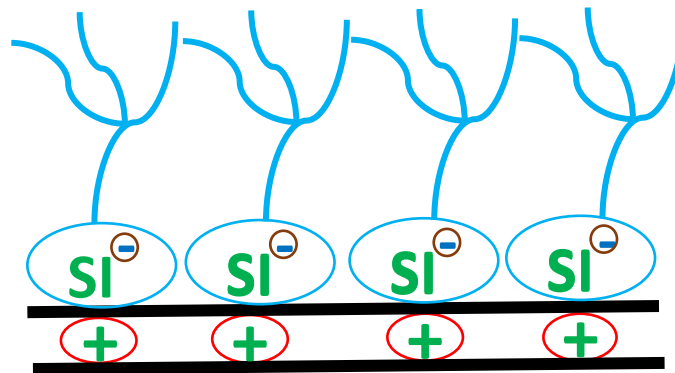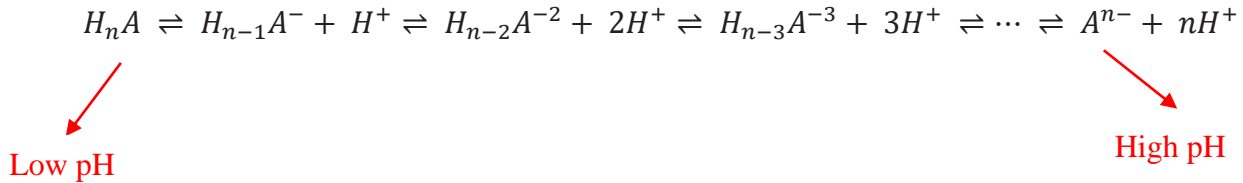
Figure 1.15. Schematic of Scale Inhibitor Adsorption on Carbonate Substrates

1.10.6. Precipitation Mechanism

The second type of inhibitor retention mechanism is by precipitation of SI, often as a divalent cation Ca^{2+} complex in a precipitation squeeze, where the long return time is controlled by the kinetics of inhibitor complex re-dissolution. We assume a precipitation reaction such as $SI + n.Ca^{2+} \rightleftharpoons SI\_Ca_n$, where $n.Ca^{2+}$ ions may bind to a single SI molecule. The solubility of this sparingly soluble salt would be described by an equilibrium solubility product, K_{sp} , of the form: $K_{sp} = [SI].[Ca]^n$ [56–58]. Recently, more emphasis has been placed on precipitation/phase separation squeeze treatments. However, in precipitating chemicals within the rock formation the possibility of the formation damage increases and this has meant that such treatments have often been avoided[59,60].

In precipitation treatments, a mildly acidic solution of the inhibitor is injected into the formation and placed several meters from the wellbore by means of a brine over flush. This process mainly depends upon the physical conditions such as the inhibitor interaction with certain divalent metal cations such as Ca^{2+} (which may either be present naturally in the reservoir or introduced with the inhibitor), pH and temperature. The inhibitor-precipitate often forms a gel-like semi-solid structure within the near-wellbore formation. Such processes can bring about extended squeeze lifetimes when compared with those achieved through a conventional adsorption/desorption approach using similar inhibitors[61–63].

The level of inhibitor in the return curve is governed by the solubility (C_s) of the inhibitor/calcium complex and the rate (r_2) of release of inhibitor into the produced water[64–66]. A mathematical model of this process, explaining the roles of both the solubility and the dissolution rate (C_s and r_2) in precipitation squeezes has been presented by Sorbie[67] and modelling work on this process dates back to the 1990s[68].

1.11. Literature Review

The squeeze technique was started after the first publication of Poetker and Stone[69] on squeezes utilising the adsorption / desorption characteristics of corrosion inhibitors. Later Smith et al.[70] and Kerver et al.[71] , extended the same ideas to inhibit calcium sulphate in water flooding projects using SIs. It was generally assumed that the adsorption and subsequent desorption of SIs was

dominated by physical processes although there did not exist in the literature a systematic study of the exact mechanisms of inhibitor adsorption from solution.

Kerver et al.[72] extended their previous work on corrosion inhibitor squeeze to a study the SI squeezes for the prevention of calcium sulphate scale deposits in oil wells. Both beaker tests for static isotherm measurement and dynamic field core floods were carried out. On the basis of their experimental results, Kerver et al. indicated that the steep slope of the adsorption isotherm at low concentrations implied that the inhibitor would be adsorbed and would desorb slowly. They also declared that the length of time that the produced fluids could supply a sufficient concentration depended on:

(i)   adsorptive capacity of the formation,

(ii)   volume of formation treated,

(iii)   well production rate and,

(iv)   desorption characteristics of the formation.

Durham[73] indicated that, since most inhibitors used for squeezing were highly ionic compounds, their bulk adsorption was probably caused by electrostatic attraction between the formation and SIs. Furthermore, this type of attraction can be readily observed with SIs, most of which are anionic in nature including acrylates, phosphate and phosphonates.

King and Warden[74], hypothesised that:

(i)   the primary means of adherence of a SI compound in sandstone in the absence of highly concentrated calcium brine is adsorption;

(ii)   adsorption refers to a plating mechanism in which a compound at the molecular level, without substantial chemical modification, adheres to the surface of the formation pore or a mineral growth in the pore, by means of electrical or physical forces;

(iii)   the amount of adsorption depends on the amount of active surface area contacted and the thickness to which the inhibitor molecules may adsorb.

Laboratory investigations of SI adsorption/desorption for field applications have employed two types of experimental approach:

(i)   static beaker tests;

(ii)   dynamic packed column and/or core displacement tests. Static beaker tests are conducted using sand, carbonate, clay or crushed core to establish bulk adsorption

isotherms and to investigate the sensitivities of adsorption to factors such as pH, temperature and time etc.

Meyers et al.[48] have summarised the laboratory design and field implementation of inhibitor squeeze treatments in the Prudhoe Bay field. In their screening of five generic phosphonate inhibitors, they concluded that DETPMP was the best inhibitor studied for use in Prudhoe Bay. It offered superior solubility, calcium tolerance, adsorption and scale inhibition compared with the other inhibitors studied. In the investigation of the adsorption/desorption behaviour of the phosphonate inhibitors, they used both crushed and consolidated reservoir rock and a simple NaCl simulated formation brine with no divalent ions present. From SI static adsorption isotherm measurements at 90°C, they found that the inhibitors showed

(i)   a very steep isotherm in the low concentration region (consistent with the Langmuir form);

(ii)   remarkable reversible desorption;

(iii)   plateau adsorption at inhibitor solution concentrations less than 25 mg/L.

They also examined the impacts of the following process parameters on inhibitor adsorption: pH, temperature, salinity, divalent cations, surfactant and winterising agents. Their main conclusions were as follows:

(i)   pH has the most significant effect on inhibitor adsorption. The adsorption of inhibitor is constant below pH4, decreased dramatically between 5 and 6, and drops essentially to zero at pH greater than 7. Thus, to maximise adsorption and to minimise shut-in time, inhibitor slugs near reservoir pH (4.7) should be injected. However, no analysis was presented as to why phosphonate adsorption was high at low pH and low at high pH in their study.

(ii)   The presence of Ca^{2+} at concentrations less than that required to precipitate the phosphonate has no effect on the adsorption of phosphonate. The adsorption of phosphonate DETPMP is enhanced by the presence of calcium at a pH of 6. The conclusion arrived by Meyers et al.[48], may be due to the low pH value they used.

(iii)   increasing the temperature from 25 to 90°C results in a 25% increase in the adsorption of DETPMP.

(iv)   by manipulating pH, temperature, inhibitor concentration, iron concentration and the calcium concentration, precipitation of iron and calcium salts can be induced.

However, they thought that although such precipitation in the matrix increases inhibitor retention, and thus treatment life, it also may reduce the near-well bore permeability and damage the well.

(v)   neither surfactant concentration (0 to 1.5 wt %), salinity (0.5 to 5 % NaCl), nor winterising agents (0 to 15 wt% methanol/0 to 15 wt% ethylene glycol) had apparent impact on the adsorption of DETPMP.

Przybylinski[75], examined five structurally different inhibitors using a dynamic adsorption desorption technique. The five inhibitors were (a) phosphonate inhibitor DETPMP; (b) an alkyl phosphonate HEDP; (c) a phosphate ester (TEAPE); (d) a tagged polyacrylic acid (PAA) and (V) a proprietary polymeric phosphonate inhibitor (PPI). The experimental work was performed with silica sand or limestone packed columns at 40°C and 80°C. Synthetic brine which had a similar composition to some oilfield brines was used. Some very interesting results were reported from this study, as follows:

(i)   the phosphonate inhibitor (DETPMP) had the highest levels of return on both sand and limestone of all inhibitors tested in this study. These laboratory results indicated that it was the best inhibitor for squeeze applications for the test conditions used.

(ii)   since adsorption/desorption depends on the partitioning of the inhibitor solution and the solid surface, the nature of the surface and the solution are both important and using an inappropriate brine may lead to false conclusions.

(iii)   precipitation can occur in reservoirs due to changes in temperature, resulting in an enhanced squeeze.

(iv)   the experimental results show that: (a) the adsorption level of phosphonate on silicate sand is higher than the value which is estimated based on simple monomolecular layer adsorption; (b) the adsorption of inhibitors increases with increase in temperature and (c) a significant fraction of the adsorbed inhibitor is not readily released to the produced brine. Thus, there is some firmly held inhibitor and some which is more readily adsorbed. These observations lead to the suggestion that two or more adsorption mechanisms are at work. These may include surface precipitation and strong adsorption.

(v)   a better indication of the suitability of an inhibitor is from kinetic desorption studies instead of the amount of inhibitor adsorbed by the formation.

The last finding from Przybylinski's work[75], regarding the importance of the kinetics of the inhibitor adsorption-desorption process, is in agreement with many researchers observations.

In order to understand the retention mechanism of phosphonate (DETPMP) in the reservoir after an inhibitor squeeze, Kan et al.[51] studied both the kinetics and the equilibrium aspects of phosphonate adsorption in the laboratory using beaker tests and sandstone core floods. They postulated that there are at least four processes involved in inhibitor adsorption:

(i)   mass-transport molecular diffusion of inhibitor in solution to the solid surface;

(ii)   acid/base dissolution of the mineral surface;

(iii)   adsorption to the surface as the result of step (II);

(iv)   ultimate solid phase maturation toward a thermodynamically stable phase, as the solid surface material interacts with the solution. They concluded that the kinetics of the slow reaction governs the phosphonate flow back phenomenon and the rate-limiting step for the slowest adsorption reaction is probably a diffusion-controlled process. The efficiency of the inhibitor squeeze can be enhanced by increasing phosphonate contact time and contact area.

Sorbie et al.[76,77] have used mathematical modelling to analyse both laboratory experiments and field systems. They have explained that the mechanism of tailing in an adsorption squeeze process is a propagation phenomenon associated with the shape of the inhibitor adsorption isotherm on the reservoir rock. They demonstrated that a sharply rising isotherm and non-equilibrium inhibitor adsorption are key factors in influencing an inhibitor squeeze.

One of these studies was on the effect of pH, Calcium concentration and temperature on the adsorption of phosphonate inhibitor onto consolidated and crushed sandstone[49]. Some interesting results were reported from this study:

(i)   in the absence of Ca^{2+} ions, the adsorption of phosphonate inhibitor (DETPMP) monotonically decreased as pH increases (at 25°C) based on the hydrogen bonding mechanism for adsorption.

(ii)   when calcium ions are present in the seawater brine (i.e. $[Ca^{2+}]$ = 415ppm; temperature = 25°C), inhibitor adsorption onto crushed rock is lower at pH_0 4 than at pH_0 2 or pH_0 6.

(iii)   at pH6, the involvement of Ca^{2+} in the inhibitor/rock interaction was clearly demonstrated (at 25°C).

(iv)   inhibitor adsorption onto crushed rock material increases at higher temperatures under all conditions.

(v)   the electrokinetic measurements on crushed rock particles in seawater solution quite clearly correlate phosphonate inhibitor adsorption behaviour with the surface charge properties (ζ-potential).

Tantayakom et al.[78] considered a kinetic study of phosphonate SI Amino-trimethylene Phosphonic Acid (ATMP) precipitation in squeeze treatments. It was concluded that pH plays an important role in controlling the precipitation of Ca-ATMP and has both positive and negative effects for field applications. At higher pH, more Ca-ATMP was precipitated; however, the precipitation was fast and more likely in the vicinity of the wellbore, thereby reducing the effectiveness of the treatment. They also suggested that nucleation kinetics play an important role in the spread of the inhibitor in the treatment zone during precipitation squeeze treatments as the injected fluid flows out into the formation.

Kahrwad et al. [10] developed a model which shows the dependence on the mass/volume (m/V) ratio if coupled adsorption/precipitation is occurring in mineral/DETPMP system and showed that apparent adsorption increases as pH of DETPMP solutions increases. At pH_0 4 only pure adsorption is observed while at pH_0 6 coupled adsorption/precipitation is dominant mechanism of DETPMP retention.

Ibrahim et al. [79] carried out static compatibility and coupled adsorption/precipitation experiments using two phosphonate SIs (DETPMP (a penta- phosphonate) and OMTHP (a hexa-phosphonate)) and several minerals. They concluded that for all SI/mineral systems, pure adsorption is observed at low Scale Inhibitor concentrations whilst coupled adsorption/ precipitation occurs at high concentrations.

Yan et al.[80] studied adsorption and precipitation of SIs on shale formations. They used two different types of shale formation (Eagle Ford and Marcellus shale) and two SIs (DETPMP and PPCA). They concluded the adsorption kinetics experiments show a fast adsorption process for DETPMP and PPCA on both shale formations, and inhibitor concentration in solution reached equilibrium between 4 and 8 h. For low phosphonate concentration ranges, the interaction between the inhibitors and both shale formations can be characterized as surface adsorption.

Above a certain concentration of inhibitors, DETPMP and calcium forms precipitate a carbonate-rich Eagle Ford shale, which increases the attachment of DETPMP on shale formations. It is found that slightly acidic pH and high calcium concentrations enhance the precipitation of DETPMP on both shales.

The adsorption of PPCA on Eagle Ford was more significant at 100% CO_2 than at 1% CO_2 condition, and high calcium levels at 100% CO_2 condition maybe the primary contributing factor for the enhancement. PPCA adsorption onto Marcellus did not exhibit a notable difference between 100% CO_2 and 1% CO_2 conditions.

The results from this study demonstrated that the interaction between inhibitor molecules and the rock surface of shales can be controlled in favour of long-term protection. pH and calcium concentrations in a particular shale formation may determine the extent to which the inhibitor species are retained and released after hydraulic fracturing. The precipitation and dissolution of calcium-inhibitor solids may be the controlling mechanism of a long-life inhibitor return. The retention and release process is more complicated in the field than lab-scale experiments due to multiple factors, such as reaction (adsorption/desorption, and precipitation/dissolution) kinetics, inhibitor interactions with other chemicals in fracturing fluids, and mass transfer limitations.

Jordana et al.[81] performed a comprehensive study on the retention and release of SI in different clay minerals. This research presents work investigating these interactions with the spectroscopic techniques commonly employed in surface chemistry. Uptake of Nitrilo-Tris Methylene-Phosphonic acid (NTMP), a model SI, by kaolin, halloysite and montmorillonite has been monitored by Liquid-Phase Nuclear Magnetic Resonance (^{31}P NMR) spectroscopy. ^{31}P NMR has also been used to follow the release of SI during desorption experiments. The adsorbed inhibitor has been detected directly and quantified with X-ray Photoelectron Spectroscopy (XPS). XPS combined with argon ion etching has also been able to distinguish between inhibitor adsorbed onto the external surface of the clays and occluded into the interlayer spacing.

They characterized NTMP after being adsorbed onto three different types of clays by XPS and ^{31}P liquid NMR. Adsorption isotherms constructed using both techniques (XPS and ^{31}P NMR) show the differences between adsorption on the external surface of a non-swelling clay, and in the interlayer pore volume of a swelling clay. NTMP was retained much better in swelling clays, such as montmorillonite, than in non-swelling clays, such as kaolin, but not all the SI may be released. Exchangeable cations present in mineral clays play a role in the retention by

complexing with the molecule and/or by catalysing its decomposition. The presence of divalent cations in the desorbing solution enhanced release of SI, but does not change the nature of the desorbing species.

Gdanski et al.[82–84] has found that static adsorption data has a direct bearing on SI adsorption/desorption in dynamic mineral packs. Furthermore, isotherm fitting with the modified Langmuir equation provided the mathematical framework for an understanding of desorption kinetics. However, the Langmuir adsorption isotherm often does not fit experimental data effectively. The Langmuir adsorption isotherm is valid only if the adsorbent material is homogeneous, both the solute and solvent have equal molar surface areas, both the surface and bulk phases exhibit ideal behaviour, and the adsorbed layer is monomolecular. The following conclusions were reported:

   (i)   a wide variety of adsorption data can be fit by using modified Langmuir equation.
   (ii)   Static adsorption isotherms are useful in determining the magnitudes of the kinetics effect on desorption in linear flow tests.
   (iii)   Siderite may be responsible for the long-term, low-level inhibitor-return profiles sometimes observed after squeeze treatments.
   (iv)   The minerals studied can be classified into three groups:
       1. strongly adsorbing (siderite)
       2. moderately adsorbing silica-like minerals (silica and kaolinite)
       3. weakly adsorbing alumina-like minerals (illite, smectite and alumina)

Kan et al.[45] has studied the inhibitor/rock interaction and factors affecting SI retention in carbonate-rich formations during squeeze treatments for four common oilfield inhibitors (three phosphonates and one poly-acrylate). In addition to calcite ($CaCO_3$) in reservoir rock, SI-Ca^{2+} solid phases are also important. Two reactions are central to inhibitor retention in carbonate-rich formation: first, reduction of calcite dissolution because of surface poisoning by the SI/Ca^{2+} coating; and second, precipitation of SI/Ca^{2+} solid with either low Ca^{2+} or high Ca^{2+} stoichiometry. For NTMP, an acidic Ca-NTMP salt is formed in a low-pH environment. In addition, two crystalline Ca-NTMP phases and an amorphous Ca-NTMP salt may form, depending on the aquatic environment. Quantitative relationships between type of inhibitor,

inhibitor acidity and concentration, together with kinetics of calcite dissolution and calcium-phosphonate precipitation are developed.

There are a few sources of calcium in a typical field squeeze:

(i) Ca^{2+} contained in the seawater and injected with inhibitor;

(ii) Ca^{2+} is injected in the overflush;

(iii) Ca^{2+} can be dissolved from calcite and solid formation minerals;

(iv) Ca^{2+} present in the formation brine.

Many laboratories result and field observations have indicated the importance of calcium to the inhibitor squeeze process. In accordance with Kan et al.[45], many researchers have found that the retention of inhibitor is significantly enhanced by the presence of calcium ions which results in an extended squeeze lifetime. However, there is no detailed analysis, in the literature, concerning this calcium enhanced retention or it is arbitrarily attributed to the precipitation between phosphonate inhibitor and calcium ions.

Tomson and Rogers[85], have extensively studied that what controls inhibitor placement in the formation. It is commonly suggested that reservoir type determines how an inhibitor is retained in a formation. This research suggested that the pill chemistry (this is the term frequently used in North America for the SI slug, as used in the UK and internationally) is also an important determinant for retention in carbonate reservoirs. Acidic pills are mostly retained near the well bore while more neutralized pills move farther into the formation. Three calcium nitrilomthylenephosphonate (NTMP) solid phases, an amorphous phase and two crystalline $Ca_{2.5}HNTMP$ phases with $pK_{SP} = 22.6$ and $pK_{SP} = 24.2$, are particularly important with respect to inhibitor retention. The relative sizes of these solid phases formed are governed by the pill composition and acidity. Nearly all of these field squeezes were done using a common phosphonate inhibitor, NTMP (nitrilotri (methylene phosphonic) acid), although similar results have been observed with several other inhibitors and blends. From these large numbers of studies and observations, the following conclusions were made:

(i)   for an acidic pill, approximately 78% of injected phosphonate precipitates in these experiments. The fraction that precipitated is inversely related to the amount of base in the pill. Most of the precipitate is near the injection port.

(ii)   for partially neutralized pill, approximately 50% of injected phosphonate precipitated at the rear end of the column.

(iii)   a portion of phosphonate was retained as the crystalline phosphonate salt and a portion of the acidic pill was retained as a more soluble calcium phosphonate salt.

Baraka-Lokmane et al.[86] studied the effect of pH and SI concentration on phosphonate–carbonate interactions. They presented results from five core floods (RC1 to RC5) using the Jurassic Portlandian limestone (φ ~19.8% and k=606 mD) with 5000 ppm, 10,000 ppm, 25,000 ppm and 27,000 ppm of partly neutralized DETPMP at pH 4 and 2. The purpose of this research was to study the effect of inhibitor concentration and pH on inhibitor adsorption and on the evolution of the inhibitor and cation (calcium and magnesium) return concentrations. This study showed that the higher the concentration of SI and the lower the pH, more calcium dissolution was observed (from the $[Ca^{2+}]$ effluents). In all treatments there was a decrease $[Mg^{2+}]$ in the effluent corresponding directly to the increase in $[Ca^{2+}]$. The effluent cation results in the long core floods support the view that both magnesium and calcium are binding strongly to the DETPMP SI. In addition, the experimental results, along with some simple modelling, greatly clarify the role of both calcium and magnesium in the mechanism of SI retention in carbonate systems. The petrography analysis also showed that core floods RC3 and RC4 (at pH 2) did not induce the formation of worm holes or micro worm holes, but core flood RC5 performed with 27,000 ppm DETPMP at pH 4 showed that the high concentration of the SI solution induced the formation of micro worm holes on the calcite crystals. The analysis of the structure of the phosphonate calcium salt shows that this salt has been precipitated, confirming that the mechanism of the DETPMP SI retention in carbonate rocks is of a precipitation type. The Atomic Force Microscopy (AFM) analysis revealed the shape of the calcium phosphonate crystals. Thin sections, Scanning Electron Microscope (SEM), Energy-dispersive X-ray spectroscopy (EDX), XPS and AFM analysis of the cores after the different core floods have shown the presence of SI salts formed within the void space and on the grains. The EDX analysis of the SI salts has revealed the presence of phosphorus. The XPS analysis has shown that core floods RC3 (25,000 ppm DETPMP at pH 2) shows more retained phosphorus (0.35%) than floods RC5 (0.30%), RC4 (0.21%), RC2 (0.17%) and RC1 (0.16%). These results show that we have more SI retention with both a high SI concentration and a low pH value, the low pH parameter seeming to be more important on SI adsorption than the concentration of the SI solution.

Tomson et al.[87] discussed the influence of metal ions, e.g., Ca^{2+}, Mg^{2+}, and Fe^{2+} on the phosphonate inhibitor retention (DETPMP (Diethylenetriamine Penta (Methylene Phosphonic acid)), BHPMP (Bis-Hexamethylenetriamine Penta (Methylene Phosphonic acid)), and release in both laboratory simulation and field case studies. These metal ions were either originally added to the inhibitor solutions or generated in-situ because of the dissolution of reservoir minerals by the acidic inhibitors. They showed Phosphonate return following an inhibitor squeeze can be modelled with three phases of return.

(i)   phase I phosphonate return corresponds to the residual phosphonate that does not attach to the solid phase and returns in 3 Pore Volume (PV);

(ii)   phase II return corresponds to the dissolution from a high-solubility solid phase;

(iii)   phase III return corresponds to the dissolution from a crystalline solubility phase. For DETPMP, Phase II return could be characterized with a solubility product, $pK_{sp}=$ 52.4 to 52.6 by assuming a stoichiometry of Ca_3H_4 DETPMP; and Phase III return corresponds to the dissolution from a crystalline solubility solid phase ($pK_{sp}=53.3$ to 54.2). BHPMP return followed three phases of return as DETPMP. The Phase III crystalline solubility (pK_{sp}) is 39.9 to 40.4 by assuming a stoichiometry of Ca_4H_2BHPMP. In addition, Cations, e.g. Ca^{2+}, Mg^{2+}, and Fe^{2+}, could be added to the inhibitor pill to enhance the inhibitor retention in the formation. Similarly, these cations could be generated in-situ by adding a strong acid to the inhibitor pill solution.

Thomas et al.[88] performed Coupled Adsorption/Precipitation tests with a Phosphonate Inhibitor and Carbonate Substrate. A series of static adsorption/precipitation tests was carried out to examine the behaviour of Diethylenetriamine Penta Methylene Phosphonic (DETPMP), when in contact with brine and calcium carbonate ($CaCO_3$). These tests are carried out at pH 2 and pH 4 and at a range of DETPMP concentrations from 0ppm to 5000 ppm. They illustrated that very low levels of adsorption are evident in tests with a full complement of divalent ions, and apparent adsorption rates are twice as high in samples with 10g of calcite as in samples with 20g of calcite. Furthermore, the initial pH of the brines does exert an influence over the result. Where the initial pH of the brine is 2, calcium levels remain at or above the initial brine concentration throughout the tests. With an initial pH of 4, however, calcium levels fall to about 80% of input. Where the calcium and magnesium are removed from the brine, this behaviour no longer holds true.

Apparent adsorption no longer follows the 2:1 trend seen in earlier tests. Where calcium has been removed from the brine, magnesium levels drop further to 55%-65% of input level, as opposed to the 80% of input where calcium is present in the brine. When magnesium is removed, a slightly larger loss of calcium is observed, down to 74% of input from 82% of input (comparing samples with 10g of calcite). Magnesium appears to be substituting for calcium in the SI-Ca/Mg precipitate when there is less calcium available in solution. These findings indicated that during squeeze treatment with phosphonate-based inhibitors, carbonate reservoirs will be subject to significant dissolution of the reservoir rock and precipitation of SI-Ca/Mg complexes in the pore space may occur.

1.12.   Relevance to the Current Study

This survey of the literature shows the history of laboratory work which has been used study the adsorption and adsorption/precipitation of SIs used in oilfield squeeze treatments. It is clear that an adsorption squeeze is governed by the inhibitor adsorption isotherm $\Gamma(C)$. However, the adsorption isotherm which is an intrinsic property of inhibitor/rock system will be a function of inhibitor concentration, pH, temperature and brine composition (e.g. Ca^{2+}, Mg^{2+}, etc…). The main mechanisms of inhibitor adsorption depend on; (i) the surface chemistry and roughness of the adsorbing minerals - silica sand, clay, kaolinite, siderite, sandstone, carbonate etc., (ii) experimental or field conditions - pH, temperature, salinity and hardness, and (iii) inhibitor properties - functional group, dissociation degree, polarity, etc. However, precipitation (Π) occurs when the SI molecule precipitates out of the solution because of the formation of an inhibitor/Ca complex. This SI/Ca complex is a sparingly soluble salt. The solubility of this sparingly soluble salt would be described by an equilibrium solubility product, K_{sp} , of the form: $K_{sp} = [SI].[Ca]^n.$

Most previous experimental work has included sandstones and some on carbonates. However, a detailed study of the interaction between SI and carbonate has not been carried out due to the complexity of their systems. Thus, this PhD thesis is to investigate the SI/carbonate systems in detail to provide a full understanding of SIs retention in carbonates and parameters which affect this. It is obvious that understanding the main retention mechanism for various SIs in carbonate

reservoirs will clearly help us in the selection of more effective SIs for squeeze treatments in carbonates.

2. CHAPTER 2: THEORY of ADSORPTION and COUPLED ADSORPTION/PRECIPITATION

2.1. Introduction

In downhole chemical scale inhibitor (SI) squeeze treatments to prevent mineral scale formation[89–92], a key issue is how long the squeeze lifetime will be. The squeeze lifetime is the time until the returned SI concentration drops below the MIC to prevent or delay scale deposition to an acceptable level; MIC = Minimum Inhibitor Concentration. The squeeze lifetime depends on the manner and degree to which the SI is retained within the porous medium. As mentioned in Chapter 1, there are two main retention mechanisms of SIs in porous media, i.e. adsorption and precipitation, which are usually denoted as Γ and Π, respectively. There is not complete agreement in the literature about when we should use one mechanistic description or another and various "schools" of thought on the retention issue have emerged, in the literature, as follows:

(i) Heriot-Watt University (HWU) – where adsorption has been described by a generalised adsorption isotherm, $\Gamma(C)$, and precipitation is described by a solubility function, $\Pi(C)$, and a dissolution rate constant (denoted, r_2);

(ii) Halliburton – Gdanski and Funkhouser[83] have described SI retention through an adsorption mechanism based on the specific mineralogy of the (sandstone) rock;

(iii) Rice University – have described SI retention by a precipitation/dissolution mechanism based on the precipitation and solubility of the various Ca-SI salts that are formed.

In fact, all of the above approaches to SI retention have some validity depending on the conditions in the system, i.e. the type of SI, the mineral substrate (sandstone, carbonate), the brine pH, the levels of divalent cations (Ca^{2+}, Mg^{2+}), the temperature, T, etc. It is more appropriate to consider **when** a given retention mechanism applies, e.g. pure adsorption (Γ), mainly precipitation (Π) or coupled* adsorption/precipitation (denoted Γ/Π). A central objective of current research within the FAST group and of this thesis is to (i) provide data for the development of a fully consistent generalised model that can describe both coupled adsorption and precipitation (Γ/Π), and (ii) devise experiments which can test this model

experimentally. (*By "coupled" here, we mean that the SI species may be involved in both adsorption and precipitation and hence these processes are not independent but are coupled together. This feature must be consistently and correctly described by any mathematical model of the coupled processes).

It is noted with regard to the adsorption (Γ) and precipitation (Π) mechanisms that it is possible to have a pure adsorption process, i.e. described by an adsorption isotherm only, $\Gamma(C)$. However, it is very rare to have a pure precipitation process, i.e. Π only, since if precipitation is occurring this implies that the solvent is a poor solvent, and this would certainly initiate some degree of adsorption on the mineral present. Therefore, for SI retention we envisage that the only 2 cases likely are (a) pure adsorption, Γ and (b) coupled adsorption/precipitation (Γ/Π). Also, as will be shown below, it is common to have pure adsorption at very low SI concentrations, with precipitation if it occurs taking place at higher SI concentrations.

2.2. Pure Adsorption
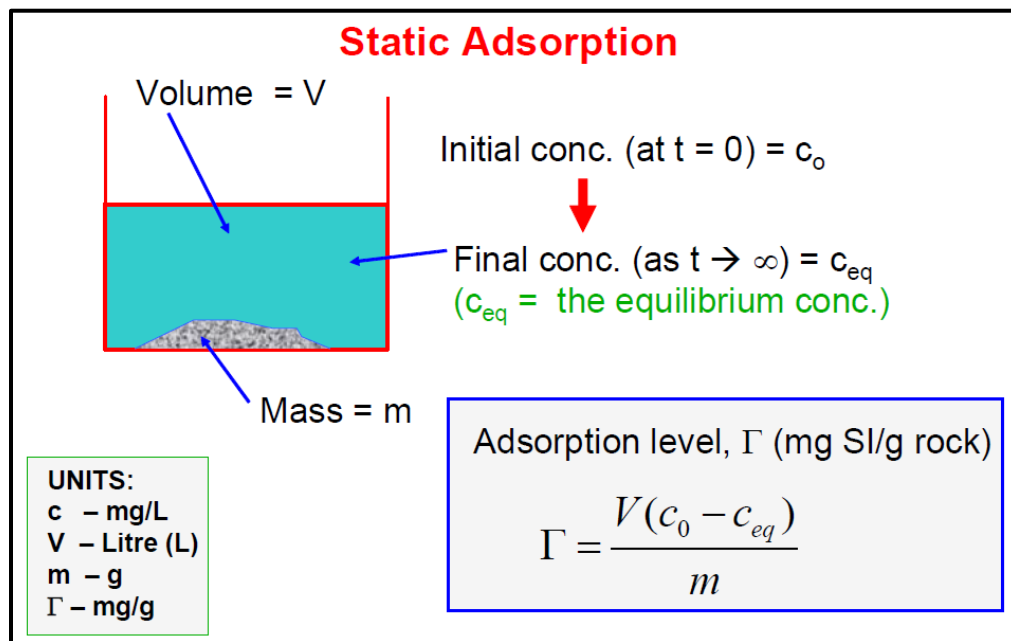
Figure 2.1. Scheme of the simple static adsorption on a crushed mineral substrate[10]

A schematic of a static adsorption experiment, i.e. where only pure adsorption occurs, is shown in Figure 2.1 where the notation is also given. A SI of initial concentration, C_o (ppm or mg/L),

in a volume, V (L), is allowed to come to equilibrium with a mass, m (g), of mineral. At equilibrium concentration of the SI, C_{eq}, then by material balance the adsorption level is as follows:

@ Initial conditions (before adsorption occurs); initial mass of SI = VCo

@ Final (equilibrium) conditions (after adsorption occurs and system reaches equilibrium); equilibrium the mass of SI = Mass adsorbed on mineral (m_1) + mass remaining in solution (m_2)

Part of the SI adsorbed on the surface of grains, $m_1 = m.\Gamma(C_{eq})$

Part of the SI left in solution (not adsorbed), $m_2 = VC_{eq}$

Since the original mass is conserved, then: $VC_o = m \Gamma(C_{eq}) + VC_{eq}$ \hfill (2.1)

If the analytical form of the isotherm is known (e.g. it is a Freundlich or a Langmuir isotherm with known parameters), then Eq. (2.1) gives a simple non-linear equation for finding C_{eq} which is the only unknown quantity. If equation (2.1) is written in another way it highlights how our experiments are performed, as follows:

$C_o = (m/V) \Gamma(C_{eq}) + C_{eq}$ \hfill (2.2)

Which indicates that the mass/volume ratio, (m/V), is an important parameter in these adsorption experiments, as already shown in Chapter 1 and will be explained further below. Defining the function $F(C_{eq})$ as follows:

$F(C_{eq}) = (m/V) \Gamma(C_{eq}) + C_{eq} - C_o$ \hfill (2.3)

At equilibrium conditions, the root of $F(C_{eq})$ is zero i.e. where:

$F(C_{eq}) = 0$ or $(m/V) \Gamma(C_{eq}) + C_{eq} - C_o = 0$ \hfill (2.4)

If we assume one of common adsorption isotherm models (Freundlich model) describes the system, the calculation of the equilibrium SI concentration by using the Freundlich form of Γ is as follows:

$$\Gamma(C_{eq}) = \alpha(C_{eq})^{\beta} \tag{2.5}$$

With $\alpha = 0.021$ and $\beta = 0.73$ where C is in ppm and Γ is in mg showing different /g rock. These parameters are not arbitrary since they relate to our experimental results. However, this case serves as a useful numerical example to demonstrate some of the calculations in the coupled adsorption/precipitation for SI/sandstone systems which is simpler than for SI/carbonates.

If the molecular weight of the SI is given by M_{SI}, then the Freundlich isotherm with molar concentration of C (M) would be:

$$\Gamma(C_{eq}) = \alpha'(C_{eq})^{\beta} \tag{2.6}$$

Where $\alpha' = (1000M)^{\beta} \cdot \alpha$.

2.3. Coupled Adsorption/Precipitation

2.3.1. SI/Sandstone System (No rock/fluid interaction)

The analysis above has been extended for pure adsorption to the case where both adsorption (Γ) and precipitation (Π) can occur at the same time. This is shown schematically in Figure 2.2 where the precipitation occurs by the formation of the calcium salt of the SI, i.e. by precipitation of *SI_Can*. In general, this precipitation reaction is as follows:

$$SI + n.Ca \rightleftharpoons SI\_Ca_n \tag{2.7}$$

Where n.Ca ions may bind to a single SI molecule. The solubility of this sparingly soluble salt would be described by an equilibrium solubility product, K_{sp}, of the form:

$$K_{sp} = [SI].[Ca]^n \tag{2.8}$$
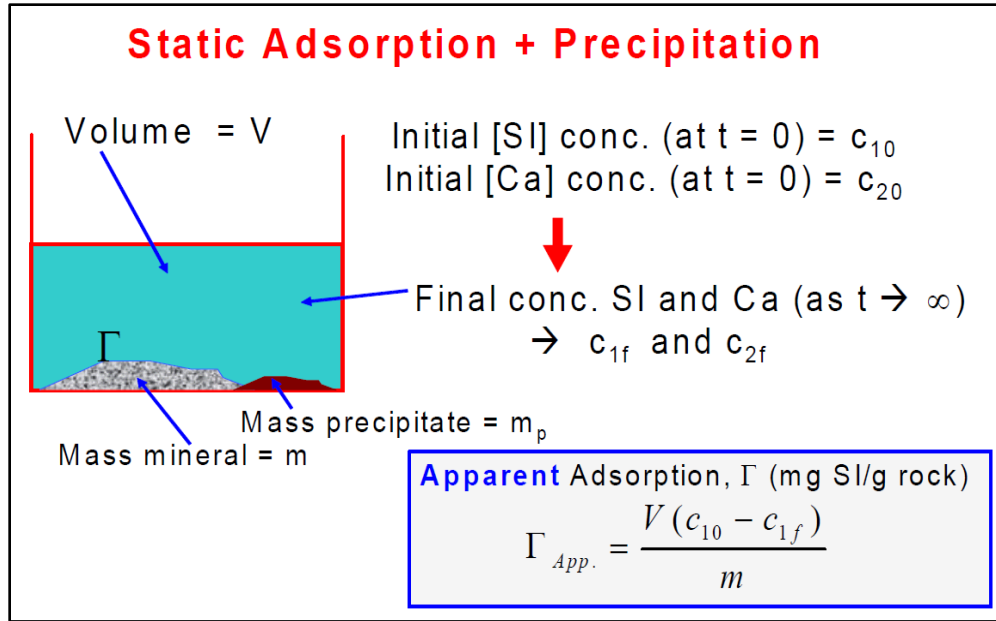
Figure 2.2. Scheme of how both coupled adsorption and precipitation can occur; this is interpreted as an "apparent adsorption"[10]

The following additional notation is introduced in Figure 2.2:

- C_{1o} and C_{1f} – initial (t=0) and final equilibrium (t→∞) SI molar concentration. (M);

- C_{2o} and C_{2f} – initial (t=0) and final equilibrium (t→∞) Ca^{2+} molar concentration. (M);

- Γ is the adsorption which depends on C_{1f}, $\Gamma = \Gamma(C_{1f})$ (mg/g);

- The precipitation process depends on both C_{1f} ([SI]) and C_{2f} ([Ca]) through K_{sp} as follows: $K_{sp} = (C_{1f}) . (C_{2f})^{n}$ in this notation when the system is in equilibrium; units of K_{sp} (M^{n+1});

- m_p is the actual mass of precipitate (SI_Ca_n) which forms.

Note that the initial and final values of SI concentration are C_{1o} and C_{1f} . Some of this SI which is "missing" from the bulk solution is adsorbed on the mineral and the remainder of it is part of the precipitate. However, if we assumed that **all** of this "missing" SI is adsorbed, then we would calculate an "apparent adsorption", Γ_{app}, as follows:

$$\Gamma_{app} = \frac{V(C_o - C_f)}{m} \tag{2.9}$$

60

This quantity is *not* the adsorbed level, it is just the *apparent* level of "adsorption" based on the SI missing from solution. Clearly, the apparent adsorption, Γ_{app}, is an over-estimate of the actual adsorption (since some of this would be precipitate) but it is what would be measured in an actual experiment if the above formula were used. We will see the use of the concept of apparent adsorption in the argument developed below.

We now derive the main equations describing coupled adsorption/precipitation based on the view of the process discussed above and shown schematically in Figure 2.2. As before, the total masses of SI and Ca, which are conserved, are given by the following expressions, where we note we are working in molar concentrations (M) for SI and Ca:

Total initial Mass of SI (which at t =0, is all in solution), $m_0 = V$ (L). M_{SI} (g of SI/mole).C_{1o} (mole of SI/L)

At equilibrium (after adsorption and precipitation):

Total mass of SI, $m_0 = V. M_{SI} .C_{1f} + (m/1000). \Gamma (C_{1f}) + \varphi. m_p$ (2.10)

Where m_p is the actual mass of precipitate which forms and φ is the fraction of the precipitate (of formula SI_Ca$_n$) which is actually SI, i.e.

$$\varphi = (\frac{M_{SI}}{M_{SI}+n.M_{Ca}})$$ (2.11)

Note that denominator of 1000 appears in Eq. (2.10) since m.Γ is in mg and all other masses in this equation are in g. Both adsorption and precipitation are contributing the change in SI concentration from C_{1o} to C_{1f} . However, the precipitate is the only cause of the change in calcium concentration from C_{2o} to C_{2f}, and since the stoichiometry is $SI + n.Ca \rightleftharpoons SI_{Ca_n}$, then the actual mass of precipitate must be given by:

$$m_p = \frac{V}{n}(C_{20} - C_{2f})(M_{SI} + n. M_{Ca})$$ (2.12)

Above equations can be used for φ and $\Gamma (C_{1f})$ in Eq. (2.10) to obtain the following expression for the mass of SI:

Total Mass SI, $m_0 = V. M_{SI} .C_{1f} + (m/1000).\Gamma (C_{1f}) + (\frac{M_{SI}}{M_{SI}+n.M_{Ca}}). \frac{V}{n}(C_{20} - C_{2f})(M_{SI} + n. M_{Ca})$

(2.13)

Which simplifies to:

Total Mass of SI, $m_0 = V. M_{SI} .C_{1f} + (m/1000). \Gamma (C_{1f}) + (\frac{M_{SI}.V}{n})(C_{20} - C_{2f})$

(2.14)

Thus, by material balance (conservation of mass of SI):

$V. M_{SI} .C_{1o} = V. M_{SI} .C_{1f} + (m/1000). \Gamma (C_{1f}) + (\frac{M_{SI}.V}{n})(C_{20} - C_{2f})$ (2.15)

Which can be divided through $V. M_{SI}$ by to obtain:

$C_{1o} = C_{1f} + (\frac{m}{1000.V.M_{SI}}). \Gamma (C_{1f}) + (\frac{1}{n}). (C_{20} - C_{2f})$ (2.16)

The main problem with the above equation is that it has 2 unknowns, C_{1f} (SI concentration) and C_{2f} (Ca concentration), which means that it cannot be solved as written. However, the Ca concentration, C_{2f}, will be eliminated by using the solubility product equation (*if there actually is a precipitate*) for the SI_Ca$_n$ – (i.e. $K_{sp} = (C_{1f}). (C_{2f})^n$) to note that:

$C_{2f} = (\frac{K_{SP}}{C_{1f}})^{\frac{1}{n}}$

Hence, this expression for C_{2f} can be substituted into Eq. (2.16) above to obtain the equation for coupled adsorption/precipitation:

$C_{1o} = C_{1f} + (\frac{m}{1000.V.M_{SI}}). \Gamma (C_{1f}) + (\frac{1}{n}). (C_{20} - (\frac{K_{SP}}{C_{1f}})^{\frac{1}{n}})$ (2.17)

As before, this equation can be rewritten in the final working form as:

$F (C_{1o}) = C_{1f} + (\frac{m}{1000.V.M_{SI}}). \Gamma (C_{1f}) + (\frac{1}{n}). (C_{20} - ((\frac{K_{SP}}{C_{1f}})^{\frac{1}{n}})) - C_{1o}$ (2.18)

Where, at equilibrium adsorption/precipitation, we simply have to solve this equation for C_{1f}, i.e. find the root of $F(C_{1o}) = 0$. Note that this is the corresponding equation to Eq. (2.16) for pure adsorption except for the additional term describing precipitation in Eq. (2.18),

i.e. $\left(\frac{1}{n}\right) \cdot (C_{20} - \left((\frac{K_{SP}}{C_{1f}})^{\frac{1}{n}}\right))$.

Note that Eq. (2.17) applies if (and only if) there is definitely a precipitate i.e. $(C_{1f}) \cdot (C_{2f})^n$ is not less than K_{sp}. If there is no precipitate, then the substitution, $C_{2f} = (\frac{K_{SP}}{C_{1f}})^{\frac{1}{n}}$, does not apply and it happens that the quantity $\left(C_{20} - \left((\frac{K_{SP}}{C_{1f}})^{\frac{1}{n}}\right)\right) < 0$ which is unphysical. Hence in solving the main working Eq. (2.18) can be used it for all cases of adsorption only or coupled adsorption/precipitation by setting the quantity $\left(C_{20} - \left((\frac{K_{SP}}{C_{1f}})^{\frac{1}{n}}\right)\right)$ to its actual value if it is $\geq$ 0, or to zero otherwise.

2.3.2. SI/Carbonate Systems

SI squeeze treatments in carbonate reservoirs are often affected by the chemical reactivity between the SI and the carbonate mineral substrate. This chemical interaction may lead to an increase in solution Ca^{2+} by mineral dissolution and subsequent precipitation of the SI through the formation of a sparingly soluble Ca/SI complex which can lead to an extended squeeze lifetime. However, the same interaction may in some cases lead to uncontrolled SI precipitation causing near-well formation damage in the treated zone[93]. This research work presents a detailed study of the various retention mechanisms of SI in carbonate formations, considering system variables such as the (carbonate) formation mineralogy, the type of SI and the system conditions. To understand the detailed SI/carbonate system, we must consider the parts of the chemical processes involved. When SI solution contacts the carbonate mineral substrate, it reacts with it chemically generally dissolving/chelating some calcium into solution. The SI can then form a SI/Ca (and SI/Ca/Mg) complex which is sparingly soluble and this may precipitate, which in

turn can affect pH. Thus, the entire system is coupled and the 3 parts of the equilibrium system are:

(i)   The dissociation of SI to form dissociated species, such as H_nA right up to A^{n-} at high pH values;

(ii)   These dissociated SI species, which are very strong chelating agents, then bind with Ca^{2+} (and Mg^{2+}) ions to form SI/Ca complexes which are known to be sparingly soluble;

(iii) The above reactions must be coupled to the carbonate system since the lower pH solution conditions and the chelating power of the dissociated SI cause the carbonate equilibrium to change.

Assume the carbonate system is illustrated in Figure *2.3* (to simplify oil and gas phases have not been taken into consideration; only the aqueous phase).
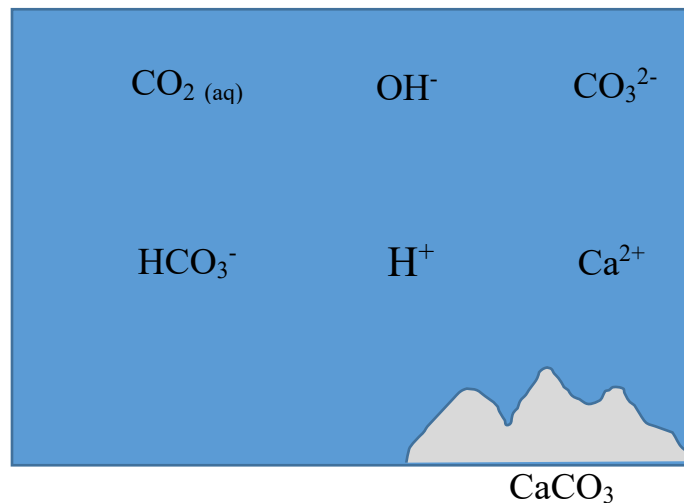
Figure 2.3. Schematic of the Carbonate Equilibrium System

The normal carbonate equilibrium equations are:

Bicarbonate Equation: $CO_2\ (aq) + H_2O \rightleftharpoons HCO_3^-\ (aq) + H^+(aq)$ (2.19)

Carbonate Equation: $HCO_3^-\ (aq) \rightleftharpoons CO_3^{2-}\ (aq) + H^+(aq)$ (2.20)

Calcium Carbonate Equation: $Ca^{2+}(aq) + CO_3^{2-}\ (aq) \rightleftharpoons CaCO_3\ (s)$ (2.21)

Water Dissolution: $H_2O \rightleftharpoons H^+(aq) + OH^-(aq)$ (2.22)
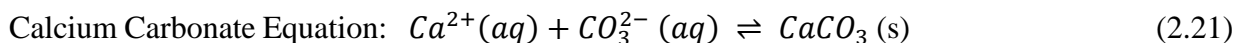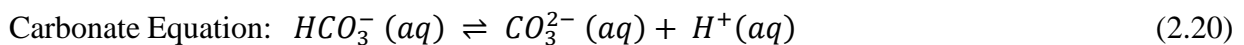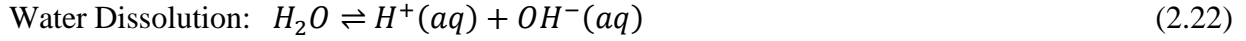
The second stage of the process is that the scale inhibitor, SI, can be considered as a weak polyacid (H_nA, where n is the number of dissociating H^+ ions). Any poly acid, H_nA, depending on the solution pH, becomes dissociated, as follows:
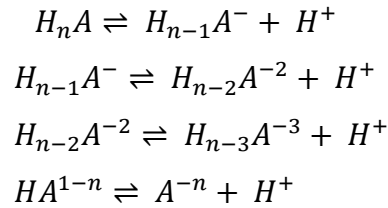
$$H_nA \rightleftharpoons H_{n-1}A^- + H^+$$
$$H_{n-1}A^- \rightleftharpoons H_{n-2}A^{-2} + H^+$$
$$H_{n-2}A^{-2} \rightleftharpoons H_{n-3}A^{-3} + H^+$$
$$HA^{1-n} \rightleftharpoons A^{-n} + H^+$$

Therefore, at very low (acidic) pH, the equilibrium is to the left and the molecule is more associated as H_nA, and at higher pH it is more dissociated, forming the anionic form of the SI.

At the third stage of this process, the dissociated SI interacts with divalent cations (particularly Ca^{2+}) and SI-M^{2+} complexes are formed.

$$SI + nCa^{2+} \rightleftharpoons SI\_Ca_n$$
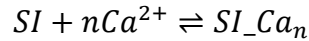
Where the stoichiometry (n) depends on the state of dissociation of the SI (weak poly acid). The SI is much more likely to complex with Ca^{2+} to form a SI/Ca complex in its dissociated form (i.e. at higher pH values) and less likely to form complexes at lower pH values. Also, complexation of the SI is favoured at higher concentrations of calcium, $[Ca^{2+}]$.

According to this discussion above, the likely mechanisms occurring here are shown schematically in Figure 2.4.
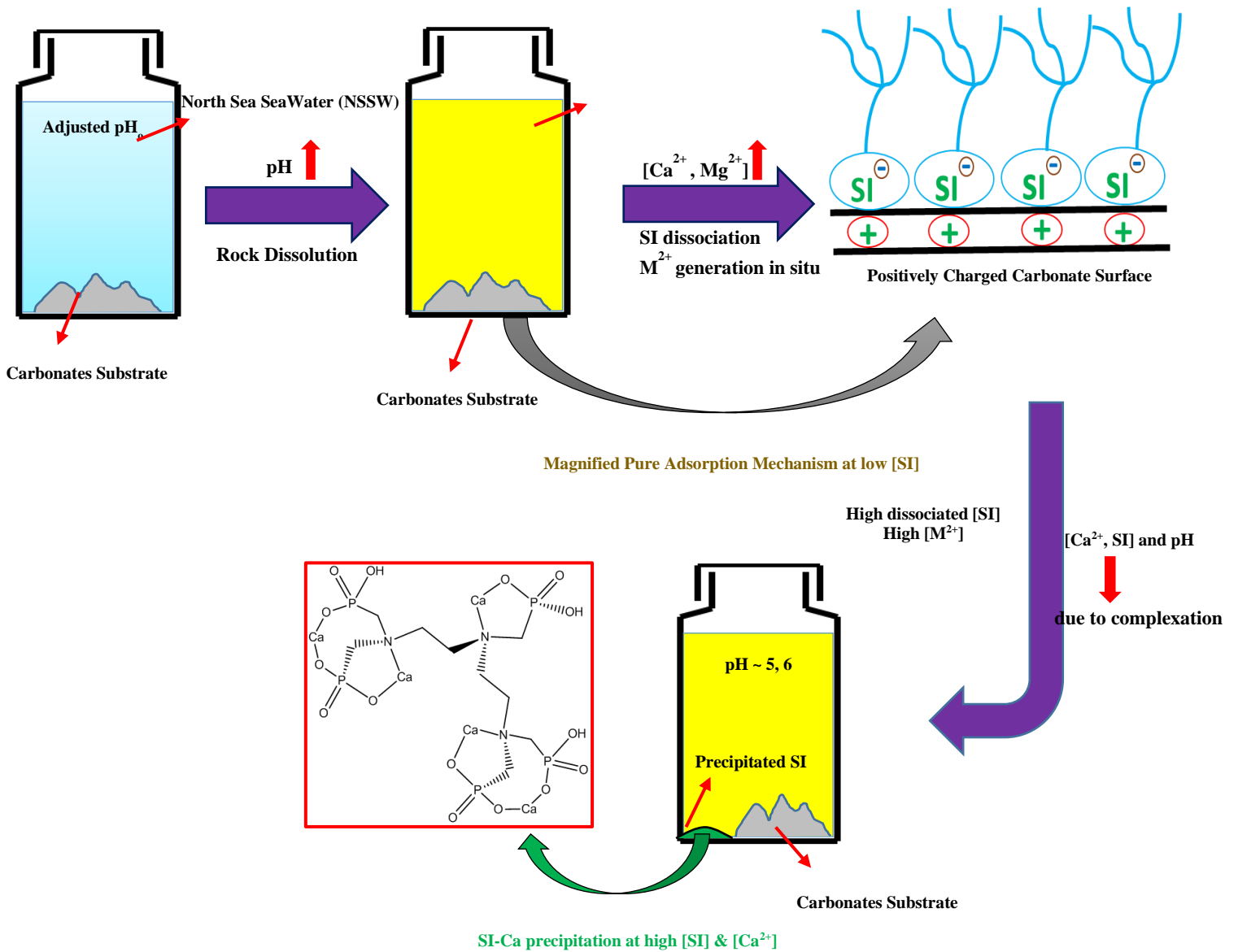
Figure 2.4. Schematic of Proposed Mechanisms of Phosphonate Scale Inhibitors Adsorption on Carbonate Rocks

2.4.   Summary and Conclusions

There are two main mechanisms of retention for scale inhibitors in porous media; adsorption and precipitation, the former mechanism is governed by electrostatic interaction between scale inhibitor and minerals of reservoir rock. However, the inhibitor interacts with divalent cations, mainly Ca^{2+},

and the inhibitor is precipitated out. Adsorption occurs at low scale inhibitor concentration, whereas precipitation in predominant at higher scale inhibitor concentration. Generally speaking, scale inhibitor squeeze treatment lifetime increases as precipitation of scale inhibitor with calcium forms. In sandstone reservoir, simple adsorption is main retention mechanism of scale inhibitors as there is no reaction between reservoir rock and the inhibitor to generate divalent cations through rock dissolution. However, in carbonate reservoirs, scale inhibitor is retained through precipitation due to high level of geochemical reactivity of reservoir rock and consequently greater concentration of divalent cations through rock dissolution. The scale inhibitor/sandstone system has been well defined and modelled by Kahrwad et al.[10] and mentioned in this chapter, whilst the scale inhibitor/carbonate system has not been well understood. This research work is an important steppingstone to know what is going on during squeezing the scale inhibitor near wellbore. We found that the entire system is defined through the three parts of the equilibrium system

(i) the dissociation of SI as a weak polyacid (H_nA) to form dissociated species, such as $H_{n-m}A^{m-}$ right up to A^{n-} at very high pH values; (ii) these dissociated SI species, which are very strong chelating agents, then bind with Ca^{2+}(and/or Mg^{2+})ions to form SI/Ca complexes, which are known to be sparingly soluble;(iii) the above reactions are coupled to the carbonate system, because the lower pH solution conditions and the chelating power of the dissociated scale inhibitor cause the carbonate equilibrium to change.

To develop a model of the entire SI / Carbonate/ solution Ca^{2+}/Mg^{2+} system, we must combine all 3 parts of the process above into a complex set of equations and solve these numerically.

An outline of how this is done is presented in the paper Silva et al[94]. The full equation set has also been developed by Sorbie (unpublished work, 2017). An attempt has been made in this thesis in Appendix 2.1 of this chapter to capture the outline of Sorbie's method, since it is not available elsewhere.

2.5. Appendix 2.1

Summary of Approach to the Coupled SI/Carbonate/Ca^{2+}-Mg^{2+} System by Sorbie (2017)

It was noted in the body of this chapter that the 3 parts of the coupled SI/Carbonate/Ca^{2+}-Mg^{2+} system must be combined mathematically and then be solved. In fact, the approach is best carried out by dealing with the systems in the following order:

1. The Carbonate system in aqueous solution;
2. The SI system, treated as a weak poly acid, H_nA;
3. The binding between the dissociated SI species (anion $H_mA^{(n-m)-}$) and the Ca^{2+}- Mg^{2+}.

The Carbonate System in the Aqueous Phase

The aqueous carbonate equilibrium system is defined by the following equilibrium equations:

Bicarbonate Equation:

$$CO_2 \text{ (aq)} + H_2O \rightleftharpoons HCO_3^- \text{ (aq)} + H^+\text{(aq)} ; \qquad K_{a1} = \frac{[HCO_3^-].[H^+]}{[CO_2]}$$

Carbonate Equation:

$$HCO_3^- \text{ (aq)} \rightleftharpoons CO_3^{2-} \text{ (aq)} + H^+\text{(aq)} ; \qquad K_{a2} = \frac{[CO_3^{2-}].[H^+]}{[HCO_3^-]}$$

Calcium Carbonate Equation:

$$Ca^{2+}\text{(aq)} + CO_3^{2-} \text{ (aq)} \rightleftharpoons CaCO_3 \text{ (s)}; \qquad K_{sp} = [CO_3^{2-}].[Ca^{2+}]$$
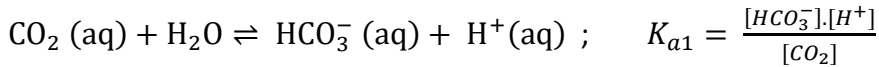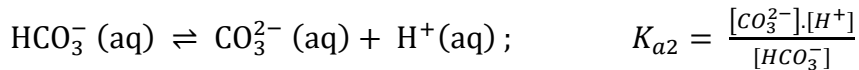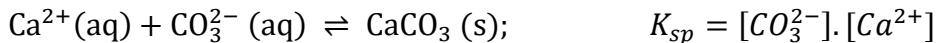
Water Dissociation:

$$H_2O \rightleftharpoons H^+\text{(aq)} + OH^-\text{(aq)} ; \qquad K_w = [H^+].[OH^-]$$

To simplify the equations above, we use the following notation for the corresponding species:

$$CO_2 \text{ (aq)} + H_2O \rightleftharpoons HCO_3^- \text{ (aq)} + H^+\text{(aq)} ; \quad K_{a1} = \frac{y_2.z}{y_1} \tag{2.23}$$

$$y_1 \qquad\qquad\qquad y_2 \qquad\qquad z$$

$$HCO_3^- \text{ (aq)} \rightleftharpoons CO_3^{2-} \text{ (aq)} + H^+\text{(aq)} ; \qquad K_{a2} = \frac{y_3.z}{y_2} \tag{2.24}$$

$$y_2 \qquad\qquad y_3 \qquad\quad z$$

$$Ca^{2+}\text{(aq)} + CO_3^{2-} \text{ (aq)} \rightleftharpoons CaCO_3 \text{ (s)} ; \qquad K_{sp} = m.\, y_3 \tag{2.25}$$

$$m \qquad\quad y_3 \qquad\qquad y_4$$

$$H_2O \rightleftharpoons H^+\text{(aq)} + OH^-\text{(aq)} ; \qquad\qquad K_w = z.\, w \tag{2.26}$$
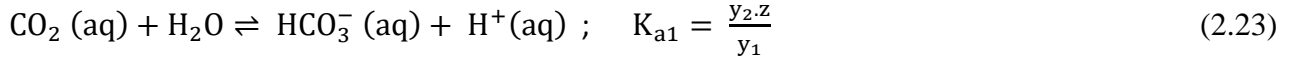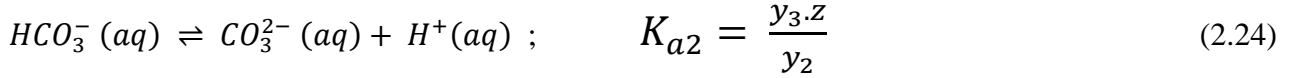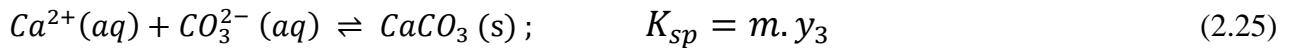
$$z \qquad\quad w$$

It is not possible to solve 4 equations (2.23, 2.24, 2.25, 2.26, and 2.27) in 7 unknowns $(y_1, y_2, y_3, y_4, m, z, w)$, and so we need 3 more equations as follows in order to solve these equations: 2 mass balance equations (for total calcium and carbon) and 1 charge balance equation.

Total C = $[CO_2] + [HCO_3^-] + [CO_3^{2-}] + [CaCO_3]$; $C_T = y_1 + y_2 + y_3 + y_4$

Total Ca = $[Ca^{2+}] + [CaCO_3]$; $Ca_T = m + y_4$

Total Charge = $-y_2 - 2.\, y_3 - w + z + 2.m$

Then:

2 mass balances: $C_T = y_1 + y_2 + y_3 + y_4$; $Ca_T = m + y_4$

1 charge balance: $Ch_T = -y_2 - 2.\, y_3 - w + z + 2.m$

Now, we have 7 equations and 7 unknowns and therefore they are in principle solvable. The equations are a set of non-linear equations. This system has a unique solution. "Equation reduction" can be done down to 1equation as follows:

$$K_{a1} = \frac{y_2 \cdot z}{y_1} \Rightarrow y_2 = \left(\frac{K_{a1}}{z}\right) \cdot y_1 \tag{2.27}$$

$$K_{a2} = \frac{y_3 \cdot z}{y_2} \Rightarrow y_3 = \left(\frac{K_{a2}}{z}\right) \cdot y_2 = \left(\frac{K_{a1} \cdot K_{a2}}{z^2}\right) \cdot y_1 \tag{2.28}$$

$$K_{SP} = m. y_3 = m. \left(\frac{K_{a1} \cdot K_{a2}}{z^2}\right) \cdot y_1 \Rightarrow y_1 = \frac{K_{SP}}{m.\left(\frac{K_{a1} \cdot K_{a2}}{z^2}\right)} \tag{2.29}$$

If we use these results in mass balance of Carbon, we obtain the equation below:

$$M_C = y_1 + y_2 + y_3 + y_4 = y_1 + \left(\frac{K_{a1}}{z}\right) \cdot y_1 + \left(\frac{K_{a1} \cdot K_{a2}}{z^2}\right) \cdot y_1 + y_4 \Rightarrow$$

$$M_C = y_1 . \left[\ 1 + \left(\frac{K_{a1}}{z}\right) + \left(\frac{K_{a1} \cdot K_{a2}}{z^2}\right)\ \right] + y_4 \Rightarrow$$

$$y_4 = M_C - y_1 . \left[\ 1 + \left(\frac{K_{a1}}{z}\right) + \left(\frac{K_{a1} \cdot K_{a2}}{z^2}\right)\ \right] \tag{2.30}$$

On the other hand, if we substitute Eq. (2.29) in Eq. (2.30), we have new equation as follows:

$$y_4 = M_C - \left[\ 1 + \left(\frac{K_{a1}}{z}\right) + \left(\frac{K_{a1} \cdot K_{a2}}{z^2}\right)\ \right] . \frac{K_{SP}}{m.\left(\frac{K_{a1} \cdot K_{a2}}{z^2}\right)} \tag{2.31}$$

or

$$y_4 (m, z) = M_C - \left[\ 1 + \left(\frac{K_{a1}}{z}\right) + \left(\frac{K_{a1} \cdot K_{a2}}{z^2}\right)\ \right] . \frac{K_{SP}}{m.\left(\frac{K_{a1} \cdot K_{a2}}{z^2}\right)} \tag{2.32}$$

Eq. (2.32) above is the key result from the carbonate system for $y_4 = [CaCO_3]$.

The Dissociation of the SI Considered as a Weak Poly Acid, H$_n$A

The second stage of the process of analysing the SI/Carbonate/Ca^{2+}-Mg^{2+} system is to consider the SI dissociation. The SIs is treated as a weak poly-acid of formula, H$_n$A, where the n is the number of H$^+$ ions that may dissociate according to the solution pH as shown below:

The first dissociation reaction is as follows:

$$H_nA\ (aq) \rightleftharpoons H_{n-1}A^-(aq) + H^+(aq)\ ; \qquad\qquad K_1 = \frac{x_2.z}{x_1}$$

$$x_1 \qquad\qquad x_2 \qquad\qquad z$$
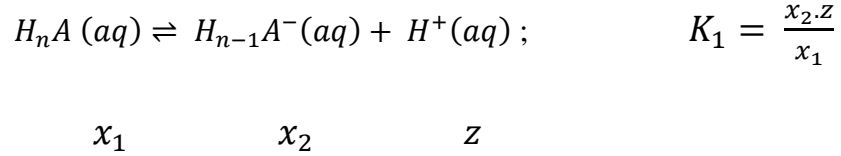
Second dissociation reaction: $H_{n-1}A^-(aq) \rightleftharpoons H_{n-2}A^{2-}(aq) + H^+(aq)\ ; \quad K_2 = \frac{x_3.z}{x_2}$

$$x_2 \qquad\qquad x_3 \qquad\qquad z$$
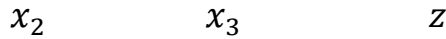
Third dissociation reaction: $H_{n-2}A^-(aq) \rightleftharpoons H_{n-3}A^{3-}(aq) + H^+(aq);\qquad K_3 = \frac{x_4.z}{x_3}$

$$x_3 \qquad\qquad x_4 \qquad\qquad z$$
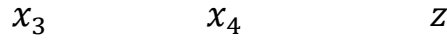
etc.. Until the final equilibrium: $HA^{(1-n)}\ (aq) \rightleftharpoons A^{-n}\ (aq) + H^+(aq)\ ; \qquad K_n = \frac{x_{n+1}.z}{x_n}$

$$x_n \qquad\qquad x_{n+1} \qquad z$$
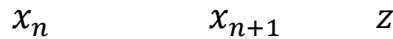
Here, we have n equations and (n+1) unknowns and thus we require another equation which is the mass balance for the A (SI) as follows:

$$M_A = x_1 + x_2 + x_3 + \cdots + x_{n+1} \tag{2.33}$$

If Eq. 2.33 is written in terms of x_1 , the expression above will be as follows:

$$x_2 = x_1\frac{K_1}{z}\ ; x_3 = x_2\frac{K_2}{z} = x_1.\left(\frac{K_1K_2}{z^2}\right)\ ; x_4 = x_3\frac{K_3}{z} = x_1.\left(\frac{K_1K_2K_3}{z^3}\right)\ \text{etc..}$$

and hence,

$$M_A = x_1 + x_1\frac{K_1}{z} + x_1.\left(\frac{K_1K_2}{z^2}\right) + x_1.\left(\frac{K_1K_2K_3}{z^3}\right) + \cdots + x_1.\left(\frac{K_1K_2...K_n}{z^n}\right)$$

or

$$M_A = x_1 \left(1 + \left(\frac{K_1}{z}\right) + \left(\frac{K_1 K_2}{z^2}\right) + \left(\frac{K_1 K_2 K_3}{z^3}\right) + \cdots + \left(\frac{K_1 K_2 \ldots K_n}{z^n}\right) \right) = x_1 . G_1(z)$$

$$\Rightarrow x_1 = \left(\frac{M_A}{G_1(z)}\right) \tag{2.34}$$

This result implies that if we know $z = [H^+]$ and M_A, then we can find all the SI dissociation species concentrations, using the results above.

Binding of the SI (dissociated H_nA) to Ca^{2+} and Mg^{2+}

The final stage as discussed above is Ca and Mg binding with the various dissociated SI species. In this part, the SI is treated as a dissociated phosphonate, for example it may be DETPMP = $H_{10}A$, where n = 10; i.e. the penta phosphonate DETPMP has 10 H^+ ions which may dissociate, and the dissociation constants, K_1, K_2, K_3, etc ... K_{10}, are known experimentally.

The charged components in the dissociated SI are ………………. binds with:

x_1 − Not involved (neutral- fully protonated) → $H_n A$ →   0 x Ca^{2+}

x_2 − 1 negative charge   → $H_{n-1}A^-$ →   0.5 x Ca^{2+}

x_3 − 2 negative charge   → $H_{n-2}A^{-2}$ →   1 x Ca^{2+}

x_4 − 3 negative charge   → $H_{n-3}A^{-3}$ →   1.5 x Ca^{2+}

etc…..

x_{n+1} − n negative charge   → A^{-n} →   (n/2)x Ca^{2+}

In the case of DETPMP, then the fully dissociated SI would form A_Ca_5 (since n = 10).

So, the corresponding binding equations are as follows:

First, the Ca/Mg – scale inhibitor (SI) binding equations are considered, as flows.

The Ca-SI Binding Reactions are …

$$Ca^{2+} + \left(\tfrac{2}{1}\right) H_{n-1}A^- \rightleftharpoons Ca^{2+} - [H_{n-1}A^-]_{\left(\tfrac{2}{1}\right)} \qquad\qquad K_{B1} = \left(\dfrac{v_2}{m_1 \cdot \left(\tfrac{2}{1}x_2\right)}\right)$$

$\quad m_1 \qquad x_2 \qquad\qquad v_2$

$$Ca^{2+} + \left(\tfrac{2}{2}\right) H_{n-2}A^{-2} \rightleftharpoons Ca^{2+} - [H_{n-2}A^{2-}]_{\left(\tfrac{2}{2}\right)} \qquad\qquad K_{B1} = \left(\dfrac{v_3}{m_1 \cdot \left(\tfrac{2}{2}x_3\right)}\right)$$

$\quad m_1 \qquad x_3 \qquad\qquad v_3$

$$Ca^{2+} + \left(\tfrac{2}{3}\right) H_{n-3}A^{-3} \rightleftharpoons Ca^{2+} - [H_{n-3}A^{3-}]_{\left(\tfrac{2}{3}\right)} \qquad\qquad K_{B1} = \left(\dfrac{v_4}{m_1 \cdot \left(\tfrac{2}{3}x_4\right)}\right)$$

$\quad m_1 \qquad x_4 \qquad\qquad v_4$

$$Ca^{2+} + \left(\tfrac{2}{n}\right) A^{-n} \rightleftharpoons Ca^{2+} - [A^{n-}]_{\left(\tfrac{2}{n}\right)} \qquad\qquad K_{B1} = \left(\dfrac{v_{n+1}}{m_1 \cdot \left(\tfrac{2}{n}x_{n+1}\right)}\right)$$
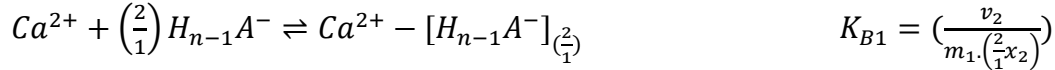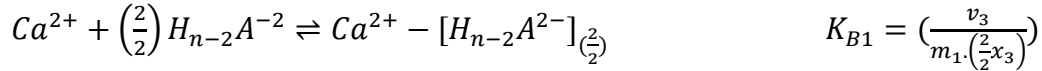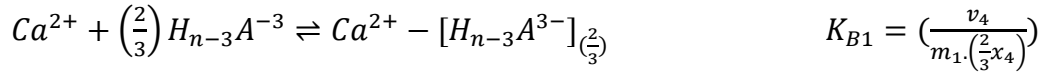
$\quad m_1 \qquad x_{n+1} \qquad\qquad v_{n+1}$

On the other hand, the MASS BALANCE for the A (SI) is …………..

$$M_A = \sum_{i=1}^{n+1} x_i + \sum_{j=2}^{n+1} \frac{2 \cdot v_j}{j-1} \qquad\qquad\qquad (2.35)$$

Likewise, the Mg-SI Binding Reactions are …

$$Mg^{2+} + \left(\tfrac{2}{1}\right) H_{n-1}A^- \rightleftharpoons Mg^{2+} - [H_{n-1}A^-]_{\left(\tfrac{2}{1}\right)} \qquad\qquad K_{B2} = \left(\dfrac{w_2}{m_4 \cdot \left(\tfrac{2}{1}x_2\right)}\right)$$
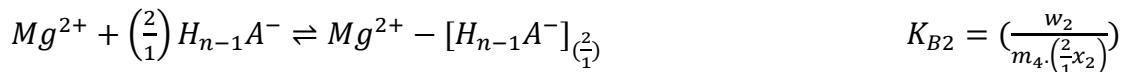
$\quad m_4 \qquad x_2 \qquad\qquad w_2$

$$Mg^{2+} + \left(\frac{2}{2}\right)H_{n-2}A^{-2} \rightleftharpoons Mg^{2+} - [H_{n-2}A^{-2}]_{\left(\frac{2}{2}\right)} \qquad\qquad K_{B2} = \left(\frac{w_3}{m_4 \cdot \left(\frac{2}{2}x_3\right)}\right)$$

$$m_4 \qquad x_3 \qquad\qquad w_3$$

$$Mg^{2+} + \left(\frac{2}{3}\right)H_{n-3}A^{-3} \rightleftharpoons Mg^{2+} - [H_{n-3}A^{-3}]_{\left(\frac{2}{3}\right)} \qquad\qquad K_{B2} = \left(\frac{w_4}{m_4 \cdot \left(\frac{2}{3}x_4\right)}\right)$$

$$m_4 \qquad x_4 \qquad\qquad w_4$$

$$Mg^{2+} + \left(\frac{2}{n}\right)A^{-n} \rightleftharpoons Mg^{2+} - [A^{n-}]_{\left(\frac{2}{n}\right)} \qquad\qquad K_{B2} = \left(\frac{w_{n+1}}{m_4 \cdot \left(\frac{2}{n}x_{n+1}\right)}\right)$$

$$m_4 \qquad x_{n+1} \qquad\qquad w_{n+1}$$

Following the equation reductions that arise from the structure of Ca/Mg_SI binding equations as follows.

First for Ca^{2+} :

$$K_{B1} = \left(\frac{v_2}{m_1 \cdot \left(\frac{2}{1}x_2\right)}\right)$$

$$\left(\frac{v_2}{m_1 \cdot \left(\frac{2}{1}x_2\right)}\right) = \left(\frac{v_3}{m_1 \cdot \left(\frac{2}{2}x_3\right)}\right)$$

$$K_{B1} = \left(\frac{v_3}{m_1 \cdot \left(\frac{2}{2}x_3\right)}\right)$$

All these expressions are the same (K_{B1}) therefore...

$$K_{B1} = \left(\frac{v_2}{m_1 \cdot \left(\frac{2}{1}x_2\right)}\right) = \left(\frac{v_3}{m_1 \cdot \left(\frac{2}{2}x_3\right)}\right) \quad \textbf{Implies =>} \quad v_3 = \left(\frac{v_2 \cdot x_3}{2 \cdot x_2}\right) \qquad\qquad (2.36)$$

On the other hand, from the SI dissociation equations mentioned above that….

$$x_3 = x_2 \frac{K_2}{z} = x_1 . \left(\frac{K_1 K_2}{z^2}\right) \quad \text{Or} \quad \frac{x_3}{x_2} = \frac{K_2}{z} \tag{2.37}$$

If the equation (4.37) is substituted in (4.36)…….

$$v_3 = \left(\frac{K_2}{2.z}\right) v_2$$

If the pattern is noted, the corresponding equations are as follows:

$$v_3 = \frac{1}{2} \left(\frac{K_2}{z}\right) v_2$$

$$v_4 = \frac{1}{3} \left(\frac{K_2 . K_3}{z^2}\right) v_2$$

$$v_5 = \frac{1}{4} \left(\frac{K_2 . K_3 . K_4}{z^3}\right) v_2$$

etc.…

$$v_{n+1} = \frac{1}{n} \left(\frac{K_2 . K_3 . K_n}{z^{n-1}}\right) v_2$$

On the other hand,

$$v_2 = 2\, m_1 . x_2 . K_{B1} = 2 m_1 . (x_1 \frac{K_1}{z}) . K_{B1} = 2 m_1 . K_{B1} . \left(\frac{K_1}{z}\right) . x_1$$

All these expressions are the same (K_{B1}) therefore….

$$v_2 = \frac{2}{1}\, m_1 . K_{B1} . \left(\frac{K_1}{z}\right) . x_1$$

$$v_3 = \left(\frac{2}{2}\right) m_1 . K_{B1} . \left(\frac{K_1 . K_2}{z^2}\right) . x_1$$

$$v_4 = \left(\frac{2}{3}\right) m_1 . K_{B1} . \left(\frac{K_1 . K_2 . K_3}{z^3}\right) . x_1$$

etc…..

$$v_{n+1} = \left(\frac{2}{n}\right) m_1.K_{B1}.\left(\frac{K_1.K_2.K_3….K_n}{z^n}\right).x_1 \qquad (2.38)$$

So, for mass balance of "A" (SI) in the Ca_SI complex, M_{A_Ca}

$$M_{A\_Ca} = \sum_{j=2}^{n+1} \frac{2.v_j}{j-1} = \left(\frac{2.v_2}{1} + \frac{2.v_3}{2} + \frac{2.v_4}{3} + \cdots + \frac{2.v_{n+1}}{n}\right) \qquad (2.39)$$

If we substitute the corresponding expressions above in equation (4.39)…………

$$M_{A\_Ca} = \frac{2}{1}.\frac{2}{1} m_1.K_{B1}.\left(\frac{K_1}{z}\right).x_1 + \frac{2}{2}.\frac{2}{2} m_1.K_{B1}.\left(\frac{K_1.K_2}{z^2}\right).x_1 + \frac{2}{3}.\frac{2}{3} m_1.K_{B1}.\left(\frac{K_1.K_2.K_3}{z^3}\right).x_1 + \cdots +$$
$$\frac{2}{n}.\frac{2}{n} m_1.K_{B1}.\left(\frac{K_1.K_2.K_3….K_n}{z^n}\right).x_1 \qquad (2.40)$$

or

$$M_{A\_Ca} = 4.m_1.K_{B1}.x_1\left[\left(\frac{K_1}{z}\right) + \frac{1}{2^2}\left(\frac{K_1.K_2}{z^2}\right) + \frac{1}{3^2}\left(\frac{K_1.K_2.K_3}{z^3}\right) + \frac{1}{4^2}\left(\frac{K_1.K_2.K_3.K_4}{z^3}\right) + \cdots +$$
$$\frac{1}{n^2}\left(\frac{K_1.K_2.K_3….K_n}{z^n}\right)\right] \qquad (2.41)$$

So the mass balance of SI/Ca^{2+} complex, M_{A_Ca}, can be written as shown below:

$$M_{A\_Ca} = 4.m_1.K_{B1}.x_1.G_2(z) \qquad (2.42)$$

If the same calculations are done for Mg^{2+}, the mass balance of A in the A_Mg complex, M_{A_Mg}:

$$M_{A\_Mg} = \sum_{j=2}^{n+1} \frac{2.w_j}{j-1} = \left(\frac{2.w_2}{1} + \frac{2.w_3}{2} + \frac{2.w_4}{3} + \cdots + \frac{2.w_{n+1}}{n}\right) \qquad (2.43)$$

A similar argument gives:

$$M_{A\_Mg} = \frac{2}{1}.\frac{2}{1} m_4.K_{B2}.\left(\frac{K_1}{z}\right).x_1 + \frac{2}{2}.\frac{2}{2} m_4.K_{B2}.\left(\frac{K_1.K_2}{z^2}\right).x_1 + \frac{2}{3}.\frac{2}{3} m_4.K_{B2}.\left(\frac{K_1.K_2.K_3}{z^3}\right).x_1 + \cdots +$$
$$\frac{2}{n}.\frac{2}{n} m_4.K_{B2}.\left(\frac{K_1.K_2.K_3….K_n}{z^n}\right).x_1 \qquad (2.44)$$

or

$$\text{M}_{A\_Mg} \quad = \quad 4.\,m_4.\,K_{B2}\,.x_1\left[\left(\frac{K_1}{z}\right) + \frac{1}{2^2}\left(\frac{K_1.K_2}{z^2}\right) + \frac{1}{3^2}\left(\frac{K_1.K_2.K_3}{z^3}\right) + \frac{1}{4^2}\left(\frac{K_1.K_2.K_3.K_4}{z^3}\right) + \cdots + \right.$$
$$\left. \frac{1}{n^2}\left(\frac{K_1.K_2.K_3\ldots K_n}{z^n}\right)\right] \tag{2.45}$$

So, the mass balance of Mg_SI complex, M_{A_Mg}, can be written as shown below:

$$\text{M}_{A\_Mg} = 4.\,m_4.\,K_{B2}\,.x_1\,.G_2(z) \tag{2.46}$$

Thus, mass balance expressions for the A (SI) for ALL of the SI complex:

– free dissociated SI + Ca_SI + Mg_SI

$$M_A = \sum_{i=1}^{n+1} x_i \; + \left(\sum_{j=2}^{n+1}\frac{2.v_j}{j-1} + \sum_{j=2}^{n+1}\frac{2.w_j}{j-1}\right)$$

$$M_{A-free} = x_1\,.G_1(z)$$

$$\text{M}_{A\_Mg} = 4.\,m_4.\,K_{B2}\,.x_1\left[\left(\frac{K_1}{z}\right) + \frac{1}{2^2}\left(\frac{K_1.K_2}{z^2}\right) + \frac{1}{3^2}\left(\frac{K_1.K_2.K_3}{z^3}\right) + \frac{1}{4^2}\left(\frac{K_1.K_2.K_3.K_4}{z^3}\right) + \cdots + \frac{1}{n^2}\left(\frac{K_1.K_2.K_3\ldots K_n}{z^n}\right)\right]$$

$$\text{M}_{A\_Ca} = 4.\,m_1.\,K_{B1}\,.x_1\left[\left(\frac{K_1}{z}\right) + \frac{1}{2^2}\left(\frac{K_1.K_2}{z^2}\right) + \frac{1}{3^2}\left(\frac{K_1.K_2.K_3}{z^3}\right) + \frac{1}{4^2}\left(\frac{K_1.K_2.K_3.K_4}{z^3}\right) + \cdots + \frac{1}{n^2}\left(\frac{K_1.K_2.K_3\ldots K_n}{z^n}\right)\right]$$

or

$$M_A = \sum_{i=1}^{n+1} x_i \; + \left(\sum_{j=2}^{n+1}\frac{2.v_j}{j-1} + \sum_{j=2}^{n+1}\frac{2.w_j}{j-1}\right) = x_1[G_1(z) + (4.\,m_1.\,K_{B1} + 4.\,m_4.\,K_{B2})\,G_2(z)] \tag{2.47}$$

$$G_1(z) = \left(1 + \left(\frac{K_1}{z}\right) + \left(\frac{K_1 K_2}{z^2}\right) + \left(\frac{K_1 K_2 K_3}{z^3}\right) + \cdots + \left(\frac{K_1 K_2 \ldots K_n}{z^n}\right) \right)$$

$$G_2(z) = \left(\left(\frac{K_1}{z}\right) + \frac{1}{2^2}\left(\frac{K_1.K_2}{z^2}\right) + \frac{1}{3^2}\left(\frac{K_1.K_2.K_3}{z^3}\right) + \frac{1}{4^2}\left(\frac{K_1.K_2.K_3.K_4}{z^3}\right) + \cdots + \frac{1}{n^2}\left(\frac{K_1.K_2.K_3....K_n}{z^n}\right) \right)$$

Which we can rearrange as follows; x_1 is a function ONLY of z= [H$^+$], m_1= [Ca^{2+}] and m_4= [Mg^{2+}]

$$x_1\,(z, m_1, m_4) = \frac{M_A}{x_1[G_1(z)+(4.m_1.K_{B1}+4.m_4.K_{B2})\,G_2(z)]}$$
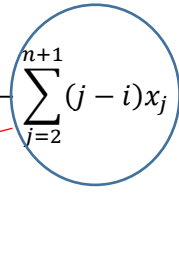
The above expression for x_1 is the key working result (from the mass balance of A, i.e. SI)

We have $y_4(m_1, z)$ and $x_1(z, m_1, m_4)$ BUT we have "used up" some mass balances (M_C and M_A). Now we need to **combine** both systems. By using $y_4(m_1, z)$ and $x_1(z, m_1, m_4)$ in 3 balance equation as shown below:

a) The system charge balance, C$_o$

b) The Calcium mass balance, M$_{Ca}$

c) The Magnesium mass balance, M$_{Mg}$

So, these are three master equations for the total system. We need to consider the equations separately.

a) The system charge balance, C$_o$

$$C_o = [H^+] + 2[Ca^{2+}] + 2[Mg^{2+}] - [HCO_3^-] - 2[CO_3^{2-}] - [OH^-] - \sum_{j=2}^{n+1}(j-i)x_j$$

The dissociated $H_n A$ (SI) species:
$$x_1 = [H_{10}A]$$
$$x_2 = [H_9 A^-]$$

$$x_3 = [H_8A^{-2}]$$

$$x_4 = [H_7A^{-3}]$$

etc……

If we look at the sum first……

$$\sum_{j=2}^{n+1} (j-i)x_j = x_2 + 2x_3 + 3x_4 + \cdots + n.x_n$$

$$= \left(\frac{K_1}{z}\right)x_1 + 2\left(\frac{K_1K_2}{z^2}\right)x_1 + 3\left(\frac{K_1K_2K_3}{z^3}\right) + \cdots + n\left(\frac{K_1K_2K_3 \ldots K_n}{z^n}\right)x_1$$

$$= x_1 \left(\left(\frac{K_1}{z}\right) + 2\left(\frac{K_1K_2}{z^2}\right) + 3\left(\frac{K_1K_2K_3}{z^3}\right) + \cdots + n\left(\frac{K_1K_2K_3 \ldots K_n}{z^n}\right)\right) = x_1 G_4(z)$$

$$\sum_{j=2}^{n+1}(j-i)x_j = x_1 G_4(z) \tag{2.48}$$

If equation (2.45) is replaced in equation (2.48)…….

$$C_o = [H^+] + 2[Ca^{2+}] + 2[Mg^{2+}] - [HCO_3^-] - 2[CO_3^{2-}] - [OH^-] - x_1 G_4(z) \tag{2.49}$$

On the other hand, $x_1 (z, m_1, m_4) = \dfrac{M_A}{x_1[G_1(z)+(4.m_1.K_{B1}+4.m_4.K_{B2})\,G_2(z)]}$

so

$$C_o = [H^+] + 2[Ca^{2+}] + 2[Mg^{2+}] - [HCO_3^-] - 2[CO_3^{2-}] - [OH^-] - x_1 (z, m_1, m_4).G_4(z) \tag{2.50}$$

Now, we eliminate bicarbonate and carbonate terms from equation (2.47) by using carbonate system equation as follows:

$$-[HCO_3^-] - 2[CO_3^{2-}] = -y_2 - 2y_3 = -\left(\frac{K_{a1}}{z}\right)y_1 - 2\left(\frac{K_{a1}.K_{a2}}{z^2}\right)y_1; \quad y_1 = \frac{K_{sp1}}{\left(\frac{K_{a1}.K_{a2}}{z^2}\right).m_1}$$

$$-[HCO_3^-] - 2[CO_3^{2-}] = -y_1\left(\left(\frac{K_{a1}}{z}\right) + 2\left(\frac{K_{a1}.K_{a2}}{z^2}\right)\right)$$

$$-[HCO_3^-] - 2[CO_3^{2-}] = = -\left(\frac{K_{sp1}}{\left(\frac{K_{a1}.K_{a2}}{z^2}\right).m_1}\right)\left(\left(\frac{K_{a1}}{z}\right) + 2\left(\frac{K_{a1}.K_{a2}}{z^2}\right)\right) = f_A(z, m_1)$$

On the other hand, $[OH^-] = \frac{K_w}{z}$
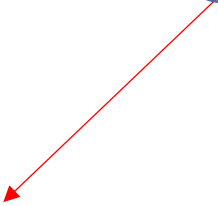
$$C_o = z + 2m_1 + 2m_4 + f_A(z, m_1) - \frac{K_w}{z} - x_1 G_4(z) \tag{2.51}$$

This equation is only a function of $z = [H^+]$, $m_1 = [Ca^{2+}]$ and $m_4 = [Mg^{2+}]$

To use this equation, we define a function F_1 as follows:

$$F_1(z, m_1, m_4) = \left[z + 2m_1 + 2m_4 + f_A(z, m_1) - \frac{K_w}{z} - x_1 G_4(z)\right] - C_o \tag{2.52}$$

b) The Calcium mass balance, M_{Ca}

$$M_{Ca} = [Ca^{2+}] + [CaCO_3] + \sum_{J=2}^{n+1} v_j$$

80

The Ca_A complexed (SI) species:

$$v_2 = [Ca\_(H_9A^-)_{2/_1}]$$

$$v_3 = [Ca\_(H_8A^{-2})_{2/_2}]$$

$$v_4 = [Ca\_(H_7A^{-3})_{2/_3}]$$

$$v_5 = [Ca\_(H_6A^{-4})_{2/_4}]$$

etc....

So, the mass balance of Ca_SI complex, M_{A_Ca}

$$M_{A\_Ca} = \sum_{j=2}^{n+1} v_j = (v_2 + v_3 + v_4 + \cdots + v_{n+1})$$

$$M_{A\_Ca} = \frac{2}{1} m_1.K_{B1}.\left(\frac{K_1}{z}\right).x_1 + \frac{2}{2} m_1.K_{B1}.\left(\frac{K_1.K_2}{z^2}\right).x_1 + \frac{2}{3} \qquad m_1.K_{B1}.\left(\frac{K_1.K_2.K_3}{z^3}\right).x_1 + \cdots +$$
$$\frac{2}{n} m_1.K_{B1}.\left(\frac{K_1.K_2.K_3....K_n}{z^n}\right).x_1$$

$$M_{A\_Ca} = 2m_1.K_{B1}.x_1\left(\left(\frac{K_1}{z}\right) + \frac{1}{2}\left(\frac{K_1.K_2}{z^2}\right) + \frac{1}{3}\left(\frac{K_1.K_2.K_3}{z^3}\right) + \frac{1}{n}\left(\frac{K_1.K_2.K_3....K_n}{z^n}\right)\right)$$

$$M_{A\_Ca} = 2m_1.K_{B1}.x_1.G_3(z) \tag{2.53}$$

$$M_{Ca} = [Ca^{2+}] + [CaCO_3] + 2m_1.K_{B1}.x_1.G_3(z)$$
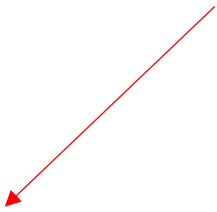
$$M_{Ca} = m_1 + y_4(z, m_1) + 2m_1.K_{B1}.x_1(z, m_1, m_4).G_3(z) \qquad (2.54)$$

This equation is also a function of $z = [H^+]$, $m_1 = [Ca^{2+}]$ and $m_4 = [Mg^{2+}]$.

Again, to use this equation, we define a function F_2 as follows:

$$F_2(z, m_1, m_4) = [m_1 + y_4(z, m_1) + 2m_1.K_{B1}.x_1(z, m_1, m_4).G_3(z)] - M_{Ca} \qquad (2.55)$$

c) The Magnesium mass balance, M_{Mg}

$$M_{Ca} = [Mg^{2+}] + \sum_{J=2}^{n+1} w_j$$

The Mg_A complexed (SI) species:

$$w_2 = [Mg\_(H_9A^-)_{2/1}]$$

$$w_3 = [Mg\_(H_8A^{-2})_{2/2}]$$

$$w_4 = [Mg\_(H_7A^{-3})_{2/3}]$$

$$w_5 = [Mg\_(H_6A^{-4})_{2/4}]$$

etc.... So, the mass balance of Mg_SI complex, M_{A_Mg}

$$M_{A\_Mg} = \sum_{j=2}^{n+1} w_j = (w_2 + w_3 + w_4 + \cdots + w_{n+1})$$

$$M_{A\_Mg} = \frac{2}{1}\, m_4 . K_{B2} . \left(\frac{K_1}{z}\right) . x_1 + \frac{2}{2}\, m_4 . K_{B2} . \left(\frac{K_1 . K_2}{z^2}\right) . x_1 + \frac{2}{3} \qquad m_4 . K_{B2} . \left(\frac{K_1 . K_2 . K_3}{z^3}\right) . x_1 + \cdots +$$

$$\frac{2}{n}\, m_4 . K_{B2} . \left(\frac{K_1 . K_2 . K_3 \ldots K_n}{z^n}\right) . x_1$$

$$M_{A\_Mg} = 2m_4 . K_{B2} . x_1 \left(\left(\frac{K_1}{z}\right) + \frac{1}{2}\left(\frac{K_1 . K_2}{z^2}\right) + \frac{1}{3}\left(\frac{K_1 . K_2 . K_3}{z^3}\right) + \frac{1}{n}\left(\frac{K_1 . K_2 . K_3 \ldots K_n}{z^n}\right)\right)$$

$$M_{A\_Mg} = 2m_4 . K_{B2} . x_1 . G_3(z) \tag{2.56}$$

$$M_{Mg} = [Mg^{2+}] + 2m_4 . K_{B2} . x_1 . G_3(z)$$

$$M_{Mg} = m_4 + 2m_4 . K_{B2} . x_1(z, m_1, m_4) . G_3(z) \tag{2.57}$$

Again, this equation is also a function of $z = [H^+]$, $m_1 = [Ca^{2+}]$ and $m_4 = [Mg^{2+}]$.

Again define the following Working equation:

$$F_3(z, m_1, m_4) = [m_4 + 2m_4 . K_{B2} . x_1(z, m_1, m_4) . G_3(z)] - M_{Mg} \tag{2.58}$$

Summary of the Equation Set for the SI/Carbonate/ Ca²⁺- Mg²⁺ System

In summary, all 3 equations shown below are ONLY functions of $z = [H^+]$, $m_1 = [Ca^{2+}]$ and $m_4 = [Mg^{2+}]$.

$$F_1(z, m_1, m_4) = \left[z + 2m_1 + 2m_4 + f_A(z, m_1) - \frac{K_w}{z} - x_1 G_4(z) \right] - C_o$$

$$F_2(z, m_1, m_4) = [m_1 + y_4(z, m_1) + 2m_1.K_{B1}.x_1(z, m_1, m_4).G_3(z)] - M_{Ca}$$

$$F_3(z, m_1, m_4) = [m_4 + 2m_4.K_{B2}.x_1(z, m_1, m_4).G_3(z)] - M_{Mg}$$

The various ancillary functions (denoted G_1 *to* G_4) required to calculate F_1, F_2 and F_3 mentioned above are summarized below:

$$x_1 (z, m_1, m_4) = \frac{M_A}{x_1[G_1(z)+(4.m_1.K_{B1}+4.m_4.K_{B2})\,G_2(z)]} \qquad \text{From the H}_n\text{A (SI) dissociation \& Ca/Mg Binding}$$

$$y_4(z, m_1) = M_C - [1 + (\tfrac{K_{a1}}{z}) + (\tfrac{K_{a1}.K_{a2}}{z^2})].\frac{K_{sp}}{m_1.(\frac{K_{a1}.K_{a2}}{z^2})} = M_C + f_A(z, m_1) \qquad \text{From the Carbonate System}$$

$$G_1(z) = \left(1 + \left(\frac{K_1}{z}\right) + \left(\frac{K_1 K_2}{z^2}\right) + \left(\frac{K_1 K_2 K_3}{z^3}\right) + \cdots + \left(\frac{K_1 K_2 \dots K_n}{z^n}\right) \right)$$

$$G_2(z) = \left(\left(\frac{K_1}{z}\right) + \frac{1}{2^2}\left(\frac{K_1.K_2}{z^2}\right) + \frac{1}{3^2}\left(\frac{K_1.K_2.K_3}{z^3}\right) + \frac{1}{4^2}\left(\frac{K_1.K_2.K_3.K_4}{z^3}\right) + \cdots + \frac{1}{n^2}\left(\frac{K_1.K_2.K_3\dots.K_n}{z^n}\right)\right)$$

$$G_3(z) = \left(\left(\frac{K_1}{z}\right) + \frac{1}{2}\left(\frac{K_1.K_2}{z^2}\right) + \frac{1}{3}\left(\frac{K_1.K_2.K_3}{z^3}\right) + \frac{1}{n}\left(\frac{K_1.K_2.K_3\dots.K_n}{z^n}\right)\right)$$

$$G_4(z) = \left(\left(\frac{K_1}{z}\right) + 2\left(\frac{K_1 K_2}{z^2}\right) + 3\left(\frac{K_1 K_2 K_3}{z^3}\right) + \cdots + n\left(\frac{K_1 K_2 K_3 \dots K_n}{z^n}\right)\right)$$

To solve these three equations which are functions of $z= [H^+]$, $m_1 = [Ca^{2+}]$ and $m_4= [Mg^{2+}]$:

$$\begin{cases} F_1(z, m_1, m_4) = 0 \\ F_2(z, m_1, m_4) = 0 \\ F_3(z, m_1, m_4) = 0 \end{cases}$$

Then Newton-Raphson method should be used. i.e. $X^{(v+1)} = x^v - H^{-1}.F^v$

The algorithm is as follows:

First Guess $\rightarrow X^v = \begin{pmatrix} z^v \\ m_1^v \\ m_2^v \end{pmatrix} = \begin{pmatrix} [H^+]^v \\ [Ca^{2+}]^v \\ [Mg^{2+}]^v \end{pmatrix}$

(Iteration counter, with first guess $v = 0$)

→ **Step A – the start of the iterations**

Now calculate vector F^v for our current iteration v ➔ $F^v = \begin{pmatrix} F_1(z^v, m_1^v, m_4^v) \\ F_2(z^v, m_1^v, m_4^v) \\ F_3(z^v, m_1^v, m_4^v) \end{pmatrix}$

Note that, if by chance $F^v = 0$ (i.e $F_1 = F_2 = F_3 = 0$) the system of equations has converged and the *z, m₁* and *m₄* values chosen would be exactly correct (rarely the case for a first guess).

Next calculate the following matrix H (called the Hessian matrix):

Calculate ➔ $H = \begin{pmatrix} \left(\frac{\partial F_1}{\partial z}\right) & \left(\frac{\partial F_1}{\partial m_1}\right) & \left(\frac{\partial F_1}{\partial m_4}\right) \\ \left(\frac{\partial F_2}{\partial z}\right) & \left(\frac{\partial F_2}{\partial m_1}\right) & \left(\frac{\partial F_2}{\partial m_4}\right) \\ \left(\frac{\partial F_3}{\partial z}\right) & \left(\frac{\partial F_3}{\partial m_1}\right) & \left(\frac{\partial F_3}{\partial m_4}\right) \end{pmatrix}$ and calculate the inverse of this H matrix, i.e.

H^{-1} where $H.H^{-1} = \begin{bmatrix} 1 & 0 & 0 \\ 0 & 1 & 0 \\ 0 & 0 & 1 \end{bmatrix}$

Then update the guess from iteration v to the next iteration $v + 1$ as follows:

$$X^{(v+1)} = X^v - H^{-1}.F^v$$

If $XX^{(v+1)} = x^v$ the iteration is over, however, you need to guess another amount until two guesses become closer.

3. CHAPTER 3: EXPERIMENTAL METHODOLOGY

3.1. Objective

The objective of this research was to investigate and identify the most important mechanisms governing the retention of scale inhibitors (DETPMP, PPCA, PFC, VS-Co and PAPE) on calcite, dolomite and limestone mineral substrates. A range of apparent adsorption/compatibility experiments (Γ_{app}) were performed and the apparent adsorption, Γ_{app}, vs. C_f, the final scale inhibitor concentration was plotted. These pots identified whether the retention mechanism was pure adsorption or coupled adsorption/precipitation through the use of two mass/volume (m/V) ratios of substrate/test volume, as explained in Chapter 2.

During these experiments, it was essential to analyse the ion concentrations of phosphorous (P) (for DETPMP, PPCA, PFC and PAPE using SI standards), calcium (Ca^{2+}), magnesium (Mg^{2+}), lithium (Li^+) and other related cations in the solution prior to and after the experiment, i.e. initial and final concentrations. These were analysed using Inductively Coupled Plasma - Optical Emission Spectroscopy (ICP-OES).The analysis of the VS-Co SI was different, as it does not contain any 'ICP-able' phosphorus in its structure, hence the wet chemical method, matrix-matched easy hyamine was used[95]. Any difference between the initial and final ion concentrations denotes whether any coupled adsorption/precipitation (Γ/Π) has taken place[10], as two different (m/V) ratios of test fluid to mineral substrate were investigated. For the compatibility tests, if any loss in SI concentration was measured and cloudiness was observed in the test solution then this was related to precipitation occurring. The SI/Ca precipitates were then studied using Environmental Scanning Electron Microscopy/ Energy Dispersive X-ray (ESEM/EDX) and Particle Size Analysis (PSA). These techniques will be described later.

3.2. Static Compatibility and Coupled Adsorption/Precipitation Experiments

3.2.1. Experimental Procedure

Static adsorption/compatibility tests were carried out over a 24-hour period, at a range of temperatures (60-95ºC) and pH values (pH_0 2, 4, 6) in a matrix of synthetic North Sea Sea Water (NSSW). The scale inhibitors were dissolved in filtered (0.45µm) NSSW at a range of concentrations (0 – 4000ppm active; VS-Co to 10,000ppm) before being individually pH adjusted to the appropriate test pH value, using dilute solutions of hydrochloride acid and sodium

hydroxide. A fixed volume of 40ml (0.040L) was then measured out and poured into its test bottle. For the static adsorption tests, the experiments were conducted using different masses of calcite, dolomite and limestone (m = 5g and 10g) at a fixed size fraction of 100-315μm to assess the coupled adsorption/precipitation behaviour. In the corresponding static compatibility tests, the experiments were performed to evaluate if any incompatibility/precipitation behaviour occurred between the product and the brine system, since no mineral substrate was present in these tests. The test solutions/bottles were placed in and left in an oven at test temperature for 24 hours before being filtered through a 0.22μm filter paper. All tests were performed in duplicate. After cooling to room temperature, the pH of the kept filtered supernatant was measured and recorded, prior to sampling. The filtered supernatant was then sampled 1ml into 9ml 1% Na^+ diluent solution before being sent to the ICP-OES for analysis alongside initial stock solutions enabling comparisons of initial and final ion concentrations. Any precipitated material/mineral substrate was rinsed on the filter paper with some distilled water and then left to dry before being analysed by ESEM/EDX or PSA.

A schematic of the experimental procedure is outlined in Figure 3.1 and a more detailed experimental procedure is outlined in Section 3.3.9.
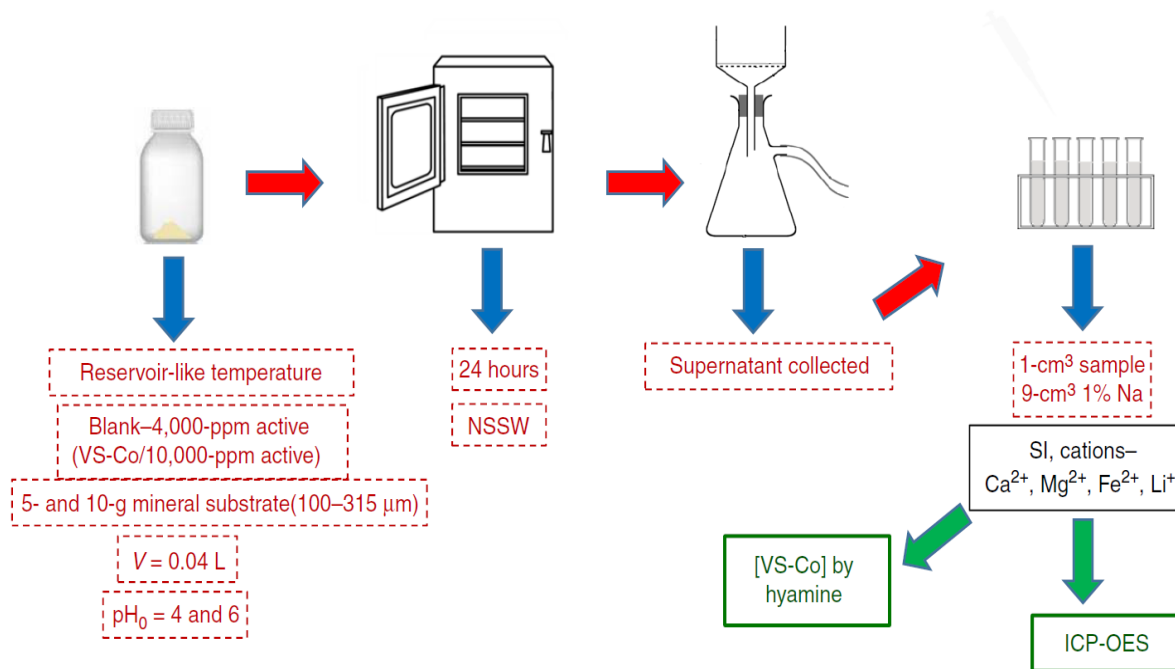
Figure 3.1. Schematic flow diagram of the static adsorption/compatibility experimental procedure[44]

Typical results of the effect of pH, mineralogy, and temperature on the bulk apparent adsorption behaviour (Γ_{app} vs. C_f) of these common commercially available SIs on a range of carbonate mineral substrates (calcite, dolomite, and limestone) will be presented in the results section. A summary of experimental conditions examined however summarizes the conditions of all the experiments performed during this work.

Table 3.1.A summary of experimental conditions examined[93]

Scale Inhibitor	Experimental Temperature (°C)	Calcite			Dolomite			Limestone	
		pH$_0$2	pH$_0$4	pH$_0$6	pH$_0$2	pH$_0$4	pH$_0$6	pH$_0$4	pH$_0$6
DETPMP	95°C	✓	✓	✓	✓	✓	✓	✓	+80°C
PPCA	95°C	✓	✓	✓	✓	✓	-	+80°C	✓
PFC	95°C	✓	✓	✓	✓	✓	✓	-	-
PAPE	80°C	-	✓	+60°C	-	✓	+60°C	-	-
VS-Co	95°C	-	✓	-	-	✓	✓	-	-

3.3.   Experimental Materials

3.3.1. Scale Inhibitors

Five scale inhibitors (SIs) were used in this work, for concentration ranges between 0 – 4,000ppm, except for VS-Co being examined over 0 – 10,000ppm. These concentrations are all 'active' ppm. The SI are chemically distinct commercial scale inhibitors widely used in oilfield applications. All of them have been extensively described in the literature and details of their chemistries and suppliers are presented in Table 3.2..

Table 3.2. Specifications of scale inhibitors

Full Name	Generic Name	Type	Chemical Structure	Activity%	Supplier
Di-Ethylene Tetra-amine Penta (methylene-phosphonic acid)	DETPMP	Phosphonate		47%	Italmatch
Poly Phosphino carboxylic Acid	PPCA	Polymeric		40.3%	BWA
P-functionalized co-polymer	PFC	Polymeric		36%	Clariant
Sulphonated Polyacrylic Acid Copolymer	VS-Co	Polymeric		35%	Nalco-Champion
Polyhydric Alcohol Phosphate Ester	PAPE	Phosphate Ester		50%	Taihe Water Treatment Company

3.3.2. Mineral Substrates

Prior to being used, the sourced carbonate mineral substrates were characterised. This involved dissolving a known amount of already crushed/washed mineral sample (0.15g) in 100ml of 10% HCl solution. The sample was then were left for 24 hrs to make sure all of the mineral was dissolved. The solution was then analysed by ICP-OES to determine the cation concentrations of specific ions such as calcium, magnesium and iron (Ca, Mg, Fe). The results are shown in Table 3.3.

Table 3.3. Characterisation of the carbonate substrates

Carbonate Type	Supplier	Calcium (mole)	Magnesium (mole)	Iron (mole)	Mg/Ca ratio
Moroccan Calcite	Geology Superstore	9×10^{-6}	3×10^{-9}	2.5×10^{-8}	3.3×10^{-4}
Skye Dolomite	UKGE	4.8×10^{-6}	5.4×10^{-6}	1.3×10^{-9}	1.11
Ayrshire Limestone	UKGE	8×10^{-6}	6.2×10^{-8}	3.8×10^{-8}	7.7×10^{-3}
Skye Limestone	UKGE	9.8×10^{-6}	2×10^{-7}	2×10^{-7}	0.021

The Moroccan calcite shows the lowest magnesium/calcium ratio in which Mg is negligible and confirms the chemical formula $CaCO_3$. For Skye dolomite the ratio of magnesium/calcium is 1.1 which is consistent with the generic formula of dolomite ($CaMg(CO_3)_2$). For both the limestone samples, some magnesium was detected, with the magnesium/calcium ratio higher in the Skye than Ayrshire sample. The amount of Iron (in moles) is greatest for the Skye limestone when compared to the other carbonate samples.

For the static adsorption tests, a previously crushed, sieved and distilled water washed/dried, size fraction of 100 - 315μm was used.

3.3.3. Test Matrix - Synthetic North-Sea Sea Water (NSSW) Brine

All brine solutions were prepared by dissolving appropriate quantities of salts in distilled water. The composition of the synthetic brine used, NSSW, is given in Table 3.4., alongside the suppliers for the analytical grade chemicals used. The brine solution was filtered through a 0.45μm filter paper to remove any suspended solid content prior to it being used in the tests. In addition, 50ppm Li^+ was added as an inert tracer to the NSSW brine to check for evaporation (if any occurred) during the heating process. The lithium results can be used to drift correct the test values if evaporation is suspected.

Table 3.4. Synthetic North Sea Seawater Water Composition (NSSW)

Ion	Concentration (ppm)	Salt Composition	Supplier	Grade	g/L
Na^+	10890	NaCl	Fisher Scientific	Analar	24.08
Ca^{2+}	428	$CaCl_2.6H_2O$	Sigma	Analar	2.34
Mg^{2+}	1368	$MgCl_2.6H_2O$	Merck	Analar	11.44
K^+	460	KCl	VWR	Analar	0.88
SO_4^{2-}	2960	Na_2SO_4	VWR	Analar	4.38
Li^+	50	LiCl	VWR	Analar	0.3055
Cl^-	19766				

3.3.4. Preparation of Diluent Solution – 1% Na^+

The diluent solution was used to dilute samples prior to them being sent for ICP-OES analysis. For all the ICP-OES samples, 1% Na^+ is used as its diluent solution to maintain the brine salinity close to the TDS of the initial NSSW test brine. This assists with the matrix matching of samples with the ICP standards allowing more accurate analysis results. All the test samples and initial stocks have undergone a x10 dilution in the diluent solution to allow the final ion concentrations to fall within the ICP-OES calibration range being used. The calculation to prepare the diluent solution was as follows:

1% Na^+ (aq) $\equiv$ 10,000ppm Na^+ (aq) $\equiv$ 25.42g of NaCl (s) in 1 litre of distilled water
So; 5 litre of distilled water, requires 25.42g x 5 = 127.10g of NaCl

3.3.5. Experimental Conditions

As previously shown in Table 3.1, numerous experiments were performed under a variety of conditions. The various conditions examined are outlined in Table 3.5.

Table 3.5. Details of Apparent Adsorption Experiment Conditions

Condition Type	Details
Temperature	95^oC all experiments 80, 60^oC only for PAPE to avoid thermal degradation
Pressure	Atmospheric, 1 bar
pH $_{initial}$ adjusted using dilute HCl and NaOH	pH_0 2, 4, 6 all experiments pH_0 4, 6 only for PAPE, VS-Co
Initial Scale Inhibitor Concentrations (active ppm)	0, 50, 100, 500, 800, 1000, 2000, 4000ppm [VS-Co]=100, 500, 1,000, 2,500, 5,000, 10,000ppm
Test volume (ml)	40ml or 0.04L
Mass of Substrate (g)	5 and 10g all experiments
Sampling times	24hrs after heating at test temperature Each test performed in duplicate
Dilution factor and diluent matrix	x10 1% Na^+ for all samples and stocks
Analysis Method	ICP-OES for SI and cation analysis Exception, [VS-Co] by Matrix Matched Easy Hyamine

3.3.6. Inductively Coupled Plasma Optical Emission Spectroscopy (ICP-OES)

ICP-OES is a method of instrumental elemental analysis. It can be used for the determination of approximately 70 elements in a variety of matrices. A plasma is an ionised gas. In ICP, an argon plasma is used. The plasma reaches temperatures of up to 10,000 K. The energy necessary to sustain the plasma is transferred electromagnetically via an induction coil (hence the term "inductively-coupled" plasma). The sample to be analysed is introduced into this hot gas through a nebulizer, which converts the liquid sample into an aerosol.

Atoms and ions from the sample are excited in the plasma and emit electromagnetic radiation in the ultraviolet and visible spectral range. The emission of light occurs as discrete lines, which are separated according to their wavelength by diffractive optics, and are utilized for

identification and quantification. Optical emission spectrometry describes a technique that is used to quantify an analysis based on the emission of light from a sample.[51].

Flow Assurance and Scale Team (FAST) have a Horiba Jobin Yvon Ultima 2 and a ThermoFisher iCAP 6300 Series Dual View (DV) upgraded to a 6500 series, Figure 3.2. They both give similar reading outputs, to within +/- 10% of each other although they work by slightly different modes. Table 3.6. highlights the individual features of the two different machines.

(a)
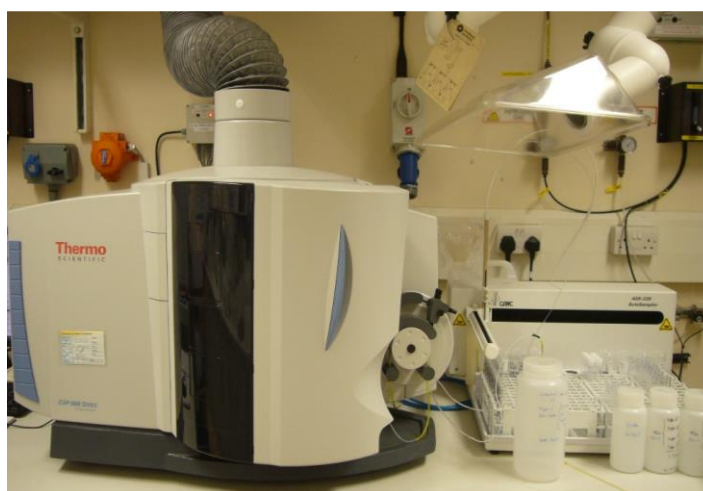
(b)

Figure 3.2.   (a) Horiba Jobin Yvon Ultima 2 and (b) Thermofisher iCAP 6300 Series Dual View

Table 3.6. The Individual Features of the Ultima 2 and upgraded iCAP 6500 DV Series

Feature	Horiba Jobin Yvon Ultima 2	Thermofisher iCAP 6300 DV upgraded to an iCAP 6500
Torch	Fully demountable vertical torch Single View Radial	Open Access to Torch Dual View: Axial & Radial
Wavelength Coverage	160-800nm Optional 120nm for UV of halogens included	166 – 847nm
Spectrometer	1m Czerny-Turner monochromator Nitrogen purged & thermostated	Echelle Type Grating
Measurement	Sequential	Simultaneous
Grating/Optics	Ion etched holographic master 110 x110mm, 2400lines/mm used in first/second order	Echelle grating 52.91 grooves/mm ruled 383mm effective focal length 9.5o UV fused silica cross dispersion prism
Spectral Resolution	10/5picometers (pcm) in first/second order <5pcm in 160-320nm <10pcm in 320-800nm	7pcm at 200nm
Detection	High Dynamic PMT Detector: Sub ppb to % level	4th Generation RACiD86 Charge Detection Device (CID)
Intensity	Gains: 10, 100	Direct measurement
Sheath Gas	Allows continuous analysis of 30% dissolved solids (DS)	Not Required 5% DS +Argon (Ar) humidifier 15% DS – Ar humidifier
Generator	Solid state, frequency stabilised, Reflected power control, air cooled	Solid state
Frequency (MHz)	40.68	27.12
Power (Watt)	Maximum 2600	750-1600
Load Coil	Water cooled	Water cooled
Argon flow (L/min)	12 (7 low-flow option)	12
Sample Introduction	Thermoregulated sample compartment, Sheath gas for reduced memory effects	Open Easy Access sample compartment
Software	ICP Analyst 5.4 - Analysis & Reporting	iTEVA Control Centre: Analyst - analysis Publisher - reporting

The procedure of conducting ICP-OES is as follows:

1. Prepare the brines/solutions required for the procedure.
2. Prepare standards for each set of analysis. Refer to the note below for the iCAP internal standard.
3. Ensure the torch/sample introduction glassware and tubing have been cleaned and correctly re-assembled.
4. Light the plasma and allow a warm up time of 1hr before initiating an analysis run. For the TF-iCAP 6500DV – a Zn stability needs to be performed after 10-15mins warm up and prior to starting the run – use the zinc stability method. A zinc stability standard is 2ppm Zn & 0.01% methanol (2ml from a 1000ppm ICP standard and 0.1ml of methanol) in 1L of distilled water.
5. Set up method and sequence.
6. **HJY – U2:** Run profiles to check background correction points for each element in the appropriate DW or brine. Set the backgrounds in the method for each element.
7. **TF – iCAP 6500DV:** Backgrounds are run automatically alongside the sample but can be manipulated afterwards.
8. **Both instruments:** Run a calibration and a set of repeats to check repeatability.
9. Check that the calibration for each element is successful and that the repeats for the standards are consistent with the expected values.
10. Samples could now be run. Samples at known concentrations are statistically analysed for their precision and accuracy, the definition of which are outlined below.

Note: In step 2, for the Thermofisher iCAP, an additional preparation of an internal standard is required. There are a number of factors to consider when choosing the internal standard:-

•   The internal standard should behave similarly to the element of interest in the plasma. For best results, where possible, the atomic (I) or ionic (II) state of the element line should match that of the internal standard line. A similar wavelength should also be used. If the element line is a low wavelength (<235nm (4xx)) then the internal standard line should also be a low wavelength. If the element line is a high wavelength (>235nm (1xx or 0xx)) then the internal

standard line should also be a high wavelength. It is also advisable to match the viewing option i.e. a radial element line with a radial internal standard line

- The most commonly used wavelengths for the yttrium internal standard are 224.306nm (for low wavelengths) and 371.030nm (for high wavelengths). Other wavelengths that can be used, although less frequently, are 324.228nm and 360.773nm

The internal standard could contain a number of different elements such as Rhodium, Scandium, Indium, Gold, Yttrium, and Caesium in 1% Nitric Acid or distilled water for sulphide/ Ethylene Diamine Tetra Acetic Acid (EDTA) containing solutions. This internal standard is sprayed at a low flow rate at all times throughout the analysis run. Caesium is sometimes present in the internal standard to reduce or stop ion suppression happening. However if it does occur then the other elements can be used to account for this ion suppression. To ensure effective mixing and reduce any air bubble effects, Triton X100 is also added to the internal standard solution if a Y-piece setup is being used. The final concentration of Triton in the internal standard is 0.1%. Table 3.7. shows the procedure of internal standard preparation for analysis.

Table 3.7. Preparation of Internal Standard

With Nitric Acid	**In Distilled Water Without Nitric Acid**
2ml 10,000ppm Y standard 400ml of 5% Nitric containing 0.1% Triton Additional 1.6ml Triton to give overall 0.1% Triton All in 2L of Distilled Water ⇨ 10ppm Y, 0.1% Triton in 1% Nitric Acid	2ml 10,000ppm Y standard 2ml Triton X100 ⇨ 10ppm Y, 0.1% Triton in DW
With Nitric Acid	**In Distilled Water Without Nitric Acid**
NOTE: When adding the Triton, have the solution already stirring with an excess of the background solution present. The Triton is extremely thick and this swirling helps it dissolution	

Accuracy is the degree of agreement between the measured value and the true value. An absolute true value is seldom known. A more realistic definition of accuracy then would be to assume it is the agreement between a measured value and the *accepted* true value.

Precision is defined as the degree of agreement between replicate measurements of the same quantity. It is the repeatability of the result. This is also known as standard deviation. However, good precision does not mean good accuracy, for instance, if there was a systematic error in the analysis. This error would not affect the precision, but it does affect the accuracy.

11. Using the diluter or a pipette, do the appropriate dilution for the elements in question, so their concentrations fit within the calibration range of the corresponding element calibration standards.
12. Run the real samples.
13. Give data to personnel responsible for the plotting of results
14. Personnel will use the appropriate ICP macro to manipulate the data to determine the concentration of the analysed samples
15. Construct a summary table of results

3.3.7. Wet Chemical Technique: Matrix-Matching Easy Hyamine

Recently, the oil industry is much more environmentally aware and one of the consequences is that more environmentally friendly scale inhibitors have been developed and applied. These are known as 'Green Scale Inhibitors' (GSI), and they do not pollute the waters around platforms and the pipeline systems through bioaccumulation and non-degradation[95]. These GSIs are also being applied in chemical squeeze treatments. Although more environmentally friendly, they bring their own set of problems to the analysis world, such as being non-phosphorus containing, making analysis by ICP non applicable. Therefore, the industry may have to resort to wet chemical techniques or other instrumentation such as HPLC (Dionex). An example of a GSI would be the VS-Co or Sulphonated Polyacrylic Acid Copolymer used during this PhD. This SI was analysed by x20 matrix-matching easy hyamine as it is non-phosphorus containing.

The development of the easy hyamine matrix matching technique evolved because of difficulties in determining low polymeric SI concentration from a restricted sample volume. The procedure for the actual detection is exactly the same as the normal easy Hyamine. However it is the steps taken before the analysis that require some thought. The final procedure developed avoids the

negative effects of the remaining chloride ion on the chelating process between the hyamine and SI. For example, a SI stock would be prepared in SW, as would happen for any experimental procedure, which would then be diluted to give a 25ppm active SI/DW stock in order to create an easy hyamine calibration range of 0-10ppm active SI/DW i.e. easy hyamine relies on the diluting out of any salts that may interfere with the SI detection. However, it was found that as the SI/SW concentration became lower in the samples, requiring a smaller dilution in DW, say a x2 dilution – 2500d and 2500s on the diluter, for a 5ml DW test solution – then a greater chloride ion concentration is present with respect to the target 0-10ppm active SI DW calibration standards. The higher concentration of chloride ions present interfere more significantly with the chelating process between the Hyamine and the SI. Therefore, the turbidity absorbance recorded for that concentration of SI is incorrect. By matrix-matching the sample and calibration standards, for example using the same dilution factor from a SW background to a DW background, gives equivalent chloride ion concentration within both. This then means that any chloride ion effects on the chelating process between the Hyamine and scale inhibitor can be negated, allowing accurate analysis to be performed for the low scale inhibitor concentration samples. For example, if a sample was thought to require a x10 dilution to give a [SI] within a 0-10ppm active SI DW calibration range, then initially 0-100ppm SW calibration standards would be prepared. These SW calibration standards would then require the same x10 DW dilution as the samples (i.e. 500s & 4500d for 5ml) and hence both the sample and calibration standards will have equivalent chloride ion concentration; thus, the sample and calibration standards will undergo similar interferences from these ions allowing accurate analysis to be performed i.e. matrix-matching. This method was used to analyze the SI concentration of VS-Co during this research.

3.3.8. Environmental Scanning Electron Microscopy - Energy Dispersive X-Ray (ESEM-EDX)

ESEM/EDX is able to image and elementally analysis a wide range of sample types without any form of preparation. It is therefore possible to examine wet, oily or outgassing samples. It is also possible to perform dynamic experiments such as wetting within the ESEM chamber, which is not otherwise possible with other conventional SEM's. ESEM/EDX analysis can be used for a

wide range of applications. FAST uses the techniques to investigate the following prior to and after an experiment:

- Mineral surfaces – dissolution effects from core flood or scale dissolvers, adhering precipitation, identifying formation damage

- Wettability Issues - oil or water wet identification when oil or water added *in situ*.

- Precipitate morphology and composition – Scale Inhibitor_Cation complexes, Naphthenate deposits, interfacial salts from mutual solvent investigations, silicate complexes, scale inhibitor interactions on scale formation

- Precipitation surface coverage – on a metal coupon, to observe if pre-treatment of a metal surface prevents surface scaling and to what degree

- Surface structures – metal, polymerics, fluorinated coatings

The machine at Institute of GeoEnergy Engineering is an XL30 ESEM with LAB_6 filament alongside an Oxford Instruments X-Max 80mm EDX detector and INCA software, shown in Figure 3.3.

Figure 3.3. ESEM - Philips XL30 at Heriot-Watt University

The General Laboratory Procedure of ESEM/EDX Analysis is fully explained in Appendix 6.1.

3.3.9. Particle Size Analyser (PSA)

Particle size and its distribution is important information required prior to executing static adsorption/precipitation or non-equilibrium sand pack experiments. For this study, sand, kaolinite and siderite minerals were measured before being used in the various experiments. Having a consistent size and distribution is important for the analysis as adsorption/precipitation (particularly adsorption) onto these minerals very much depends on their particle size and distribution (i.e. specific surface area). The Malvern Master Sizer MS-20 was used to measure particle size and its distribution. Refer to Figure 6.7 (Malvern Master Sizer MS-20 Instruction Manual)

This machine uses the principle of laser diffraction to determine the particle size of the precipitate of $SI-M^{2+}$ described in Chapter 4. The technique of laser diffraction is based around the principle that particles passing through a laser beam will scatter light at an angle that is directly related to their size.

The Operation Procedure of Particle Size Analyser (PSA) is fully explained in Appendix 6.2.

3.3.10. Detailed Experimental Procedure for the Static Adsorption/Compatibility Tests

1. Prepare NSSW brine by dissolving the relevant salts in distilled water and subsequently filter this brine through a 0.45μm filter paper.
2. Prepare a 10,000-ppm SI stock solution in the test brine and further dilute to appropriate SI concentrations (50, 100, 500, 800,1,000 2,000 and 4000ppm) for the adsorption test in the same test brine. Exception: [VS-Co] $_{initial}$=100, 500, 1,000, 2,500, 5,000 and 10,000ppm.
3. Record the pH and then adjust the pH of all stock solutions (blanks and SI/SW samples) to the required initial test pH value: i.e. pH_0 2, 4 and 6.
4. Prepare two sets of bottles - one for adsorption (contains mineral) testing, and the other for compatibility (no mineral present) testing. Prepare duplicate sample bottles for each test condition for adsorption, but only one for compatibility.
5. Weigh samples of mineral substrate into appropriately labelled 150 cm^3 plastic bottles (m= 5 and 10 g).
6. Pipette 40 cm^3 of the appropriate SI solution into each bottle (V=0.04 L).

7. Cap the bottles and shake for 5 seconds before placing in an oven at test temperature (^{o}C) and atmospheric pressure.

8. Check the bottle caps for tightness after 1 hour and tighten if loose, to avoid evaporation.

9. After 24 hours in the oven, remove the test bottles and immediately filter through individual 0.22-μm membrane filters; keep the labelled mineral/precipitate on their filter papers and the separate supernatant solutions.

10. Leave the filtered supernatant solution to cool to room temperature for approximately 24 hours.

11. Measure the post-test pH.

12. Sample the filtered supernatant using a pipette, and dilute the sample volume in a known matrix volume (x10 1% Na$^+$) ready for analysis alongside the associated stock solutions by inductively coupled plasma-optical emission spectrometry (ICP-OES) for [SI], [Ca^{2+}], and [Mg^{2+}]. Exception: Analyse the [SI] of the VS-Co samples/stocks by the wet chemical matrix-matched easy hyamine technique instead of ICP-OES[95]

13. Plot up the data generated

14. Perform ESEM/EDX analysis and PSA on the collected and dried solid phases (precipitate/mineral combined and separate) to analyse the morphology and particle size of the mineral-substrate grains and any bulk precipitate formed.

15. Analyse and interpret all the results

The schematic of the static adsorption and compatibility experiment was illustrated previously in Figure 3.1.

3.3.11. Typical Test Schedule Example (Bottle Test)

The bottles were numbered to track each concentration used. Experiments at each concentration were performed in duplicate to assure the consistency of the results.

Bottle No.	[SI], ppm active	Bottle No.	[SI], ppm active
1	Blank	S1a (95^{0}C)	0
2	Blank	S2a (95^{0}C)	50
3	50	S3a (95^{0}C)	100
4	50	S4a (95^{0}C)	500
5	100	S5a (95^{0}C)	800
6	100	S6a (95^{0}C)	1000
7	500	S7a (95^{0}C)	2000
8	500	S8a (95^{0}C)	4000
9	800	S1b (Room Temperature)	0
10	800	S2b (Room Temperature)	50
11	1000	S3b (Room Temperature)	100
12	1000	S4b (Room Temperature)	500
13	2000	S5b (Room Temperature	800
14	2000	S6b (Room Temperature)	1000
15	4000	S7b (Room Temperature)	2000
16	4000	S8b (Room Temperature)	4000

4. CHAPTER 4: EXPERIMENTAL RESULTS and DISCUSSION

4.1. Introduction

In this Chapter, we present some of the main experimental findings of this thesis. The results are presented as follows:

(i)   The solubility of calcite and dolomite in North Sea Sea Water (NSSW) and in distilled water (DW) – Section 4.2

(ii)   The Phosphonate Scale Inhibitors Retention in Carbonates (dolomite and calcite) – Section 4.3

(iii)   The Polymeric Scale Inhibitors (PPCA and PFC) Retention in Carbonates (calcite and dolomite) – Section 4.4

(iv)   The Phosphate Ester Scale Inhibitors Retention (at two different reservoir temperature; T= 80°C & 60°C) in Carbonates (calcite and dolomite) – Section 4.5

(v)   Comparison of the Phosphonate and Polymeric Scale Inhibitors (DETPMP & PPCA) Retention on Limestone Substrates – Section 4.6

Finally, a full overview and summary of all of this work, including the overall conclusions and findings of this research, are presented in the Chapter 5.

4.2.   Solubility of Calcite & Dolomite in NSSW & DW

In this section, we present the results on the solubility of calcite and dolomite in North Sea Water (NSSW) and Distilled Water (DW). No scale inhibitor was used in these measurements, and so these can be considered as being "baseline" mineral solubility experiments. To measure the solubility of calcite and dolomite, these mineral substrates were put in plastic bottles with two different masses of mineral (m= 5& 10 g); then NSSW and DW adjusted to various initial pH values (pH$_0$= 2, 4, 6 & 8) were added to the bottles. The samples were put in an oven at a reservoir like temperature (T=95°C) for 24 hrs. Then, they were taken out and filtered. The supernatant solutions were analysed by ICP to look at initial and final concentrations of divalent cations ($[Ca^{2+}]$, $[Mg^{2+}]$) and also final pH of supernatants were measured and recorded.
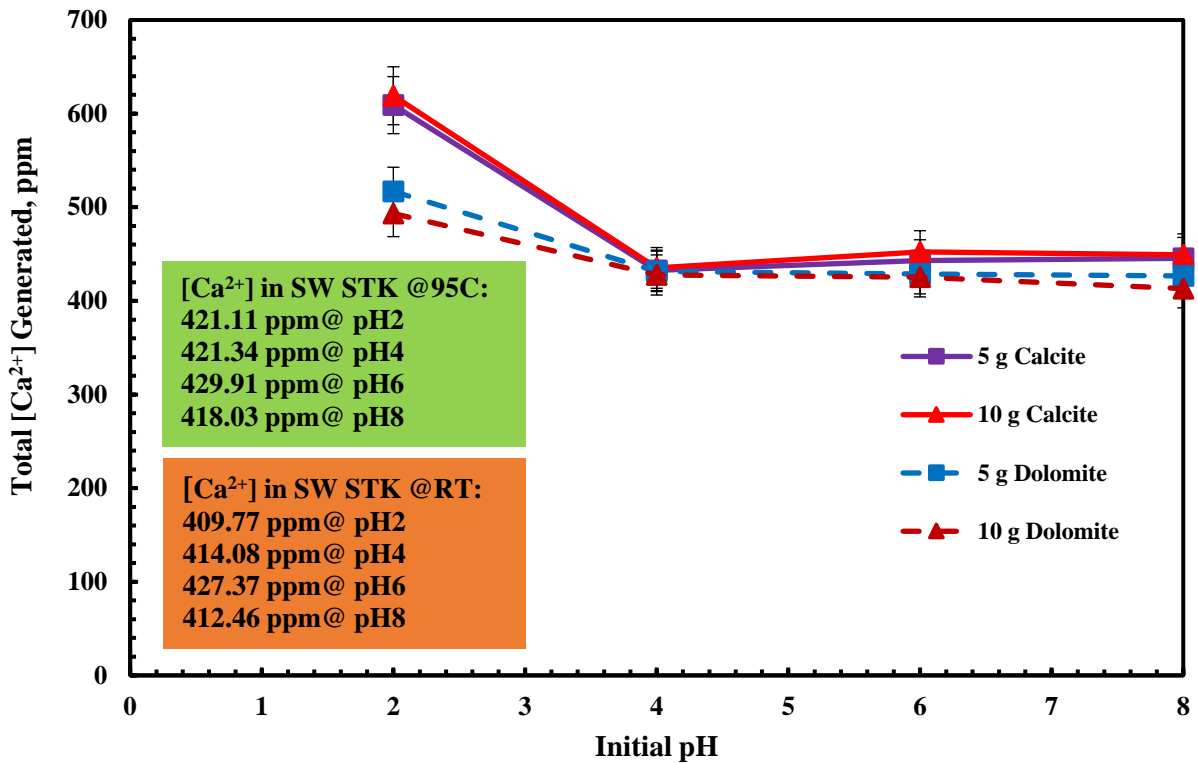
Figure 4.1. Total [Ca^{2+}] Generated In Situ for Calcite & Dolomite with NSSW at Different pH Values

As shown in Figure 4.1, for lower initial pH (pH = 2), the amount of calcium generated in situ by the carbonate rock dissolution increases. This is simply due to acid dissolution of the carbonates (both calcite and dolomite). However, the rock dissolution is negligible as pH changes from pH_0 4 to pH_0 8. In addition, at pH_0 2, the amount of calcium generated through rock dissolution is higher for the calcite/NSSW system than for the dolomite/NSSW system. It is due partly to the lower amount of calcium in dolomite compared to calcite, and also to the fact that dolomite is somewhat less reactive.
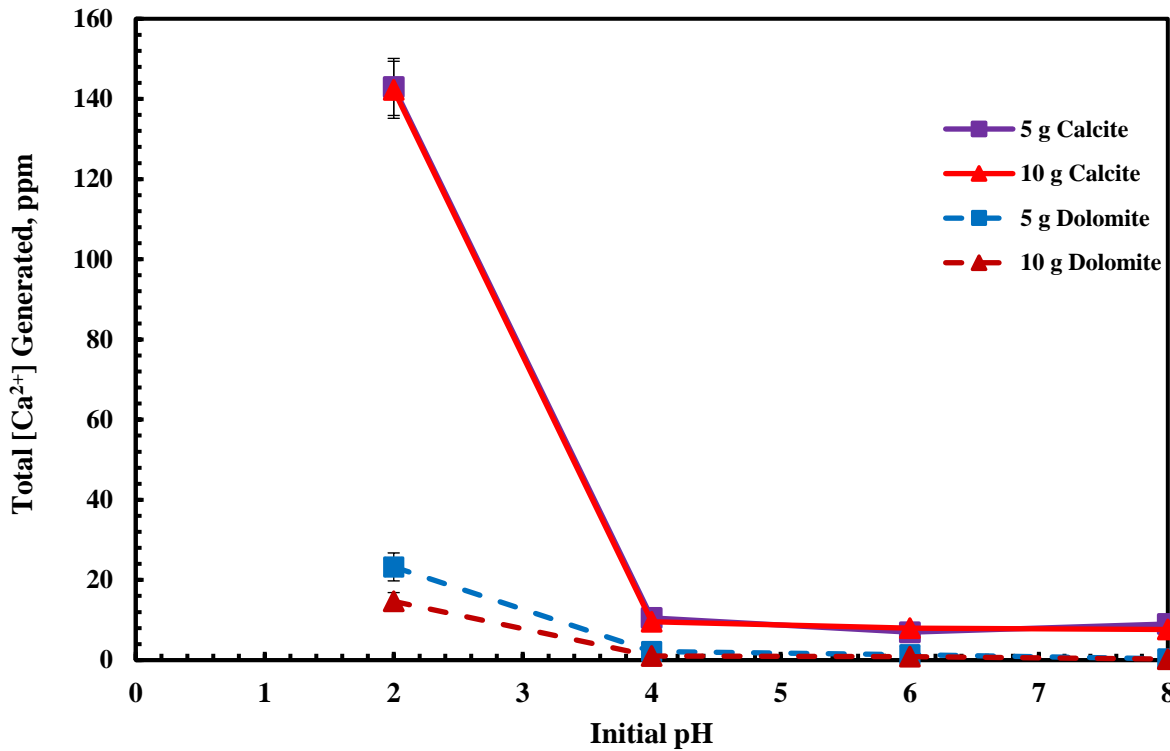
Figure 4.2. Total [Ca^{2+}] Generated In Situ for Calcite & Dolomite with Distilled Water (DW) at Different pH Values

The corresponding calcite and dolomite solubility in distilled water (DW) at the same initial pH values (pH$_0$= 2, 4, 6 & 8) is shown in Figure 4.2, [Ca^{2+}] generated in situ by rock dissolution for the pH0 2 case is again the highest amount is 140 ppm and 20 ppm for calcite and dolomite; the results above for NSSW were ~ 179 ppm and 79 ppm for calcite and dolomite cases, respectively. Thus, NSSW is able to dissolve more carbonates than DW. In addition, calcium generated in situ in calcite is higher than in dolomite, as the later has less calcium content than the former and the dolomite is less reactive.
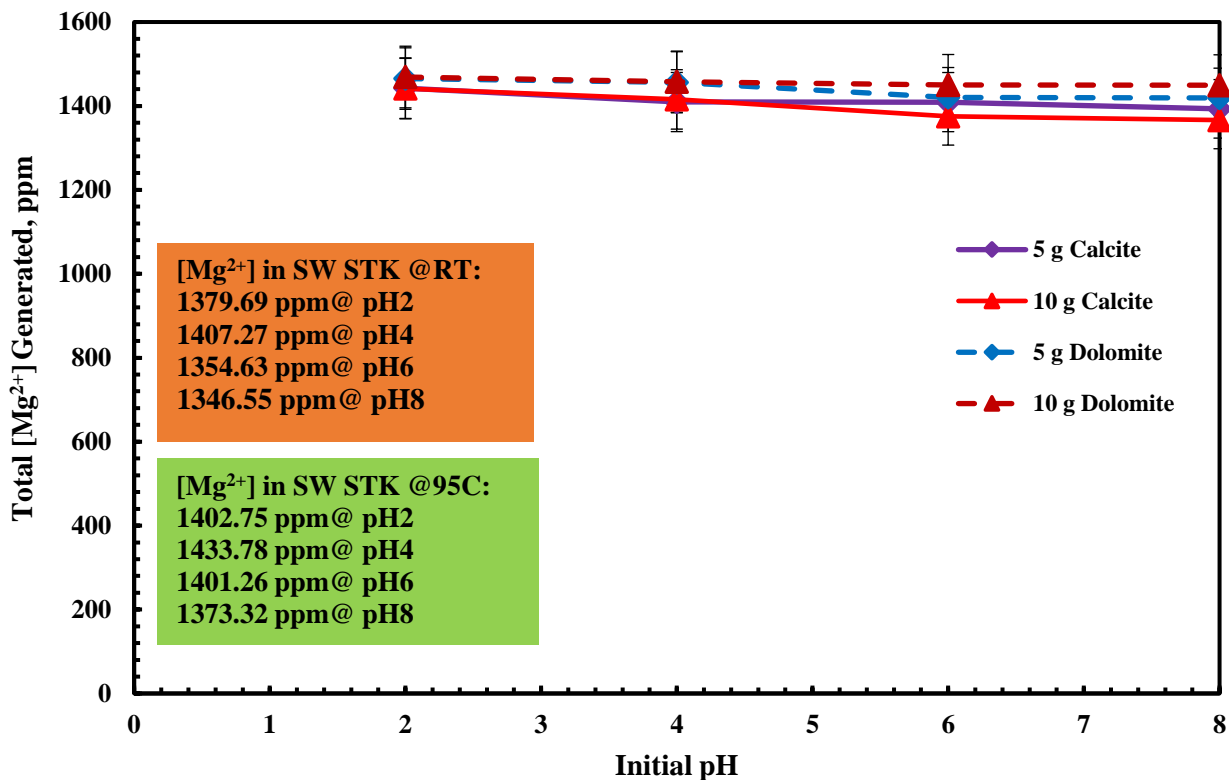
Figure 4.3. [Mg^{2+}] Generated In Situ for Calcite & Dolomite with NSSW at Different pH Values

Figure 4.3 shows the amount of magnesium (Mg^{2+}) generated in situ through rock dissolution in NSSW; note that the difference is not obvious in this case since the NSSW already contains about 1400ppm Mg^{2+}. The Mg^{2+} generated in the dolomite/NSSW system (~66ppm) is more than that in the calcite/NSSW system (~39 ppm). This is related to higher amount of magnesium in dolomite. Furthermore, [Mg^{2+}] generated through rock dissolution is negligible and does not change significantly as pH is increased (contrary to [Ca^{2+}] generated in situ results).
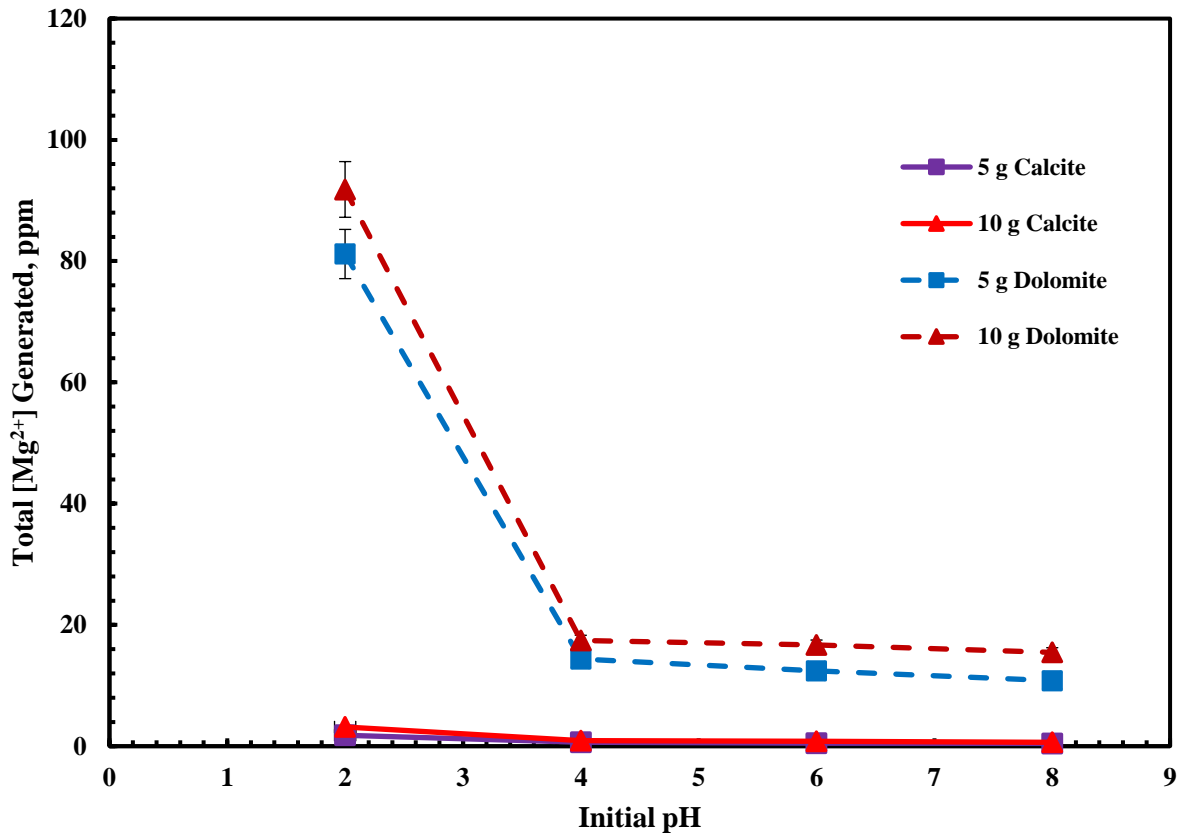
Figure 4.4. [Mg^{2+}] Generated In Situ for Calcite & Dolomite with DW at Different pH Values

The Mg^{2+} results for the carbonate/DW systems are shown in Figure 4.4. At the lowest pH value (pH$_0$=2), rock dissolution occurs in dolomite/DW system and some magnesium is leached out of system (~ 80 ppm). However, once the solution pH is increased, the amount of magnesium generated decreases to 20 ppm and does not change very significantly at higher initial pH values. In the calcite/DW system, this amount of Mg^{2+} is ~ 3 ppm at pH$_0$ = 2 and is even less at higher initial pH values. These results are simply because of the fact that there is a very small amount of Mg in the calcite sample, and fairly significant amounts in the dolomite (approx. CaMg (CO$_3$) $_2$).
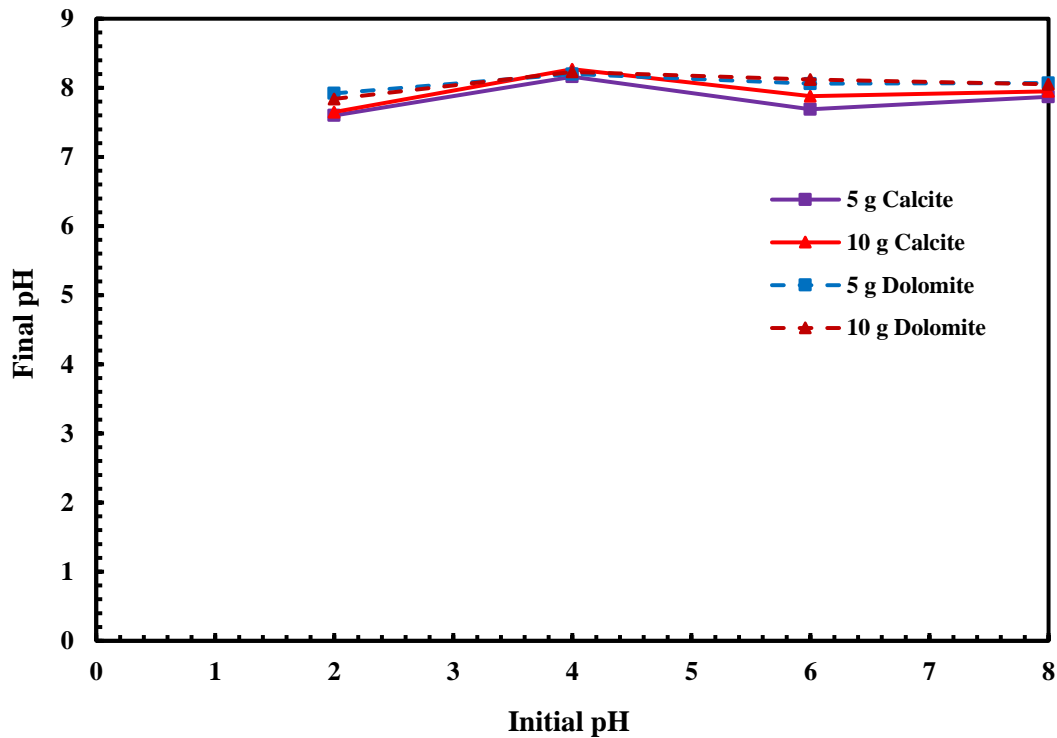
Figure 4.5. Final pH for Calcite and Dolomite with SW at Different pH Values

As seen in Figure 4.5, the final pH of the solution increases as the carbonates contact with NSSW because of rock dissolution. In addition, in all initial adjusted pH values, final pH is around 8 for both calcite and dolomite substrates, although this amount is slightly higher for the dolomite/NSSW system. This implies that the aqueous system is buffered because of the presence of carbonate minerals.
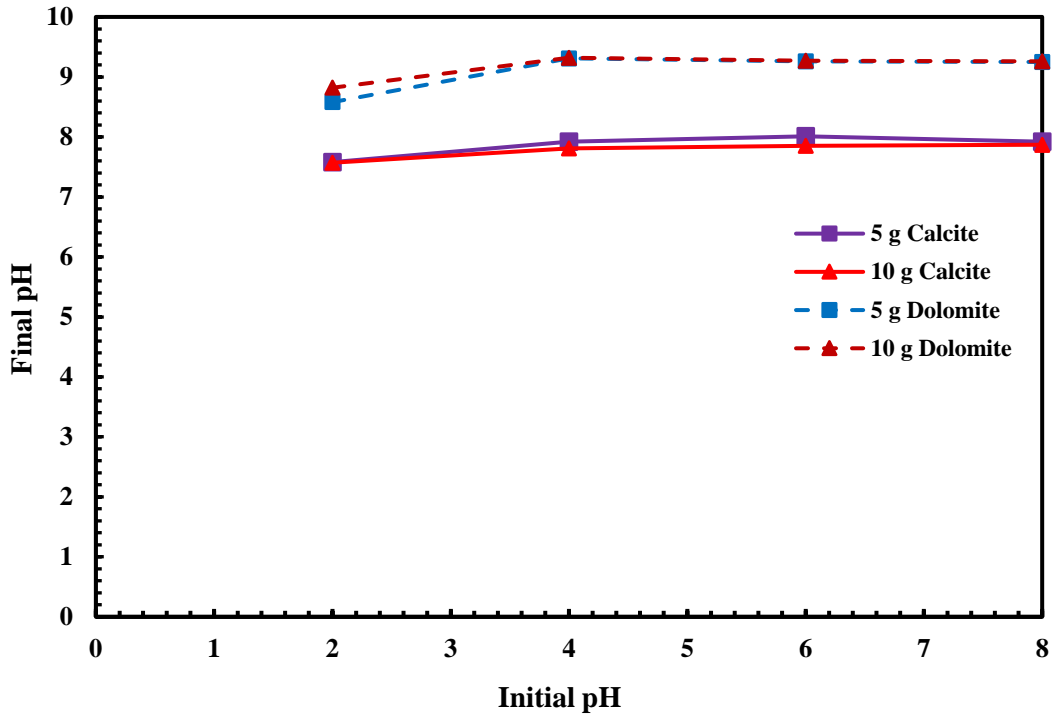
Figure 4.6. Final pH for Calcite and Dolomite with DW at Different pH Values

Figure 4.6 shows the corresponding final pH results for calcite and dolomite in DW are rather different to those in NSSW (above). The final pH values for the dolomite/DW system are higher than those for the calcite/DW system, as shown in Figure 4.6; the final pH for the dolomite/DW system is around pH_f ~9 while this is pH_f ~7.5 for the calcite/DW system.

To sum up this section, some conclusions as follows:

1) As pH is reduced, the amount of divalent cations (Ca^{2+}, Mg^{2+}) generated in situ by rock dissolution increases.

2) The amount of calcium generated through rock dissolution is higher in the calcite/NSSW system than for the dolomite/NSSW system. This is attributed to the relatively lower amount of calcium in dolomite compared to calcite, and the lower reactivity of the dolomite.

3) NSSW is able to dissolve more carbonates than DW, so more divalent cations are generated in carbonates/NSSW system in comparison with carbonates/DW.

4) More magnesium is produced in dolomite than in calcite as dolomite has a far higher magnesium content than calcite

5) Final pH of solution increases as the carbonates contact with NSSW because of rock dissolution. In addition, in all initial adjusted pH values, final pH is around 8 for both calcite and dolomite substrates, although this amount is a little bit higher for dolomite/NSSW in comparison with calcite/NSSW.

6) Final pH of dolomite/DW is higher than that of calcite/DW system as shown above (pH_f for dolomite/DW system is around 9 while this amount is ~7.5 for calcite/DW system). This change might be attributed to the carbon dioxide (CO_2) content of these system.

These findings presented in this part help us to understand behaviour of different SIs in terms of retention on carbonates which will be brought later on.

4.3.   Phosphonate Scale Inhibitors Retention in Carbonates

Experimental Results for "Apparent Adsorption", Γ_{app}

The aim of this section is to investigate dominant mechanisms governing the retention of Di-Ethylene Tetra- amine Penta (DETPMP) on two different carbonate substrates, calcite and dolomite. This commonly applied phosphonate scale inhibitor (SI) is readily detectable via "P" by Inductively Coupled Plasma- optical emission spectrometry (ICP-EOS). This has been done by carrying out a range of static "apparent adsorption" experiments where we plot the apparent adsorption, Γ_{app} vs. C_f the final SI concentration as a function of (m/V) where m is the mass of substrate (calcite and dolomite) and V is the solution volume. As explain in Chapter 2, this allows us to easily identify SI concentration regions when pure adsorption (Γ) occurs and where coupled adsorption/precipitation (Γ/Π) occurs. These apparent adsorption plots are measured for a specific fraction size of the crushed carbonate substrates ($100\text{-}315\mu m$) as well as at various (m/V) ratios. All of the SI/calcium precipitates have been examined using Environmental Scanning Electron Microscope / Energy-dispersive X-Ray (ESEM/EDX). In addition, the impact of the initial pH of the solution on apparent adsorption of DETPMP inhibitor was studied for two carbonate mineralogies (calcite and dolomite) at a reservoir like temperature, T=95°C. For these static apparent adsorption tests, the experiments were conducted using m= 5 and 10 g of carbonate substrates for a fixed volume (V= 40 ml) of solution, i.e. for two (m/V) ratios. As

the experimental results presented below will show, only 2 values of (m/V) are required to clearly establish the 2 retention regimes, i.e. pure adsorption (Γ) and coupled adsorption/precipitation (Γ/Π). In the corresponding compatibility tests (no mineral present), the experiments were performed to investigate the intrinsic precipitation behaviour of the solution, since no mineral was present in these tests. Hence, any loss in SI concentration from solution in these compatibility tests must be due to pure precipitation (Π only).

In this section, we present the experimental results under the following headings:

Apparent adsorption of DETPMP on Moroccan Calcite and Skye Dolomite:

The results of the static coupled adsorption/precipitation (Γ/Π) experiments; referred to as "apparent adsorption" experiments, are plotted as Γ_{app} vs. C_f, the final concentration of SI in solution in the manner of a "normal" adsorption isotherm. Figure 4.7 (a), Figure 4.7(b) & Figure 4.7(c) show the apparent adsorption level vs. final SI concentration of scale inhibitor for two masses (m = 5g and 10g) of 100-315μm size fraction of calcite and dolomite as a function of the final scale inhibitor concentration (Γ_{app} vs. C_f) in synthetic NSSW at T = at 95°C for initial pH$_0$ = 2, 4 & 6, respectively.
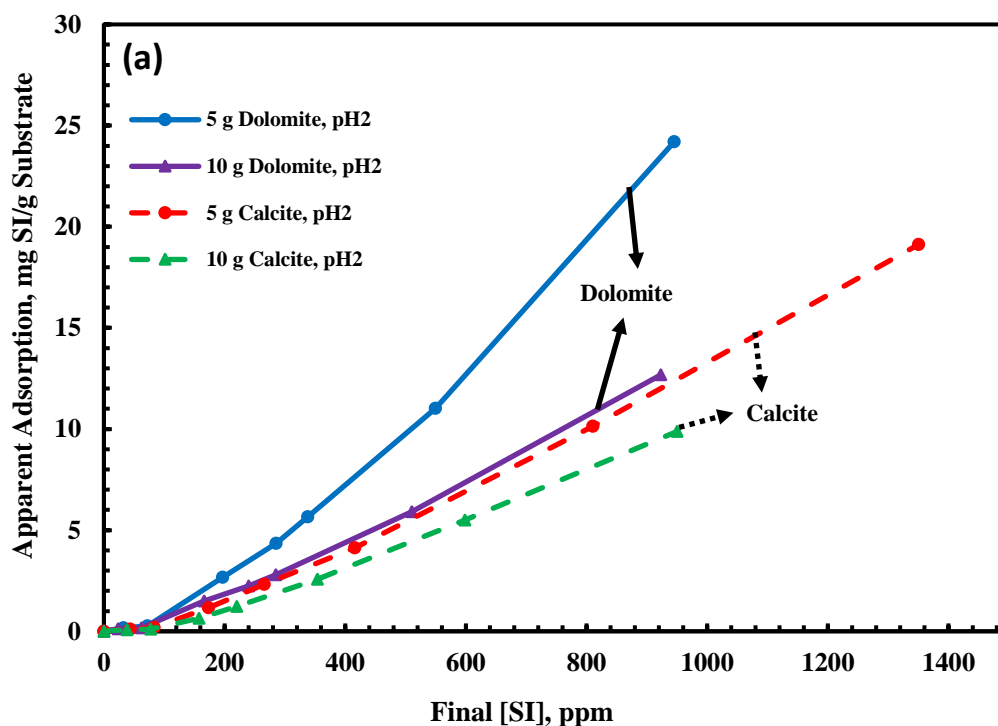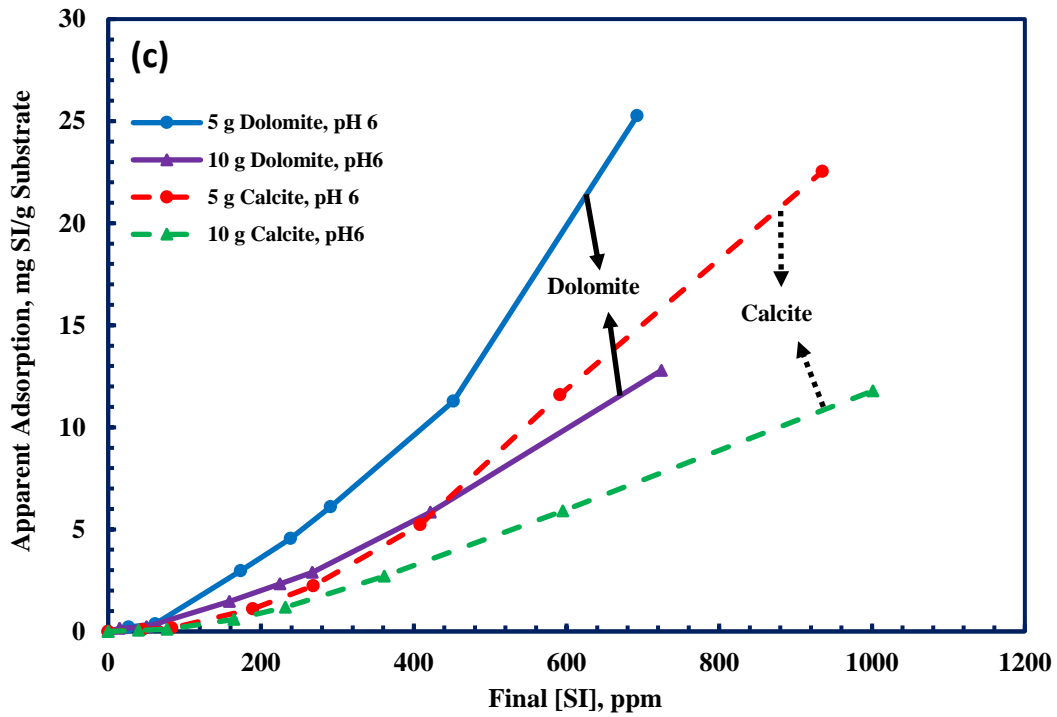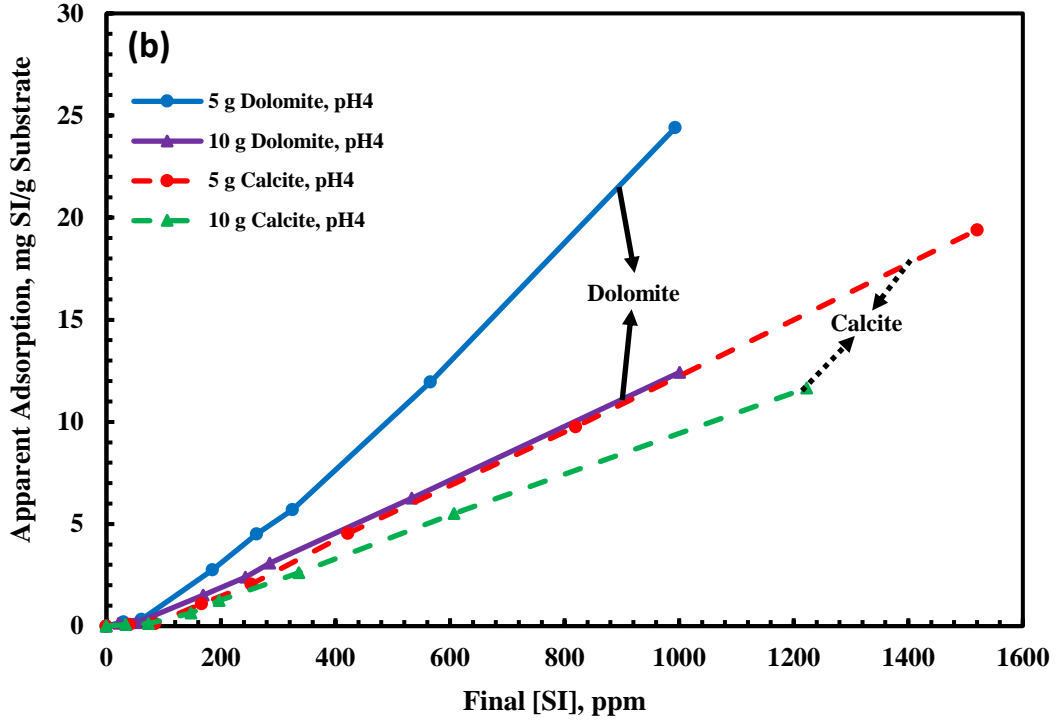
Figure 4.7. Comparison of apparent adsorption for DETPMP- i.e. Γ_{app} vs. C_f - onto two masses (m = 5g and 10g) of calcite and dolomite for initial pH values of (a) pH_0 2 (b) pH_0 4 (c) pH_0 6; all experiments at T = 95°C

The results in these figures clearly show regions of both pure adsorption (Γ) and coupled adsorption/precipitation (Γ/Π) at different DETPMP concentrations regardless of the type of

substrate and initial pH value. DETPMP in NSSW shows pure adsorption behaviour up to [DETPMP] ~100ppm and then a much wider region of coupled adsorption/precipitation behaviour above ~100ppm, where the apparent adsorption measurements diverge for different m/V values. These results also show that coupled adsorption/ precipitation is the dominant retention mechanism over all of the [DETPMP] concentration region > 100ppm. The apparent adsorption values are in the region of 5-25 (mg SI/g substrate) which are much greater than the normal lower pure adsorption levels of 0-2 (mg SI/g substrate). Thus, the regions of pure adsorption and coupled adsorption/ precipitation behaviour are unequivocally demonstrated for DETPMP on calcite and dolomite for all initial pH values.

The DETPMP/dolomite and DETPMP/calcite systems both qualitatively show very similar trends in apparent adsorption. However, there are some quantitative differences between these two systems, in that the apparent adsorption of DETPMP is higher for the dolomite system than for the calcite system. This is actually rather surprising, since it is well known that calcite is rather more chemically reactive than dolomite. This result has been repeated in our laboratory and has been reproduced several times on the Moroccan calcite and Skye dolomite samples used in this work. To explain this finding, we must first present the additional final pH and $[Ca^{2+}]$ data for each of the above experiments.

Final pH Values, pH_f: In all apparent adsorption experiments, for the various initial pH values (pH_0 2, 4, 6), the final pH values (pH_f) were measured, as were the final $[Ca^{2+}]_f$ values in every case (presented below). All the pH results are presented in Figure 4.8 (a), Figure 4.8(b) and Figure 4.8(c), each corresponding to the apparent adsorption results in Figure 4.7 above. Also shown in these figures are the pH results for the compatibility (no mineral present) tests and these show that there are no noticeable changes in pH in the pure compatibility test at initial adjusted pH_0 2 and 4 (Figure 4.8 (a) and Figure 4.8(b)). Thus, DETPMP is completely compatible with NSSW in the absence of calcite/dolomite mineral up to [DETPMP] =4000ppm in the solutions at pH_0 2 and 4. However, when the initial pH is increased to pH0 6 (Figure 4.8(c)), the final pH in the compatibility tests declines gradually which indicates that there is some incompatibility between DETPMP and divalent cations (Ca^{2+} and Mg^{2+}) in the NSSW and this is giving some precipitate, even in the absence of carbonate mineral.

Figure 4.8 (a), Figure 4.8(b) and Figure 4.8(c) also show the final pH values (pH_f) in the presence of calcite and dolomite for all initial pH conditions and DETPMP concentrations used in the apparent adsorption experiments. Thus, every pH_f point in these figures corresponds to one of the apparent adsorption points (or compatibility test – no mineral) in Figure 4.7(a), Figure 4.7(b) and Figure 4.7(c). Once substrates (calcite and dolomite) are added to the DETPMP solution, the pH rises from their initial values (pH_0 2, 4 and 6) to pH ~ 8 due to dissolution of calcite/dolomite substrate in the scale inhibitor solution (or in the brine in the compatibility tests). At DETPMP concentrations of ~100ppm, the retention regime changes from pure adsorption (Γ) to coupled adsorption/ precipitation (Γ/Π), and we observe that the pH decreases quite sharply. This is obviously associated with the precipitation process and this will be explained later. The detailed results for pH_f in Figure 4.8(a), Figure 4.8(b) and Figure 4.8(c) show that the final pH values of the solutions in the calcite/DETPMP system are less than the final pH values in the dolomite/DETPMP system solutions. For the **DETPMP/calcite system**, for pH_0 2, the pH goes from pH_f = 7.5 (brine only) down to pH_f ~5 as the DETPMP concentration increases; the corresponding result for pH_0 4 are pH_f ~7.5 (brine only) and pH_f ~5.5 (high DETPMP concentration), and for pH_0 6 are pH_f ~7.5 - 8 (brine only) and pH_f ~6 (high DETPMP concentration). For the **DETPMP/dolomite system**, for pH_0 2, the pH goes from pH_f ~8.2 (brine only) down to pH_f ~6 as the DETPMP concentration increases; the corresponding result for pH_0 4 are pH_f ~8.2 (brine only) and pH_f ~6 (high DETPMP concentration) and for pH_0 6 are pH_f ~8.2 (brine only) and pH_f ~7 (high DETPMP concentration).
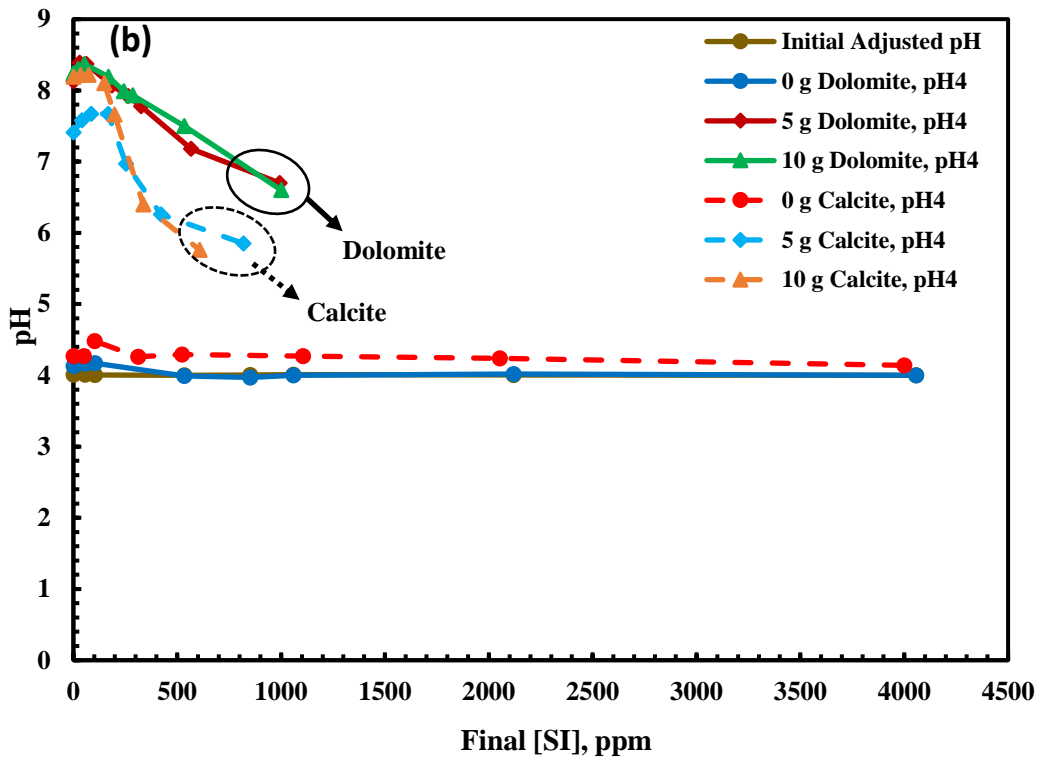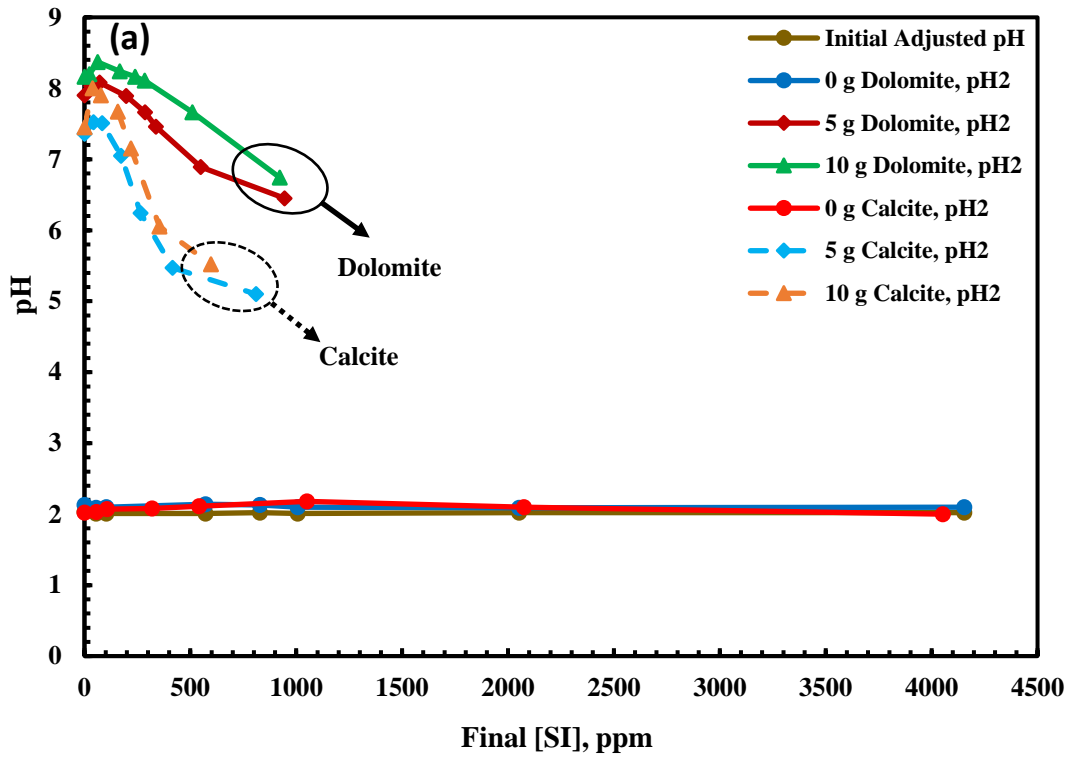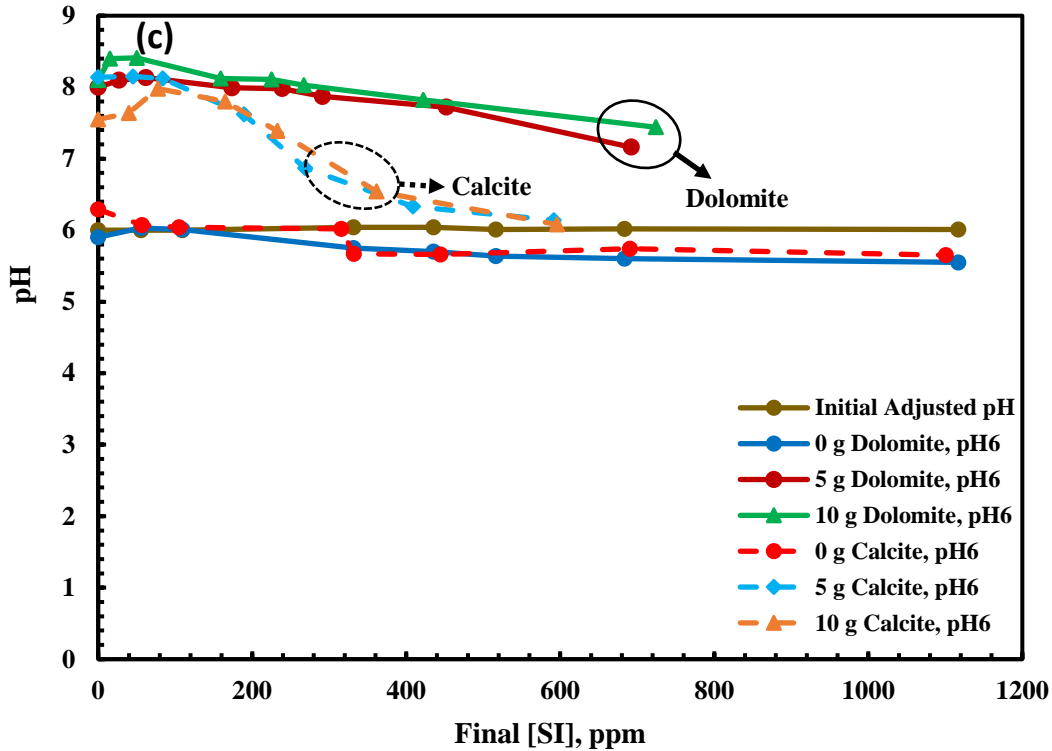
Figure 4.8. Comparison of pH for DETPMP onto two masses (m = 5g and 10g) of calcite and dolomite at (a) pH_0 2 (b) pH_0 4 (c) pH_0 6 & T = 95°C for all tests

Final Calcium Concentrations, $[Ca2+]_f$: For all of the apparent adsorption vs. C_f measurements, the final levels of solution calcium ion concentrations, $[Ca^{2+}]_f$, have also been measured by ICP-OES. These calcium results are presented as *normalised* concentrations, i.e. $([Ca^{2+}]_f /[Ca^{2+}]_0)$ in Figure 4.9(a), Figure 4.9(b) and Figure 4.9(c); the initial calcium concentration in the NSSW is $[Ca^{2+}]_0 = 428ppm$. Again, we first focus on the normalised calcium results for the compatibility (no mineral) tests in these figures; clearly the compatibility results for the pH_0 2 and 4 cases in Figure 4.9(a) and Figure 4.9(b) show that the solutions are completely compatible since normalised calcium $([Ca^{2+}]_f /[Ca^{2+}]_0) = 1$ at all DETPMP concentration. However, for the pH_0 6 case in Figure 4.6(c), the normalised calcium $([Ca^{2+}]_f /[Ca^{2+}]_0)$ is < 1 and drops as low as ~0.4 (~170 ppm) at the highest DETPMP concentration tested, showing that this solution is incompatible and some precipitation occurs (of SI/Ca complex). We now consider the cases in the presence of the carbonate minerals and it is clear from these results that the carbonate rock is taking part in the reaction scheme to some degree in most of these cases. In all cases (pH_0 2, 4 and 6) the final calcium levels are always higher for the calcite than for the dolomite, confirming that the calcite in indeed more reactive. Most calcite dissolution is, as

expected, observed in the pH_0 2 case in Figure 4.9(a) where the normalised calcium level reaches ($[Ca^{2+}]_f /[Ca^{2+}]_0$) ≈ 1.6 (~680 ppm); for the DETPMP/calcite system it is also found that the final ($[Ca^{2+}]_f /[Ca^{2+}]_0$) ≈ 1.2 for pH_0 4 and ≈ 1.05 for pH_0 6. In contrast, the dolomite behaviour is rather different. Only in the pH_0 2 case, for lower values of DETPMP concentrations do we see normalised calcium > 1; in fact it is ~1.3 – 1.4 for DETPMP at values of final SI concentration, C_f <500ppm. In the other higher initial pH cases where pH_0 4 and 6, then the normalised calcium is reduced below 1 in nearly all cases for the DETPMP/dolomite system.   This implies that the precipitate (the DETPMP/Ca complex) in the dolomite case actually removes any leached Ca from the carbonate rocks and some of the initial solution calcium from the system. This will be quantified and demonstrated further in the mass balance calculation presented below.

117
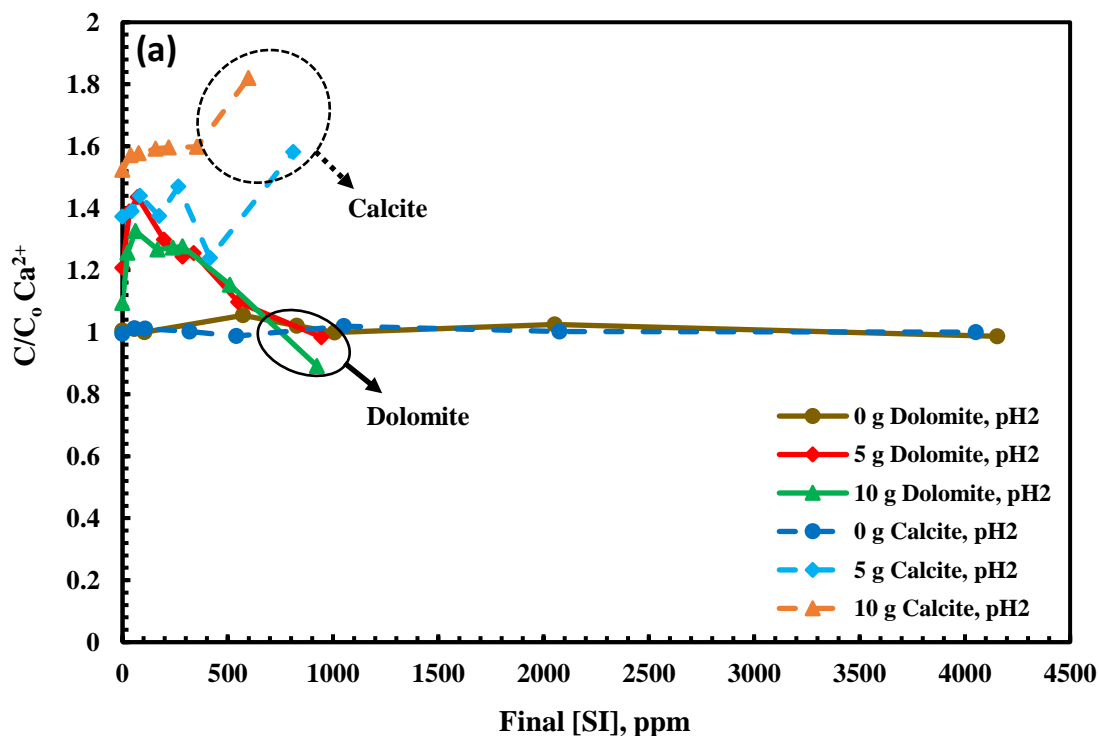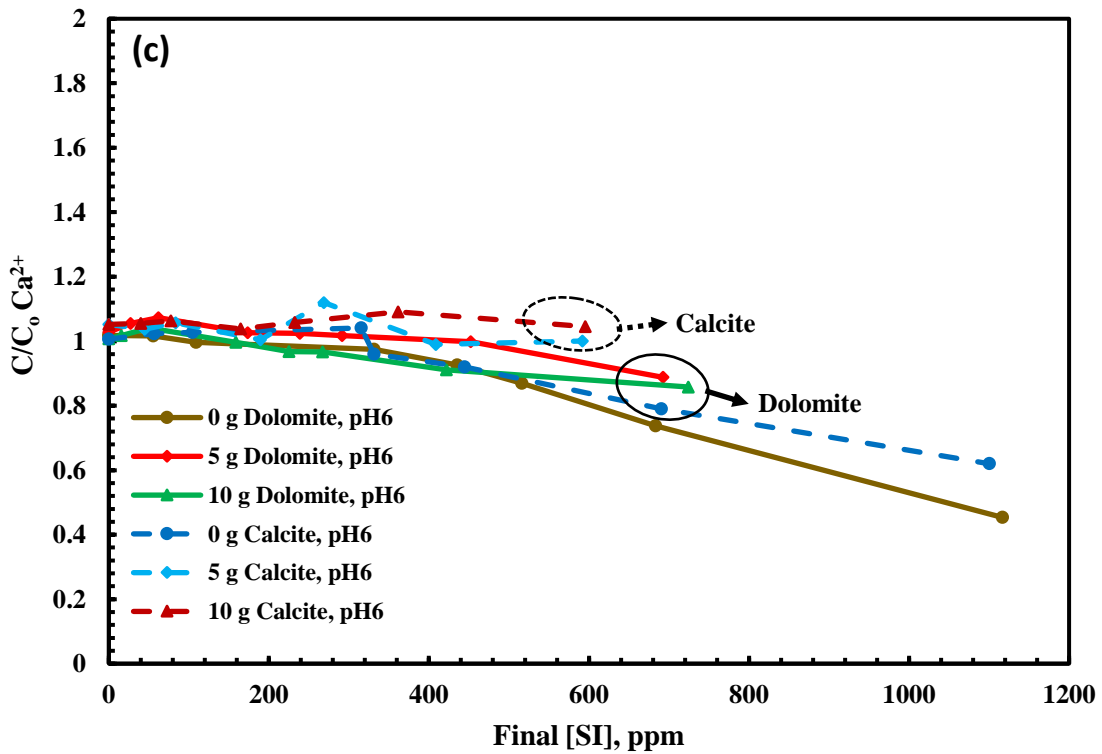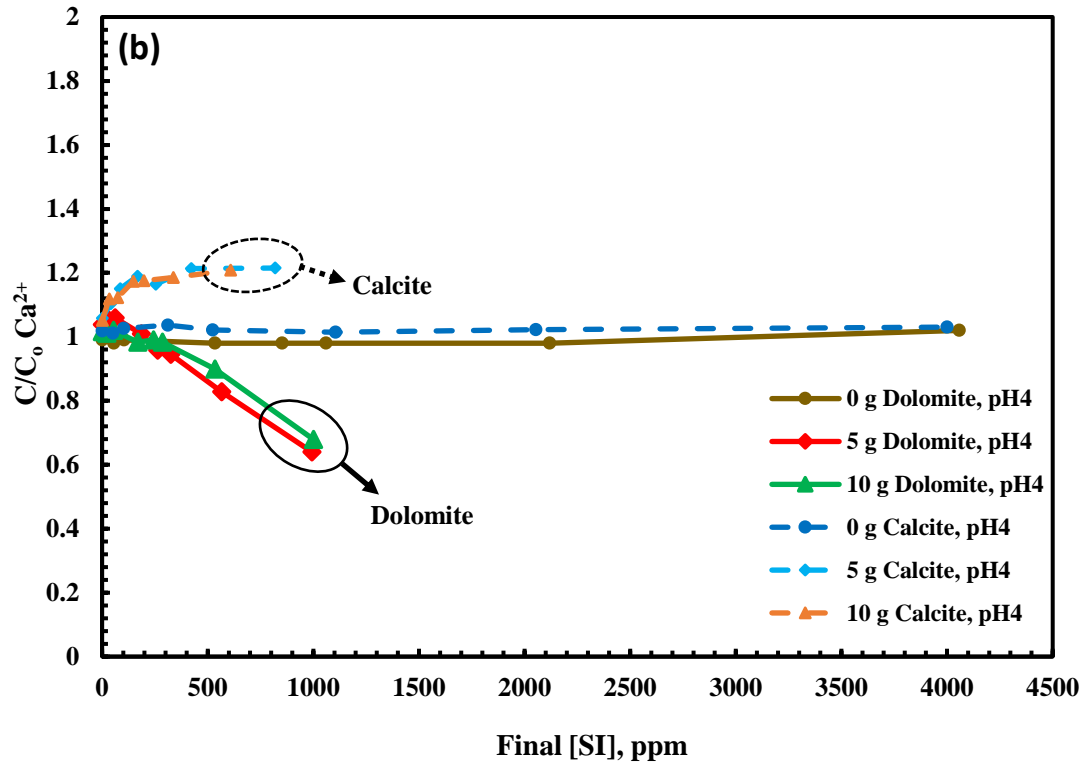
Figure 4.9. Comparison of C/C_0 Ca^{2+} for DETPMP onto two masses (m = 5g and 10g) of calcite and dolomite at (a) pH_0 2 (b) pH_0 4 (c) pH_0 6 & T = 95°C for all tests

118

ESEM/EDX Analysis for DETPMP-Dolomite and DETPMP-Calcite Systems: After the filtration of the solids (either just mineral substrate or substrate + precipitated SI/Ca complex), the filter papers were dried, photographed and used for ESEM/EDX analysis. This was carried out to investigate the morphology of the precipitated complex in the presence of calcite and dolomite substrate. In particular, we wished to establish if the precipitate was formed as a grain coating around the calcite and dolomite particles or whether it formed independently as a bulk solution precipitate.

Figure 4.10 and Table 1.1. and Table 4.2. present ESEM/EDX results for the DETPMP/calcite system, and Figure 4.11 and Table 4.3. & Table 4.4 present the ESEM/EDX results for the DETPMP/dolomite system.
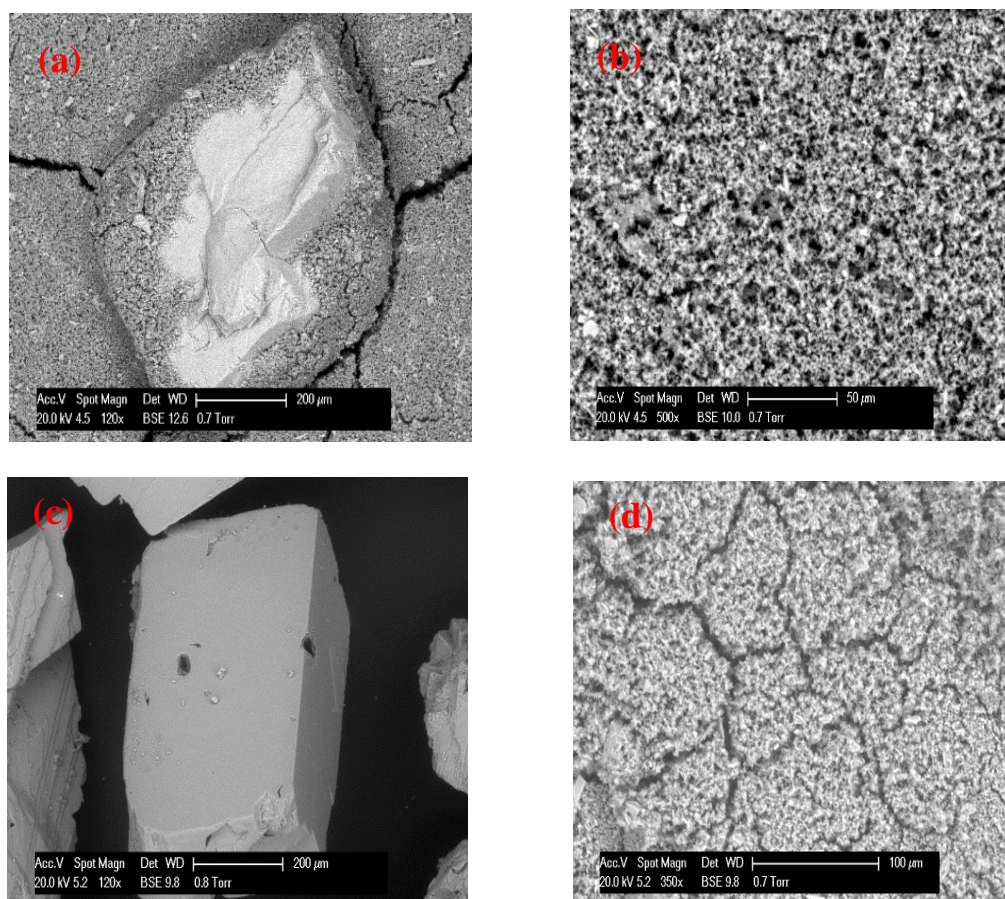
Figure 4.10. Morphology of calcite grains and precipitate at 4000ppm DETPMP from ESEM photographed samples a) calcite grain (pH0 2) b) bulk precipitate (pH$_0$ 2) c) calcite grain (pH$_0$ 4) d) bulk precipitate (pH$_0$ 4) e) calcite grain (pH0 6) f) bulk precipitate (pH$_0$ 6) g) bulk precipitate, compatibility test, pH$_0$ 6

Table 4.1. EDX analysis of 4000ppm DETPMP for 100-315µm calcite at pH$_0$ 2& 4 from ESEM

Element	Calcite grain 4000 ppm (pH$_0$ 2) % Weight	% Atomic	Bulk precipitate 4000 ppm (pH$_0$ 2) % Weight	% Atomic	Calcite grain 4000 ppm (pH$_0$ 4) % Weight	% Atomic	Bulk precipitate 4000ppm (pH$_0$ 4) % Weight	% Atomic
C	18	27	20	30	37	48	8	12
O	49	56	40	52	48	45	51	64
Na	2	1	1	1	-	-	3	2
Mg	2	2	4	3	-	-	5	4
P	8	5	15	8	0.4	0.2	14	9
Cl	3	1	3	2	-	-	6	3
Ca	18	8	11	8	16.6	6.8	13	7

Table 4.2. EDX analysis of 4000ppm DETPMP for 100-315μm calcite and Compatibility test at pH_0 6 from ESEM

Element	Calcite grain 4000 ppm (pH_0 6)		Bulk precipitate 4000 ppm (pH_0 6)		Compatibility Test 4000 ppm (pH_0 6)	
	% Weight	% Atomic	% Weight	% Atomic	% Weight	% Atomic
C	10	17	-	-	17	26
O	49	61	54	69	40	47
Na	1	1	3	3	2	2
Mg	1	1	8	6	8	6
P	3	2	18	12	19	11
Cl	1	1	6	5	7	4
Ca	35	17	11	5	7	4

As shown in Figure 4.10 and Table 4.1 &Table 4.2. for the DETPMP results at pH_0 4 & 6, phosphorous is clearly detected at a high level (~15% by weight) in the finer precipitate which forms in the bulk mainly on the filter paper. This is illustrated in Figure 4.10(a) & Figure 4.10(b) and Table 1.1. (DETPMP/Calcite at pH_0 2). However, there is a detectable amount (~8% by weight) on the calcite grains themselves for the 4000ppm DETPMP case at pH_0 2 (Figure 4.10(a), Table 4.1). This amount is possibly some of the SI/Ca precipitate adhering to the calcite surface or is part of the adsorbed SI. Therefore, we observed no "surface coating" of the SI/Ca complex around the calcite grains in these experiments, and we see no evidence for the hypothesis of "surface poisoning" by the Ca-DETPMP complex. In addition, the amount of phosphorus detected by EDX for two different initial pH values, pH_0=2 and 4, are quite similar (~ 15% by weight) and it confirms that the amount of apparent adsorption for these pH values are quite similar, as shown in Figure 4.10(a) & Figure 4.10(b).

As pH is increased from 2 to 6, the SI interacts more with Ca^{2+} from the NSSW in the compatibility test (no substrate) showing DETPMP is incompatible with NSSW at pH_0 6 (contrary to pH_0 2& 4). Hence, a similar quantity of phosphorous is detected at 4000 ppm in the compatibility test (~18% by weight; see Figure 4.10(g)) which is similar to the phosphorus detected in the adsorption test (~ 18% by weight) (Figure 4.10(f)). Furthermore, as the pH of the DETPMP solutions increases, the amount of phosphorous detected clearly increases which supports the corresponding static apparent adsorption experimental results.
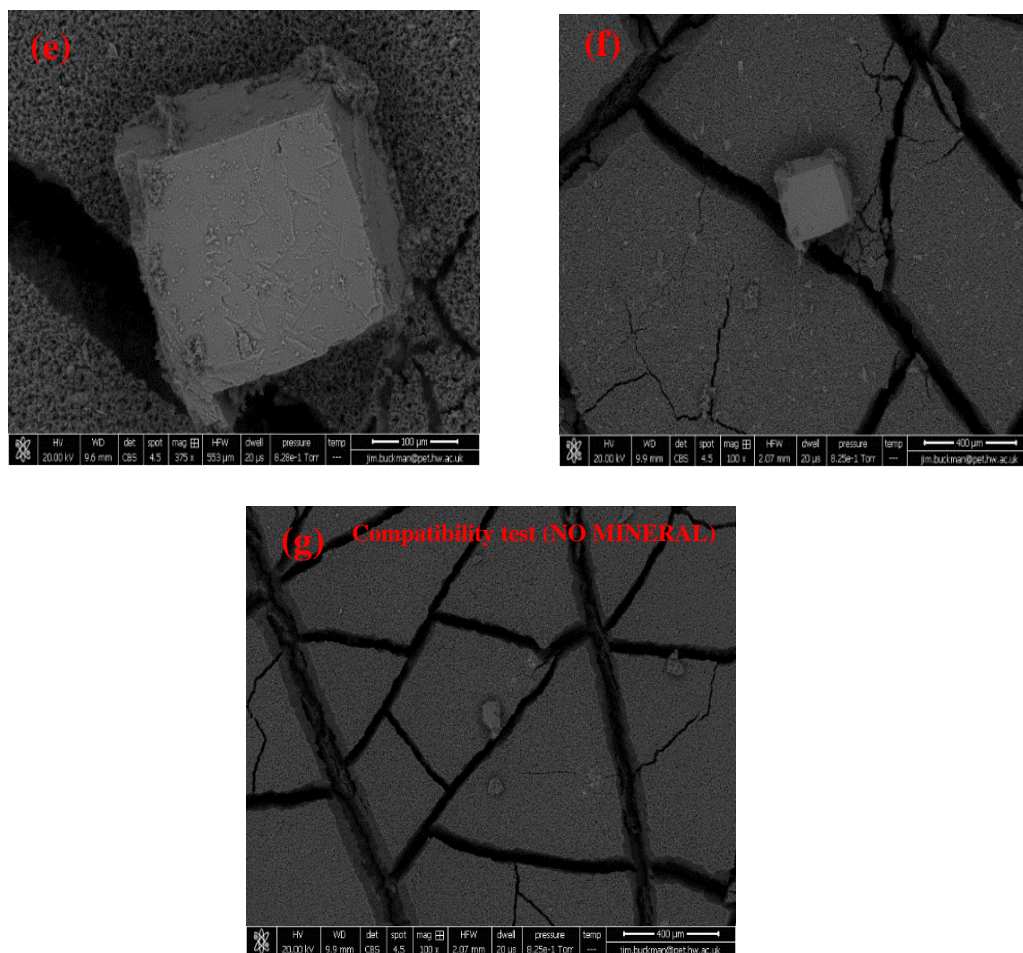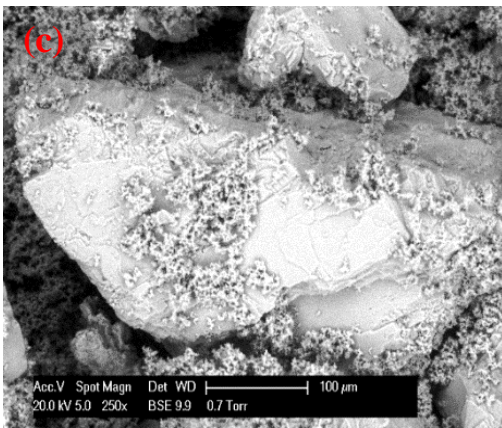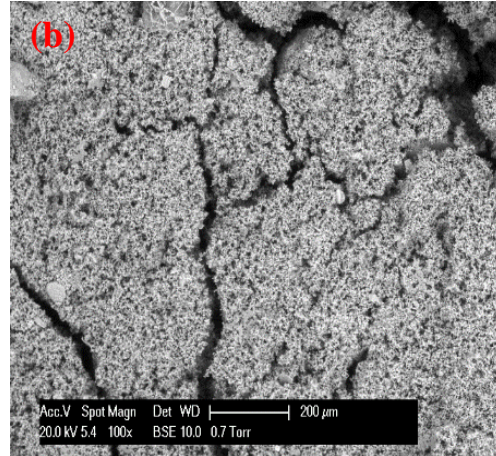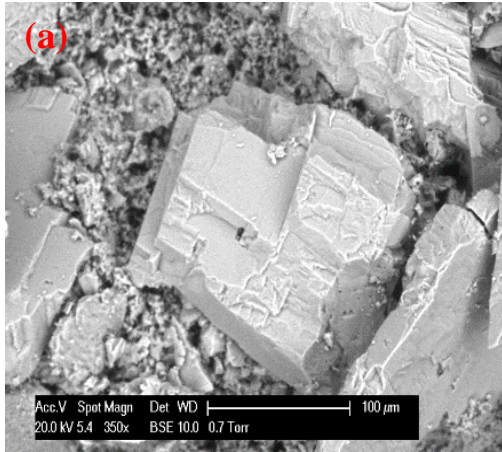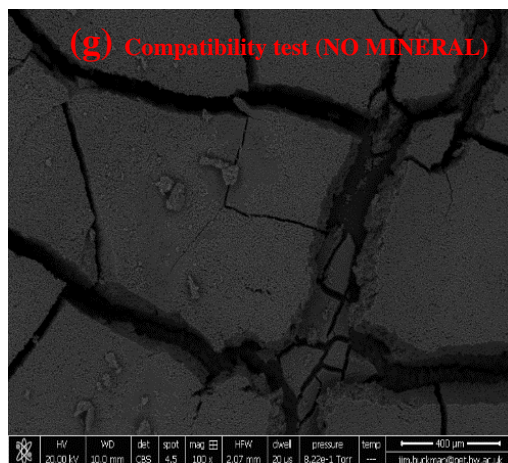
Figure 4.11. Morphology of dolomite grains and precipitate at 4000ppm DETPMP from ESEM photographed samples a) dolomite grain (pH_0 2) b) bulk precipitate (pH_0 2) c) dolomite grain (pH_0 4) d) bulk precipitate (pH_0 4) e) dolomite grain (pH_0 6) f) bulk precipitate (pH_0 6) g) bulk precipitate, compatibility test, pH_0 6

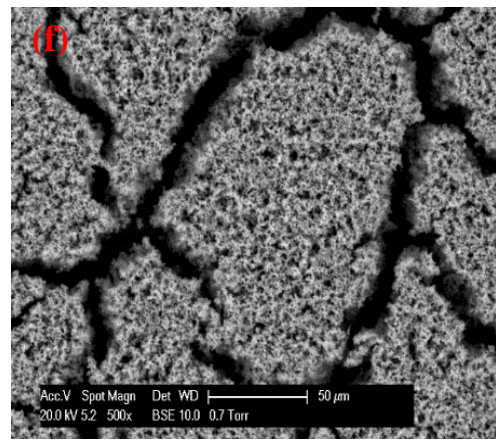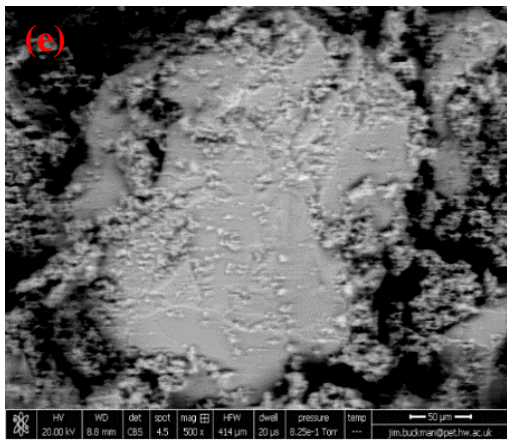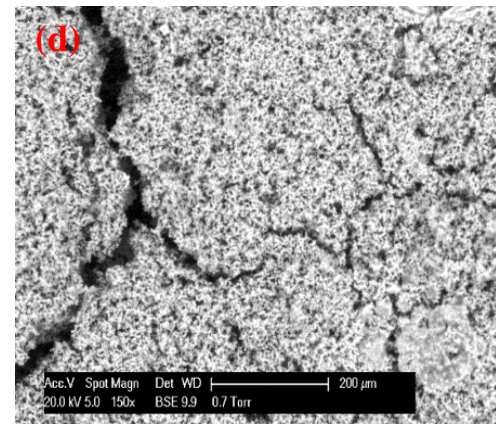Table 4.3. EDX analysis of 4000 ppm DETPMP for 100-315 µm dolomite at pH_0 2& 4 from ESEM

Element	Dolomite grain 4000 ppm (pH_0 2) % Weight	% Atomic	Bulk precipitate 4000 ppm (pH_0 2) % Weight	% Atomic	Dolomite grain 4000 ppm (pH_0 4) % Weight	% Atomic	Bulk precipitate 4000ppm (pH_0 4) % Weight	% Atomic
C	15	22	19	28	-	-	19	28
O	55	62	49	54	63	77	47	52
Mg	9	6	7	5	14	11	7	5
P	4	2	13	7	2	1	13	7
Cl	1	1	2	2	1	1	5	2
Ca	16	7	10	4	20	10	8	6

Table 4.4. EDX analysis of 4000 ppm DETPMP for 100-315 µm dolomite and Compatibility test at pH_0 6 from ESEM

Element	Dolomite grain 4000 ppm (pH_0 6) % Weight	% Atomic	Bulk precipitate 4000 ppm (pH_0 6) % Weight	% Atomic	Compatibility Test 4000 ppm (pH_0 6) % Weight	% Atomic
C	17	24	5	11	12	21
O	54	59	25	38	33	43
Na	8	7	9	9	9	7
Mg	6	3	21	16	25	16
P	2	1	7	5	8	5
Ca	13	6	33	21	13	8

As shown in Figure 4.11 and Table 4.3. & Table 4.4 for the DETPMP/dolomite tests, high levels of phosphorus (P) have been detected in the compatibility test for 4000 ppm DETPMP (~25%) which is similar to the quantity of phosphorous detected at 4000 ppm in the adsorption test (~21% by weight) at pH_0 6. However, there are some detectable quantities of P on the dolomite grains themselves, as for the 4000 ppm DETPMP cases ([P] ~ 6% by weight on the grains) which are possibly due to some of the SI/Ca precipitate adhering to the dolomite surface or it may possibly be a part of the adsorbed SI. In addition, the amount of calcium, magnesium and phosphorus detected by EDX at two initial adjusted pH values (pH_0 2&4) are quite similar which confirms that the amount of missing phosphorus and cations due to the formation of SI/M^{2+} complex in the corresponding apparent adsorption experiment are very similar. However, when the pH is increased to pH_0=6, the quantity of phosphorus detected increases remarkably (~21% by weight), which is more than in the pH_0 2 &4 cases and this again proves that pH plays a more important role in the formation of DETPMP/Ca complex than the amount of calcium, which is higher for the acidic pH values, pH_0 2 & 4. Thus, the higher the pH, the more DETPMP retention on the substrate (i.e. more precipitation) occurs. Furthermore, the amount of phosphorus detected through EDX analysis for DETPMP/dolomite system is greater than for the DETPMP/calcite which supports the apparent adsorption results reported above.

Mass Balance Calculation for the DETPMP/Carbonate System

Mass Balance Equations: Figure 4.12 shows a schematic of the mass balances occurring in an apparent adsorption experiment, where Figure 4.12 (a) shown the initial (t=0) state of the system. This shows the situation at $t = 0$, immediately after the carbonate substrate (of mass = m) is added to the DETPMP solution at a given initial pH= pH_0 and Ca^{2+} (denoted $C_{1,0}$) and DETPMP concentration (denoted $C_{2,0}$). The resulting equilibrium system is shown in Figure 4.12(b), where the supernatant has a final level of [Ca^{2+}] = $C_{1,f}$ and [DETPMP] = $C_{2,f}$, and the pH = pH_f. A mass of precipitated complex (SI_Ca_n where n = stoichiometry, the number of Ca ions per molecule of DETPMP) has formed and is denoted by Π and the final mass of carbonate substrate is denoted m'. Note that precipitation Π is in units of moles (or mass) per unit volume of liquid. Since some carbonate dissolution has occurred then, $m' < m$. In addition, there may be some actual SI adsorption on the carbonate substrate which we denote Γ, but we have demonstrated

by measurement (in Figure 4.7) that this level is very small. By definition, apparent adsorption is given as follows in the notation above as:

$$\Gamma_{app} = \frac{V\,(C_{1,o} - C_{1,f})}{m} \tag{4.1}$$

and this is the reported value in Figure 4.7. The full physico-chemical description of the process is shown in Figure 4.7 and hence, we may write this same quantity, Γ_{app}, as:

$$\Gamma_{app} = \frac{m'.\Gamma + V.\Pi}{m} \tag{4.2}$$

Since Γ is actually very small and ($\frac{m'}{m} = 0.99$), then $\Gamma_{app} \approx (\frac{V}{m})^{\Pi}$ to a very good approximation.

The mass balance for calcium can now be written as follows, where the initial total mass of Ca, $M_{Ca.T}$, is given by (see Figure 4.12(a)):

$$M_{Ca.T} = V.C_{1,0} + f_{Ca1}.m \tag{4.3}$$

Where f_{Ca1} is the mass fraction of Ca in the carbonate substrate (e.g. for $CaCO_3$, the $f_{Ca1} = 0.407$). The mass balance for total calcium at equilibrium is as follows:

$$M_{Ca.T} = V.C_{1,f} + f_{Ca2}.\,\Gamma_{app}.m + f_{Ca1}.\,m' \tag{4.4}$$

Where f_{Ca2} is the mass fraction of Ca in the SI_Ca$_n$ precipitation complex. This is more complicated to obtain since the stoichiometry of the SI_Ca$_n$ complex, i.e, n, varies with solution chemistry, particularly pH. However, common phosphonates, including DETPMP, have been studied by Shaw et al.[96] and this quantity can be estimated (see below).

The expressions in equation (4. 3) and (4. 4) for the total amount of calcium, $M_{Ca.T}$, are the same quantity and hence:

$$V.C_{1,0} + f_{Ca1}.m = V.C_{1,f} + f_{Ca2}.\,\Gamma_{app}.m + f_{Ca1}.\,m' \tag{4.5}$$

and this can be rearranged to:

$$f_{Ca1}.\,(m - m') = V.\,(C_{1,f} - C_{1,0}) + f_{Ca2}.\,\Gamma_{app}.m \tag{4.6}$$

the quantity on the left hand side (LHS) above is clearly the mass of calcium dissolution from the carbonate substrate, $M_{Ca.D}$. Thus, the quantity ($M_{Ca.D} = V.\,(C_{1,f} - C_{1,0}) + f_{Ca2}.\,\Gamma_{app}.m$) can be

calculated from measured quantities if f_{Ca2} can be obtained. The related quantity of the mass of calcium in both the precipitate and the solution, $M_{Ca.P}$, is given by:

$$M_{Ca.P} = V.C_{1,f} + f_{Ca2}. \Gamma_{app}.m \qquad (4.7)$$

And clearly the quantities $M_{Ca.D}$ and $M_{Ca.P}$ are related by:

$$M_{Ca.D} = M_{Ca.P} - V.C_{1,0} \qquad (4.8)$$

Thus, the total calcium generated by carbonate rock dissolution is equal to the sum of the amount involved in complexation/precipitation and that remaining in solution, minus the initial mass of calcium present in solution ($V.C_{1,0}$). To calculate the f_{Ca2}, we use a combination of experimental data suggested by the modelling developed by Silva et al.[94] as shown in Figure 4.13.

$[Ca^{2+}]_0 = C_{1,0}$

$[DETPMP]_0 = C_{2,0}$

V= Volume of Solution

m= mass of substrate

No Precipitation (Π=0)

a) Before precipitation

$[Ca^{2+}]_f = C_{1,f}$

$[DETPMP]_f = C_{2,f}$

V

m'   Π

$\Gamma_{app,f}$

b) After precipitation
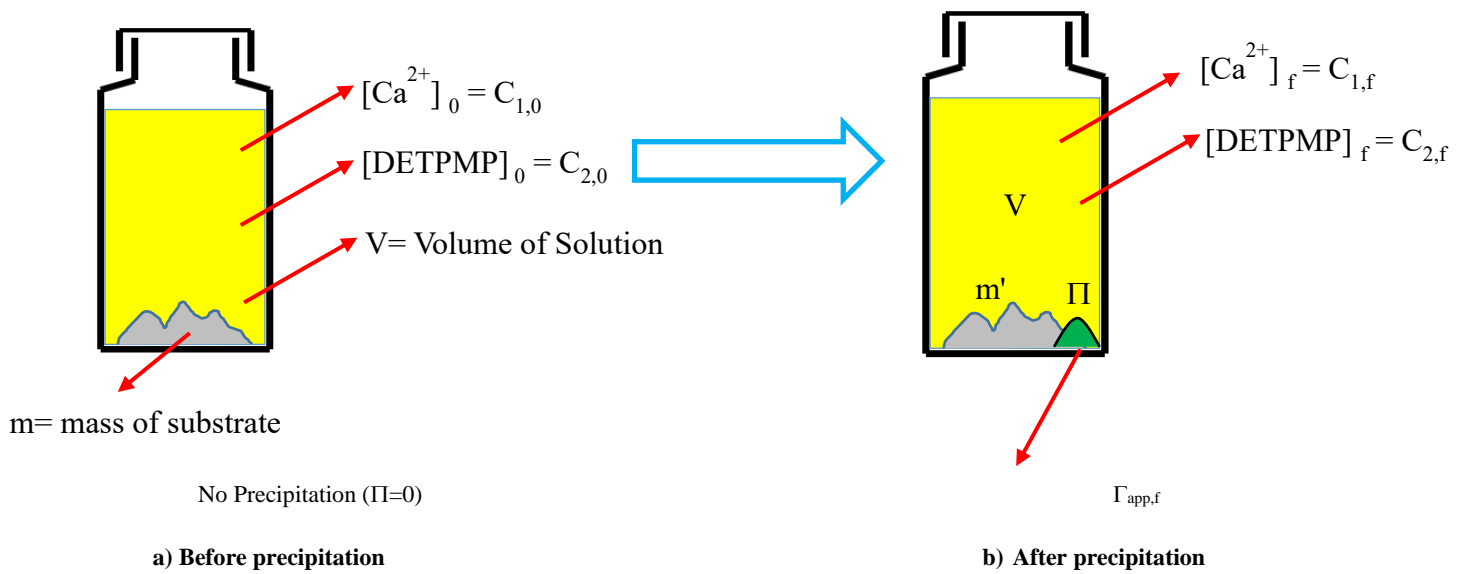
Figure 4.12. Schematic of Scale Inhibitor/ Rock system a) before precipitation b) after precipitation[97]
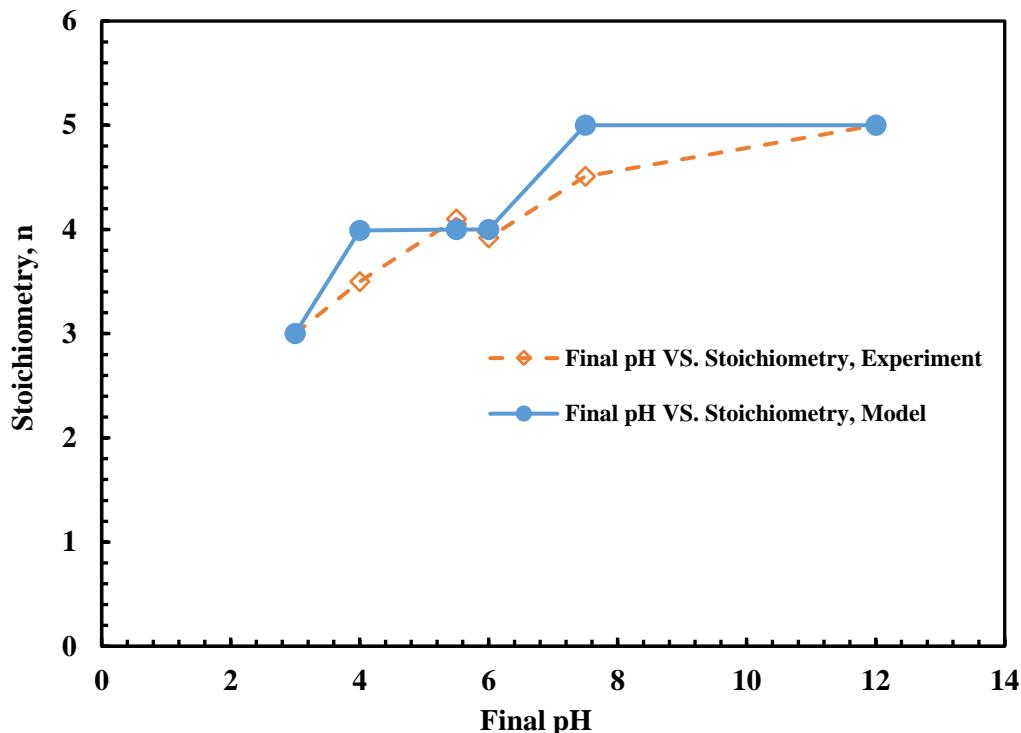
Figure 4.13. Match between experimental and modelling results for stoichiometry of Ca^{2+} involved in complexation with DETPMP as a function of the final pH; Silva et al.[94]

Mass Balance Results: The mass balance approach presented above is now used to calculate various useful quantities. Firstly, the calculated amount of Ca^{2+} generated by carbonate rock dissolution is shown for all apparent adsorption experiments in Figure 4.14 for calcite and in Figure 4.15 for dolomite. Note that in these figures we plot the amounts of calcium vs. the *initial* DETPMP concentrations and that results for calcite are up to 2000ppm of DETPMP (Figure 4.14), and for dolomite they are given up to 4000ppm (Figure 4.15); also note that the apparent adsorption results for both the m = 5g and 10g substrate masses (duplicates of each) are combined, as shown in the error bars. Both of these figures are qualitatively similar in that more Ca dissolution from the rock occurs at lower initial pH_0 values and as the DETPMP concentration increases; that is rock dissolution is enhanced both by lowering pH (more acid) and by increasing [DETPMP] (more complexation). Relatively more Ca dissolution occurs for calcite than dolomite, which is best seen by comparing the initial [DETPMP] = 2000ppm results in Figure 4.14 and Figure 4.15; this comparison shows that for [DETPMP] = 2000ppm for pH_0 2, then ~21mg of Ca is produced by rock dissolution for calcite, and ~16 mg Ca for dolomite. However,

the rock Ca dissolution amounts are quite similar for both calcite and dolomite at the other initial values of pH_0 4 and 6.
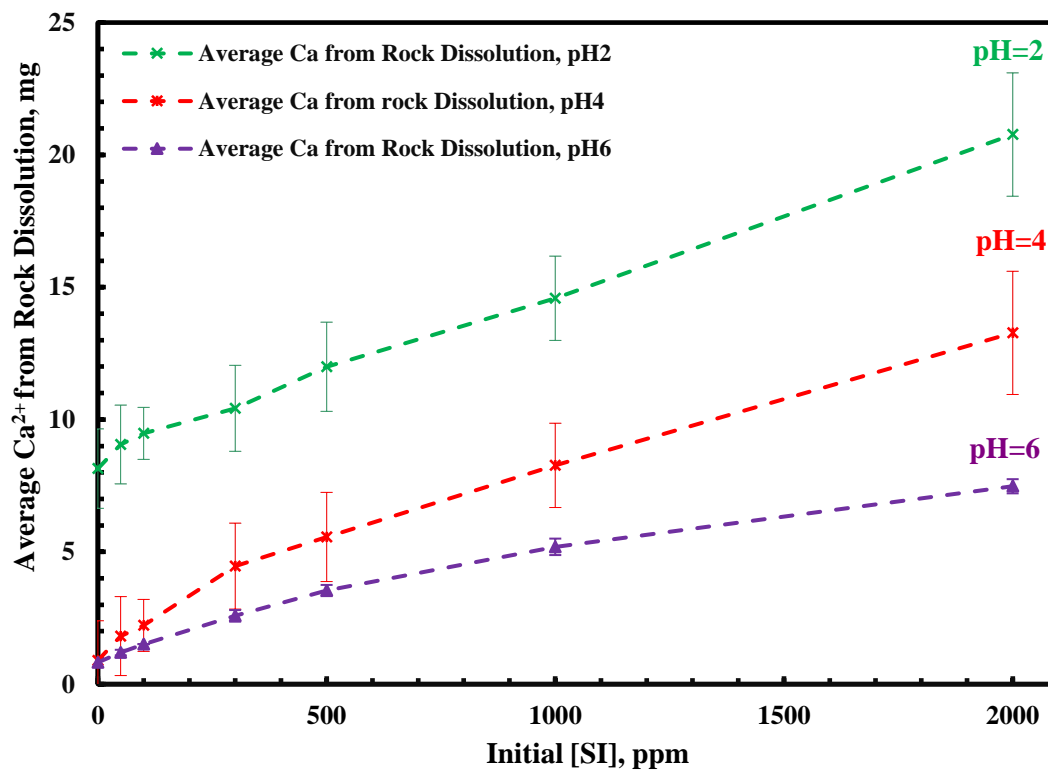
Figure 4.14. Average Calcium Generated from Calcite Dissolution Results
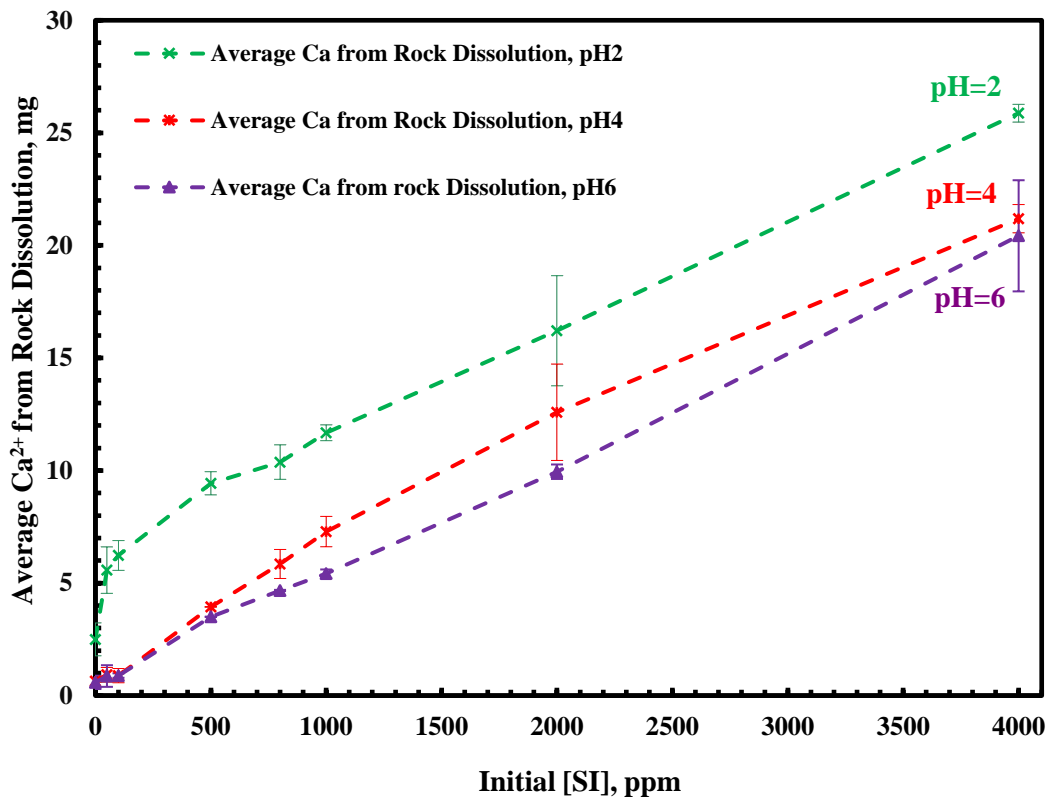
Figure 4.15. Average Calcium Generated from Dolomite Dissolution Results

The mass balance analytical approach above is now used to determine how much calcium is involved in complexation and how much is left in solution. We calculate both the average amount of calcium in solution and the average amount in the precipitate for every apparent adsorption experiment; "average" in this context means an average over both the (duplicate samples) of the m = 5g and 10g results. Figure 4.16 and Figure 4.17 show the "Ca in solution" and the "Ca in precipitate" results for all experiments for calcite and dolomite, respectively. Both of these figures for calcite and dolomite show that for [DETPMP] up to and including the 100ppm level, all the calcium is in the solution and none is in the precipitate, since obviously no precipitate formed. At DETPMP concentrations above 100ppm, then some calcium is shown as being in the precipitate and this amount increases in all cases as the concentration increases and this quantity (and the proportion of the total Ca in the precipitate) also increases as pH_0 increases. Plotting the results in this way highlights that more calcium is observed in the precipitate in the dolomite case (Figure 4.16) compared with the calcite case (Figure 4.17), which is completely consistent with the direct apparent adsorption results (Γ_{app}) themselves.
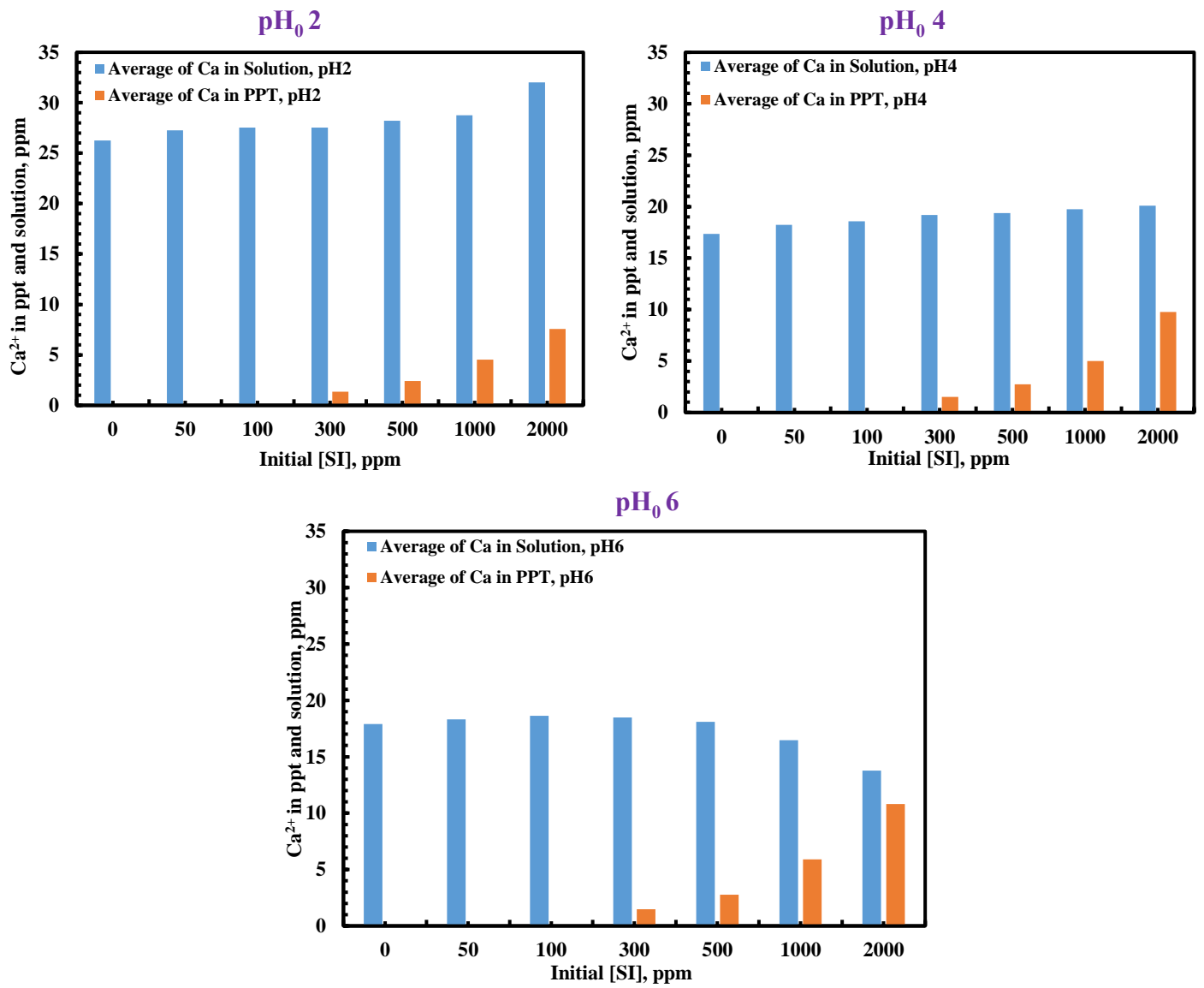
Figure 4.16. Calcium in Precipitation (PPT) and Solution Results in DETPMP/Calcite System
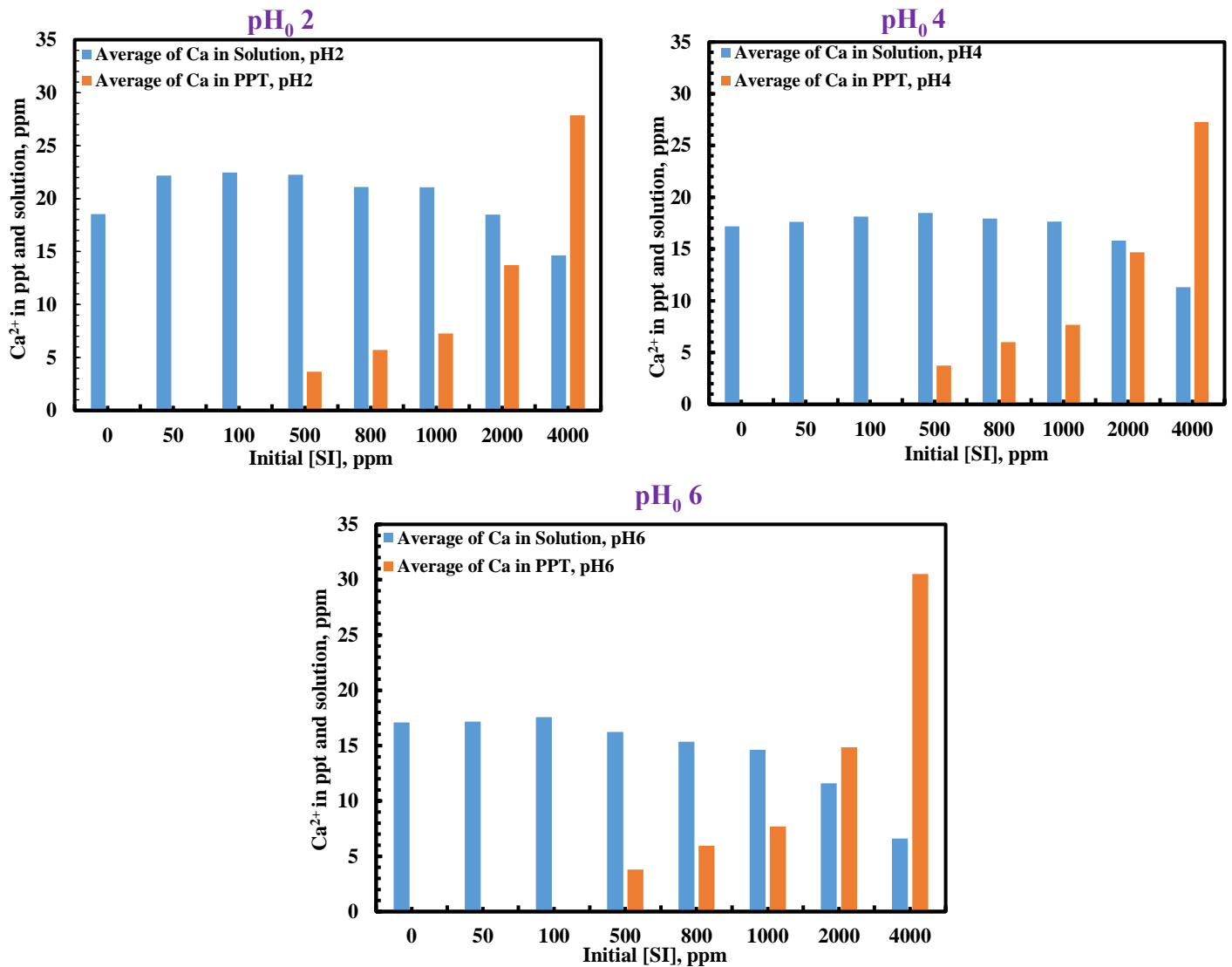
Figure 4.17. Calcium in Precipitation (PPT) and Solution Results in DETPMP/Dolomite System

Description and Explanation of the Observed Apparent Adsorption Results

The Chemical System: The DETPMP/carbonate system in the experiments reported in this work is governed by 3 main chemical processes, as follows:

(i)   **DETPMP as a weak poly-acid:** Phosphonate scale inhibitors dissociate like weak poly-acid, where DETPMP can be considered as the weak poly-acid, $H_{10}A$. The process can be viewed as the successive dissociation shown in Figure 4.18:
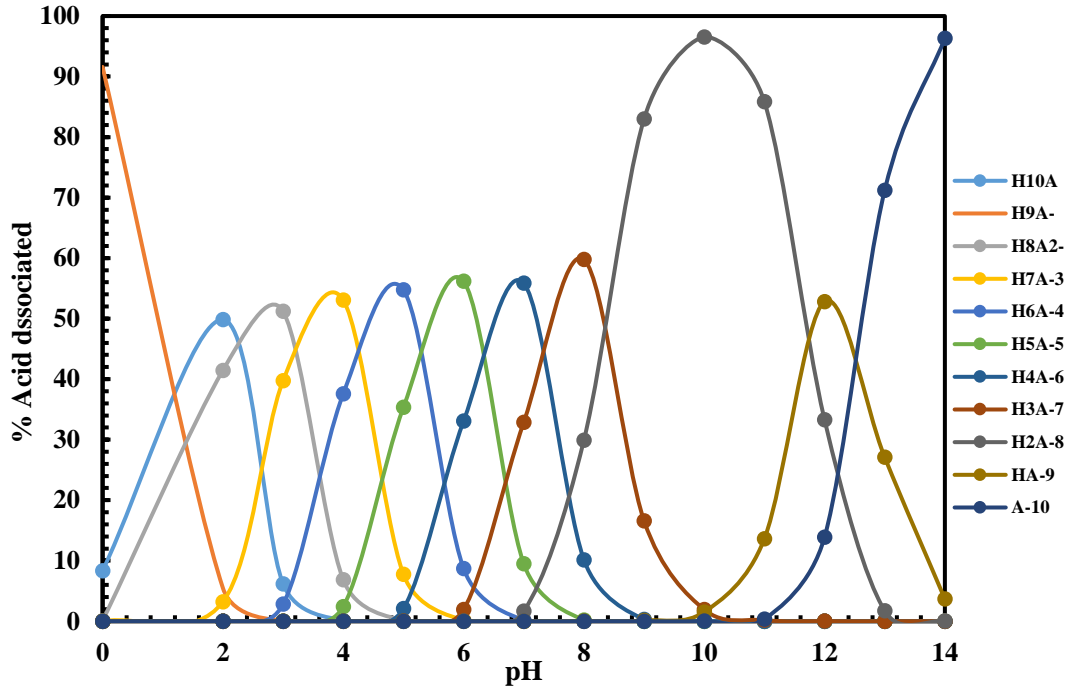
Figure 4.18. Speciation of DETPMP (H10A) with pH[36]

As shown in Figure 4.18, at very low (acidic) pH, the equilibrium is to the left and the molecule is more associated as $H_{10}A$, and at higher pH it is more dissociated into $m.H^+$ and $H_{10-m}A^{m-}$. The dissociated $H_{10-m}A^{m-}$ species is much more likely to complex with Ca^{2+} to form a SI/Ca complex in its dissociated form (i.e. at higher pH values) and less likely to form complexes at lower pH values[96,98]; see (ii) below. Essentially, whatever other reactions are happening in the system, the DETPMP molecule responds to the local pH by speciating to the appropriate changed entity, as follows:

$$H_nA \longrightarrow H_{n-1}A^- + H^+$$

$$H_{n-i}A^{-i} \longrightarrow H_{n-(i+1)}A^{-(i+1)} + H^+ \qquad\qquad i = 1, 2, \ldots, n$$
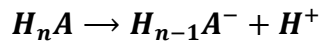
(ii)   **Ca/Mg – SI Binding and Complex Formation:** complexation between the dissociated SI (DETPMP) and the Ca^{2+} (and Mg^{2+}) occurs to form a complex denoted SI_Ca_n, which is sparingly soluble and may precipitate. The stoichiometry is described by the

n, which is the ratio of Ca ions to DETPMP molecules.   The complexation process of SI with divalent cations (mainly Ca^{2+}) is described as follows:

$$Ca^{2+} + \left(\frac{2}{i}\right)H_{n-1}A^{-i} \rightarrow Ca^{2+}[H_{n-1}A^{-i}]_{\left(\frac{2}{i}\right)} \qquad\qquad i = 1, 2, ..., n$$

$$Mg^{2+} + \left(\frac{2}{i}\right)H_{n-1}A^{-i} \rightarrow Mg^{2+}[H_{n-1}A^{-i}]_{\left(\frac{2}{i}\right)} \qquad\qquad i = 1, 2, ..., n$$
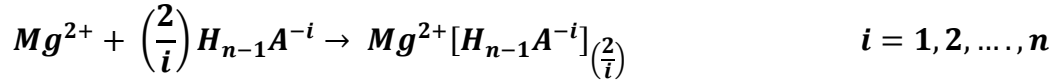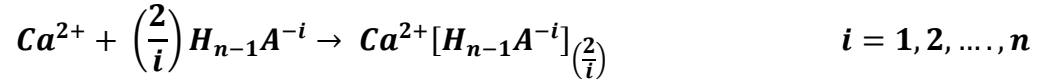
(iii)　　**The Carbonate System:** the interaction of the SI dissociation and the Ca/Mg binding with the carbonate system. That is, the CO_2/bicarbonate/carbonate coupled aqueous and the rock dissolution of the calcite/dolomite, as follows:

$$CO_2 + H_2O \rightarrow HCO_3^- + H^+$$

$$HCO_3^- \rightarrow CO_3^{2-} + H^+$$

$$CaCO_3\ (s)\ \rightarrow Ca^{2+} + CO_3^{2-}$$

$$CaMg(CO_3)_2\ (s)\ \rightarrow Ca^{2+} + Mg^{2+} + 2CO_3^{2-}$$

$$H_2O \rightarrow OH^- + H^+$$
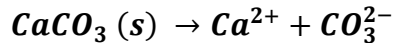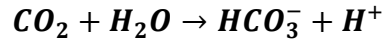
Describing this overall process requires a coupled set of equilibrium equation representing each process, and such a model is describing in Silva et al.[94]. In addition, in Chapter 2, Appendix 2.1 a full model of the process is described. This model requires that we know the quantities of Ca^{2+} generated by rock dissolution, how much is involved in complexation (to form SI_Ca$_n$) and how much remains in solution (as free Ca^{2+} or as soluble SI_Ca$_n$ complex).   Work on applying this model to analyze the results presented here is in progress.

Analysis of the Key Observations: We now consider the apparent adsorption experiments reported in this work in the light of the chemical system described immediately above. That is we wish to explain the observed Γ_{app} vs. C_f results using the supporting measurements of the pH_f and $[Ca^{2+}]_f$ which we have for all Γ_{app} experiments.   As noted above, the ideal case would be to model the complete system in a rigorous manner and reproduce all the results quantitatively. This activity is in progress and here we will consider just *two* key observations which we will explain qualitatively; these are as follows:

(1) *System Behaviour:* That the qualitative behaviour of the calcite and dolomite systems are very similar in terms of the Γ_{app} vs. C_f results for each and the related behaviour of the pH_f and $[Ca^{2+}]_f$.

(2) *Calcite vs. Dolomite Γ_{app}:* That the Γ_{app} for the dolomite case is (counter intuitively) *higher* than for calcite, although calcite is certainly rather more "reactive".

The first point on **system behaviour** above is simply a description of the 3-part chemical system above. That is, when the carbonate mineral is put into the DETPMP/brine solution (which contains ~428ppm Ca^{2+} already) at a given initial pH_0, then several coupled chemical reactions occur, as follows: (i) re-speciation of the DETPMP ($H_{10}A$) in the changing pH solution, (ii) acid dissolution of the rock to produce more Ca^{2+} in solution (more at pH_0 2 than for pH_0 4 or 6), (iii) calcium SI binding to the SI in solution which takes up both the existing Ca^{2+} in solution as well additional Ca^{2+} from the rock to form a SI_Ca_n complex (n = stoichiometry), (iv) the SI_Ca_n complex is sparingly soluble (especially for higher n values) and this may precipitate, (v) the resulting pH changes which occur in this coupled system of reactions leading to the final pH = pH_f. It is evident for this description that the two main factors affecting the amount of precipitation of the DETPMP_Ca_n complex are the pH which determines the degree of dissociation of the DETPMP ($H_{10}A$) and the level of solution Ca^{2+}. More precipitate is expected at higher pH and higher solution $[Ca^{2+}]$; but the question remains: *which of these 2 effects - pH or $[Ca^{2+}]$- is more important in the DETPMP/carbonate system?*

Accepting the above as a qualitative description of the system behaviour, we now go on to explain why we observe the **calcite vs. dolomite** result, i.e. that Γ_{app} is higher for dolomite. In fact, answering the question immediately above also explains why we see the higher Γ_{app} for dolomite. We conclude from pH_f and $[Ca^{2+}]_f$ results that **pH** is in fact the more important factor for the formation of DETPMP_Ca_n complex. In all cases in Figure 4.8, the final pHf was *higher* for dolomite than for calcite, but results in Figure 4.9 show that the $[Ca^{2+}]_f$ was actually *higher* in all cases for calcite. Since it is the same SI (DETPMP) , then it will behave according to whichever factor has the greater effect – pH or $[Ca^{2+}]$ - and it is evident from our results that pH (i.e. the degree of dissociation of the $H_{10}A$ = DETPMP) is more important than the calcium level in solution.

To Sum up this section, the bulk "apparent adsorption" behaviour (Γ_{app} vs. C_f,) one of the most widely applied phosphonate scale inhibitors (DETPMP) on calcite and dolomite mineral substrates has been studied. An extensive series of apparent adsorption experiments were carried out for DETPMP in North Sea Seawater (NSSW) brine at T = 95°C. In addition to measuring Γ_{app} at 2 (m/V) ratios at 3 initial pH_0 values (2, 4 and 6) for a wide range of DETPMP concentrations from 0 to 4000ppm, the final pH_f and $[Ca^{2+}]_f$ values were also measured for all cases. In all experiments where precipitates were formed (of DETPMP_Ca_n complex; n = stoichiometry), these were studied by performing both ESEM and EDX measurement to establish the morphology of the deposits (ESEM) and their compositions (EDX).

A qualitative chemical description of the DETPMP/carbonate system in the experiments reported in this work is presented and it is believed that it is described by 3 main chemical processes, as follows: (i) The treatment of the DETPMP as a weak poly-acid, in this case described by $H_{10}A$, and this of course speciates into higher charged components as pH increases described a set of dissociation contacts. (ii) The binding of Ca^{2+} (and also Mg^{2+}) to the dissociated DETPMP species to form a complex denoted DETPMP_Ca_n, which may precipitate since it is sparingly soluble. (iii) The previous processes are coupled to normal aqueous carbonate system i.e. CO_2/bicarbonate/carbonate/$CaCO_3$ – $CaMg(CO_3)_2$. A qualitative explanation of our results can be given based on this view. A more quantitative model is in development to describe this full coupled system Silva et al[94].

The specific conclusions from this work are as follows:

1. Regions of both pure adsorption (Γ) and coupled adsorption precipitation (Γ/Π) are clearly observed for DETPMP on both calcite and dolomite substrates. Pure adsorption (Γ) is observed in the very low SI concentration region ($\leq 100\ ppm$) on both calcite and dolomite. However, precipitation is more dominant for SI/carbonate retention than adsorption for both calcite and dolomite, in the sense that it occurs over a much wider [SI] range, >100+ppm. The actual amount of precipitate formed varies from case to case, depending on the SI concentration, substrate (calcite/dolomite), initial pH_0 and temperature T (although a fixed T = 95°C was used in this work).

2. Qualitatively, both the DETPMP/dolomite and DETPMP/calcite systems behave quite similarly, in that they both show very similar trends in apparent adsorption and in the resulting final pH and final $[Ca^{2+}]$ behaviour. For both the DETPMP/dolomite and DETPMP/calcite systems, apparent adsorption (Γ/Π) increases with increased pH and $[Ca^{2+}]$. However, there are some quantitative differences between these systems in that (i) apparent adsorption is *higher* for dolomite than for calcite, (ii) the final pH_f is also higher for dolomite than calcite, and (iii) the final $[Ca^{2+}]_f$ is lower for dolomite than calcite. These observations are related through a complex coupling of the SI/substrate chemistry where the joint effect of the higher final pH of the DETPMP/dolomite system leads to a more dissociated DETPMP and a higher Γ_{app} resulting in a lower final Ca^{2+} level. Indeed, this results demonstrates that the formation of DETPMP/Ca complex is more affected by pH than by $[Ca^{2+}]$. Previous work has shown that this is *not* the case for the polymeric scale inhibitor, PPCA, which shows the opposite effect, i.e. $[Ca^{2+}]$ is more important than pH in determining the amount of precipitated SI/Ca complex.

3. All solid samples (carbonate substrate and SI/Ca complex precipitate) were examined by ESEM to establish the morphology of the precipitates in particular, and EDX to establish their compositions. ESEM/EDX results detected high levels of P (phosphorus; from the DETPMP) concentrations in the deposit where clear Γ/Π occurred and these increase as Γ_{app} (precipitation) increases. Very little P is detected directly on the calcite or dolomite grain surfaces although traces are sometimes seen. No evidence is seen of any "coating" or "poisoning" of the SI/Ca complex on the calcite or dolomite grains. Thus, the DETPMP/Ca complex precipitation is principally a bulk solution phenomenon rather than being a grain surface reaction.

4. Mass balance calculations showed that the level of calcium generated in calcite is higher than in dolomite as we expected (calcite has relatively more calcium than dolomite). In addition, the amount of calcium left in solution in calcite/DETPMP system is higher than in dolomite/DETPMP system. Also, the calcium extent of complexation in dolomite/DETPMP system is higher than in calcite/DETPMP system; this extent relates to the stoichiometry, n, in the DETPMP_Ca_n complex.

5. An equilibrium model describing the inhibitor dissociation (where DETPMP = $H_{10}A$, a weak poly acid), the Ca- binding to the dissociated SI species and the precipitation of the SI_Ca_n complex, coupled to the carbonate system has been applied to qualitatively to explain theses experimental findings.

4.4.   Polymeric Scale Inhibitors Retention in Carbonates

In this section, the bulk "apparent adsorption" behaviour (Γ_{app}, vs. C_f) of two polymeric scale inhibitors (SI), PolyPhosphino Carboxylic Acid (PPCA) and Phosphorus-Functionalized Co-Polymer (PFC), onto carbonate mineral substrates (calcite and dolomite) has been studied for initial solution pH values of pH_0 = 2, 4 and 6. In nearly all cases, precipitates formed at higher SI concentrations were due to the formation of sparingly soluble SI/Ca complexes. A systematic study has been carried out on the SI/Ca precipitates formed, by applying both Environmental Scanning Electron Microscopy - Energy Dispersive X-Ray (ESEM/EDX) and particle size analysis (PSA), and this identifies the morphology and the approximate composition of the precipitates.

For PPCA, at all initial solution pH values, regions of pure adsorption (Γ) ([PPCA] <100ppm) and coupled adsorption/ precipitation (Γ/Π) are clearly observed for both calcite and dolomite. PFC at pH_0 = 4 and 6 also showed very similar behaviour with a region of pure adsorption (Γ) for [PFC] < 500ppm and a region of coupled adsorption/precipitation (Γ/Π) above this level. However, the PFC/calcite case at pH 2 showed only pure adsorption, while the PFC/dolomite case at pH 2 again showed coupled adsorption/ precipitation at higher PFC concentrations. For both SIs on both carbonate substrates, precipitation is the more dominant mechanism for SI retention than adsorption above a minimum concentration of approximately 100 – 500 ppm SI. The actual amount of precipitate formed varies from case to case, depending on the specific SI, substrate (calcite/dolomite) and initial pH (pH_0 2, 4 and 6).

Although the qualitative behaviours of both PPCA and PFC were similar on both carbonate substrates, the apparent adsorption of PPCA was higher on calcite than on dolomite, and the apparent adsorption of PFC was higher on dolomite than on calcite. We discuss here how these observations are related to the reactivity of the different carbonate minerals, the resulting final

pH (which affects the dissociation of the SI), Ca-SI binding and the solubility of the resulting complex.

Here, we present the results of the static coupled adsorption/precipitation (Γ/Π) experiments; which we have referred to as apparent adsorption experiments. Figure 4.19 and Figure 4.20 show the apparent adsorption level of PPCA and PFC for two different masses (m = 5g and 10g) of 100-315μm calcite and dolomite as a function of the final SI concentration in synthetic NSSW at initial pH values of pH = 2, 4 and 6 at 95°C, respectively.
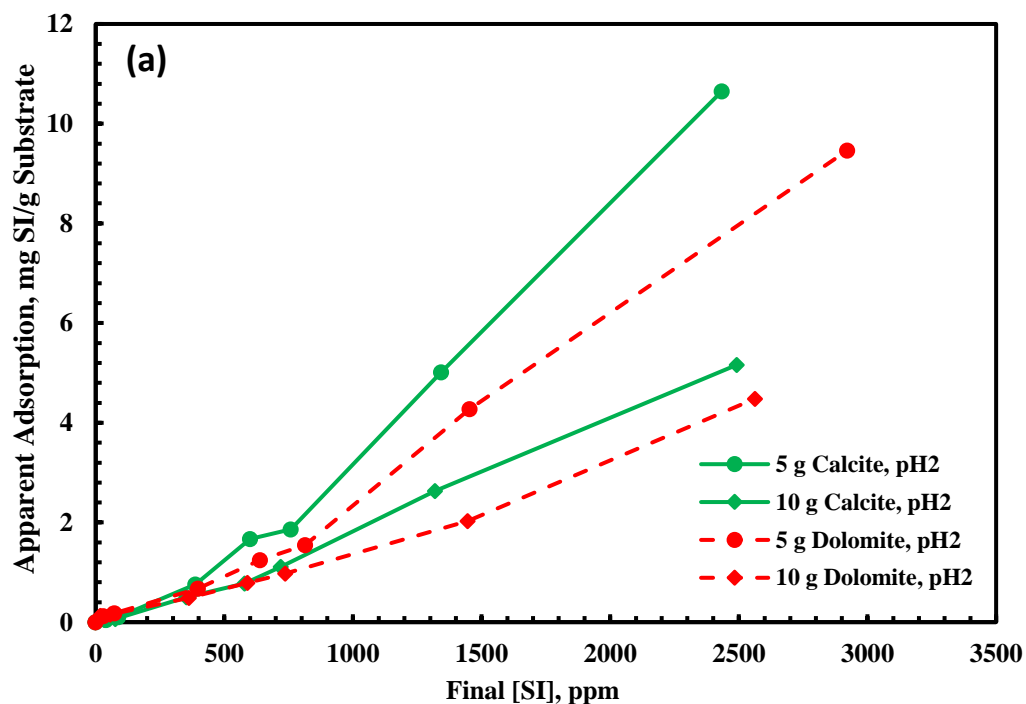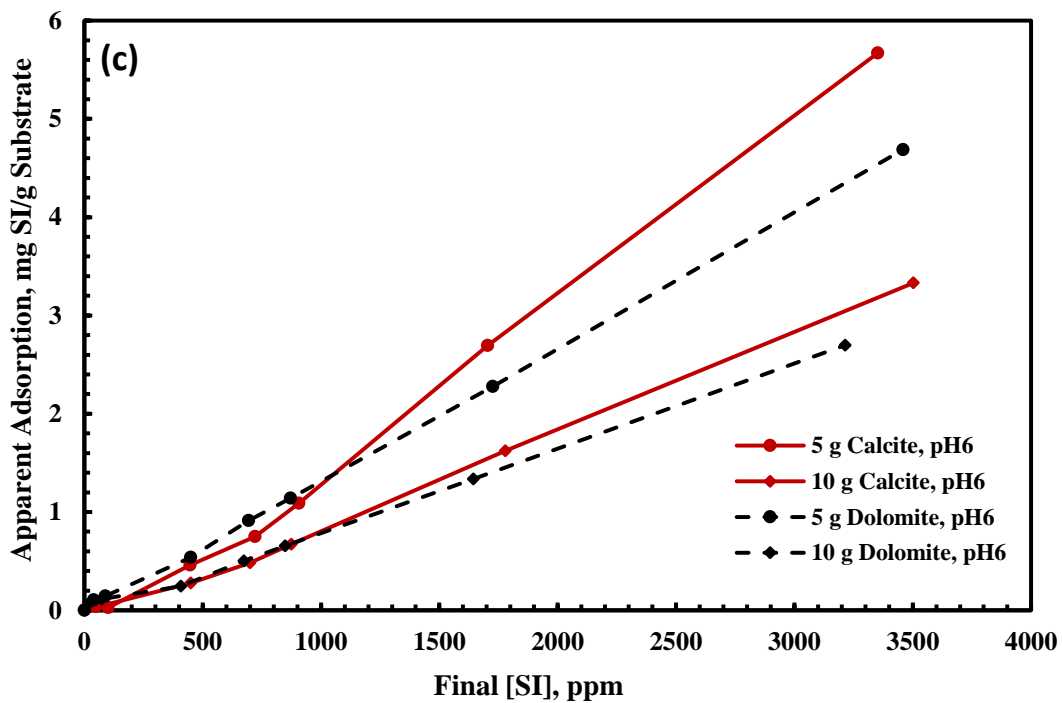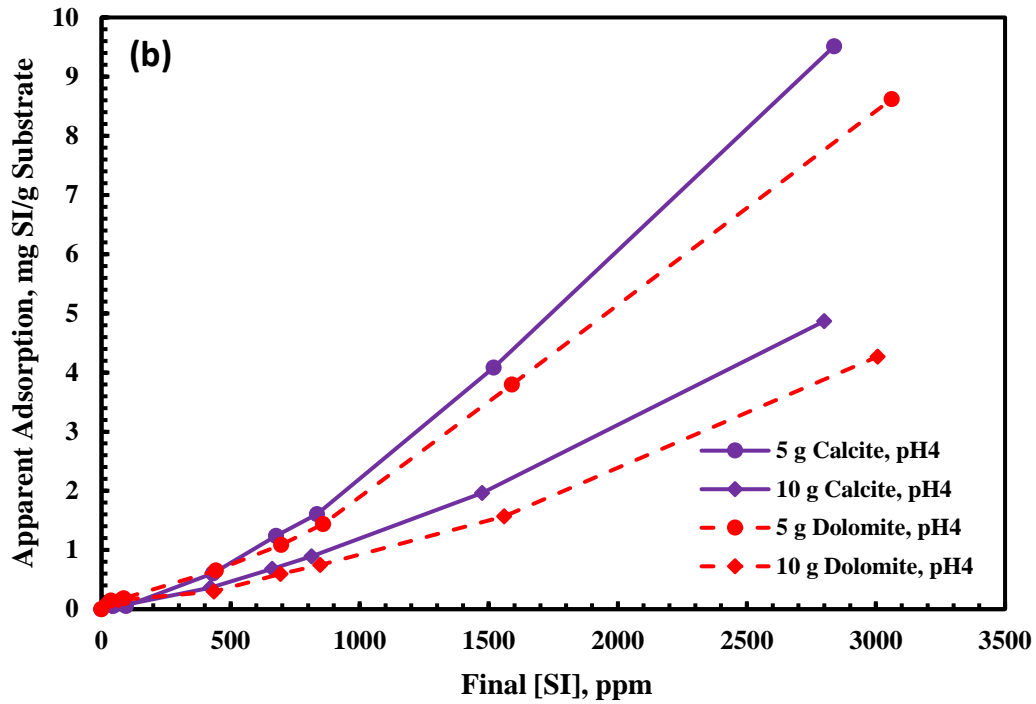
Figure 4.19. Comparison of apparent adsorption for PPCA onto two masses (m = 5g and 10g) of calcite and dolomite at T = 95°C and (a) $pH_0 2$, (b) $pH_0 4$, (c) $pH_0 6$
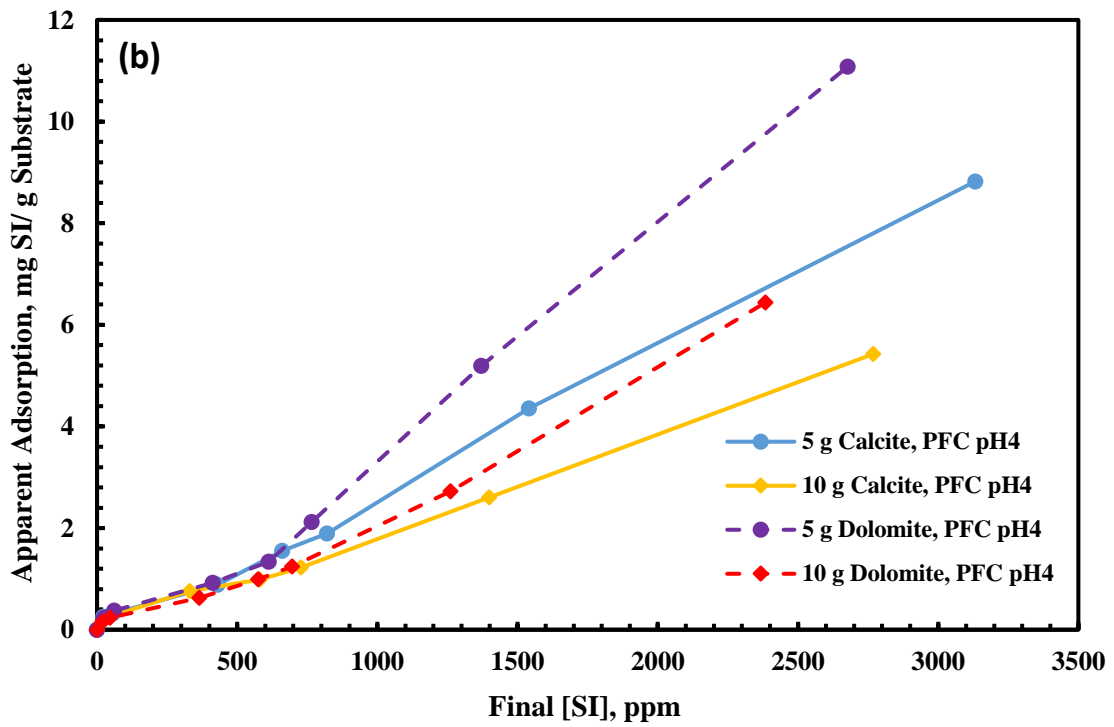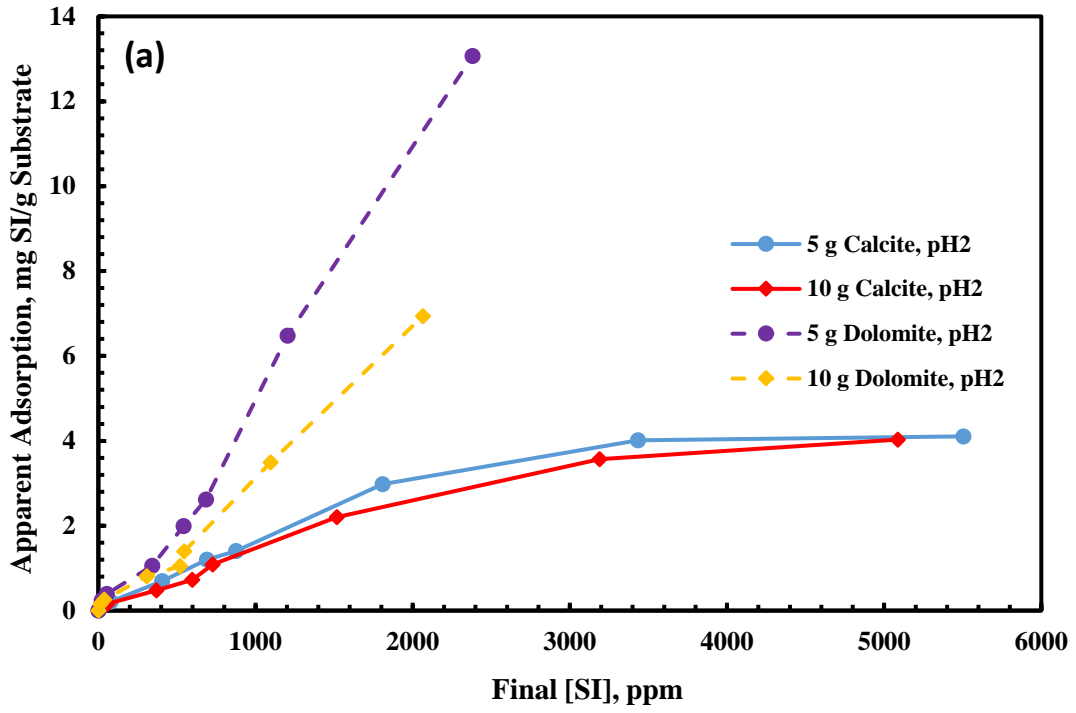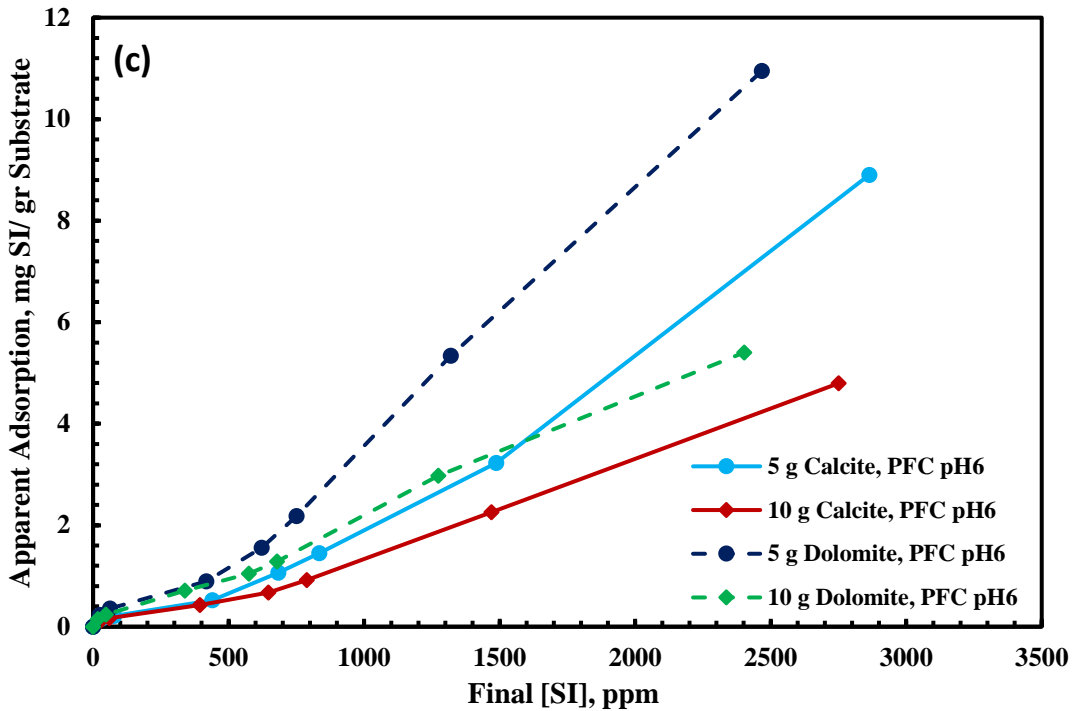
Figure 4.20. Comparison of apparent adsorption for PFC onto two masses (m = 5g and 10g) of calcite and dolomite at T = 95°C and (a) pH_0 2, (b) pH_0 4, (c) pH_0 6

The results in Figure 4.19 and Figure 4.20 clearly show regions of both pure adsorption (where apparent adsorption levels for different (m/V) ratios overlap) and coupled adsorption/precipitation (where results from different (m/V) values diverge) for PPCA, regardless of the type of carbonate substrate and the initial solution pH. However, PFC is retained on calcite through a pure adsorption mechanism at initial adjusted pH_0 2 (Figure 4.20(a)). Note that the [PFC] was increased to 6,000 ppm to make sure pure adsorption occurs at the PFC/calcite system at initial adjusted pH_0 2. As seen in Figure 4.20(a), the results have converged, and it was confirmed that pure adsorption is the main retention mechanism for the PFC/calcite system at initial adjusted pH_0 2. At the other initial pH values (pH_0 4 and 6), both pure adsorption and coupled adsorption/precipitation were observed for PFC (similar to PPCA). PPCA in NSSW has pure-adsorption behaviour up to approximately 100 ppm and coupled adsorption/ precipitation for [PPCA]>100 ppm. PFC shows a larger region of pure adsorption (C only) at lower PFC concentrations (up to approximately 500 ppm) compared with PPCA at initial adjusted pH 4 and 6. That the adsorption region for PFC is more significant than for the PPCA is probably because of the presence of more sulfonate groups on the PFC, whereas PPCA has mainly carboxylic acid groups[36].

The most interesting specific observations from these initial apparent-adsorption results are the following.

1. For PPCA, the amount of apparent adsorption, Γ_{app}, decreases as pH increases. At lower pH values, the PPCA solution is more acidic and dissolves more carbonate substrate, generating more divalent cations in situ. Therefore, the dissociated PPCA will interact with the additional divalent cations, particularly Ca^{2+}, in the solution, leading to more precipitation (i.e., observed as a higher apparent adsorption). At higher pH values (pH_0 6), the PPCA would be somewhat more dissociated (more negative species, A^-, in solution), but the amounts of Ca^{2+}, and $[Mg^{2+}]$ dissolved into the solution would be much less. Thus, the effect is an increased level of precipitation (i.e., a higher apparent adsorption) at the lower initial pH level.

2. Qualitatively, both the PPCA/dolomite and PPCA/calcite systems behave quite similarly in that they both show very similar trends in apparent adsorption. However, there are quantitative differences between these PPCA/dolomite and PPCA/calcite systems in that apparent adsorption is less for the dolomite than for the calcite. This might be attributed to the Ca concentration, which PPCA needs in order to precipitate. Because calcite contains relatively more Ca than dolomite, the former produces more Ca in situ than the latter, and subsequently PPCA has a higher apparent adsorption on calcite substrate compared with dolomite. Therefore, Ca availability contributes more than pH to form a SI/Ca^{2+} complex in the PPCA/carbonate system.

3. For PFC, the apparent adsorption, Γ_{app}, is approximately the same at pH_0 6 and 4, whereas in the PFC/calcite system at pH_0 2, only pure adsorption is observed. This is because the sulfonate functional group has high tolerance to divalent cations because it is more acidic, and the sulfonate group interacts less with Ca^{2+}. However, at higher pH values (pH_0 4 and 6), the SI becomes more dissociated and interacts more with Ca to form a PFC/Ca precipitate. Moreover, the PFC has been more retained on dolomite substrate than on calcite because the final pH is higher in the dolomite/PFC system than in the calcite/PFC system. PFC has more P content than PPCA, therefore the former is more susceptible to pH than the latter. Thus, PFC becomes more dissociated in the PFC/dolomite system than in the PFC/calcite case, and consequently more apparent adsorption occurs. Thus, pH would contribute more than Ca affinity to form a SI/Ca^{2+} complex in the PFC/carbonate system, which is different from the apparent adsorption behaviour of PPCA in the carbonate system.

4. The region of pure adsorption (Γ) is more extensive for PFC than for PPCA. The pure Γ region extends up to [PFC] of approximately 500 ppm and [PPCA] of approximately 100 ppm because of the presence of more phosphonate groups on the PFC, whereas PPCA mainly has carboxylic acid groups[36].

To understand the SI apparent adsorption behaviour and the effect of both pH and Ca^{2+}, the likely mechanisms occurring here are shown schematically in Figure 4.21. When the SI first contacted the carbonate formation, it dissolved the rock, increasing the pH value to 7 and 8 for calcite and dolomite substrates, respectively. This increase in solution pH then causes the inhibitor to become more dissociated. All SIs are a weak polyacid (e.g., H_nA), which dissociates as follows:

$$H_nA \leftrightarrows H_{n-1}A^- + H^+ \leftrightarrows H_{n-2}A^{2-} + 2\,H^+ \leftrightarrows H_{n-3}A^{3-} + 3\,H+ \leftrightarrows \ldots\ldots \leftrightarrows A^{n-} + n\,H^+$$

Low pH   *High pH*

At given pH:

$$H_{n-m}A^{m-} \leftrightarrows \text{Polyanion}$$

Dissociated Polymeric Scale Inhibitor
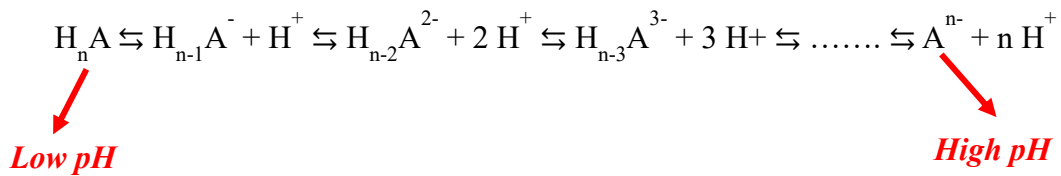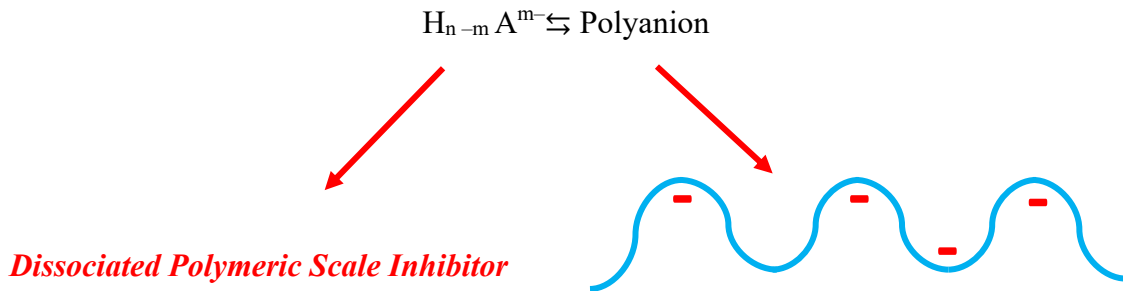
Thus, it is adsorbed on the surface as

Positively Charged Carbonate Surface
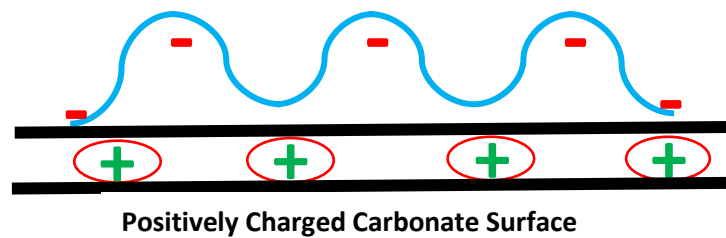
Figure 4.21. Schematic of polymeric SI adsorption on carbonate substrates

143

Therefore, at very low (acidic) pH, the equilibrium is to the left and the molecule is more associated as H_nA; at higher pH, it is more dissociated into H^+ and A^{n-}, where the A^{n-} is the remainder of the molecule as shown (approximately) in the preceding schematic. Note that the PPCA structure is quite accurate (with molecular weight=approximately 3,500 Daltons), but the PFC is approximate, and P is higher (approximately 2%) than in PPCA (approximately 0.5%)[36]. In PFC, the P is attached in the monomers making up the copolymer, whereas in PPCA, it is as shown on the backbone. Thus, the schematic adsorption and precipitation might be shown as after dissociation of SI at high pH, the inhibitor interacts with Ca^{2+} to form the SI/Ca^{2+} complex:

$$H_{n-m}\,A^{m-} + Ca^{2+} \leftrightarrows Ca\text{-}SI\ (aq) \leftrightarrows Ca\text{-}SI\ (s)$$

Solubility = C_S　　　　　　**Precipitate**
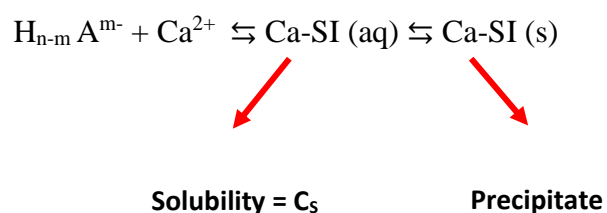
To support these observations, further ancillary results will be presented here on carbonate dissolution (changing $[Ca^{2+}]$ and $[Mg^{2+}]$ in solution) and on the final pH values of the system. Further ESEM-EDX and PSA data are also presented here on the precipitates (and carbonate substrates) themselves.

Figure 4.22 and Figure 4.23 present the final pH results for PPCA (Figure 4.22) and PFC (Figure 4.23) for both the blank and apparent-adsorption experiments on calcite and dolomite given in Figure 4.19 and Figure 4.20. First, we note from the blank-solution results that the pH remained at its initial value (pH_0 2, 4, or 6) for all SI concentrations in the absence of carbonate substrate for both PPCA and PFC. In the presence of a carbonate mineral substrate, these final pH results give a good indicator of the total system response.

We summarize these results as follows.

1. For PPCA (at the higher concentrations), the final pH values for initial solution pH_0 2, 4, and 6 were pH=7, 7 to 7.3, and 8, respectively, for calcite, and pH=7.6 to 8, 7.5 to 8.3, and 8 to 8.2, respectively, for dolomite. A somewhat-higher final pH value was found for dolomite than for calcite for all initial pH values.

2. For PFC (at the higher concentrations), the final pH values for initial solution pH_0 2, 4, and 6 were pH=5 to 5.1, 5.6 to 6, and 6 to 6.3, respectively, for calcite, and pH=7.6 to 8.2, 6.9 to 7.8,

and 7.6 to 7.9, respectively, for dolomite. A higher final pH value was again found for dolomite compared with calcite for all initial pH values.

3. Overall, PFC results in a lower final pH value than PPCA under all initial conditions for both carbonate minerals.
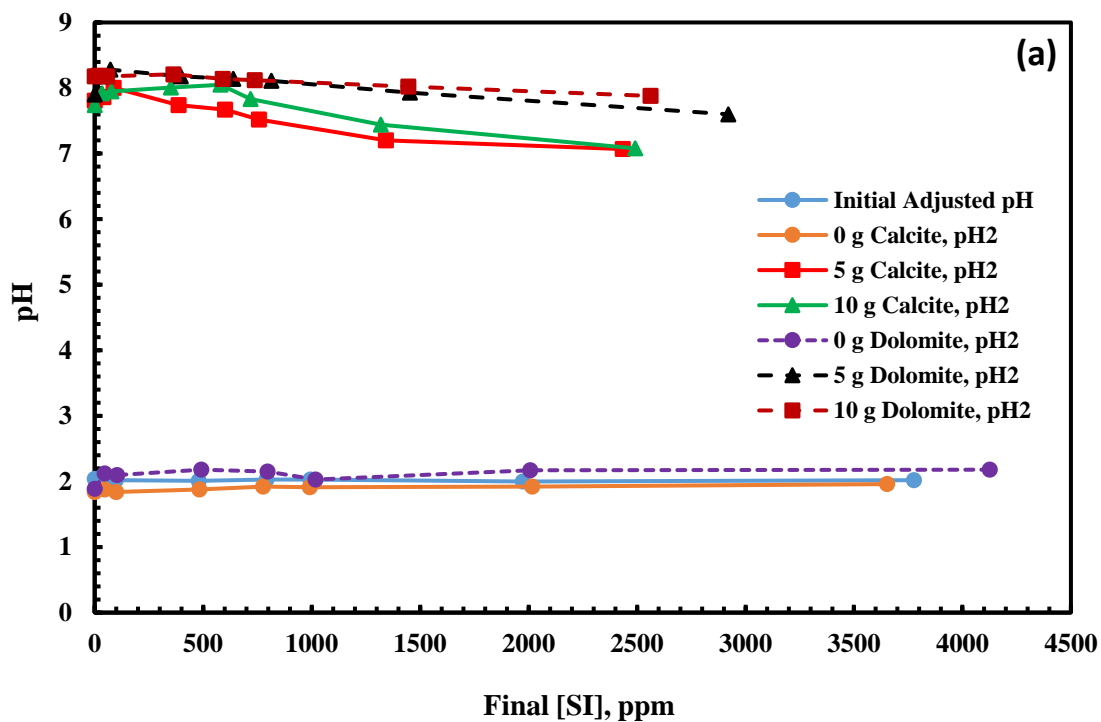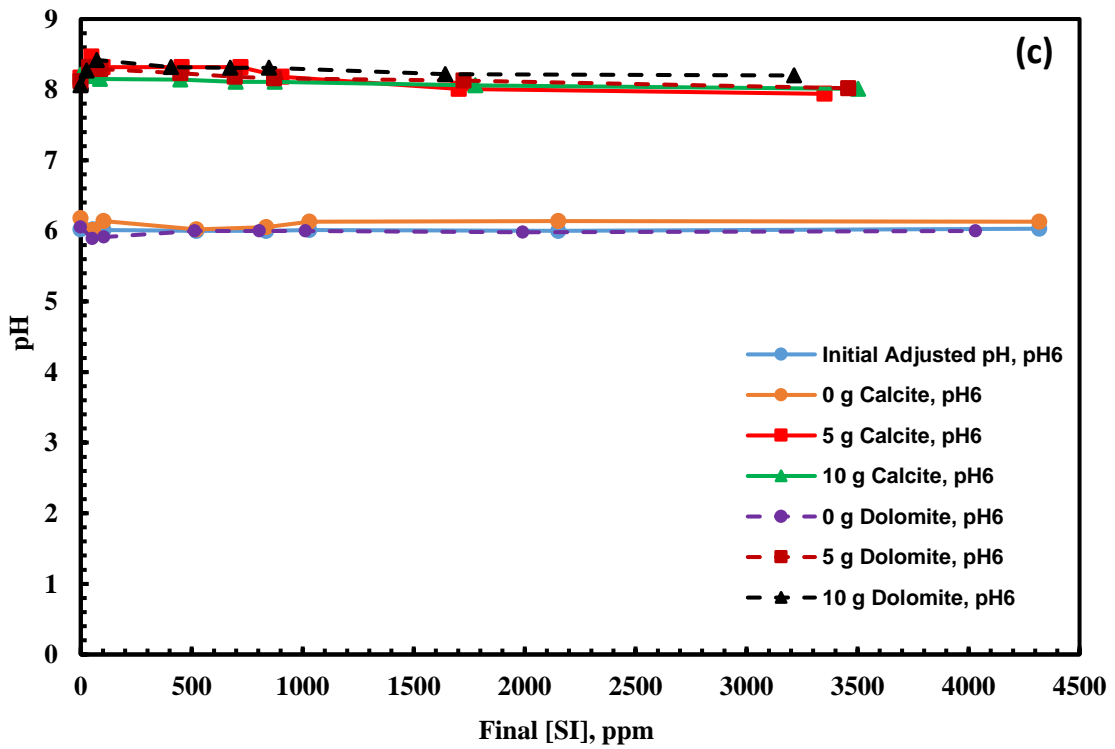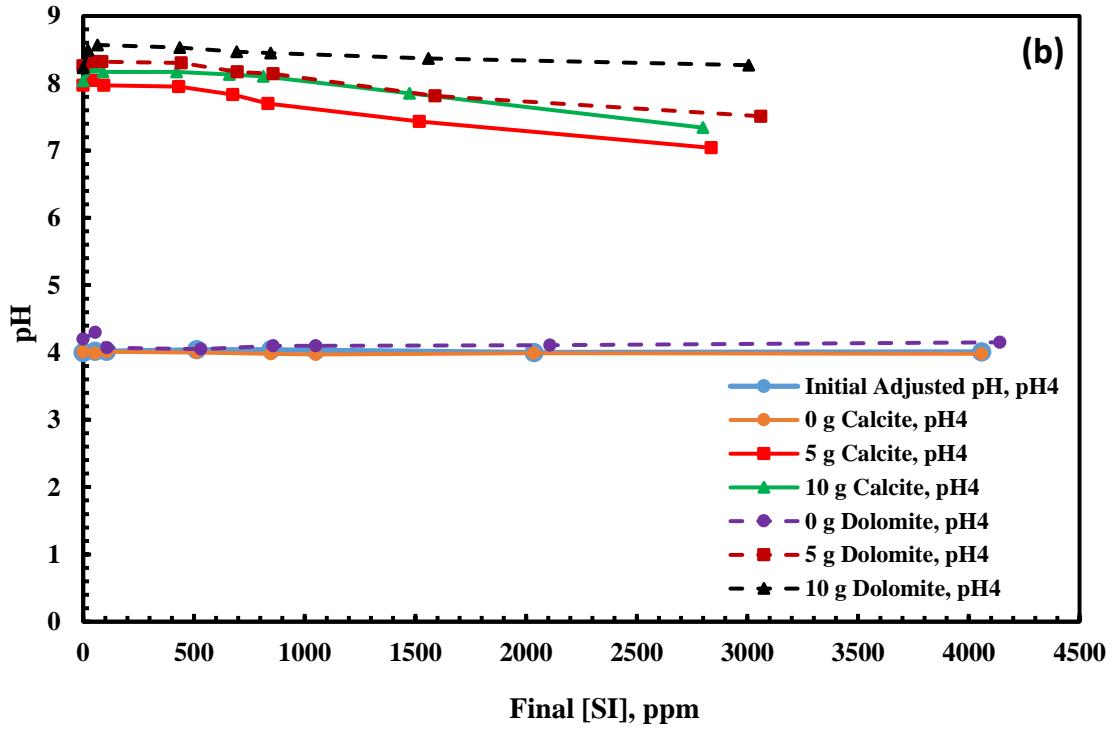
Figure 4.22. Comparison of pH for PPCA onto two masses (m = 5g and 10g) of calcite and dolomite at T = 95°C, pH$_0$ 2, 4 and 6
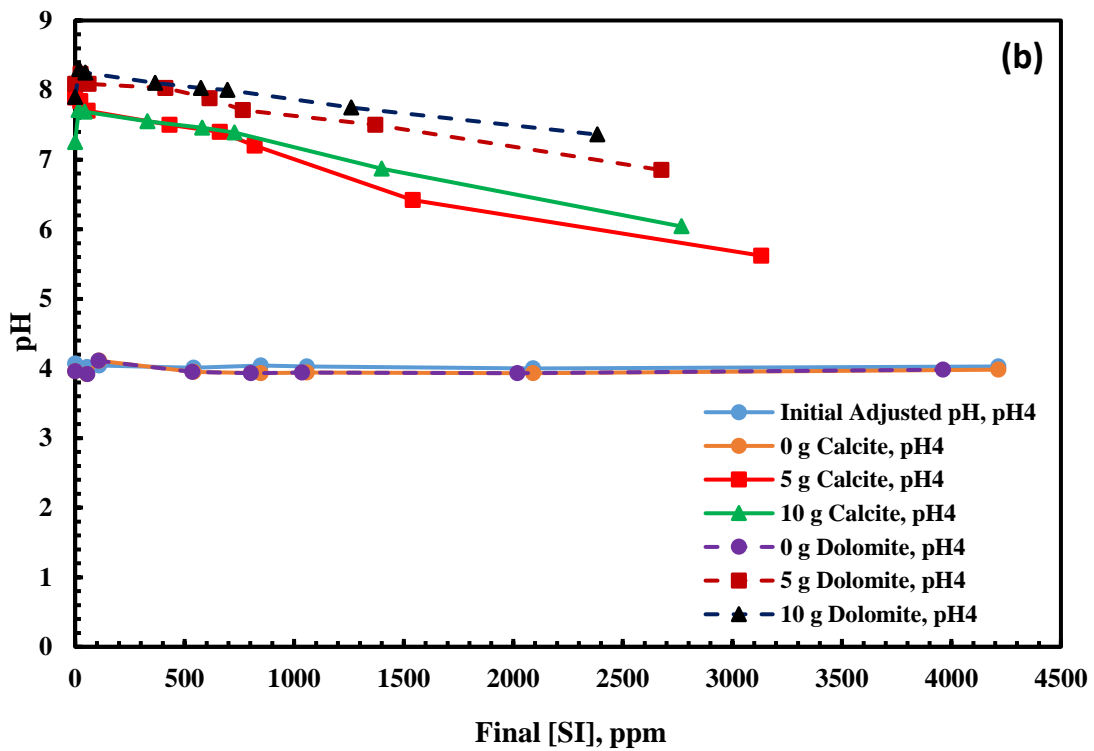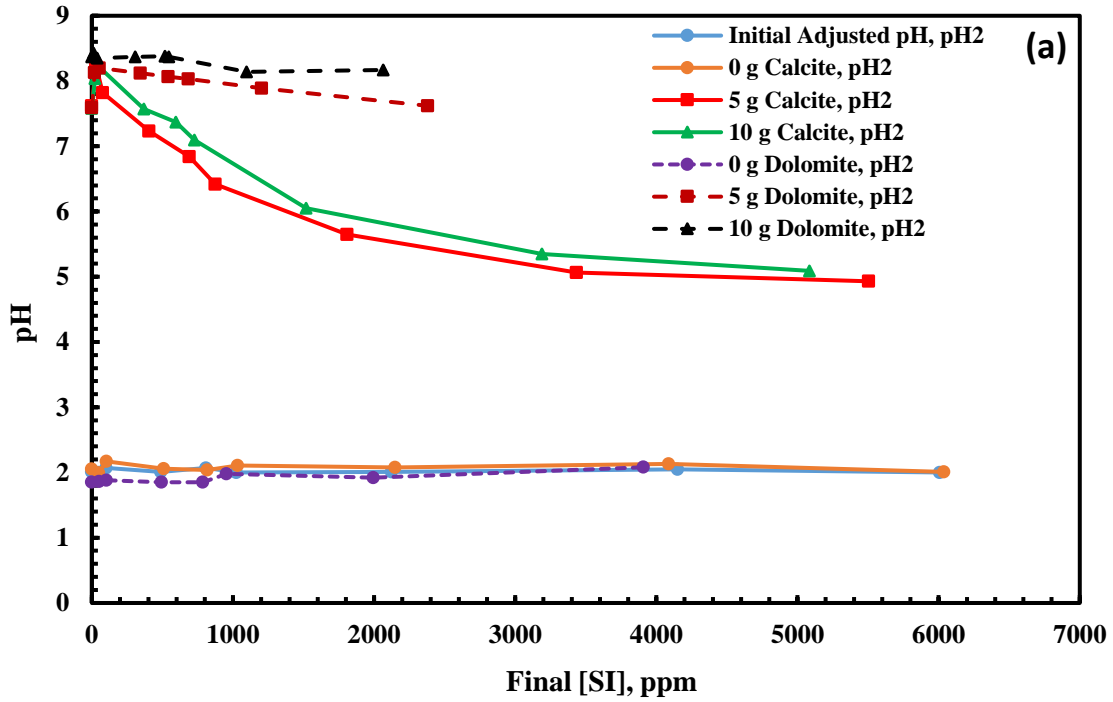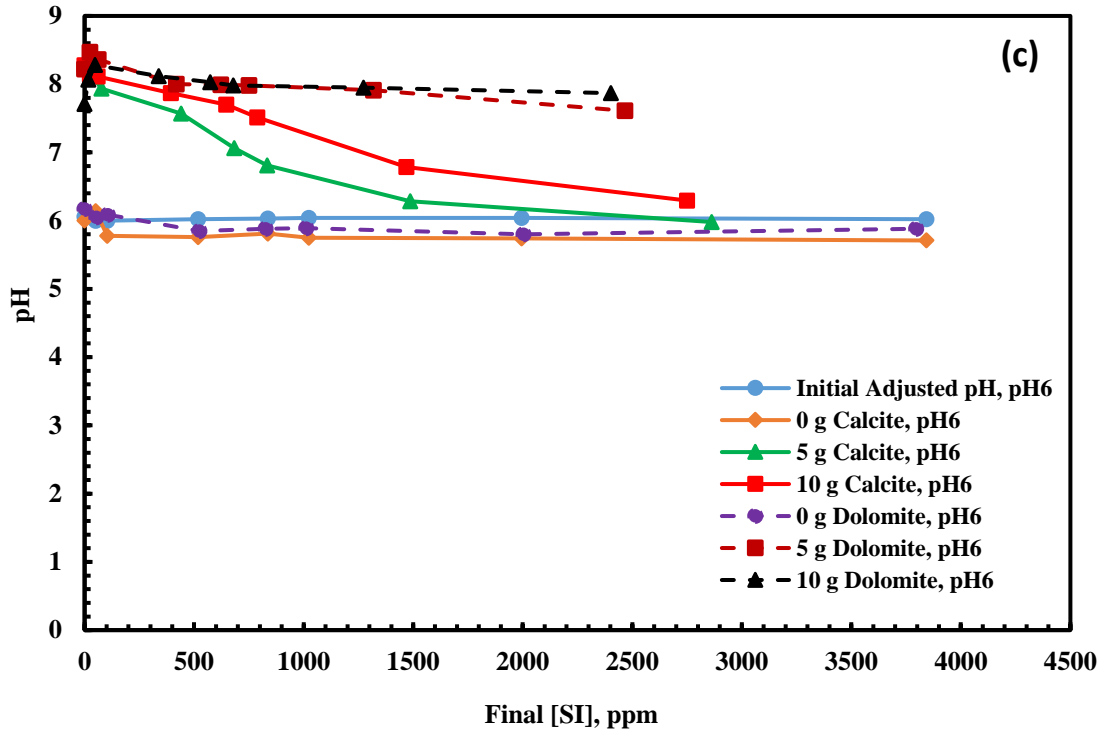
Figure 4.23. Comparison of pH for PFC onto two masses (m = 5g and 10g) of calcite and dolomite at T = 95°C, pH$_0$ 2, 4 and 6

Here, we present final divalent cation (mainly Ca^{2+} & Mg^{2+}) levels for PPCA and PFC for both the blank and apparent adsorption experiments on calcite and dolomite given in Figure 4.19 and Figure 4.20. The initial solution (synthetic seawater) has a calcium level of, $[Ca^{2+}]$ = 428ppm (approximately 10.7mM) and a magnesium level of, $[Mg^{2+}]$ = 1368ppm (approximately 57mM). Figure 4.24 and Figure 4.27, these are the Ca^{2+} and Mg^{2+} levels to which results are normalized and present the final differences in normalized $[Ca^{2+}]$ for both compatibility and adsorption tests for the PPCA/carbonate and PFC/carbonate systems.

In summary, the final normalized calcium results from these figures show the following:

1. None of the blanks (i.e., with no carbonate substrate present) in Figure 4.24 and Figure 4.25 show any significant deviations from normalized $[Ca^{2+}]$ = 1, indicating that all solutions are completely compatible and there is no loss of Ca^{2+} by precipitation for any of the initial pH/[SI] conditions;

2. For both SIs (PPCA and PFC) and both carbonate minerals (calcite and dolomite), the normalized $[Ca^{2+}]$ is well above unity for all initial pH$_0$ 2, 4 solutions. From normalized

148

$[Ca^{2+}] \sim x1.8$–$x3$ and $[Ca^{2+}] \sim x1.4$–$x1.8$ for PPCA/carbonate, and $[Ca^{2+}] \sim x2$–$x3$ and $[Ca^{2+}] \sim x1.4 - x1.6$ for PFC/carbonate, respectively (although all final pH values are well above this value);

3. All initial pH_0 6 cases (PPCA, PFC and calcite/dolomite) give normalized $[Ca^{2+}]$ levels that are mostly less than or slightly greater than unity (PFC/calcite has a normalized $[Ca^{2+}]$ $x1.03 - 1.07$).
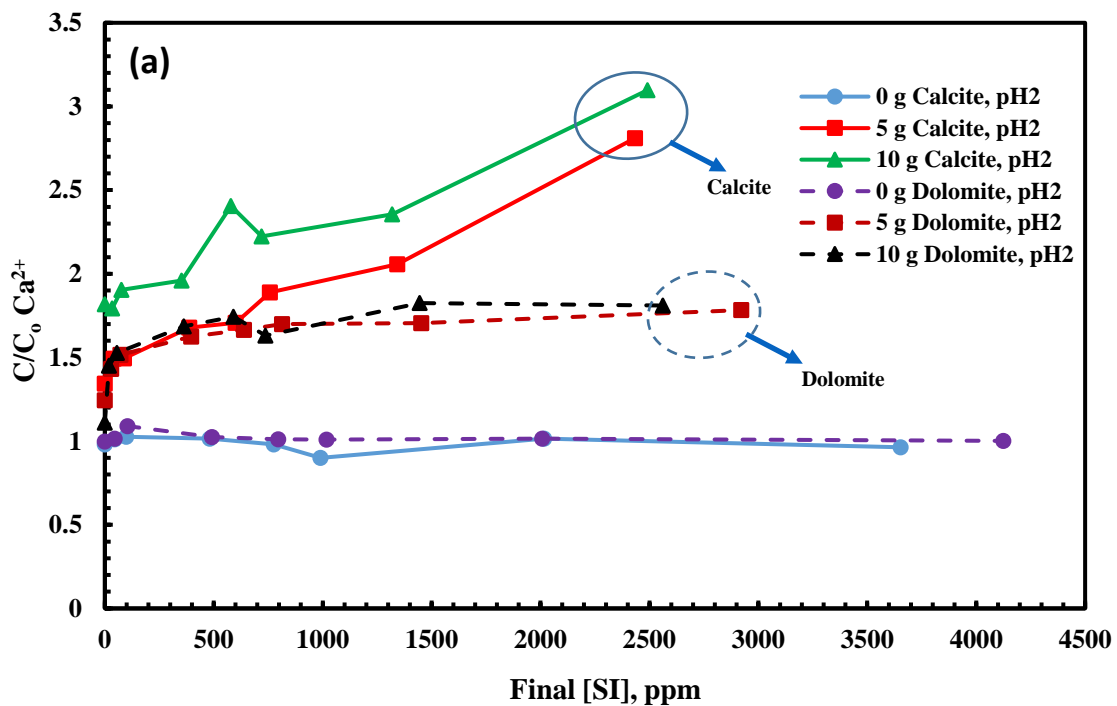
Figure 4.24. Comparison of Changes in normalized C/C_0 of $[Ca^{2+}]$ in calcite and dolomite systems vs. final [PPCA] at pH_0 2, 4 and 6
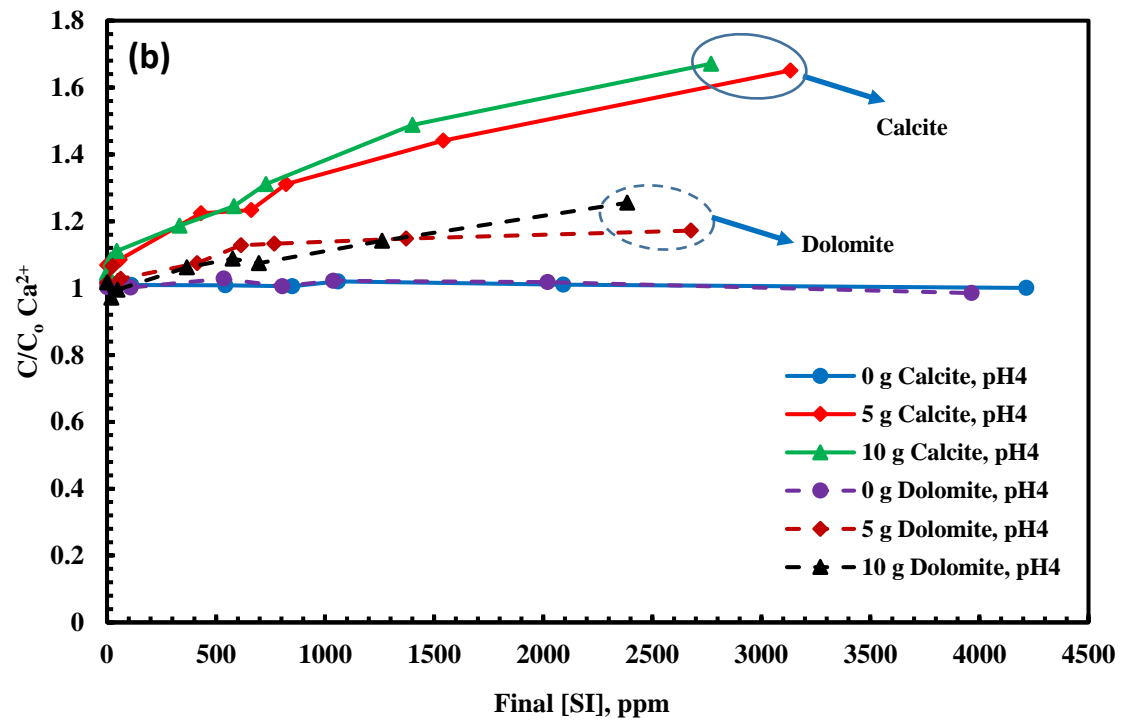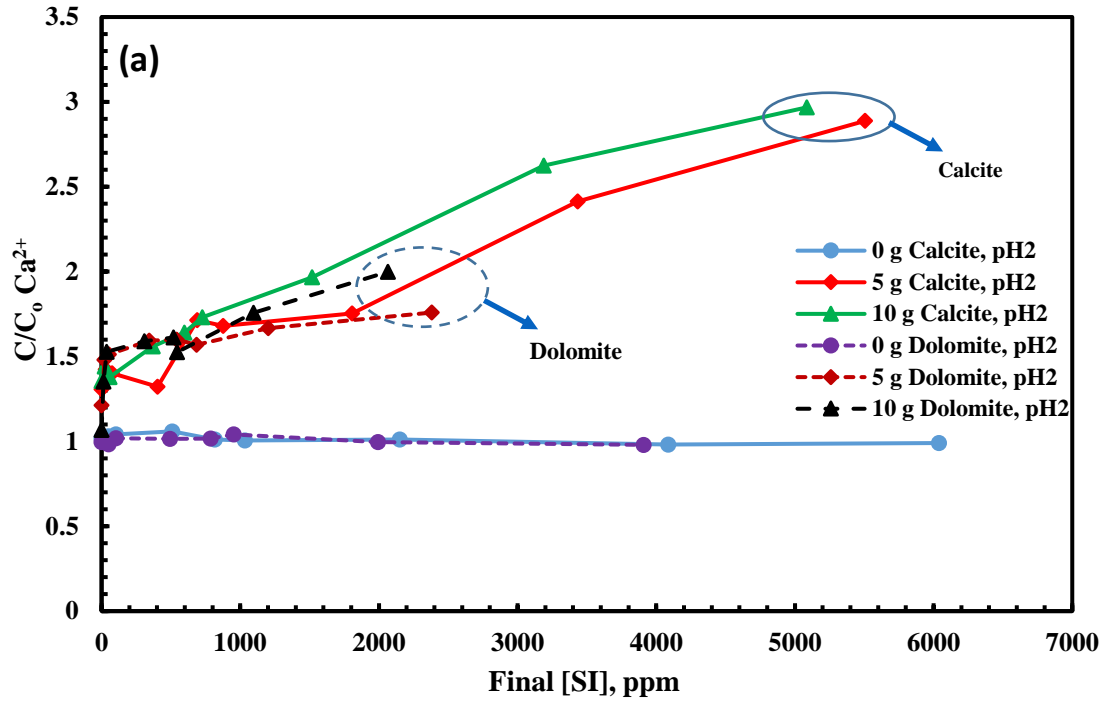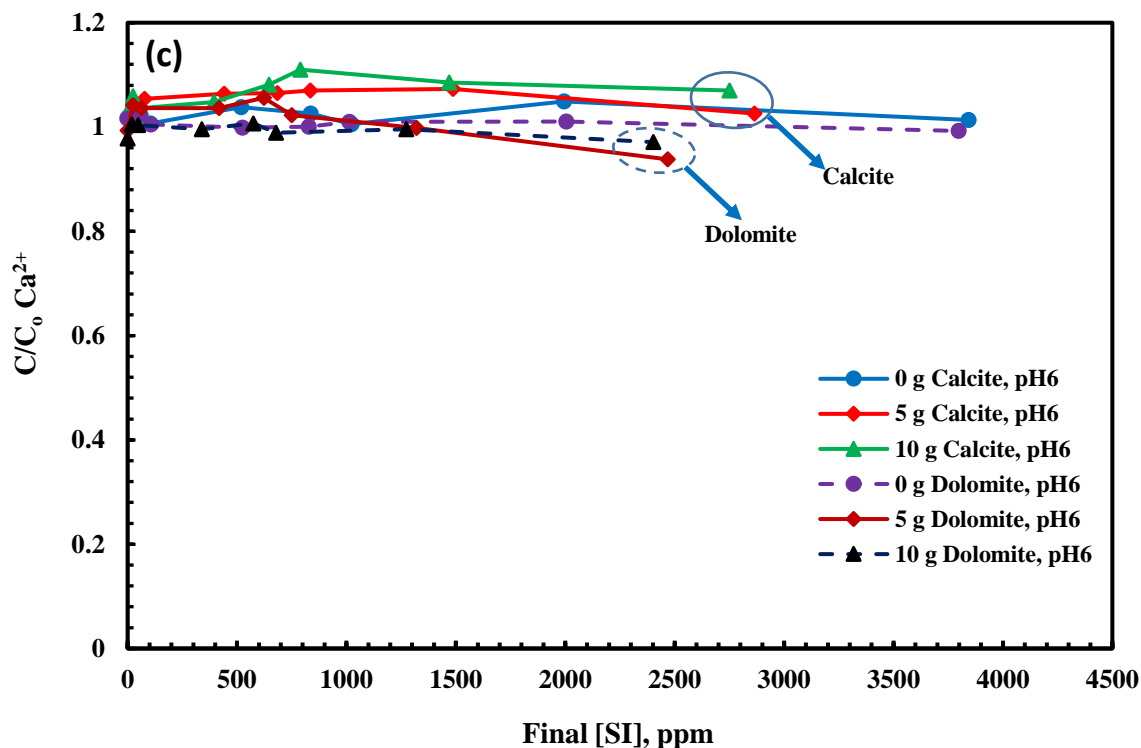
Figure 4.25. Comparison of Changes in normalized C/C_0 of $[Ca^{2+}]$ in calcite and dolomite systems vs. final [PFC] at pH_0 2, 4 and 6

We note that initial and final levels of Mg^{2+} were also measured in all apparent adsorption experiments but the results indicated that the role of Mg was secondary in these polymeric SI systems. In summary, the final normalized magnesium results from these figures show the following:

1. Firstly, none of the blanks (i.e. with no carbonate substrate present) in Figure 4.26 and Figure 4.27 show any significant deviations from normalized $[Mg^{2+}] = 1$, indicating that all solutions are completely compatible and there is no loss of Mg^{2+} by precipitation for any of the initial pH/[SI] conditions;

2. For both SIs (PPCA and PFC) and both carbonate minerals (calcite and dolomite), the normalized $[Mg^{2+}]$ is well above unity for all initial pH_0 2, 4 solutions; from normalized $[Mg^{2+}] \sim$ x1.1–0.9 and $\sim$x1.2–x1.1 for PPCA/carbonate; $\sim$x1 and $\sim$ x1.2 – x 1.1 for PFC/carbonate, respectively (although all *final* pH values are well above this value – see above);

All initial pH_0 6 cases (both PPCA, PFC and calcite/dolomite) give normalized $[Mg^{2+}]$ levels that are mostly below or just above unity. According to these results, Ca is mainly involved and Mg is hardly involved in complexation with these SI. Moreover, in the PPCA/calcite and PFC/calcite systems, final $[Mg^{2+}]$ levels off at a normalised value of $[Mg^{2+}]$ <1 which confirms that magnesium is somewhat involved in the complexation process, but not as significantly as calcium. In the dolomite/SI systems, normalised values of $[Mg^{2+}]$ is around 1, which means that the consumption of magnesium in the interaction with the SIs and gain from dolomite dissolution is approximately balanced.
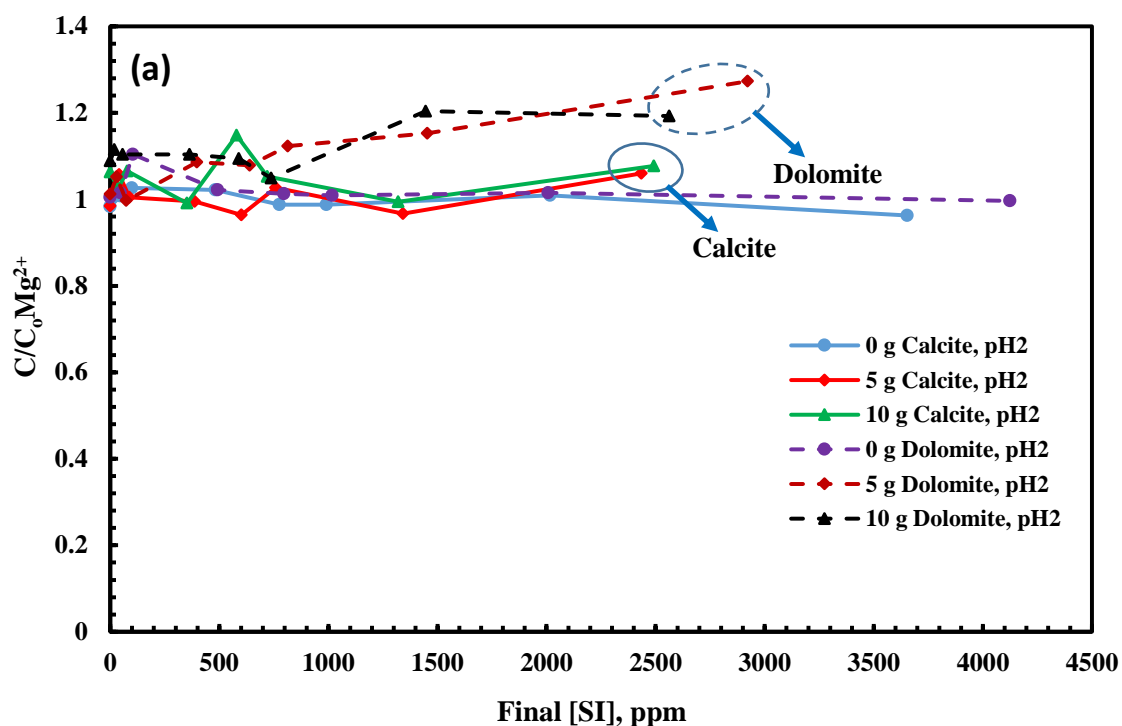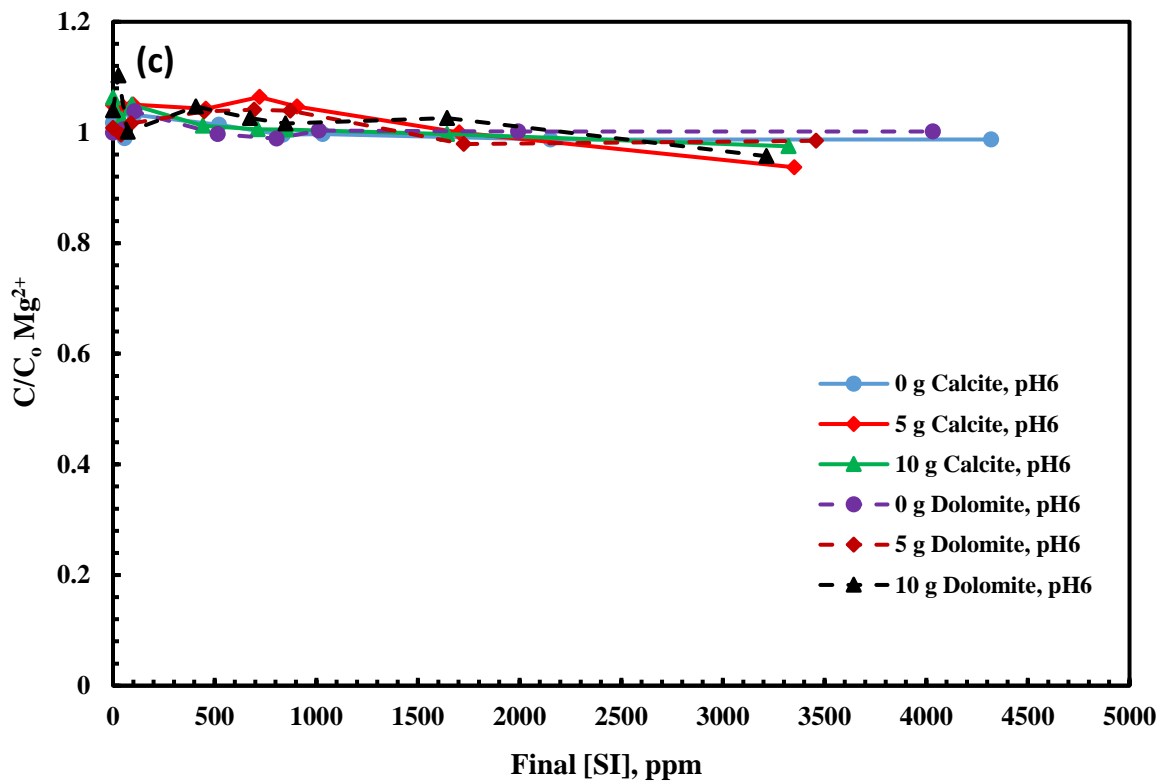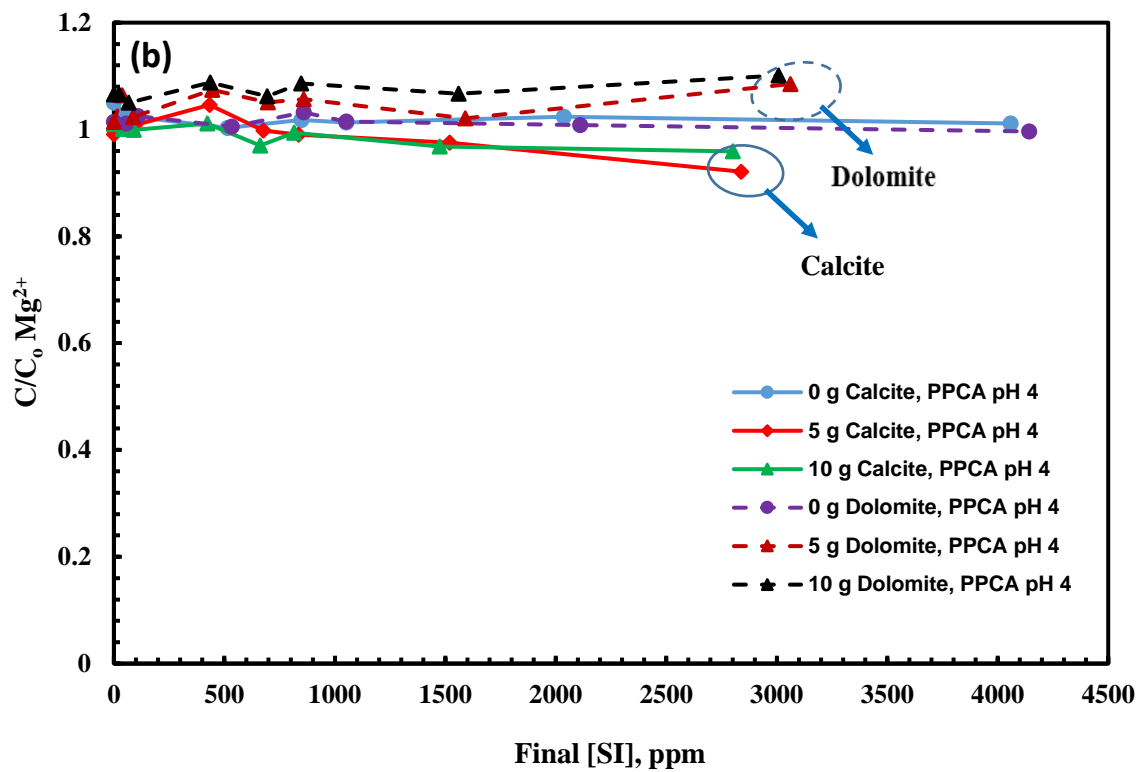
Figure 4.26. Comparison of Changes in normalized C/C_0 of $[Mg^{2+}]$ in calcite and dolomite systems vs. final [PPCA] at pH_0 2, 4 and 6
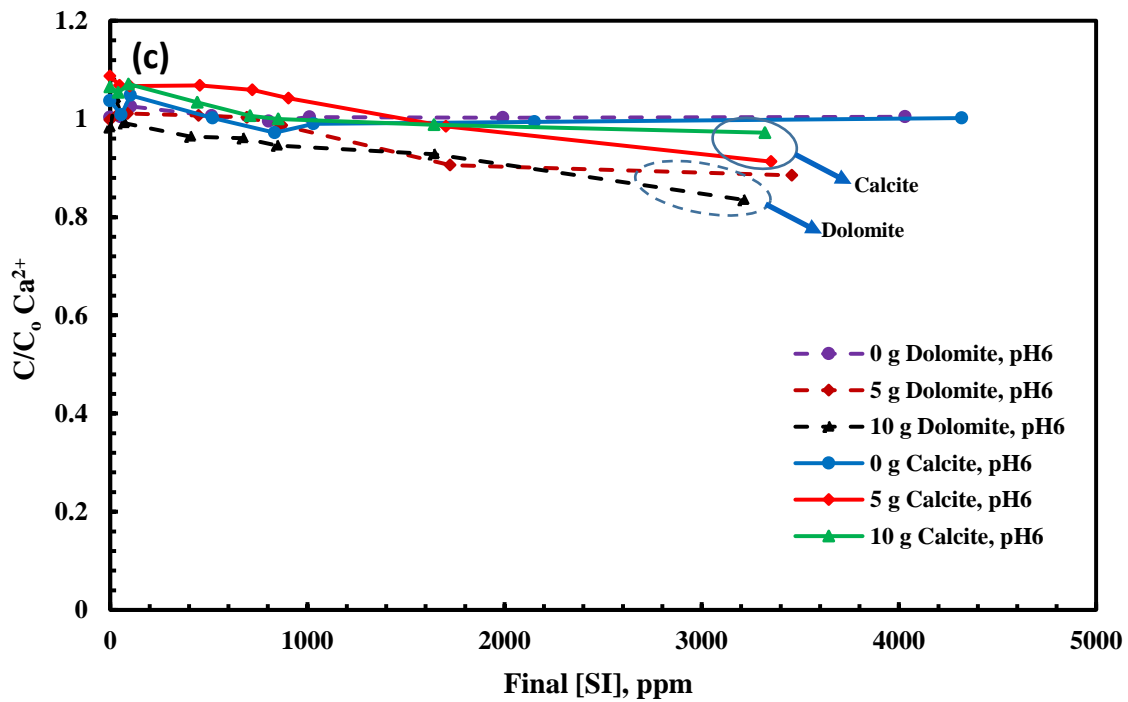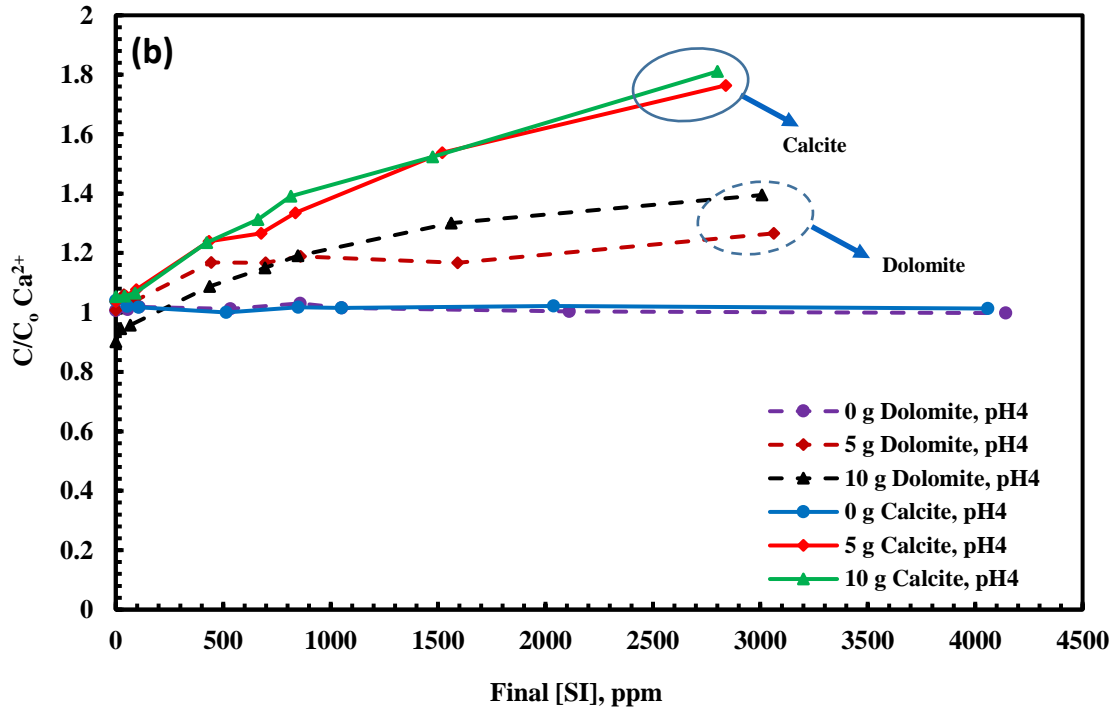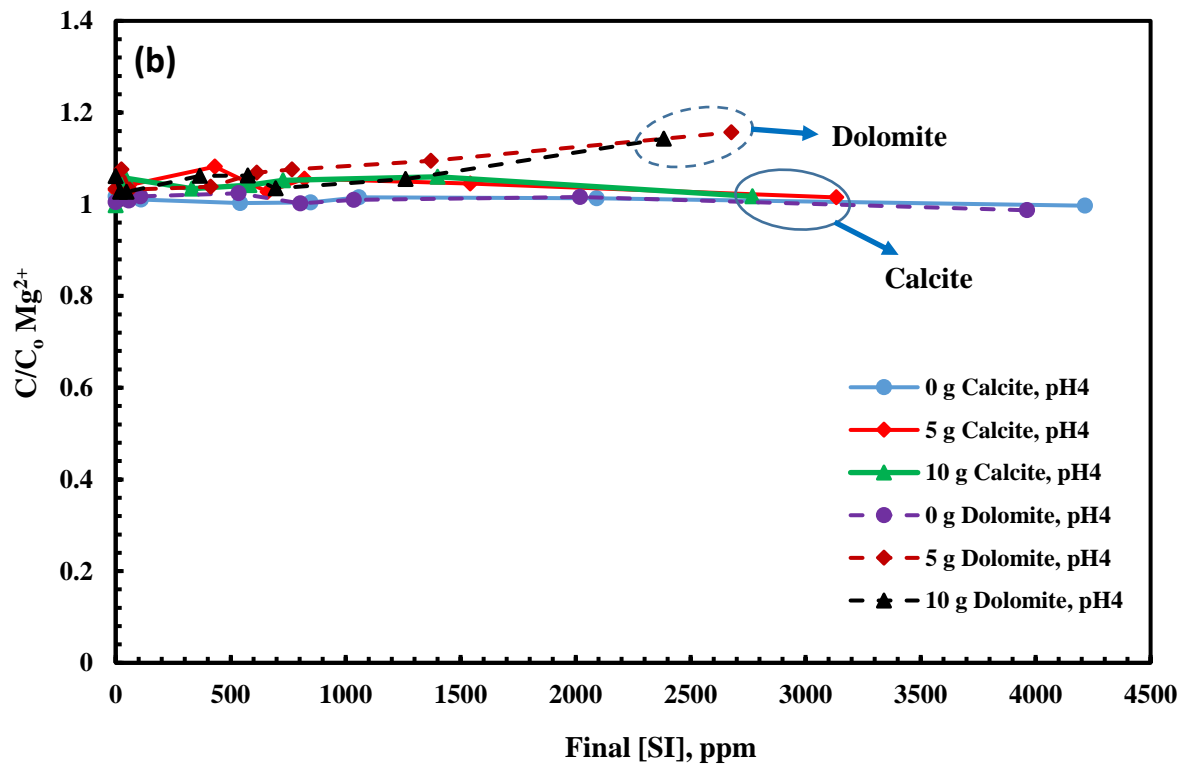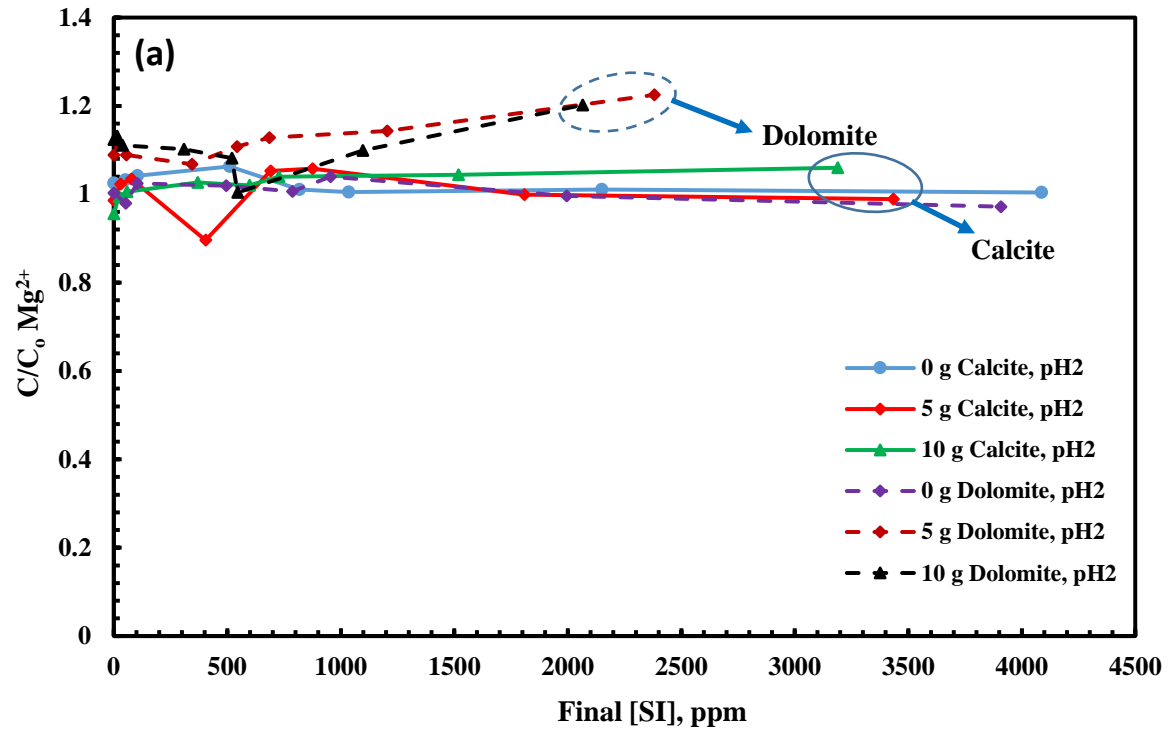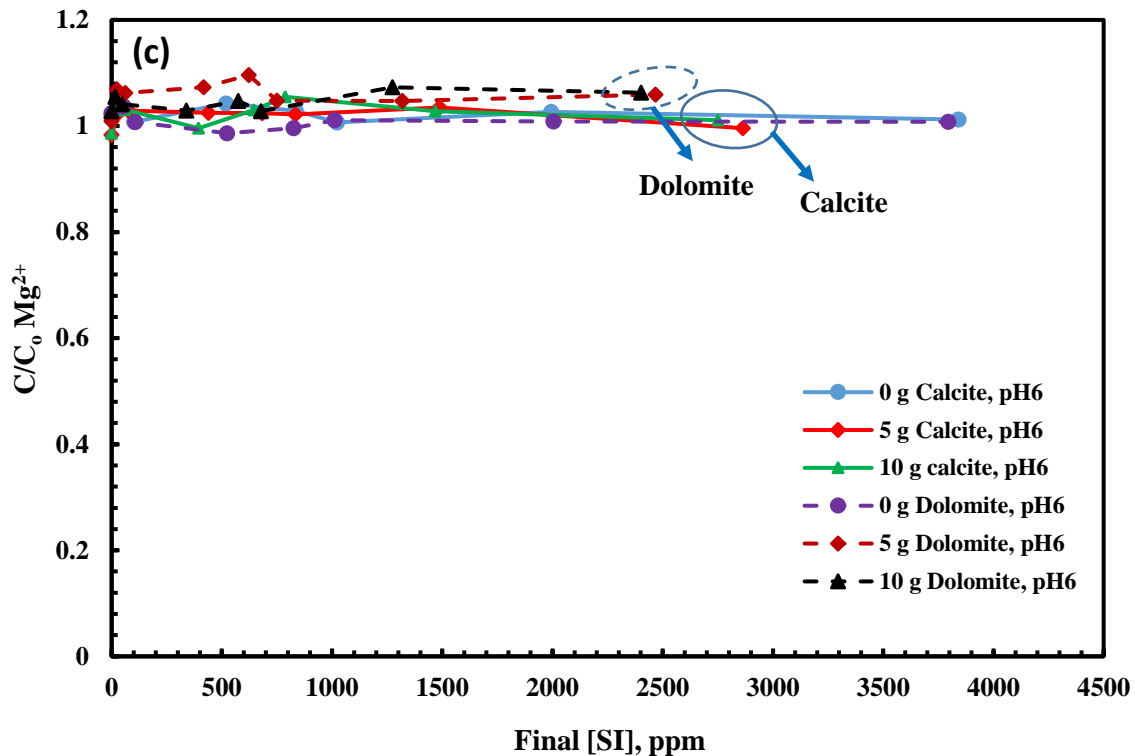
Figure 4.27. Comparison of Changes in normalized C/C_0 of $[Mg^{2+}]$ in calcite and dolomite systems vs. final [PFC] at pH_0 2, 4 and 6

ESEM/EDX Results: ESEM/EDX analysis was used to examine the surface of the carbonates both before and after treatment in all of the apparent adsorption experiments reported above. After filtration, all the filter papers containing calcite/dolomite substrates and the precipitated complex (if present) for each of the PPCA and PFC concentrations tested were dried and taken for ESEM-EDX analysis. The results are shown by presenting the directly observed ESEM images in the figures along with some representative EDX compositions from these images as tables of % (weight and atomic) of the various elements present; the latter results are approximate but can be taken as "semi-quantitative". We have studied all of the precipitates where they occurred in these experiments, but we focus here only on the highest concentration results since these are the cases for which the most precipitate was obtained, and which show the clearest results. PSD results, however, are shown for all cases below. Figure 4.28 shows the ESEM results for the 4000ppm PPCA case at pH_0 2 where PPCA has the highest Γ_{app} in both calcite and dolomite. This figure shows significant amounts of smaller sized granular precipitate, particularly in Figure 4.28(b) and Figure 4.28(d), which focus specifically on this precipitate.

156

The precipitate occurs mainly as a separate material rather than coating the carbonate grains. From the solution ICP results, this precipitate certainly contains both Ca and PPCA (P). However, the EDX detects no phosphorus (P) for these cases but it does detect Ca, and so we do not show the results tables here. No P is detected mainly because of the low content of phosphorus in PPCA (~0.5% of P)[36].
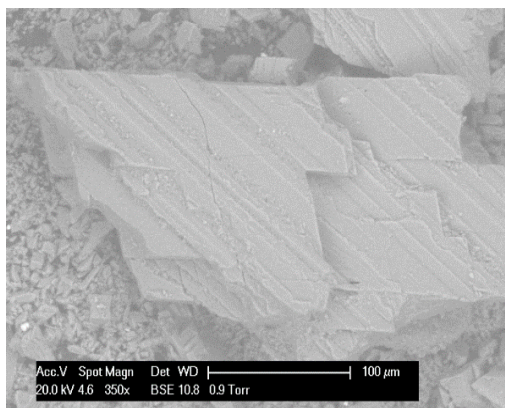
a) 4000 ppm, 100-315 µm Calcite, pH2
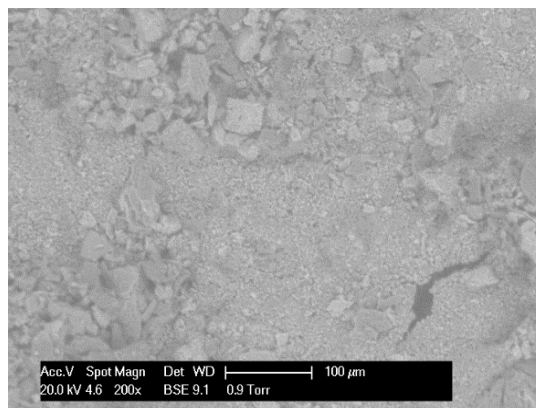
b) Precipitate, 4000 ppm, 100-315 µm Calcite, pH2
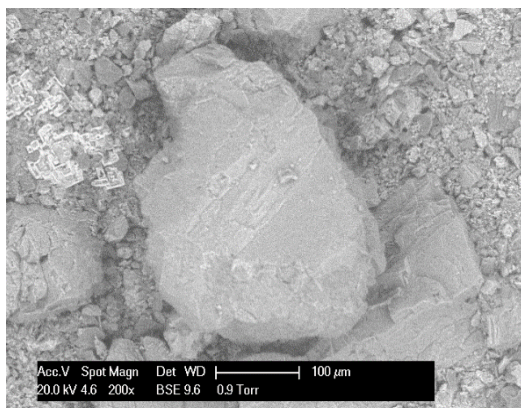
c) 4000 ppm, 100-315 µm Dolomite, pH2
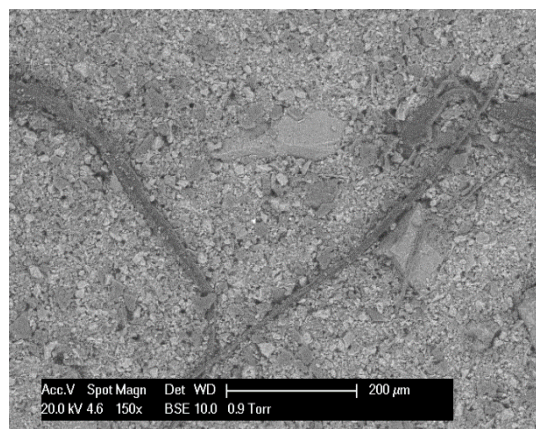
d) Precipitate, 4000 ppm, 100-315 µm Dolomite, pH2

Figure 4.28. Morphology of 4000 ppm PPCA Samples for 100-315 µm calcite and dolomite at pH_0 2 on ESEM photographed samples

PFC contains a higher proportion of P than PPCA and is much more detectable by EDX. Results for the 4000ppm PFC precipitates formed at pH_0 2, pH0 4 and pH_0 6 for both calcite and dolomite are shown in Figure 4.29 (pH_0 2), Figure 4.30 (pH_0 4) and Figure 4.31 (pH_0 6) (ESEM images)

157

and Table 4.5. (pH$_0$ 2), Table 4.6 (pH$_0$ 4) and Table 4.7 (pH$_0$ 6) (corresponding % weight/atomic by EDX).
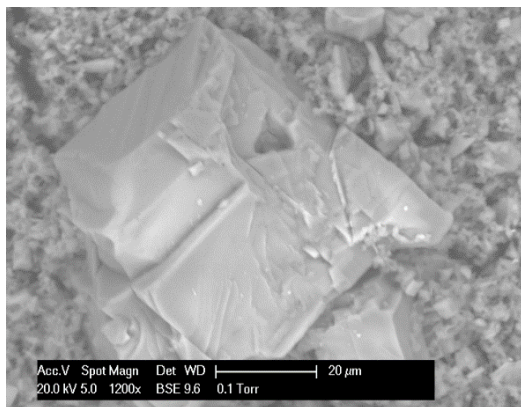
a) Calcite grain, 4000 ppm PFC, pH$_0$2
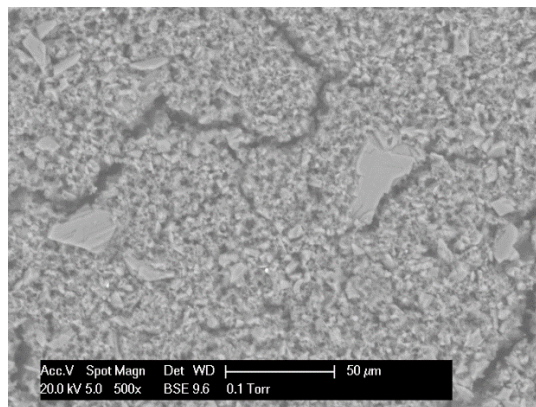
b) Fine solids deposited, 4000 ppm PFC, calcite, pH$_0$2
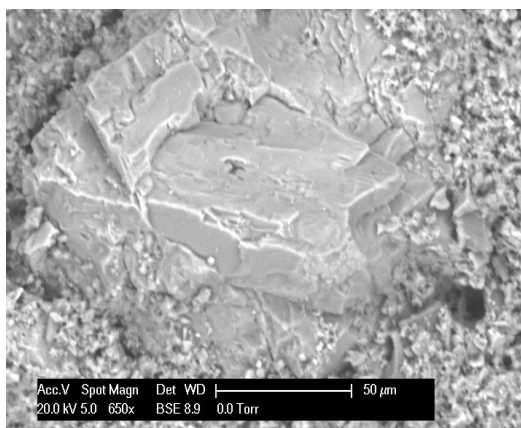
c) Dolomite grain, 4000 ppm PFC, pH$_0$2
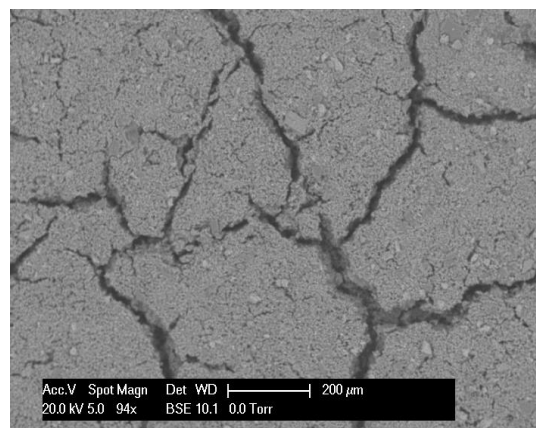
d) Precipitate, Dolomite, 4000 ppm PFC, pH$_0$2

Figure 4.29. Morphology of 4000 ppm PFC Samples for 100-315 µm calcite and dolomite at pH$_0$ 2 on ESEM Samples

Table 4.5. EDX analysis of 4000 ppm PFC for 100-315 µm calcite and dolomite at pH_0 2

Element	Calcite grain 4000 ppm (pH02)		Sublayer calcite 4000 ppm (pH02)		Dolomite grain 4000 ppm (pH02)		Bulk precipitate 4000ppm (pH02)	
	% Weight	% Atomic	% Weight	% Atomic	% Weight	% Atomic	% Weight	% Atomic
C	-	-	-	-	15	22	-	-
O	33	52	28	45	56	61	36	52
Na	5	6	11	12	2	2	6	6
Mg	2	2	3	3	10	7	19	18
P	1	1	2	2	1	0.5	4	3
S	3	2	3	3	1	0.5	4	3
Cl	7	5	17	12	3	2	8	5
Ca	49	32	36	23	11	5	21	13

As shown in the Figure 4.29 and Table 4.5. , a significant amount of phosphorus was detected by EDX in the PFC/dolomite case (~4% wt) and a small amount of P is seen around dolomite grains which may be due to SI or SI/Ca precipitate adhering on the surface of dolomite. It should be mentioned that although PFC has been retained by pure adsorption on the calcite grain, some phosphorus was detected by EDX in the sublayer of the calcite grains (~2%wt) and around the calcite grains (~1% wt.); both of these levels are less than what were found in the PFC/dolomite system.
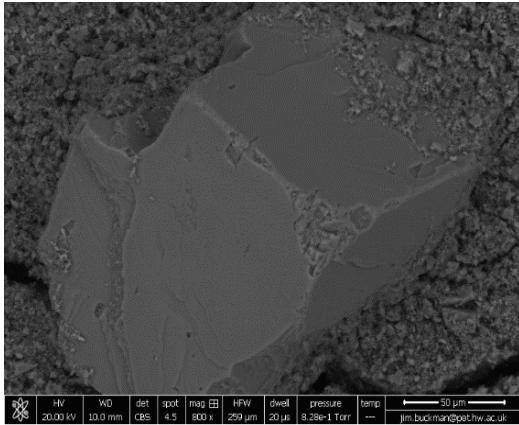
a) Calcite grain, 4000 ppm PFC, pH$_0$4
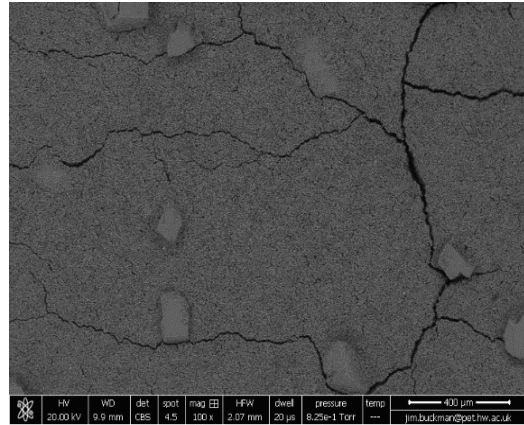
b) Precipitate, Calcite, 4000 ppm PFC, pH$_0$4
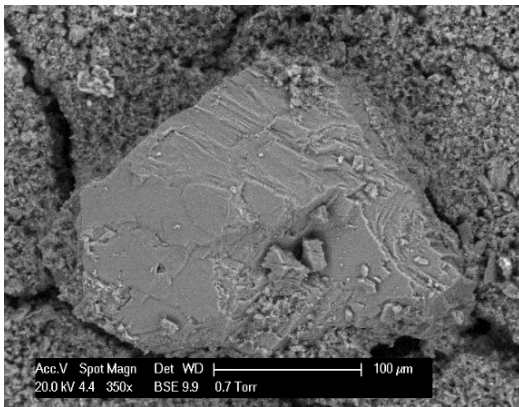
c) Dolomite grain, 4000 ppm PFC, pH$_0$4
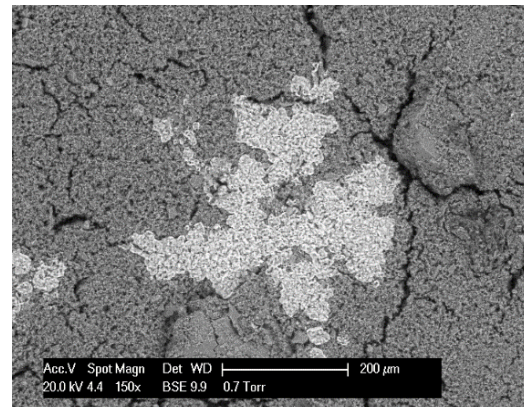
d) Precipitate, Dolomite, 4000 ppm PFC, pH$_0$4

Figure 4.30. Morphology of 4000 ppm PFC Samples for 100-315 µm calcite and dolomite at pH0 4 on ESEM Samples

Table 4.6. EDX analysis of 4000 ppm PFC for 100-315 µm calcite and dolomite at pH$_0$ 4

Element	Calcite grain 4000 ppm (pH04)		Bulk precipitate 4000 ppm (pH04)		Dolomite grain 4000 ppm (pH04)		Bulk precipitate 4000ppm (pH04)	
	% Weight	% Atomic	% Weight	% Atomic	% Weight	% Atomic	% Weight	% Atomic
C	-	-	-	-	15	13	-	-
O	59	77	50	66	54	61	55	71
Na	2	2	3	3	2	1	6	5
Mg	3	1.5	7	7	8	6	10	9
P	3	2	11	7	2	1	3	2
S	2	1	7	5	2	1	3	1
Cl	1	0.5	4	3	14	6	7	4
Ca	30	16	18	10	15	1	16	8

As shown in Figure 4.30 and Table 4.6 for the PFC results, phosphorus is clearly detected at a high level in the finer PFC/Ca precipitate which forms in the bulk (P ~11% and 3% by weight for calcite and dolomite respectively). However, in addition, there is a smaller but detectable amount of P on the calcite and dolomite grains (~3% and 2% by weight, respectively) for the 4000ppm PFC case. This lower amount is possibly due to some of the PFC/Ca precipitate adhering to the calcite or dolomite surface or is part of the adsorbed SI. Some significant levels of sulphur (~2.12 % by weight) have been detected in the SI/dolomite case, appearing as some white spots on bulk precipitate (see Figure 4.30(d)), which may come from the PFC SI.

ESEM/EDX results for the 4000ppm PFC case at pH_0 6 for both calcite and dolomite are shown in Figure 4.31 and Table 4.7. These results for the PFC/dolomite case show that phosphorus is again clearly detected at a significant level (~3%) in the finer precipitate which forms in the bulk. This is similar to the phosphorus levels detected for the PFC/Calcite case (~3%). In addition, there is a detectable amount of P (~ 3% by weight, ~ 0.3% by weight) on the dolomite and calcite grains themselves, respectively; possibly due to some of the SI/Ca precipitate adhering to the dolomite and calcite surfaces or may be part of the adsorbed SI. Furthermore, as the pH of the PFC solutions increases in the dolomite case, the amount of phosphorus detected, clearly increases (~ 3% and ~4% by weight at pH 4 and 6 respectively). In addition, it should be mentioned that in the PFC/dolomite system, Ca/Mg ratio for pH_0 4 & 6 are quite similar (~1.6) while this ratio decreases as pH is reduced to pH=2 (Ca/Mg: 1.1). Moreover, the Ca/P ratio is higher than Mg/P for all initial pH values which confirms that calcium interacts more strongly with the inhibitor. In the PFC/calcite case, Ca/Mg ratio is higher than in the dolomite system.
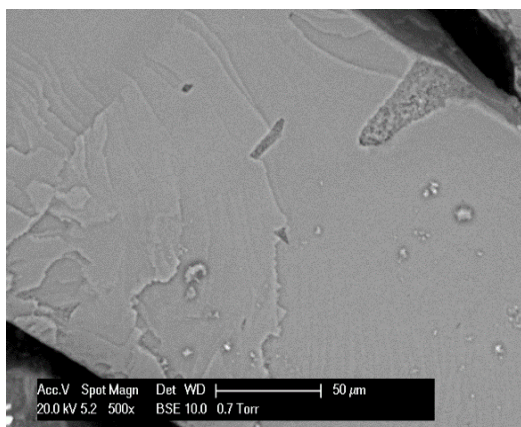
a) Calcite grain, 4000 ppm PFC, $pH_0 6$
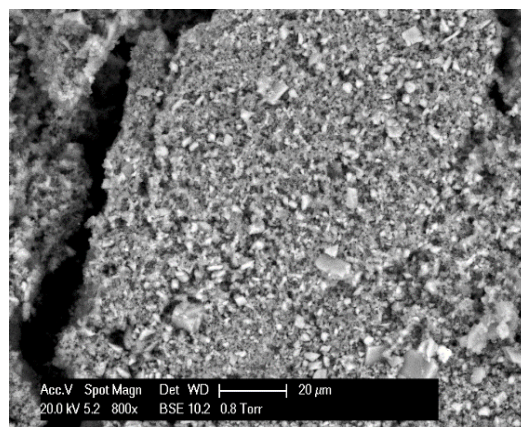
b) Precipitate, Calcite, 4000 ppm PFC, $pH_0 6$
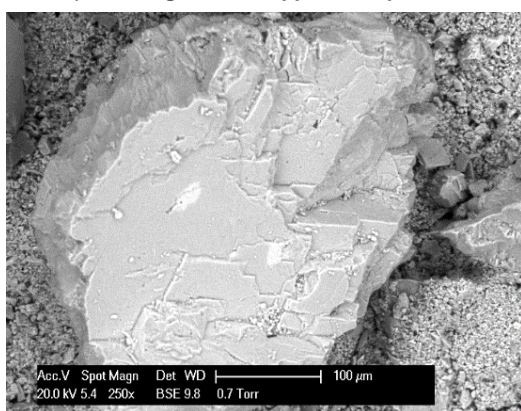
c) Dolomite grain, 4000 ppm PFC, $pH_0 6$
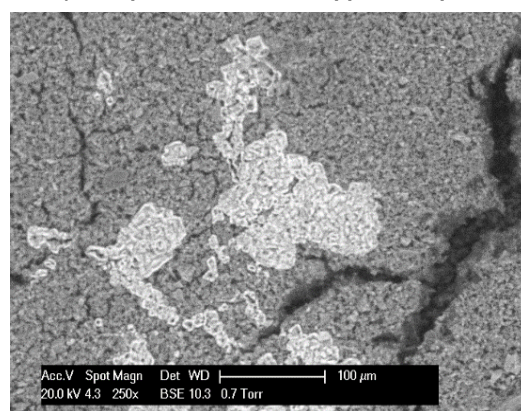
d) Precipitate, Dolomite, 4000 ppm PFC, $pH_0 6$

Figure 4.31. Morphology of 4000 ppm PFC Samples for 100-315 µm calcite and dolomite at pH_0 6 on ESEM Samples

Table 4.7. EDX analysis of 4000 ppm PFC for 100-315 µm calcite and dolomite at pH_0 6

Element	Calcite grain 4000 ppm ($pH0$ 6)		Bulk precipitate 4000 ppm ($pH0$ 6)		Dolomite grain 4000 ppm ($pH0$ 6)		Bulk precipitate 4000ppm ($pH0$ 6)	
	% Weight	% Atomic	% Weight	% Atomic	% Weight	% Atomic	% Weight	% Atomic
C	13	22	21	31	20	28	21	31
O	51	61	49	54	51	54	44	49
Na	1	0.5	3	2	2	2	7	5
Mg	-	-	2	2	4	5	6	4
P	0.3	0.2	3	2	3	12	3	2
S	-	-	2	1	-	-	2	1
Cl	1	0.3	4	2	2	1	7	4
Ca	34	16	16	7	18	8	10	4

Particle Size Analysis (PSA) & Particle Size Distributions (PSDs): Since we could not detect any phosphorus in PPCA/Carbonates by EDX, we required a method to carry out Particle Size Analysis (PSA). Particle size distributions (PSDs) were measured for all precipitates which formed in the apparent adsorption experiments. A Particle Size Analyser (PSA) manufactured by the Malvern Company was used. Firstly, the particle size analysis for the larger pure calcite/dolomite (100-315 µm) was performed using a 300 mm Lens (the largest one which can only detect larger particle of order ~100+ µm) to measure the PSD and then similar PSD measurements were performed using the smaller 75mm lens (suitable for PSD down to ~1+ µm sizes). Results are first shown for the larger particle distributions in Figure 4.32 (a) (for PPCA/calcite) and Figure 4.32 (b) (for PPCA/dolomite). We show PSA for PPCA/carbonate substrates at pH2 since this is the case for which most precipitate was observed.
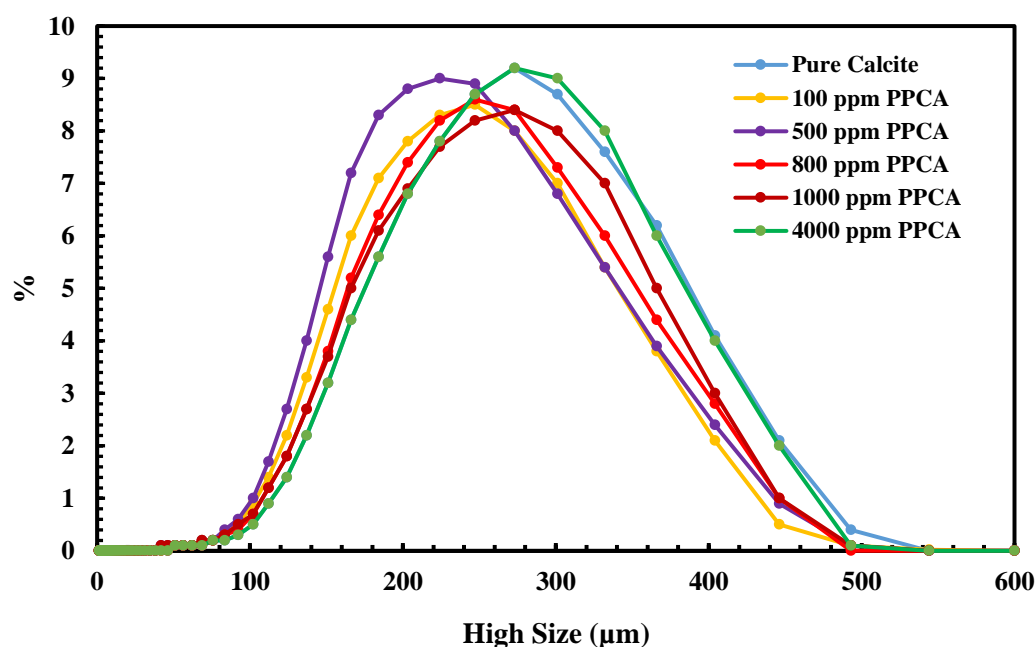
a) Larger grain sizes, 100-315 µm Calcite, pH$_0$ 2

163
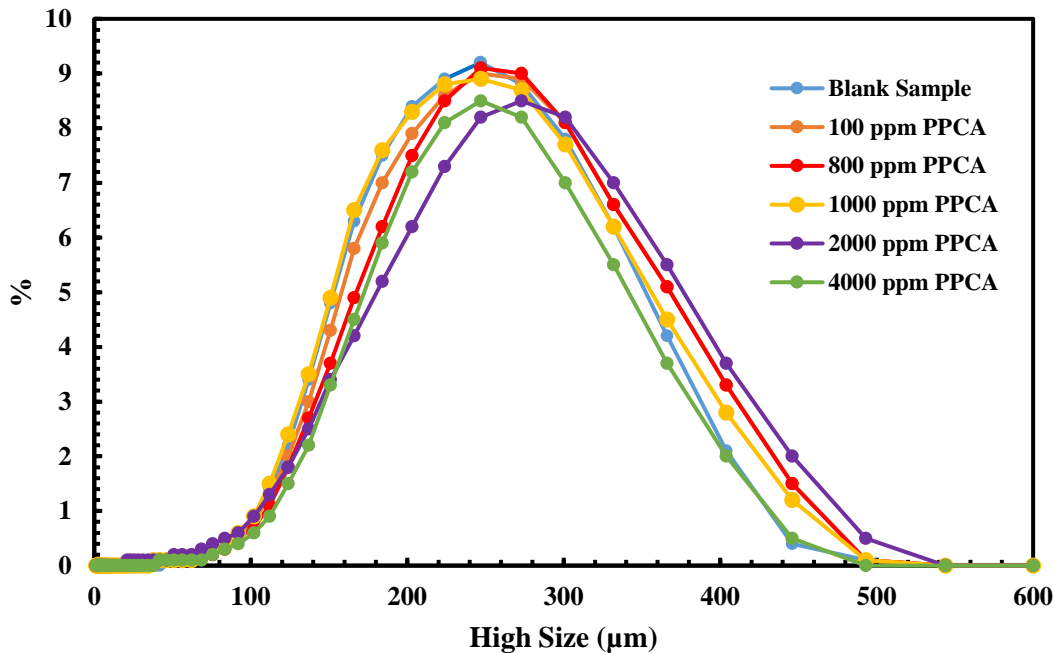
b) Larger grain sizes, 100-315 μm Dolomite, pH_0 2

Figure 4.32. Particle Size Analysis for 100-315 μm calcite and dolomite residue at different concentrations and pH_0 2 with the 300 mm lens

The PSD results in Figure 4.32 show that there is good consistency in the measurement of the carbonate particle sizes with the 300mm lens for both experiments. For these cases, we see that only large particle sizes are observed and are broadly in agreement with the calcite/dolomite size range we expect. When these same sample cases were examined by the smaller lens (45 mm lens) which can "see" much smaller particles (from ~1 – 20 μm), we see no fine particles of this size for the 100ppm case; see Figure 4.33– the "flat line". However, when at increased PPCA concentrations where the system is going from a region of pure adsorption to coupled adsorption/precipitation, we now see peaks of PSD between ~1 – 10 μm (Figure 4.32). Clearly, these populations of smaller particles are the SI/Ca precipitated material which forms as this finer material; note that this is clearly distinguishable from the calcite/dolomite grains (which are much bigger as shown in Figure 4.32 and this can also be seen directly from the ESEM results in Figure 4.28).
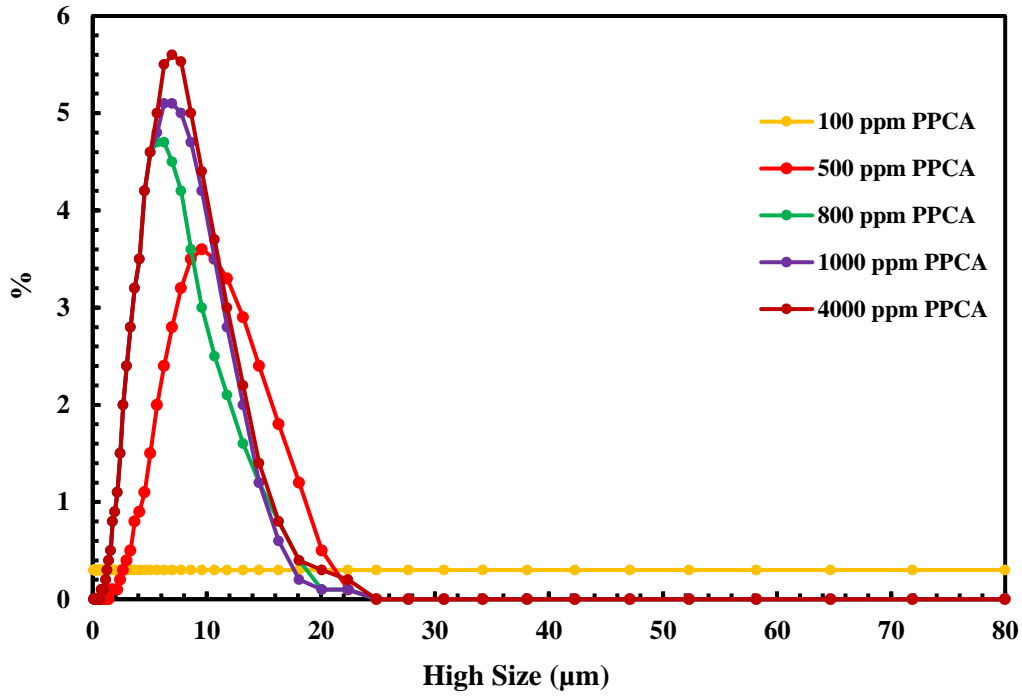
a) Small precipitate particles, 100-315 μm Calcite, pH$_0$ 2
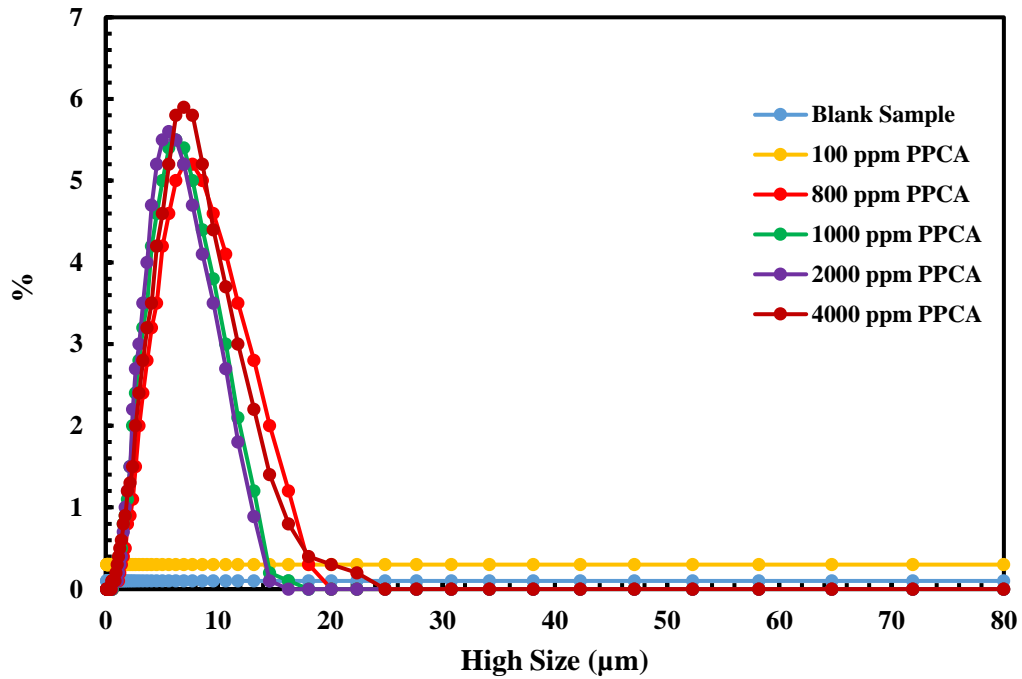
b) Small precipitate particles, 100-315 μm Dolomite, pH$_0$ 2

Figure 4.33. Particle Size Analysis for 100-315 μm precipitate deposited on filter paper at different concentrations and pH$_0$ 2 with 45 mm lens

In this section, results have been presented for a range of apparent adsorption experiments for the polymeric SIs PPCA and PFC on the carbonate minerals calcite and dolomite. The results are plotted as graphs of Γ_{app}, vs. C_f, at different (m/V) ratios, as shown in Figure 4.19 and Figure 4.20. In these experiments, the initial pH was fixed (at pH_0 2, 4, or 6), as was the initial amount of Ca in the solution ($[Ca^{2+}]_0$ =428 ppm), but both of these quantities changed at equilibrium; pH always increased and the final normalized $[Ca^{2+}]$ was either greater than unity (initial pH_0 2 and 4) or approximately unity (pH_0 6). Final pH and final $[Ca^{2+}]$ levels were measured for all experiments (i.e., for each concentration point in the apparent-adsorption curve). In addition, all precipitates were analysed using ESEM-EDX and PSA. These carbonate systems are much more chemically reactive than sandstone minerals (e.g., quartz, feldspar, and clays), which have already been studied extensively. The inhibitor solution reacts chemically with the rock to change the solution pH and $[Ca^{2+}]$ levels such that, for the higher SI concentrations, precipitation of a sparingly soluble SI/Ca complex is formed, giving a region where coupled adsorption/precipitation (denoted Γ/Π) occurs. The detailed observations (described previously) for apparent adsorption, the corresponding final pH and normalized $[Ca^{2+}]$ behaviour, and the ESEM-EDX/ PSA results are summarized in Table 4.8.. It is these results that we must explain qualitatively, and in due course reproduce by modelling.

Table 4.8. Summary of apparent adsorption, the corresponding final pH values and normalized [Ca^{2+}] observations, and the ESEM-EDX and PSA results from the experiments

OBSERVATIONS on Apparent Adsorption Level - both Calcite and Dolomite
(Γ_app results for m = 5g at highest SI conc.; units mg/g)

Scale Inhibitor (SI)	Calcite pH =2	Dolomite pH=2	Calcite pH =4	Dolomite pH=4	Calcite pH =6	Dolomite pH=6	NOTES
PPCA	10.7	9.5	9.5	8.5	5.7	4.7	1. **PPCA** Γ_{app} Calcite > Dolomite
So ==>	Γapp_Cal >	Γapp_Dol	Γapp_Cal >	Γapp_Dol	Γapp_Cal >	Γapp_Dol	& Γ_{app} at pH 2 > Γ_{app} at pH 4 > at pH 6
PFC	4.1	13	8.8	11.1	8.9	10.9	2. **PFC** Γ_{app} Calcite < Dolomite
So ==>	Γapp_Cal <	Γapp_Dol	Γapp_Cal <	Γapp_Dol	Γapp_Cal <	Γapp_Dol	& Γ_{app} at pH2 < Γ_{app} at pH 4 ≈ at pH 6 (for Calcite) & Γ_{app} at pH2 > Γ_{app} at pH 4 ≈ at pH 6 (for Dolomite)

OBSERVATIONS on Final pH and [Ca^{2+}]

	Final pH (higher SI conc.; range, m = 5 - 10g)						Final normalised [Ca^{2+}] (range m = 5 - 10g)					
Scale Inhibitor (SI)	Calcite pH 2	Calcite pH 4	Calcite pH 6	Dolomite pH2	Dolomite pH 4	Dolomite pH 6	Calcite pH2	Calcite pH 4	Calcite pH 6	Dolomite pH2	Dolomite pH 4	Dolomite pH 6
PPCA	~7.08	7.04 - 7.34	7.94-8.02	7.6-7.88	7.51-8.01	8.0 - 8.2	x2.8-3.1	x1.8	x0.91 - 0.97	x1.78-1.8	x1.26- 1.4	x0.84 - 0.89
PFC	4.93-5.09	5.62 - 6.04	6.0 - 6.3	7.62-8.17	6.85 - 7.36	7.61 - 7.87	x3	x1.66	x1.03 - 1.07	x1.76-2	x1.17 - 1.26	x0.94 - 0.97

OBSERVATIONS ON ESEM/EDX and Particle size distributions

Scale Inhibitor (SI)	ESEM	EDX	PSA
PPCA	1. Smaller sized precipitates observed for **both** PPCA and PFC.	1. No P detected in PPCA precipitates or on surface - % P too low (must be present)- Ca observed.	1. For both PPCA and PFC precipitates confirmed in size range 1 - 10µm.
PFC	2. Mostly separate precipitate but very small amounts seen adhering to calcite and dolomite.	2. Much P seen in PFC precipitates in particular - some P on surfaces	2. Very distinct larger PSD (100 - 500 µm) seen for rock grains.

The specific conclusions from this section are the following.

1. Both pure adsorption (Γ) and coupled adsorption/precipitation (Γ/P) regions are clearly observed for PPCA, on both dolomite and calcite, for initial pH values of pH$_0$ 2, 4, and 6. This is also the case for PFC at pH$_0$ 2, 4, and 6, except in the case at pH$_0$ 2, where PFC shows only pure adsorption on calcite because the sulfonate functional group is more acidic, and this group has higher tolerance (lower binding) to Ca^{2+}.

2. Precipitation is more dominant for SI/carbonate retention than adsorption in the sense that it occurs over a much wider SI range, above a minimum concentration of approximately 100 ppm (for PPCA) and approximately 500 ppm (for PFC). This is probably because of the presence of more sulfonate groups on the PFC, whereas PPCA mainly has carboxylic acid groups.

167

3. The actual amount of precipitate formed varies from case to case, depending on the specific SI (different chemistries), the substrate (calcite or dolomite), initial pH (different levels of rock dissolution and divalent-cation generation in situ), and temperature T (although a fixed T=95°C was used in this work). In the low-SI-concentration region (<100 ppm for PPCA and<500 ppm for PFC), only pure adsorption (Γ) is observed. Hence, in a squeeze treatment in the lower SI tail, the dynamic region of the return curve would be controlled by the relevant low-concentration region of the adsorption isotherm, $\Gamma(C)$. However, the general "loading" of the formation with SI/M^{2+} complex (i.e., the total amount retained as a "reservoir" of SI within the formation) would be as a result of the precipitation/dissolution process.

4. For PPCA, the main observations are that the apparent adsorption (Γ_{app}) levels are higher for lower initial pH conditions (lower initial pH, more Ca generation in situ, more SI/M^{2+} complex formation), and higher for calcite than for dolomite (more Ca content relatively in calcite than in dolomite). It confirms that the level of Ca contributes to the PPCA retention in carbonate formations.

5. For PFC, the main observations are that the apparent-adsorption (Γ_{app}) levels are approximately the same at pH_0 4 and 6, and higher for dolomite than for calcite (the final pH value of the PFC/dolomite system is higher than that of the PFC/calcite case; as a result, PFC becomes more dissociated in the former system and consequently shows higher retention). We also note that one case, PFC on calcite at pH_0 2, shows only pure adsorption (the more acidic sulfonate functional group has high tolerance to Ca^{2+}). This observation for the PFC/carbonate system is different from the PPCA/carbonate case.

6. Results from ESEM-EDX and PSA generally confirm and are consistent with the static apparent-adsorption results. For both PPCA and PFC, it is clear from the ICP-OES results that both Ca and P are lost from the solution and form a precipitate. This precipitate can be observed directly by ESEM, where a distinct granular precipitate sized much smaller than the carbonate grains (approximately 100 to 400 mm) is observed. This is further confirmed by PSA using the smaller (45-mm) lens, which detects a precipitate with a size range of approximately 1 to 10 mm. EDX does not detect any P in the PPCA/Ca precipitate because the P content of PPCA is too low to detect using this method, but it does detect Ca. For the PFC/Ca precipitate, EDX does easily detect high P concentrations in the deposit where clear C/P has occurred, and the EDX levels are

higher as Γ_{app} (precipitation) increases. Very little P is detected directly on the calcite or dolomite grain surfaces, but traces are sometimes seen.

4.5.   Phosphate Ester Scale Inhibitors Retention in Carbonates

In this section, we investigated the retention of the environmentally friendly SI, polyhydric alcohol phosphate ester (PAPE), on calcite and dolomite substrates. Elemental analysis of the supernatant solution as well as pH measurement and environmental scanning electron microscopy (ESEM) with energy dispersive X-ray analysis (EDX) were all used to investigate SI retention and to identify the morphology/composition of the resultant SI−Ca precipitates. Results revealed that PAPE was retained by calcite via pure adsorption at an initial test pH (pH_0) of 4 and then precipitated at pH_0 6. In contrast, the PAPE/dolomite system was found to be effectively pH-independent, with precipitation dominating at both pH_0 values. Any temperature effect was negligible for dolomite/PAPE retention, whereas with calcite, retention was smaller at lower temperature, which is attributed to the temperature-dependence of the substrate solubility. Overall, the final pH of the system and the resulting degree of SI dissociation contributed more to PAPE retention than did the final calcium concentration. EDX analysis confirmed scale-inhibitor phosphorus in the deposited solids, indicating coupled adsorption/precipitation. This phosphorus increased with the amount of precipitation and with the temperature, confirming the corresponding static adsorption test results.

First of all, we present the impact of pH on the apparent adsorption of PAPE on both calcite and dolomite. From the stock solution of [SI] = 10000 ppm active PAPE, lower SI concentrations of 50, 100, 500, 800, 1000, 2000, and 4000 ppm were prepared by dilution and used for the apparent adsorption and compatibility (no mineral substrate) experiments. The pH values of the various PAPE solutions were adjusted to initial pH values (pH_0) of 4 or 6 for the various experiments. Because of the lower thermal stability of PAPE, the maximum temperature for the experiments was limited to 80 °C.
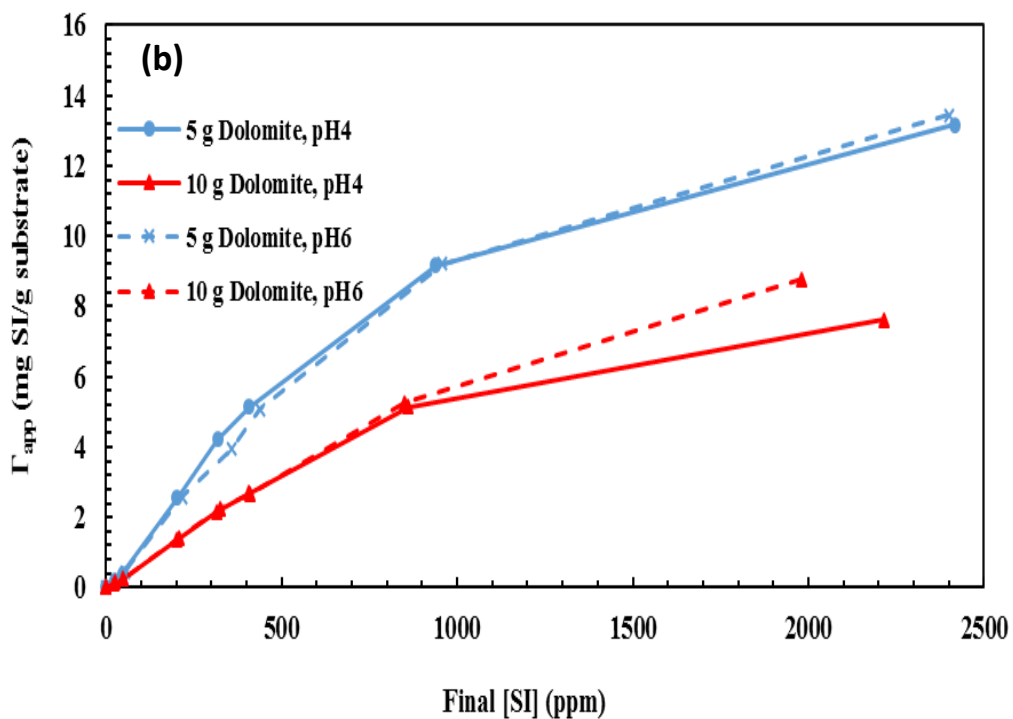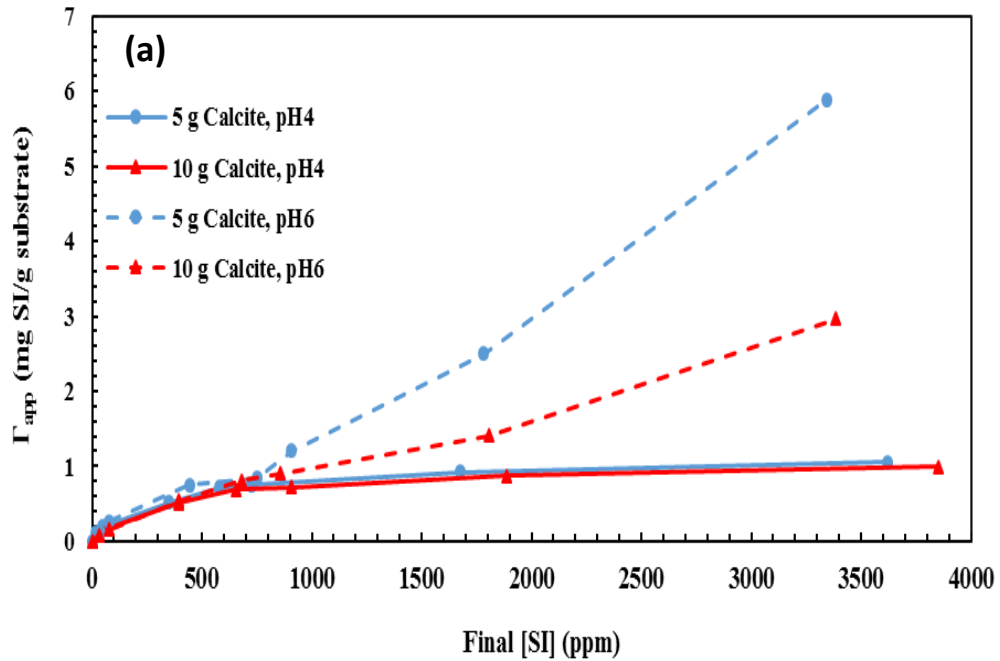
Figure 4.34. Apparent adsorption (Γ_{app}, vs. C_f) for PAPE with 5 and 10 g of (a) calcite and (b) dolomite at pH_0 4 & 6; T = 80°C

Figure 4.34 (a) shows that, for calcite at pH_0 4 (solids lines), pure adsorption was observed for all concentrations of PAPE. For the same substrate at pH_0 6 (dashed lines, Figure 4.34(a)), pure adsorption was observed up to ~800 ppm with deviation at higher PAPE concentrations

indicating the occurrence of coupled adsorption/precipitation (Γ/Π)[10,79]. This behaviour can be explained by the pH-dependence of scale inhibitor dissociation in relation to the final pH of the solutions. It has been shown previously that at lower pH values, phosphonate inhibitors are less dissociated, which would lead to lower propensity for precipitation and therefore lower apparent adsorption[42,99].

For the PAPE/dolomite system shown in Figure 4.34 (b), both pure adsorption and coupled adsorption/precipitation predominates for both initial pH values. Only pure adsorption was seen for [SI] up to ~100 ppm, but above a PAPE concentration of 100ppm, the curves deviate indicating a change in retention regime to coupled adsorption/precipitation. Unlike the calcite system, the apparent adsorption of the PAPE/dolomite system was effectively pH independent[43,44].

When compared with the retention mechanisms of other scale inhibitors, it is believed that the weak polyacidic nature of PAPE could lead to a greater degree of dissociation at higher pH. This may be attributed to the different chemistry of the PAPE/carbonate systems compared to the retention of other conventional inhibitors (phosphonate and polymeric scale inhibitors) where the retention increases as pH increases for phosphonate SIs and as pH decreases for polymeric inhibitors[42,79]. Here, PAPE was retained more on dolomite than on calcite, which is consistent with previous phosphonate inhibitor/carbonate system observations. This can be related to the higher final pH values in the PAPE/dolomite system compared to those for the PAPE/calcite system (see the corresponding figures showing final pH below). Since the inhibitors such as PAPE can be considered as weak polyacids, schematically represented as H_nA, these can be partly dissociated (i.e. $H_nA \leftrightarrows H^+ + H_{n-1}A^-$). Therefore, at very low (acidic) pH, the H_nA equilibrium is to the left and the molecule is more associated as H_nA, and at higher pH it is more dissociated into H^+ and $H_{n-1}A^-$. The SI (H_nA) is much more likely to complex with Ca^{2+} to form a SI/Ca complex in its dissociated form (i.e. at higher pH values) and less likely to form complexes at lower pH values[98,100].

In the PAPE/dolomite system, the final pH is higher than for PAPE/calcite, due to the higher solubility of dolomite in the matrix brine (NSSW), so the PAPE inhibitor would therefore be somewhat more dissociated (more $H_{n-m}A^{m-}$ in solution) than in calcite. Thus, PAPE is much more likely to interact with divalent cations and form $SI-M^{2+}$ in dolomite than in calcite[43]. Hence, it

171

was observed that the degree of apparent adsorption of PAPE on dolomite was more than on calcite, even though the calcium content of calcite was relatively higher than that of dolomite. It can therefore be concluded that pH, in particular pH_f, controls PAPE retention in carbonate systems as opposed to the calcium concentration. These results have implications on the application pH that should be used when PAPE is deployed in carbonate reservoirs.

Now, we study the impact of temperature on PAPE retention in carbonates. As PAPE was seen to be retained more on the carbonate substrates at pH_0 6, the experiments were repeated at an initial pH of 6 and a temperature of 60°C to investigate the effect of temperature on apparent adsorption.
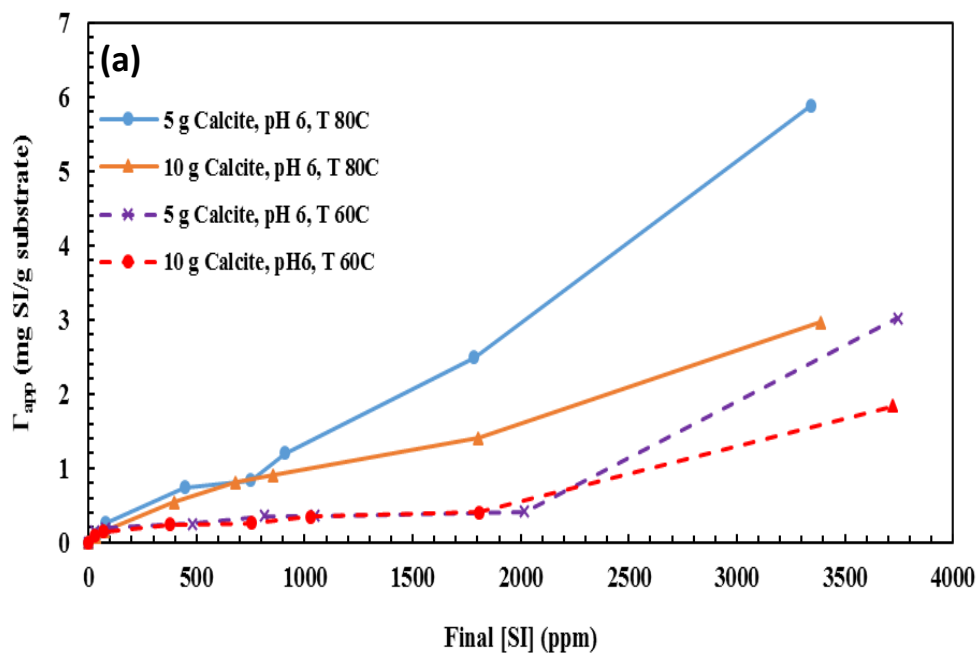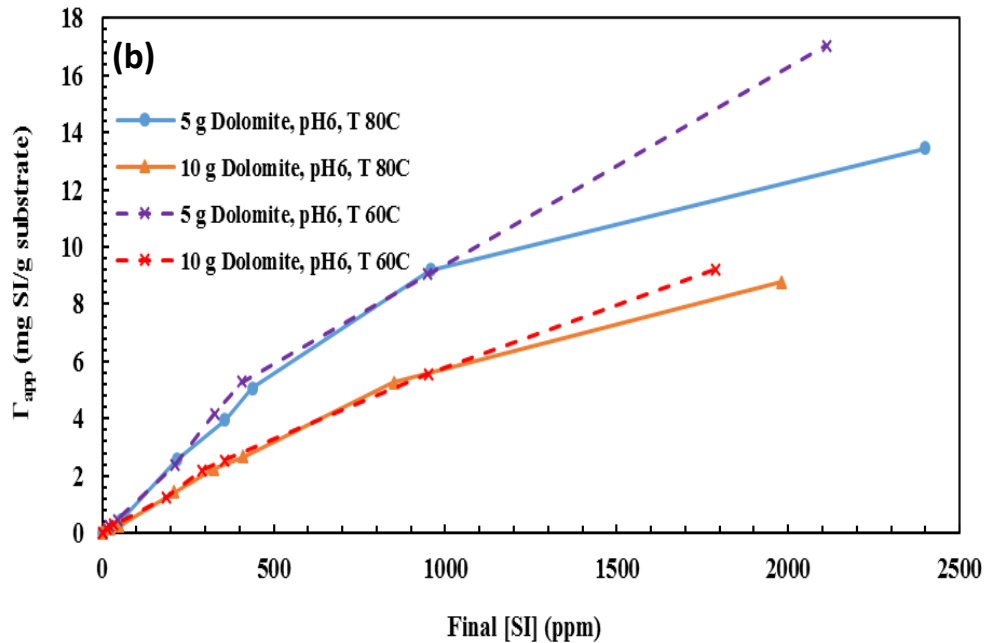
Figure 4.35. Apparent adsorption (Γ_{app} vs. C_f) for PAPE with 5 and 10 g of (a) calcite and (b) dolomite at T = 60 & 80°C; pH_0 6

As shown in Figure 4.35(a), the resultant Γapp with calcite was lower at 60°C than at 80°C. Calcite is less soluble at higher temperature, however the interactions between the scale inhibitor and Ca^{2+}, including the strength of $SI-M^{2+}$ binding, increases significantly with temperature and thus the solubility of the $SI-M^{2+}$ complex decreases, resulting in more precipitation/retention[101]. The dominant retention mechanism of PAPE with calcite at 60°C changes from coupled adsorption/precipitation to pure adsorption, although both mechanisms exist above 2000 ppm PAPE. In fact, temperature affected apparent adsorption of PAPE on calcite quite significantly. It was therefore concluded that PAPE works more effectively at higher temperature in calcite formations, at least in terms of retention, although there may be chemical stability issues at elevated temperature.

The Γ_{app} of PAPE on dolomite was not as temperature dependent (Figure 4.35 (b)) as it was for calcite, with apparent adsorption increasing as lower temperature only at the highest PAPE concentration[52]. These results show that PAPE has good retention characteristics at both temperatures and is therefore a good SI candidate for these reservoir and operational conditions.

When the scale inhibitor is injected into carbonate formations, the SI (weak polyacid) solution contacts the carbonate mineral substrate and causes rock dissolution leading to an increase of

initial pH to ~7 and 8 for calcite and dolomite substrates, respectively. The increased solution pH causes the inhibitor to become more dissociated, and these negatively charged species (dissociated scale inhibitor) are then able to be adsorbed onto the positively-charged rock surface through electrostatic interactions[49]. In addition, if the scale inhibitor concentration is sufficiently high, Ca^{2+} binds with the dissociated scale inhibitor (SI-Ca^{2+} complexation)[96]. Thus, the entire system is coupled and the 3 parts of the equilibrium system are:

(i)   The dissociation of SI as a weak polyacid (H_nA) to form dissociated species, such as $H_{n-m}A^{m-}$ right up to A^{n-} at very high pH values;

(ii)   These dissociated SI species, which are very strong chelating agents, then bind with Ca^{2+} (and/or Mg^{2+}) ions to form SI/Ca complexes which are known to be sparingly soluble;

(iii)   The above reactions are coupled to the carbonate system since the lower pH solution conditions and the chelating power of the dissociated SI cause the carbonate equilibrium to change.

To explain these observations, further ancillary results will be presented below on carbonate dissolution and on the final pH values of the system. Figure 4.36(a) and Figure 4.36(b) show the final solution pH as a function of final SI concentration for the corresponding apparent adsorption experiments presented in Figure 4.34(a) and Figure 4.34(b).
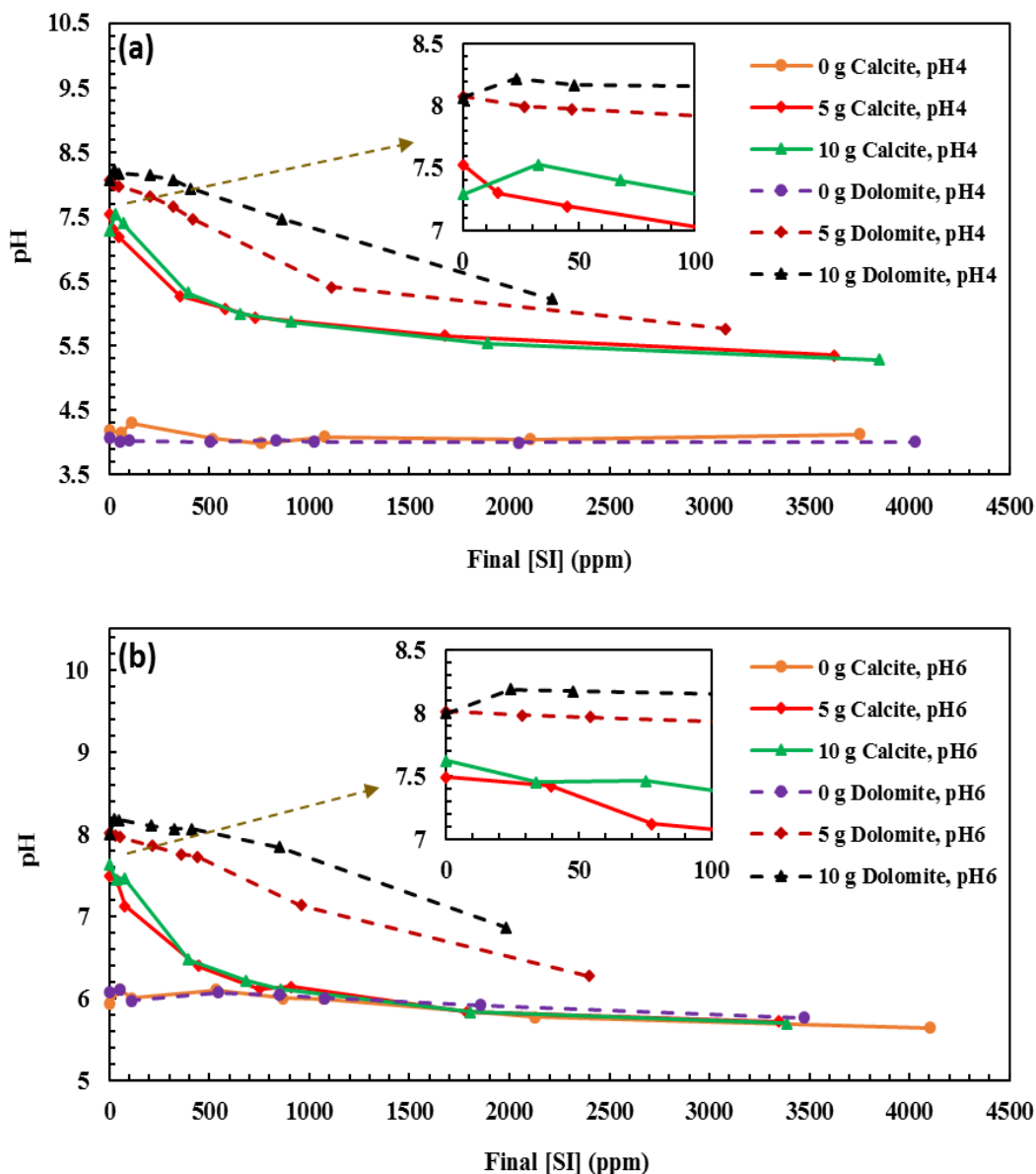
Figure 4.36. Final pH as a function of [PAPE] with 0, 5 or 10 g of calcite or dolomite at T = 80°C, (a) pH_0 4 and (b) pH_0 6

For pH_0 4 at 80°C compatibility tests (no substrate) there was no noticeable change in final pH (see Figure 4.36(a)), showing that PAPE was compatible with NSSW at these conditions. The final pH increased when the tests were repeated in the presence of 5 or 10 g of either carbonate substrate due to the dissolution of calcite or dolomite with the associated liberation of Ca^{2+} (& Mg^{2+} for dolomite) and carbonate (CO_3^{2-})[45]. This trend was observed until the retention regime changed from pure adsorption to coupled adsorption/precipitation, at which point the divalent cations generated *in situ* were consumed by the formation of a SI-M^{2+} complex[87]. The final pH

for dolomite was higher than the calcite system, resulting in a greater degree of PAPE dissociation and a higher tendency for apparent adsorption (as shown in Figure 4.34(a) and Figure 4.34(b)).

When the tests were repeated at pH0 6 (Figure 4.36 (b)), a slight decrease in final pH (to ~pH 5.6) was noted at high [PAPE] in the absence of any carbonate substrate, suggesting a slight incompatibility of the SI with NSSW at these conditions. This incompatibility is not desirable, as the inhibitor should precipitate far away from the wellbore, therefore it would be prudent to inject PAPE/NSSW at a lower pH to avoid this issue.

The final solution pH as a function of final scale inhibitor concentration is shown in Figure 4.37(a) and Figure 4.37(b) for the carbonate systems at T = 60°C and 80°C, for a single pH_0 of 6.
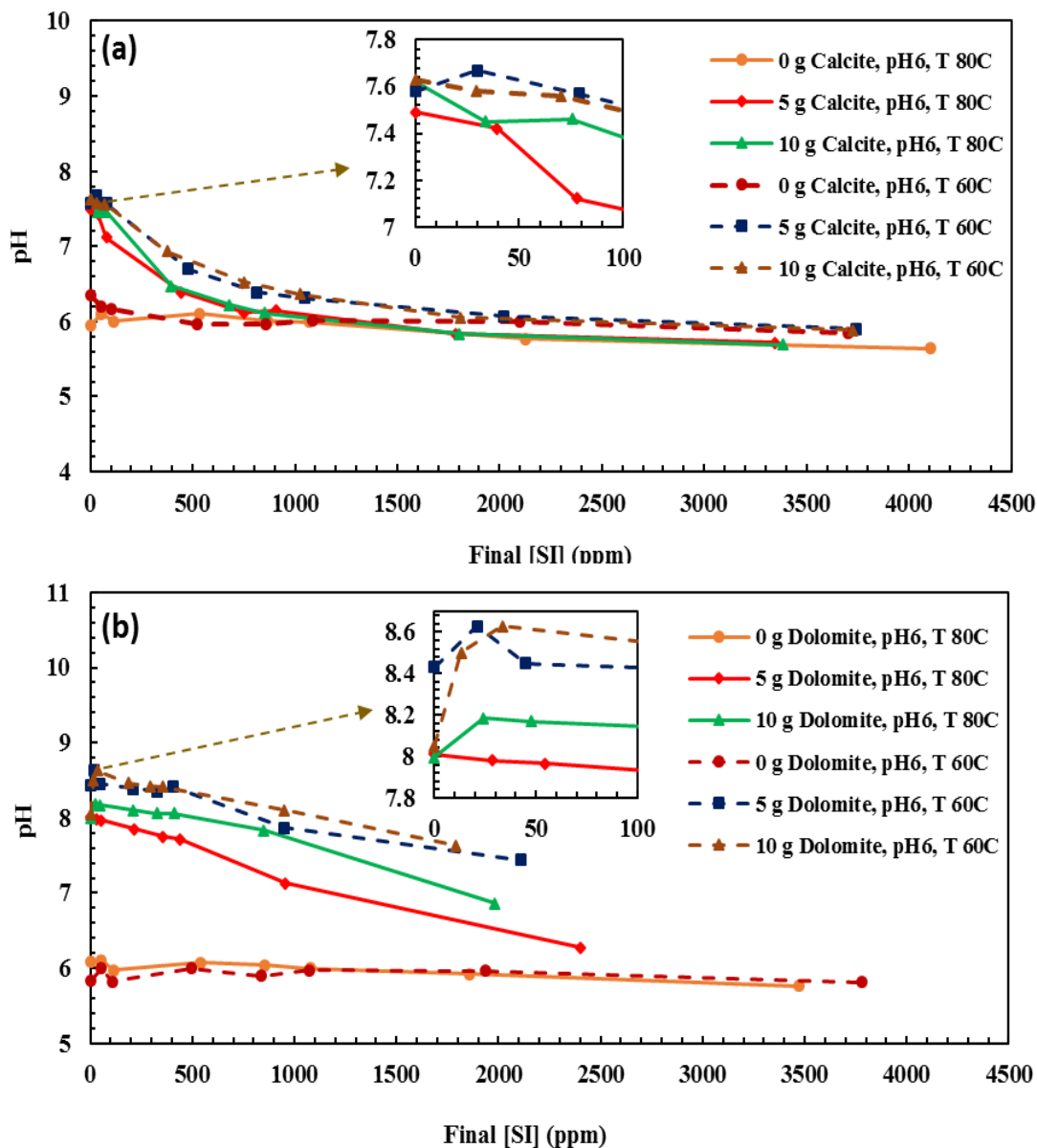
Figure 4.37. Final pH as a function of [PAPE] with 0, 5 and 10 g of (a) calcite or (b) dolomite at T = 60 & 80°C, pH$_0$ 6

Figure 4.37 (a) shows that PAPE was not compatible with NSSW at 60°C which was similar to the PAPE/NSSW behaviour at 80°C (Figure 4.36(b)). Thus, the final pH at the highest concentration ([PAPE] = 4000 ppm), decreased due to the reaction between PAPE and the calcium in NSSW. In the presence of calcite, the final pH of the scale inhibitor solution increased due to rock dissolution and then decreased due to a change in the retention mechanism from pure adsorption to coupled adsorption/precipitation along with the associated phosphorus and calcium removal from solution due to complexation and precipitation. Moreover, the final pH at 60°C

decreased so sharply that it was lower than the pH required for PAPE dissociation[96,99]. In other words, the scale inhibitor was in its more associated form and the apparent adsorption of PAPE on the calcite mineral at the lower temperature was reduced and the dominant mechanism of retention was pure adsorption[43]. However, at 4000 ppm, PAPE was sufficiently dissociated that the retention mechanism switched to precipitation. Thus, the retention mechanism of PAPE on calcite was dependent on temperature; lower temperature results in less dissociated PAPE and accordingly less precipitation. In the PAPE/dolomite system (Figure 4.37 (b)), the final pH values for 60°C and 80oC were quite similar from 0 – 2000 ppm, however, the pH at 4000 ppm, T = 60°C was a little higher than that at T = 80°C, which indicates greater PAPE dissociation and supports the conclusion that the apparent adsorption of PAPE on dolomite is greater at 60°C than at 80°C for [PAPE] = 4000 ppm (Figure 4.37 (b)).

To further establish the pure adsorption and coupled adsorption/precipitation behaviour, changes of $[Ca^{2+}]$ and $[Mg^{2+}]$ concentration were measured before and after the experiments[79]. Results are shown in Figure 4.38(a) and Figure 4.38(b), where a decrease in divalent ions from input concentration can be attributed to the precipitation of a M^{2+}-PAPE complex and any increase was due to carbonate substrate dissolution. That said, it is possible for $[Ca^{2+}]$ to reach levels above the input concentration and for precipitation to occur as the $[Ca^{2+}]$ increases due to dissolution and $[Ca^{2+}]$ decreases because of complexation. These figures show the calcium and magnesium concentrations normalised to their initial solution values of $[Ca^{2+}]_0 = 428$ ppm and $[Mg^{2+}]_0 = 1368$ ppm.

Figure 4.38. Comparison of C/C_0 Ca^{2+} for PAPE with 0, 5 or 10 g of calcite or dolomite at T = 80°C, (a) pH0 4 and (b) pH_0 6

As shown in Figure 4.38(a), at pH_0 4 there was no noticeable change in normalised $[Ca^{2+}]$ in the absence of calcite or dolomite substrates (compatibility tests), therefore PAPE was seen to be compatible with NSSW at this pH_0. Furthermore, in the presence of calcite, the calcium

concentration increased as a function of PAPE concentration up to ~1.6 times the initial value[52]. For dolomite, calcium decreased as [PAPE] increased, down to approximately a third of input concentration for 4000 ppm SI.

When the tests were repeated at pH_0 6 (Figure 4.38 (b)), calcium consumption was noted in the compatibility tests due to chemical reaction between SI and calcium from the solution, which confirms PAPE was incompatible with NSSW at pH_0 6. In addition, the normalised calcium concentration was lower for pH_0 6 than pH_0 4 for both substrates, due to the low-pH-driven dissolution (~ 0.4 and ~ 1 in dolomite and calcite, respectively)[102].
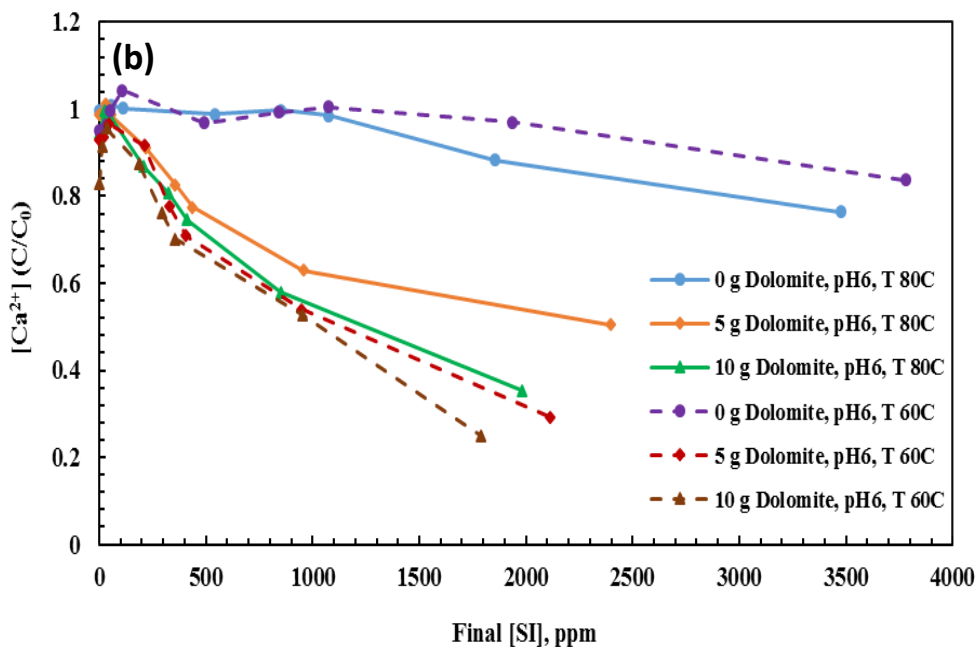
Figure 4.39. Comparison of C/C0 Ca^{2+} for PAPE with 0, 5 and 10 g of (a) calcite or (b) dolomite at T = 60 & 80°C, pH_0 6

The calcium concentration decreased in the absence of a carbonate substrate (Figure 4.39(a)) and Figure 4.39(b)), indicating that PAPE was incompatible with NSSW in these conditions. For 2000 and 4000 ppm PAPE, a SI-M^{2+} complex was formed at 80°C, while 4000 ppm PAPE was required for precipitation at 60°C, suggesting that PAPE incompatibility increased at higher temperature. Because the solubility of PAPE-Ca^{2+} was lower at higher temperature, this results in more precipitation being formed at higher temperature.

In the PAPE/calcite system, the normalised calcium concentration in PAPE/calcite system at 60°C levelled off ~ 1, which means that all calcium generated *in situ* was consumed and there was no excess calcium in solution, while in the same system at 80°C, normalised $[Ca^{2+}]$ decreased even below the baseline, which means that some calcium was consumed from the NSSW. Indeed, the calcium involved in complexation for PAPE/calcite system at 60°C was less than that at 80°C, meaning that less reaction occurred at lower temperature leading to less apparent adsorption[43].

Figure 4.39 (b) shows that the calcium decrease for dolomite was more significant than for calcite, and this is thought to be due to the lower solubility of dolomite at these conditions[52]. Furthermore, the normalised calcium concentration in the dolomite system was similar at both

temperatures, except for the highest [PAPE] = 4000 ppm, ~ 0.6 and 0.5 at 60 & 80°C, respectively, meaning that calcium consumption was about the same.

The level of Mg^{2+} should also be taken into account when examining the retention of PAPE and research has shown that magnesium has a poisoning effect for phosphonate scale inhibition performance[103]. The normalised magnesium concentration is presented to in Figure 4.40(a) and Figure 4.40(b); note that Mg is present in the initial NSSW brine ($[Mg^{2+}]_0$ = 1368 ppm) and it may be available from the dolomite substrate ($CaMg(CO_3)_2$) but it is only present at trace levels in calcite.
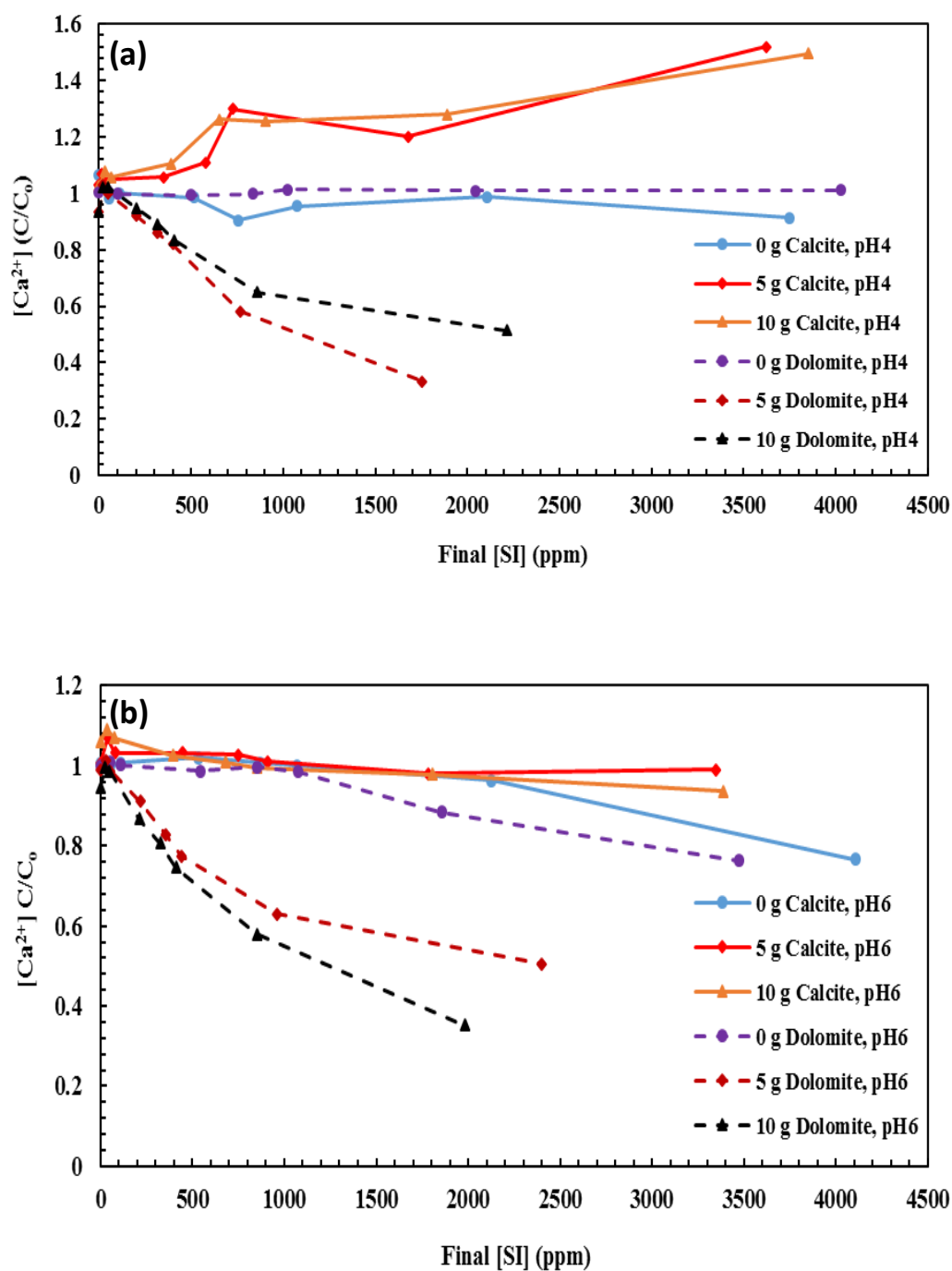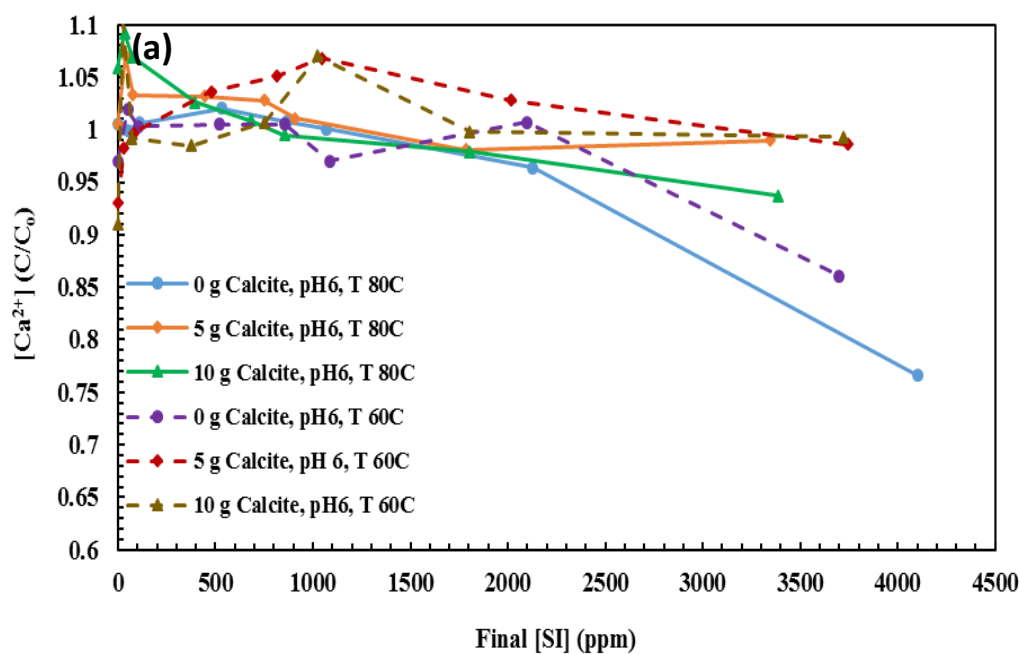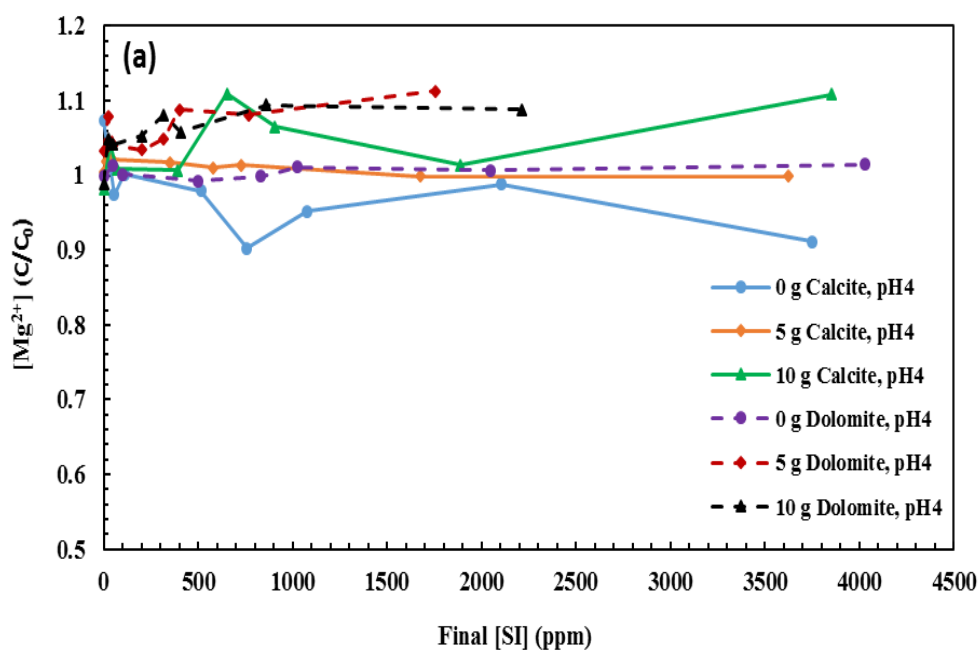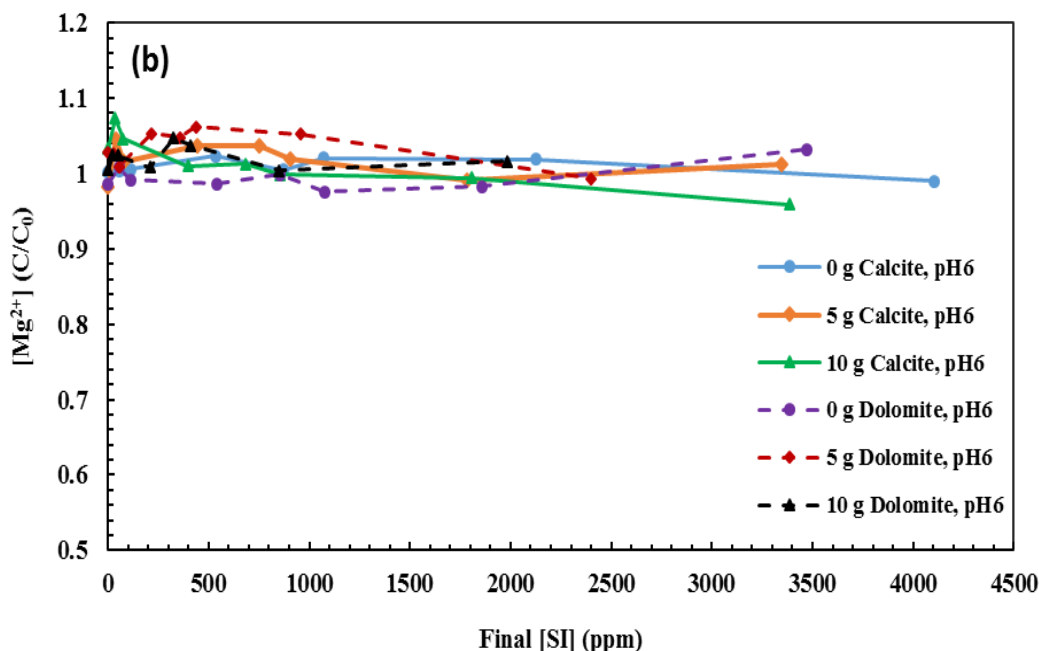
Figure 4.40. Comparison of C/C0 Mg^{2+} for PAPE with 0, 5 and 10 g of calcite and dolomite at T = 80°C, (a) pH_0 4 and (b) pH_0 6

As shown in Figure 4.40(a) and Figure 4.40(b), there was no significant change in Mg^{2+} concentration in the compatibility tests, *i.e.* no reaction/precipitation. When dolomite was present in the SI solutions, a continuous increase in the normalised magnesium concentration was observed ($[Mg^{2+}] \sim$ x1.1), which was higher at pH_0 4 for Ca^{2+} (due to complexation of SI-Ca^{2+}). However, at pH_0 6, *in* situ magnesium generation (for dolomite) was less than that at pH_0 4 and the overall result was that the final magnesium levels in solution approximately levels off at a normalised value of $[Mg^{2+}] \sim 1$. The change in magnesium concentration was insignificant in comparison to the calcium concentration, indicating that magnesium is effectively not involved in any chemical reactions with PAPE to form a complex, while the calcium concentration changes more significantly, clearly demonstrating that it has greater tendency to complex with PAPE than the magnesium does (Figure 4.40 (a) and Figure 4.40(b))[87]. The initial and final Mg^{2+} concentrations were also measured for the 60°C (not presented here) and were seen to be identical to those at 80°C, indicating that the role of Mg^{2+} was also secondary in these systems.

Now, SI/Ca complex should be analysed by ESEM/EDX analytical method as performed before for DETPMP and PFC cases. So, after filtration, all of the solids collected from the static

apparent adsorption tests were examined using ESEM/EDX to investigate the morphology of the precipitated complex in the presence of calcite and dolomite substrates and to analyse the surface elemental composition of all the solids present[42,79].
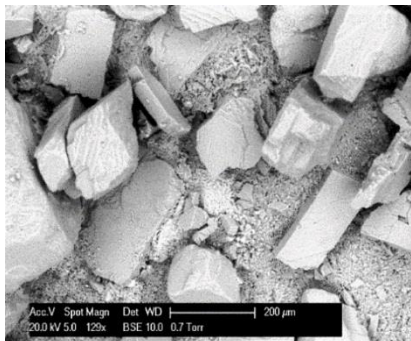
a) Calcite grain, 1000 ppm PAPE
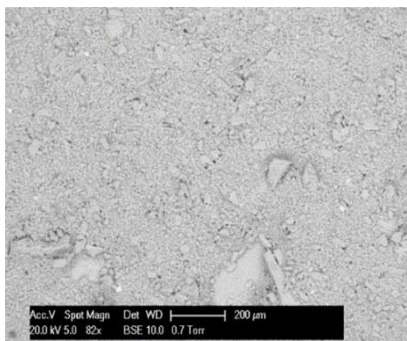
b) Fine solids deposited, calcite, 1000 ppm PAPE
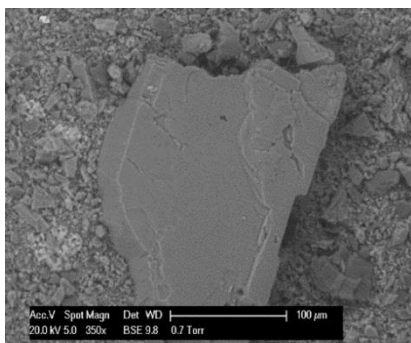
c) Calcite grain, 4000 ppm PAPE
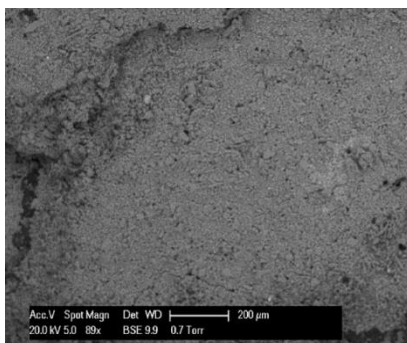
d) Fine solids deposited, calcite, 4000 ppm PAPE
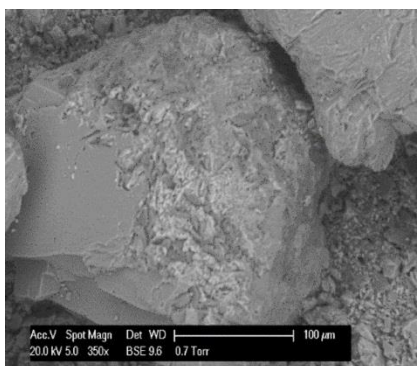
e) Dolomite grain, 1000 ppm PAPE
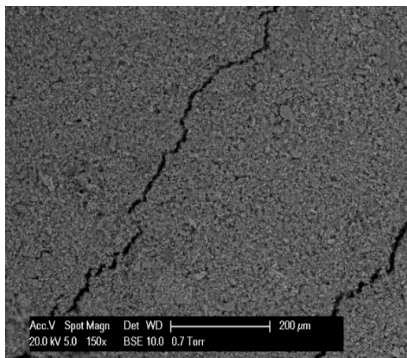
f) Precipitate, dolomite, 1000 ppm PAPE
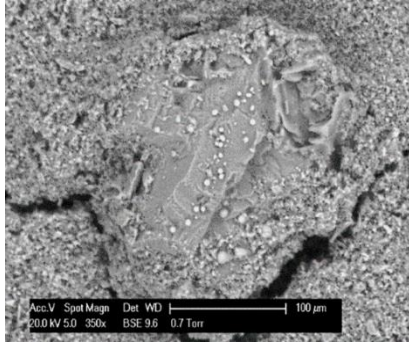
g) Dolomite grain, 4000 ppm PAPE
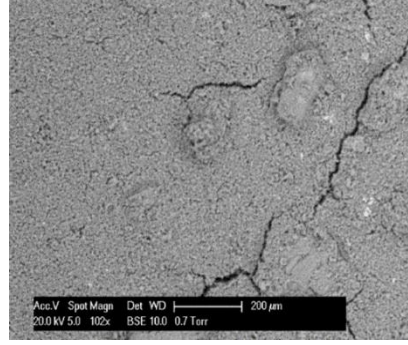
h) Precipitate, dolomite, 4000 ppm PAPE

Figure 4.41. ESEM images of solids recovered from tests at 1000 and 4000 ppm PAPE at pH_0 4, T = 80°C

Table 4.9. EDX analysis of the solids from 1000 and 4000 ppm PAPE for 100-315 µm calcite at pH_0 4, T = 80°C

	Calcite grain 1000 ppm		Fine Solids Deposited 1000 ppm		Calcite grain 4000 ppm		Fine Solids Deposited 4000ppm	
Element	% Weight	% Atomic	% Weight	% Atomic	% Weight	% Atomic	% Weight	% Atomic
C	18	29	12	20	14	20	13	20
O	41	48	52	63	56	62	53	64
Na	7	6	-	-	1	0.5	-	-
Mg	-	-	1	0.4	11	9	0.23	0.48
P	-	-	1.46	0.3	-	-	1.26	0.68
Cl	8	4	0.54	0.3	1	0.5	0.45	0.24
Ca	26	13	33	16	17	8	32	15

Table 4.10. EDX analysis of the solids from 1000 and 4000 ppm PAPE for 100-315 µm dolomite at pH_0 4, T = 80°C

	Dolomite grain 1000 ppm		Bulk Precipitate 1000 ppm		Dolomite grain 4000 ppm		Bulk Precipitate 4000 ppm	
Element	% Weight	% Atomic	% Weight	% Atomic	% Weight	% Atomic	% Weight	% Atomic
C	13	19	15	23	13	20	12	19
O	58	65	54	61	54	62	54	62
Na	-	-	-	-	2	1	1	1
Mg	11	7	-	-	8	5	8	5
P	-	-	1	1	5	3	6	4
Cl	1	1	1	1	1	1	2	1
Ca	17	8	29	14	17	8	17	8

The results in Figure 4.41and Table 4.9. , show that phosphorous (indicative of the PAPE scale inhibitor) was clearly detected at low levels (1.26% and 1.46% at both 1000 ppm and 4000 ppm, respectively) on the calcite substrate. The amount of phosphorus did not change significantly as [SI] increased, which suggests that the retention regime at pH_0 4 was pure adsorption. In other words, the Ca/P ratio becomes constant as [PAPE] increases which confirms the corresponding apparent adsorption of PAPE on calcite at pH_0 4 (Table 4.10), phosphorous was clearly detected at high levels (~5 % at 4000 ppm PAPE), significantly higher than was detected for calcite grains. In addition, phosphorus was detected around the dolomite grains (Figure 4.41(e) & Figure 4.41 (g)), which indicated the SI-Ca precipitate adhering to the dolomite surface. Moreover, the phosphorus detected by EDX in the bulk precipitate for dolomite increased in line with PAPE concentration, contrary to the calcite system, which adds further evidence that PAPE retention differs between these systems. PAPE is retained on dolomite through coupled adsorption/precipitation while pure adsorption is the predominant mechanism with calcite[44].

a) Calcite grain, 4000 ppm PAPE

b) Precipitate, Calcite, 4000 ppm PAPE

c) Precipitate, Dolomite, 4000 ppm PAPE

d) Compatibility test, 4000 ppm PAPE
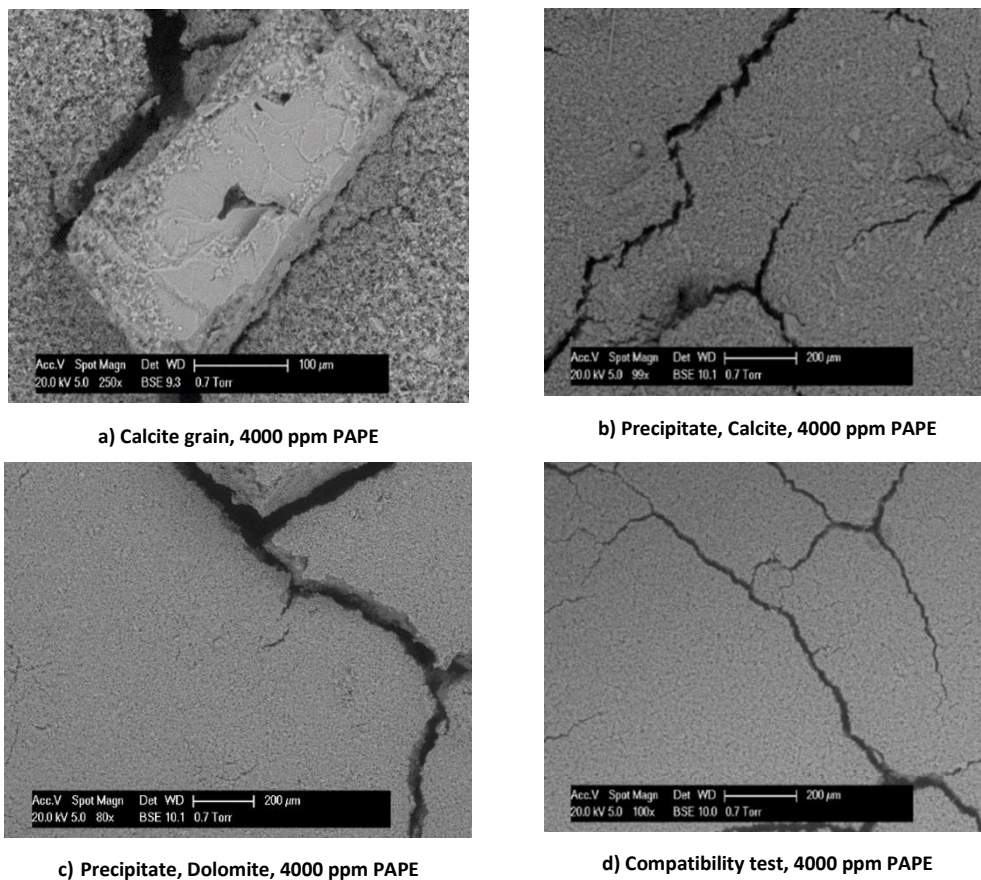
Figure 4.42. ESEM images of solids recovered from tests calcite and dolomite grains at 4000 ppm PAPE at pH_0 6, T = 80°C

Table 4.11. EDX analysis of the solids from 4000 ppm PAPE for 100-315 µm calcite and dolomite at pH_0 6, T = 80°C

Element	Calcite grain 4000 ppm		Bulk Precipitate 4000 ppm (PAPE/Calcite)		Bulk Precipitate 4000 ppm (PAPE/Dolomite)		Compatibility test 4000ppm	
	% Weight	% Atomic	% Weight	% Atomic	% Weight	% Atomic	% Weight	% Atomic
C	13	21	11	18	-	-	12	19
O	51	60	52	61	55	71	52	60
Na	1	1	1	1	2	2	2	1
Mg	3	2	3	3	6	5	4	4
P	7	4	9	5	18	12	15	9
Cl	2	4	2	1	5	3	4	2
Ca	23	11	21	11	14	7	11	5

As shown in Figure 4.42 and Table 4.11, a high level of phosphorus (15 wt%) was detected in the compatibility test for 4000 ppm PAPE, while the quantity of phosphorous detected at 4000 ppm with calcite and dolomite in the bulk precipitate were 9 and 18 wt%, respectively. There was also a significant amount of phosphorus (7 wt%) detected on the calcite grains themselves at 4000 ppm PAPE, which suggests SI-Ca precipitate adhering to the calcite surface or (less likely) part of an adsorbed SI layer[42]. Moreover, as the pH of the PAPE solutions increased, the amount of phosphorus detected in bulk precipitate clearly increased. Finally, the extent of phosphorus detected for dolomite was higher than for calcite, which confirms the corresponding apparent adsorption results.

a) Calcite grain, 4000 ppm PAPE, pH_0 6, T = 60°C   b) Precipitate, calcite, 4000 ppm PAPE, pH_0 6, T = 60°C

c) Precipitate, dolomite, 4000 ppm PAPE, pH_0 6, T = 60°C   d) Compatibility test, 4000 ppm PAPE, pH_0 6, T = 60°C
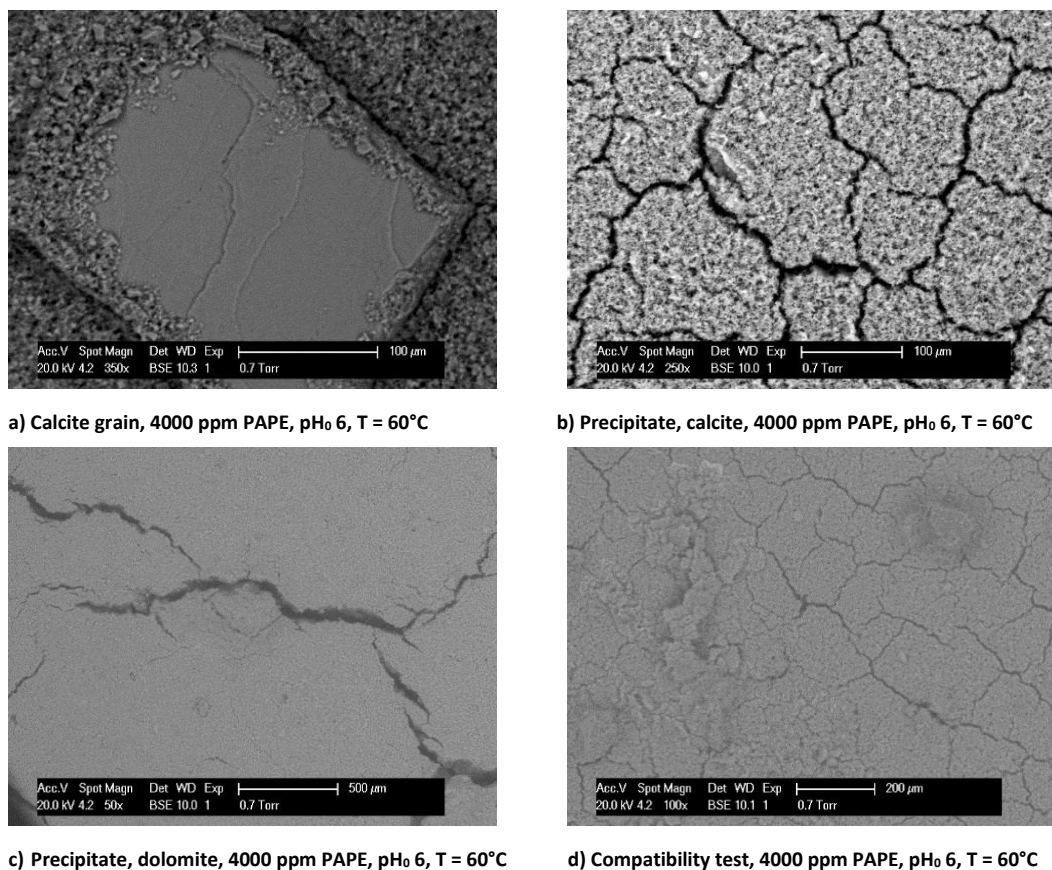
Figure 4.43. ESEM images of solids recovered from tests calcite and dolomite grains at 4000 ppm PAPE at pH_0 6, T = 60°C

Table 4.12. EDX signals on the solids from 4000 ppm PAPE for 100 – 315 µm calcite and dolomite at pH_0 6, T = 60°C

	Calcite grain 4000 ppm		Bulk Precipitate 4000 ppm (PAPE/Calcite)		Bulk Precipitate 4000 ppm (PAPE/Dolomite)		Compatibility test 4000ppm	
Element	Weight %	Atomic %	Weight %	Atomic %	Weight %	Atomic %	Weight %	Atomic %
C	14	23	12	19	11	17	-	-
O	54	63	50	61	52	62	41	58
Na	1	0.7	1	1	1	1	3	3
Mg	1	1	2	1	8	6	8	8
P	2	1	5	3	8	5	20	15
Cl	1	0.3	1	1	2	1	8	5
Ca	27	12	29	14	18	7	20	11

As shown in Figure 4.43 and Table 4.12., there was significant phosphorus detected in the samples (bulk precipitation for both PAPE/carbonates and compatibility test (no minerals present)) and the amount of phosphorus in the calcite system was lower than for the dolomite system and these results are consistent with the corresponding apparent adsorption results. In addition, PAPE was seen to be incompatible with NSSW as bulk precipitation was observed in the absence of minerals (Figure 4.43 (d)). The quantity of phosphorus in the compatibility experiment at 60°C was ~ 20% wt and 15% wt at 80°C. For calcite, the amount of phosphorus detected, either around the calcite grain or in bulk precipitation, was lower at lower temperature (2 and 5 wt%, and 7 and 9 wt% for the calcite grain and bulk precipitate at 60 and 80°C, respectively). In the PAPE/dolomite system, the phosphorus content was greater at 80°C for the highest concentration of PAPE (4000 ppm), which indicates that PAPE retention was greater at 80°C than at 60°C (18 and 8 wt% at 80°C and 60°C, respectively).

To sum up this section, the bulk "apparent adsorption" behaviour (Γ_{app} vs. C_f,) of PAPE scale inhibitor (SI) on calcite and dolomite mineral substrates has been studied over a range of conditions. A systematic application of ICP-OES (to determine [P] from the SI, [Ca^{2+}] and [Mg^{2+}]), pH analysis and ESEM/EDX of the SI/Ca precipitates formed has allowed for the rationalisation of the results in reference to the intrinsic functionality of the scale inhibitor and the reactivity of the carbonate mineral substrates.

The specific conclusions from this work are as follows:

1. Both pure adsorption (Γ) and coupled adsorption precipitation (Γ/Π) regimes were clearly observed for PAPE with a dolomite substrate at pH_0 4 and 6, while for the PAPE and calcite case at initial adjusted pH 4, only pure adsorption was observed at 80°C. However, precipitation is more dominant for PAPE/carbonate retention than adsorption. At 60°C and pH 6, the situation is different in that pure adsorption is the dominant retention regime for calcite/PAPE, while in the PAPE/dolomite system, precipitation is the dominant mechanism.

2. In general, the degree of apparent adsorption increased at higher pH for PAPE/calcite system (contrary to polymeric scale inhibitors). In the PAPE/calcite system at pH_0 4, the retention regime was only pure adsorption, while for PAPE/dolomite and PAPE/calcite systems at pH_0 6, precipitation was the more dominant mechanism.

3. The amount of apparent adsorption in the PAPE/dolomite system was seen to be effectively pH independent, which is quite different to the PAPE/calcite system in which the apparent adsorption was greater at higher pH.

4. For all concentrations of PAPE, the amount of apparent adsorption on calcite was lower at 60°C than at 80°C. In contrast, apparent adsorption did not change due to temperature for the PAPE/dolomite system, except at [PAPE] = 4000 ppm, where precipitation was lower at 80°C.

5. The carbonate mineralogy plays an important role in determining the detailed retention mechanism of PAPE in carbonate systems. Greater retention was observed for PAPE with dolomite than on calcite, despite the former being less chemically reactive. Therefore, during the design of squeeze treatments in carbonate formations, the rock composition should be taken into consideration.

6. Calcium has much higher affinity for chemical interaction with PAPE than magnesium. Thus, it is mainly the calcium-PAPE complex that is involved in the retention process.

7. In the PAPE/calcite system, apparent adsorption increased at higher temperature, which may be a kinetic effect leading to the rapid formation of a SI-Ca^{2+} complex. However, in the PAPE/dolomite system, apparent adsorption did not change noticeably as a function of temperature, possibly highlighting the dominance of pH in this system. For PAPE/calcite, both temperature and pH affected retention.

8. Results from the ESEM/EDX generally confirm and are very consistent with the static adsorption results. EDX detectable phosphorus levels (indicating the presence of the PAPE inhibitor) were observed in the precipitated deposits formed by combined Γ/Π. The amount of phosphorus detected, though not strictly quantitative, was seen to increase as Γ_{app} (precipitation) increased. In addition, phosphorus (PAPE) was detected on the surface of the calcite or dolomite grains directly, with the amount detected higher at 80°C than at 60°C (only at 4000 ppm for dolomite), in line with the corresponding apparent adsorption results.

4.6. Phosphonate and Polymeric Scale Inhibitors Retention on Limestone Substrates

We have already studied the apparent adsorption of three types of SIs (Phosphonate (DETPMP), Polymeric (PPCA, PFC) and Phosphate Ester (PAPE) inhibitors) on two carbonate substrates (calcite and dolomite) in previous sections of this chapter. In this section, we examine the apparent adsorption of DETPMP & PPCA on two limestone samples to investigate effect of this mineralogy on apparent adsorption.

4.6.1. DETPMP retention on Limestone

Similar apparent adsorption/compatibility results are now presented for DETPMP as a typical example of a phosphonate SI. DETPMP was made up as a stock solution at [SI] =10000 ppm active and this was subsequently used to make the various concentrations in the apparent adsorption experiments, in exactly the same manner as for [DETPMP] in section 4.2. pH was measured for all the stock solutions and was later adjusted to pH_0 4& 6. Static adsorption/ compatibility tests were carried out at the pH_0 4& 6 of the DETPMP solutions at 95°C. Figure 4.44 & Figure 4.45 show the apparent adsorption level of scale inhibitor (DETPMP in mg SI / g rock) for two masses, m = 5g and 10g, of 100- 315 μm limestone samples as a function of the final scale inhibitor concentration.
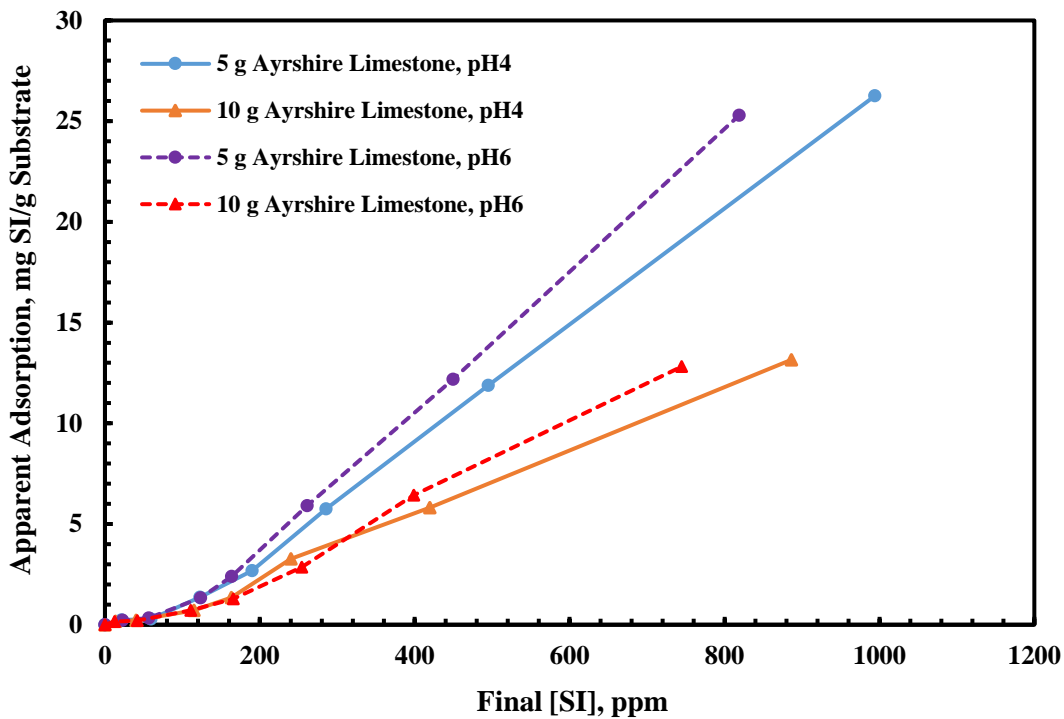
Figure 4.44. Apparent adsorption (Γ_{app} vs. C_f) for DETPMP onto 2 masses (m = 5g and 10g) of Ayrshire Limestone at two different pH values (pH$_0$ 4, 6); T = 95°C
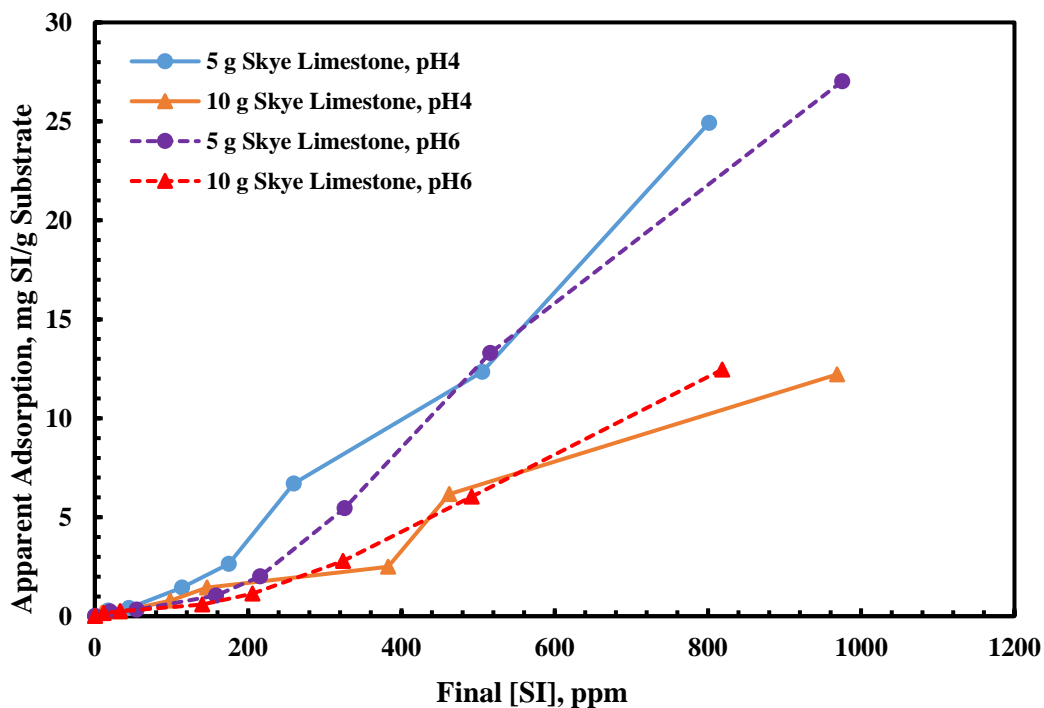
Figure 4.45. Apparent adsorption (Γ_{app} vs. C_f) for DETPMP onto 2 masses (m = 5g and 10g) of Skye Limestone at two different pH values (pH$_0$ 4, 6); T = 95°C

192

As shown in these figures, apparent adsorption of DETPMP increases as pH increases. This may be ascribed to higher dissociation of DETPMP at pH_0 6; i.e. the SI (DETPMP) is much more likely to complex with Ca^{2+} to form a SI/Ca complex in its dissociated form (i.e. at higher pH values) and less likely to form complexes at lower pH values. Although the amount of apparent adsorption in both systems are similar qualitatively, the compositions of SI-M^{2+} analysed by EDX which come up later are different. In addition, apparent adsorption of DETPMP on Skye limestone is a little higher than on Ayrshire as the former has more iron which has been involved in complexation and thus more retention[104].

The pH changes in the DETPMP/Ayrshire Limestone and DETPMP/Skye Limestone apparent adsorption experiments are plotted as a function of final SI concentration (C_f) in Figure 4.46 & Figure 4.47.
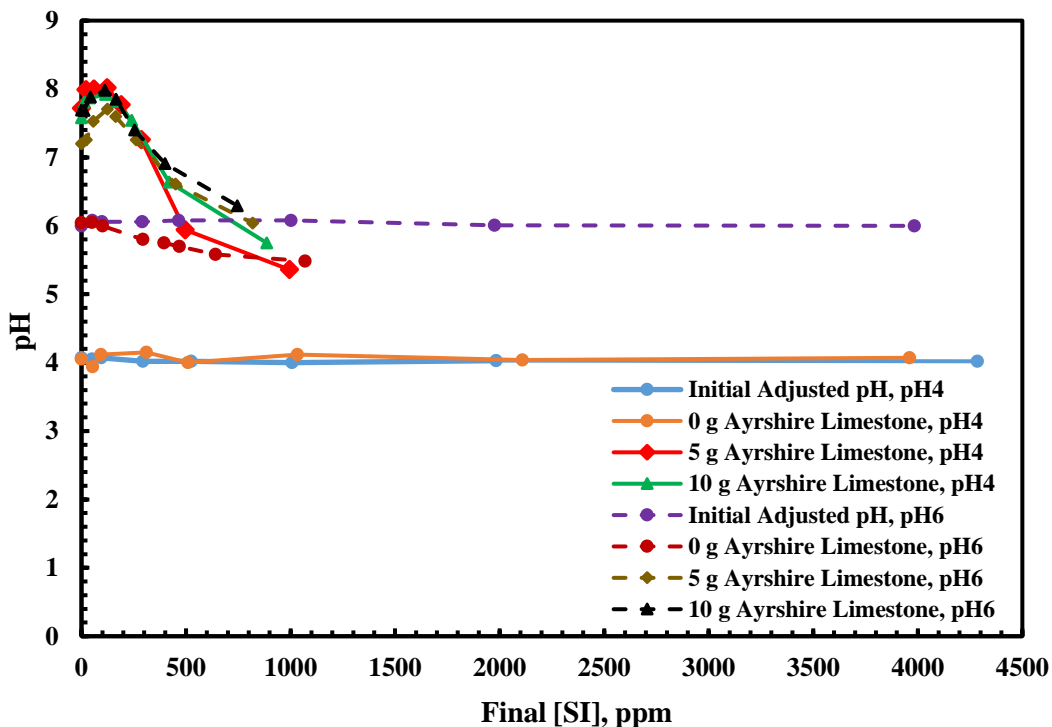
Figure 4.46. Comparison of pH for DETPMP onto 2 masses (m = 5g and 10g) of Ayrshire Limestone at two different initial pH values (pH_0 4, 6); T = 95°C
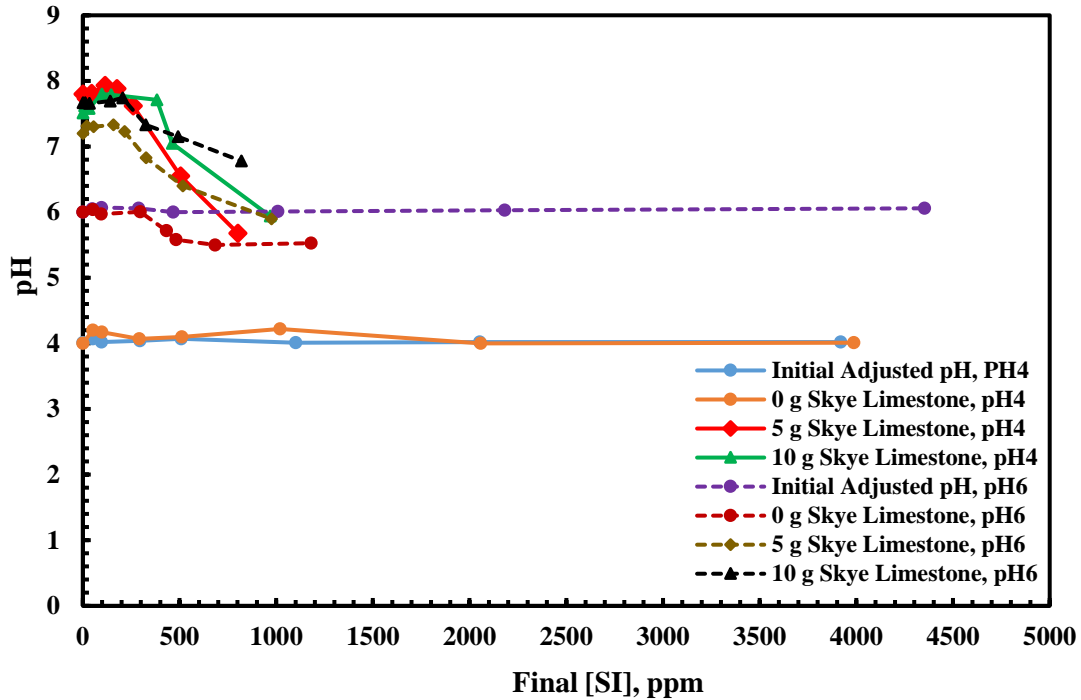
Figure 4.47. Comparison of pH for DETPMP onto 2 masses (m = 5g and 10g) of Skye Limestone at two different initial pH values (pH$_0$ 4, 6); T = 95°C

The results in Figure 4.46 & Figure 4.47 show that there are no noticeable changes in pH in the pure compatibility tests (no limestone present) at initial adjusted pH$_0$ 4. Thus, DETPMP is completely compatible with NSSW at pH$_0$ 4 in the absence of mineral in the solution. However, once pH is increased to pH$_0$6, DETPMP is not compatible with NSSW anymore as final pH starts to decrease from 1000 ppm. This means, DETPMP has become enough dissociated and it attracts calcium which is necessary for complexation from NSSW solution. However, if limestone substrates are added to the DETPMP solution, the pH rises from its initial value pH (pH$_0$ 4&6; initially adjusted pH) to pH ~ 8 due to dissolution of limestone substrates in a scale inhibitor solution and divalent cations, particularly Ca^{2+}, Mg^{2+} and Fe^{2+} (in Skye limestone case), are leached out of substrates. As the retention regime changes from pure adsorption to coupled adsorption/ precipitation, pH then decreases due to chemical reaction between SI and divalent cations. It should be mentioned that final pH for pH$_0$ 6 is slightly higher than for pH$_0$ 4 in both DETPMP/limestone systems which shown DETPMP has capacity to adsorb cations for precipitation and consequently more apparent adsorption at the corresponding pH (pH$_0$ 6).

Figure 4.48 &Figure 4.49 show the changes of [Ca^{2+}] in solution before and after the experiments in the SI/limestone systems in NSSW for both the adsorption and the compatibility tests.

194
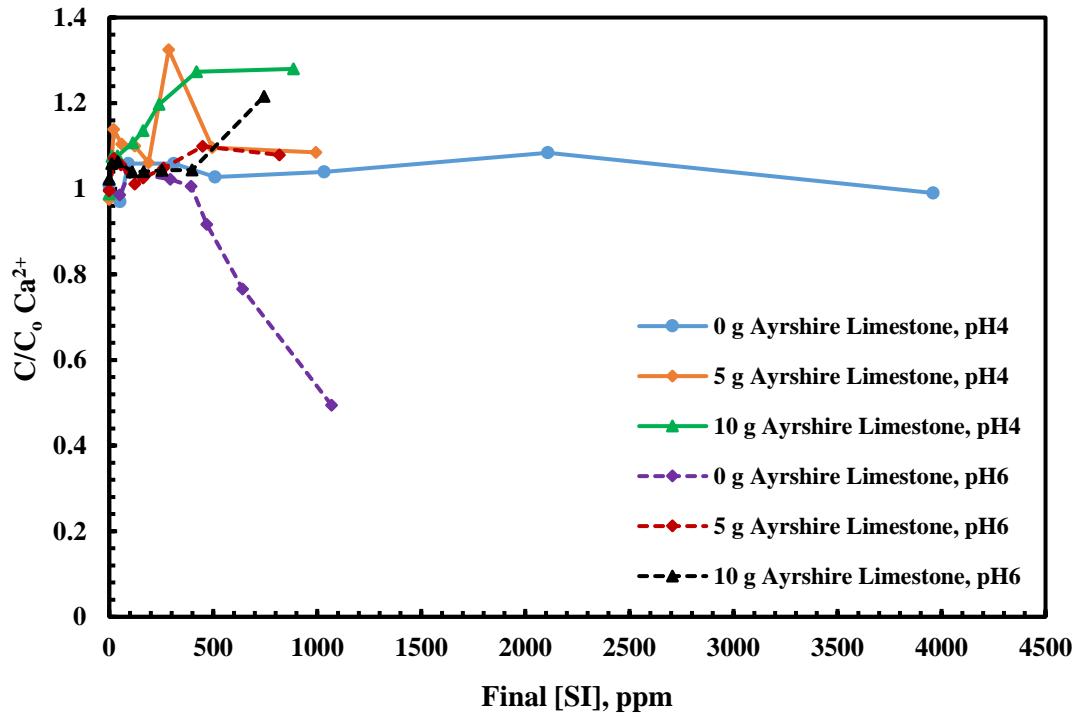
Figure 4.48. Comparison of C/C_0 of $[Ca^{2+}]$ trends for DETPMP/Ayrshire limestone systems in different pH values (pH$_0$ 4, 6); T= 95°C
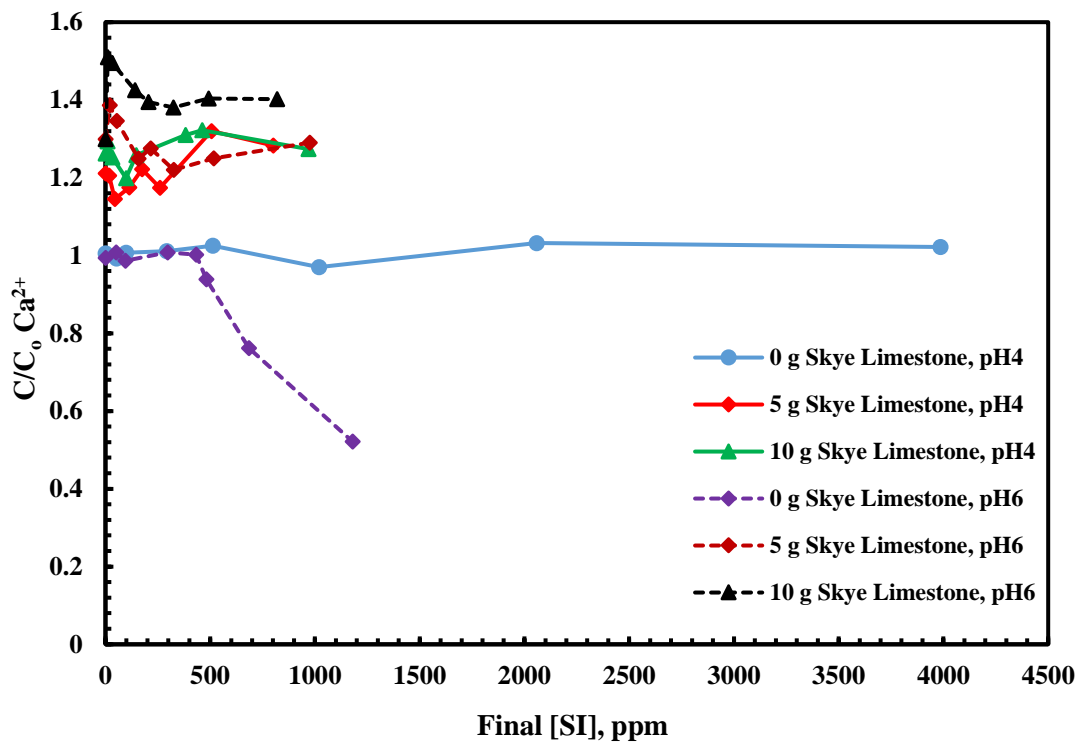
Figure 4.49. Comparison of C/Co of $[Ca^{2+}]$ trends for DETPMP/Skye limestone systems in different pH values (pH$_0$ 4, 6); T = 95°C

Figure 4.48 & Figure 4.49 show that there are no significant changes in Ca^{2+} concentration for compatibility tests at pH_0 4 while at pH_0 6 as mentioned above, DETPMP is incompatible with NSSW and forms complex with calcium present in SW. The differences if final pH and Ca are all consequences of the balance between the carbonate substrate dissolution and precipitation of the SI/Ca complex. They can only be explained properly by modelling.
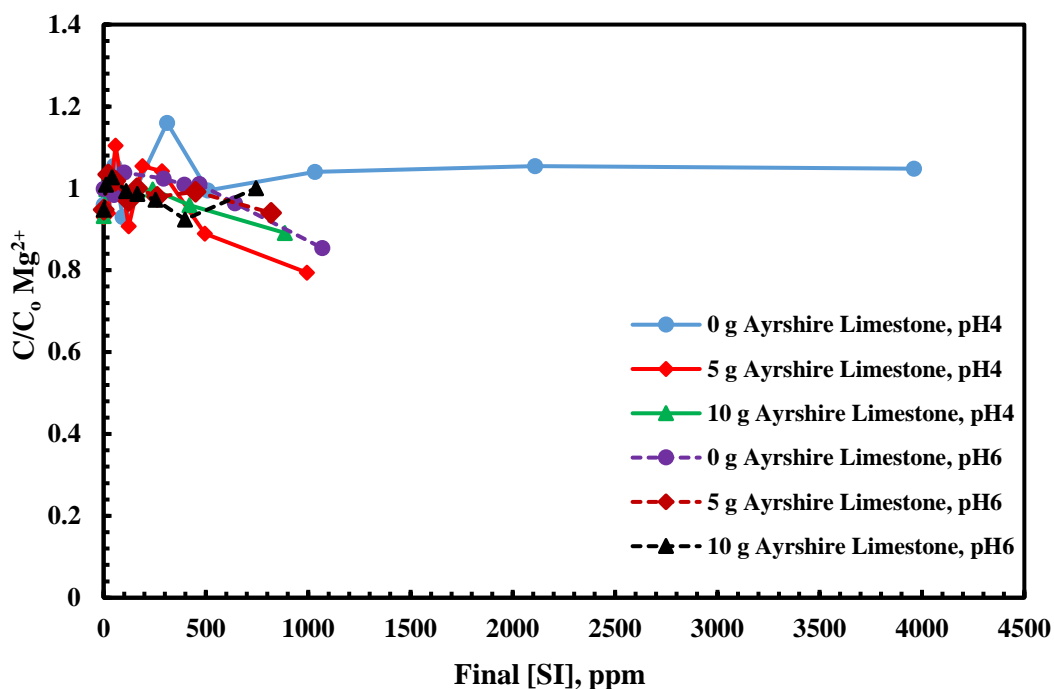
Figure 4.50. Comparison of C/C_0 of $[Mg^{2+}]$ trends for DETPMP/Ayrshire limestone systems in different pH values (pH_0 4, 6); T = 95°C
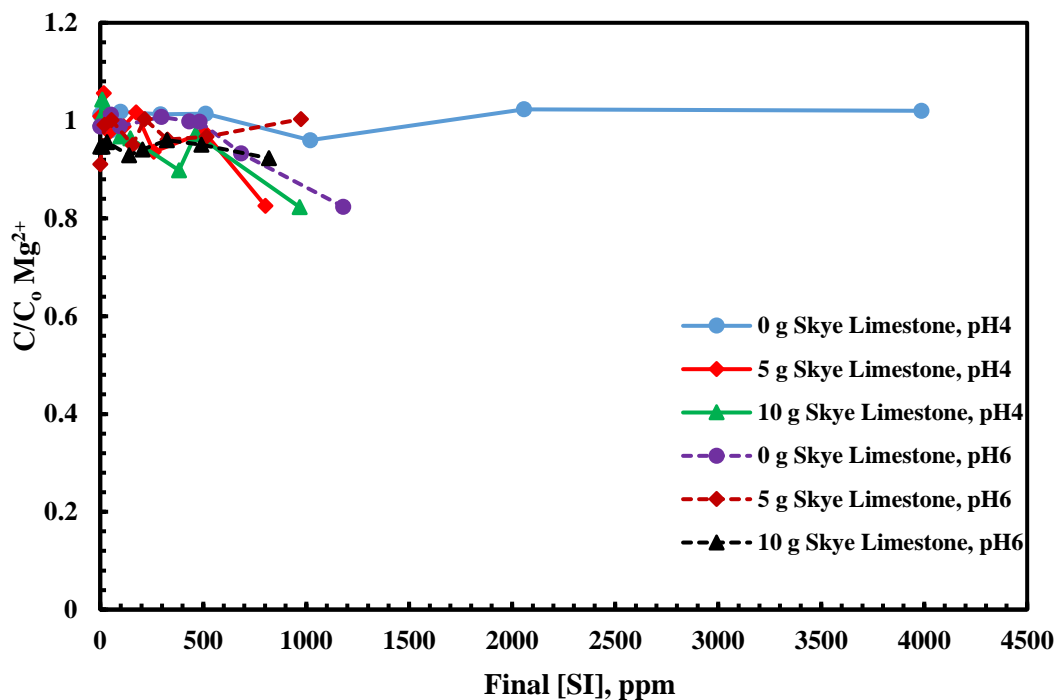
Figure 4.51. Comparison of C/C_0 of $[Mg^{2+}]$ trends for DETPMP/Skye limestone systems in different pH values (pH_0 4, 6); T = 95°C

As shown in Figure 4.50 & *Figure 4.51*, there is no significant change in $[Mg^{2+}]$ in the compatibility test at pH_0 4. However, once pH is increased to pH_0 6, the normalised concentration of magnesium reduces because of Mg^{2+} involvement in complexation process with SI. In addition, once limestone samples are added to DETPMP solution, some more magnesium is leached out of system because of rock dissolution and final $[Mg^{2+}]$ levels off at a normalised value of $[Mg^{2+}]$ ~ 1 which also confirms that magnesium is not significantly involved in the complexation process.

In addition, to confirm the corresponding apparent adsorption results, all of the solids collected from the static apparent adsorption tests for the DETPMP/Skye limestone and DETPMP/Ayrshire limestone systems have been examined as before using ESEM/EDX analysis.
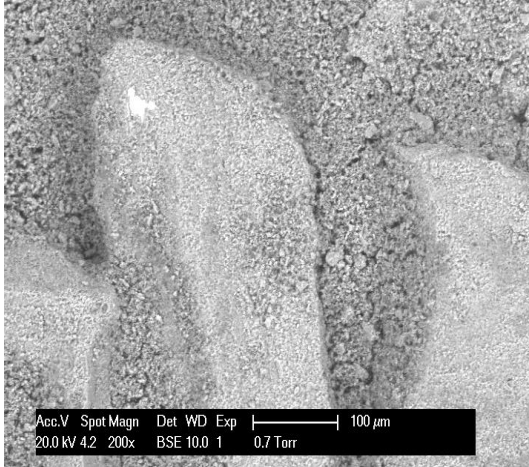
a) Skye Limestone grain, 4000 ppm DETPMP
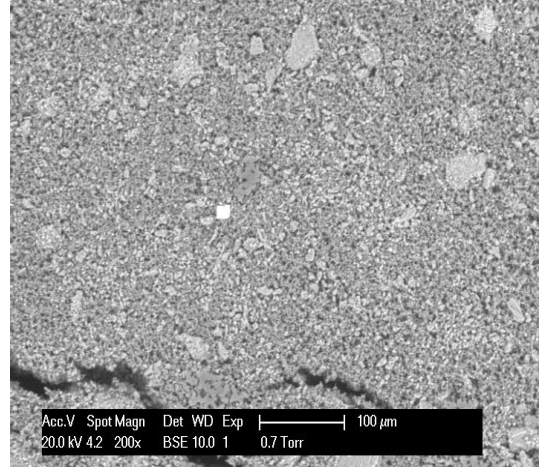
b) Precipitate, 4000 ppm DETPMP, Skye Limestone
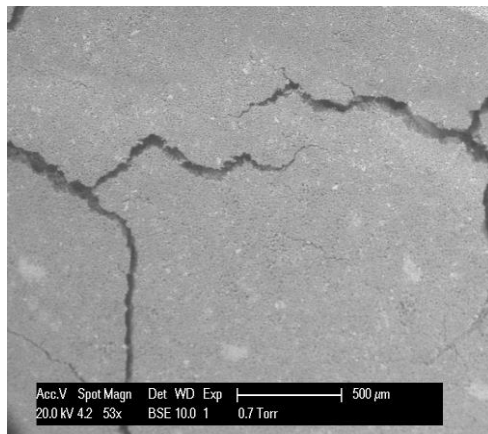
c) Precipitate, 4000 ppm DETPMP, Ayrshire Limestone

Figure 4.52. Morphology of Skye and Ayrshire grains and Bulk Precipitation at 4000 ppm DETPMP at pH_0 4, T=95°C on ESEM photographed samples

Table 4.13. EDX signals on the 4000 ppm DETPMP for 100-315 µm Skye and Ayrshire Limestone at pH_0 4, T=95°C from ESEM

Element	Skye Limestone grain 4000 ppm		Bulk Precipitate 4000 ppm (DETPMP/Skye Limestone)		Bulk Precipitate 4000 ppm (DETPMP/Ayrshire Limestone)	
	% Weight	% Atomic	% Weight	% Atomic	% Weight	% Atomic
C	15	23	3	3	8	12
Na	1	1	2	3	1	1
Mg	2	1	5	5	4	3
P	4	2	13	10	14	9
S	1	0.5	0.5	0.5	-	-
Cl	1	1	4	4	4	2
K	1	0.5	0.5	0.5	-	-
Ca	18	8	34	20	17	9
O	57	63	38	54	52	64

As shown in Figure 4.52 and in

Table *4.13*., phosphorous is clearly detected at a high level (~13% & ~14% by weight for Skye and Ayrshire limestone Samples, respectively) in the finer precipitate which forms in the bulk, mainly on the filter paper. However, there is a remarkable detectable amount (~4% by weight for Skye limestone) on the Skye limestone grains which is most probably some of the SI/Ca precipitate adhering to the Skye limestone surfaces or (less probably) could be part of the adsorbed SI. In addition, the amount of phosphorous detected in DETPMP/Skye limestone system is higher than DETPMP/Ayrshire limestone which confirms the SI retains more or less in both limestone samples.
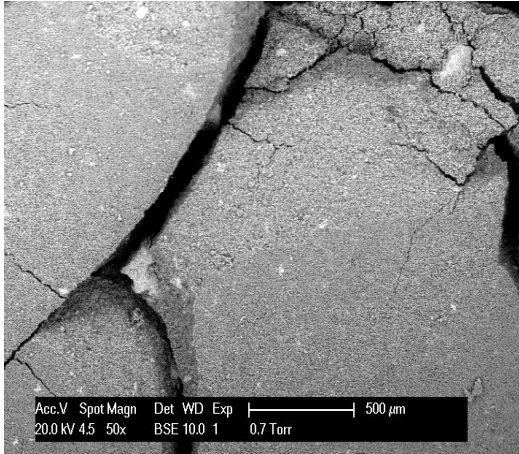
a) Precipitate, 4000 ppm DETPMP, Skye Limestone
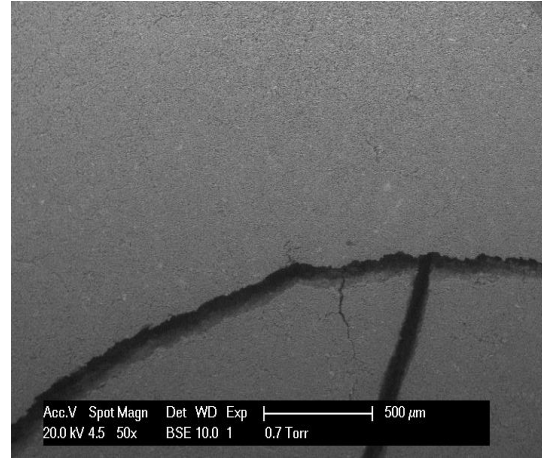
b) Precipitate, 4000 ppm DETPMP, Ayrshire Limestone
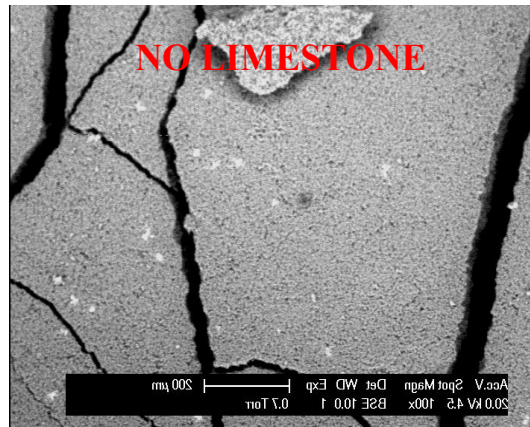
c) Precipitate, 4000 ppm DETPMP, Compatibility test

Figure 4.53. Morphology of Skye and Ayrshire grains and Bulk Precipitation at 4000 ppm DETPMP at pH_0 6, T=95°C on ESEM photographed samples

Table 4.14. EDX signals on the 4000 ppm DETPMP for 100-315 µm Skye and Ayrshire Limestone at pH_0 6, T=95°C from ESEM

Element	Bulk Precipitate 4000 ppm (DETPMP/Skye Limestone)		Bulk Precipitate 4000 ppm (DETPMP/Ayrshire Limestone)		Bulk Precipitate 4000 ppm (Compatibility test)	
	% Weight	% Atomic	% Weight	% Atomic	% Weight	% Atomic
O	53	68	54	73	37	53
Na	3	3	3	2	6	5
Mg	7	7	5	4	14	12
P	18	12	11	6	23	14
S	1	1	-	-	1	1
Cl	5	3	5	2	10	7
Ca	11	5	22	13	9	8
Fe	2	1	-	-	-	-

The results in Figure 4.53 and Table 4.14., show that phosphorous is clearly detected at high levels (~23% by weight for the 4000 ppm DETPMP cases, respectively) in the compatibility test. Furthermore, there is also a high detectable amount (~ 18 and 11% by weight at 4000 ppm for Skye and Ayrshire limestone samples, respectively) in the finer precipitate which forms in the bulk and is mainly retained on the filter paper. It should be mentioned that in DETPMP/Skye limestone system, some Iron (~ 2% by weight) has been detected that leads to more DETPMP retention in Skye limestone. In addition, the Iron has not been detected at the same system, pH_0 4.

4.6.2. PPCA Retention on Limestone Substrates

First, a stock scale inhibitor (SI) concentration at 10000 ppm active (ppm = mg/L) was prepared and used to make the various SI concentrations in the experiments. SI concentrations of 50, 100, 500, 800, 1000, 2000 and 4000 ppm were used in all the experiments. pH was measured for all the stock solutions and was later adjusted to an initial value of pH_0 4& 6 to investigate impact of pH on apparent adsorption.

To interpret the results here, we note that the inhibitors such as PPCA can be considered as weak acids, schematically represented as HA. These can be partly dissociated (i.e. $HA \leftrightarrows H^+ + A^-$) with a relatively low K_a value (where $K_a = [H^+][A^-]/[HA]$ and this is usually of order $K_a \sim 10^{-4} - 10^-$

5). Therefore, at very low (acidic) pH, the HA equilibrium is to the left and the molecule is more associated as HA, and at higher pH it is more dissociated into H^+ and A^-. The SI (HA) is much more likely to complex with Ca^{2+} to form a SI/Ca complex in its dissociated form (i.e. at higher pH values) and less likely to form complexes at lower pH values. Also, complexation of the SI is favoured at higher concentrations of calcium, $[Ca^{2+}]$. In fact, the SI species such as PPCA are actually weak **poly**-acids where, for example, DETPMP has 10 dissociating Hs. That is, DETPMP can be denoted schematically as $H_{10}A$ and dissociation is described by a series of 10 K_a values, K_{a1}, K_{a2} etc.
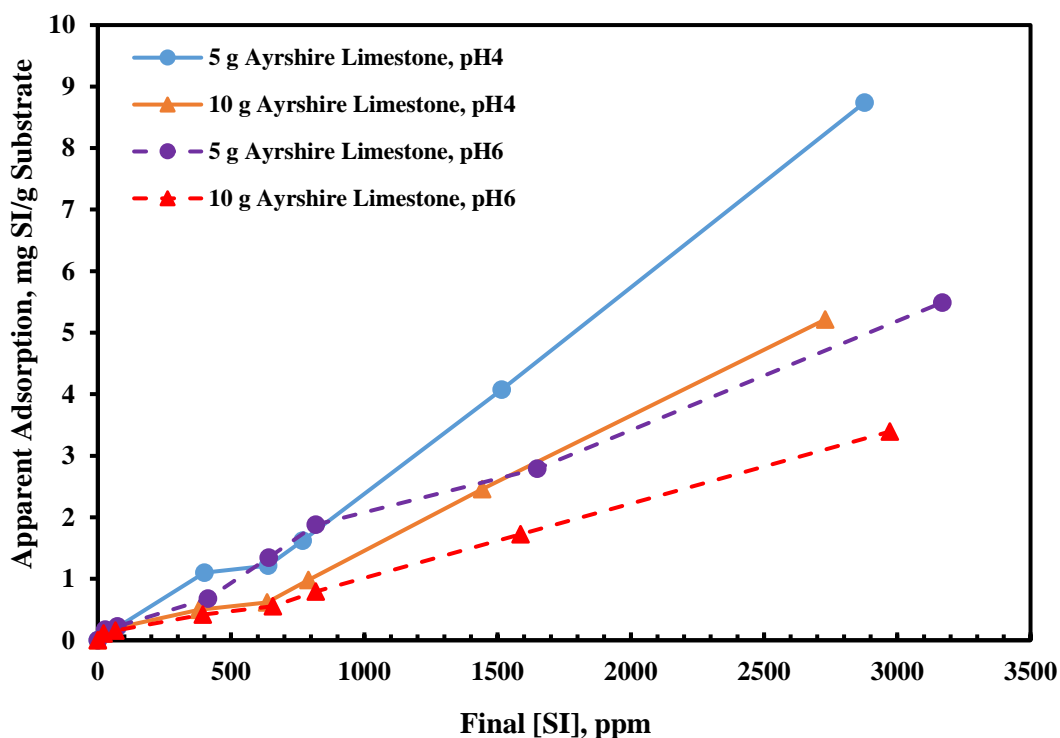
Figure 4.54. Apparent adsorption (Γ_{app} vs. C_f) for PPCA onto 2 masses (m = 5g and 10g) of Ayrshire Limestone at two different pH values (pH$_0$ 4, 6); T = 95°C

202
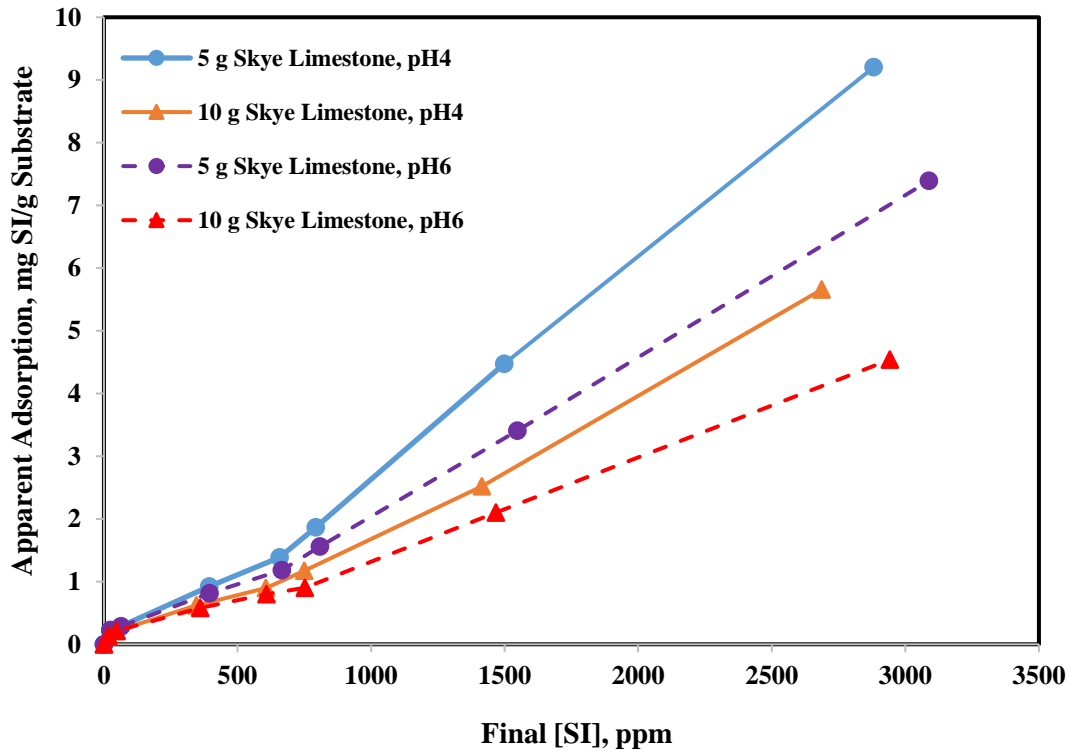
Figure 4.55. Apparent adsorption (Γ_{app} vs. Cf) for PPCA onto 2 masses (m = 5g and 10g) of Skye Limestone at two different pH values (pH$_0$ 4, 6); T = 95°C

Figure 4.54 & Figure 4.55 show the results for apparent adsorption vs. the final SI concentration (Γ_{app}, vs. C_f) for 2 masses of calcite and dolomite substrates (m = 5g and 10g). The results clearly indicate that both pure adsorption and coupled adsorption/precipitation took place at both initial adjusted pH values (pH$_0$ 4&6). Only pure adsorption is seen for [SI] up to ~100ppm, before the different (m/V) curves start to deviate, indicating that coupled adsorption/precipitation behaviour was occurring. In addition, the results in the figures also show that for PPCA, coupled adsorption/ precipitation is the predominate mechanism for its retention in both limestone porous media. Moreover, apparent adsorption increases as pH decreases. At pH$_0$ 4, the PPCA solution is more acidic and can dissolve more carbonate substrate and accordingly more divalent cations will be generated in situ. So, the dissociated PPCA will interact with the increased divalent cations by carbonate rock dissolution, leading to more precipitation (i.e. an observed higher "apparent adsorption"). At pH$_0$ 6, the PPCA would be somewhat more dissociated (more A$^-$ in solution) as described above, but the amount of divalent cations dissolved into solution would be much less. Also, the effect of the carbonate is to drive the final pH up to about pH ~8 (see results below). The net effect here is that it is at the lower pH (initial pH$_0$ 4) where a higher [M^{2+}] is

203

dissolved into solution and the pH is increased in any case (by the carbonate dissolution); thus, the effect is an increased level of precipitation (i.e. a higher "apparent adsorption") at this lower pH level.

Figure 4.56 & Figure 4.57 show the pH trend in solution as a function of final SI concentration for the corresponding apparent adsorption experiments in Figure 4.54 & Figure 4.55.
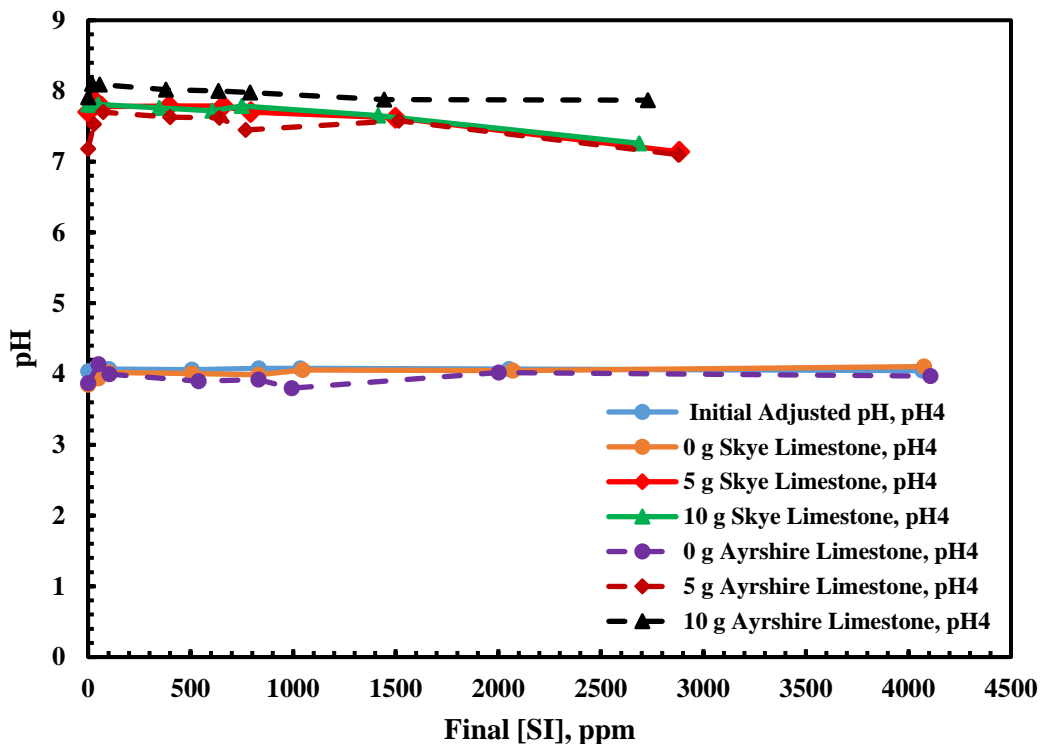
Figure 4.56.   pH trend for different masses of Ayrshire limestone & Skye limestone (100-315 µm) versus final [PPCA] at pH_0 4; T=95°C
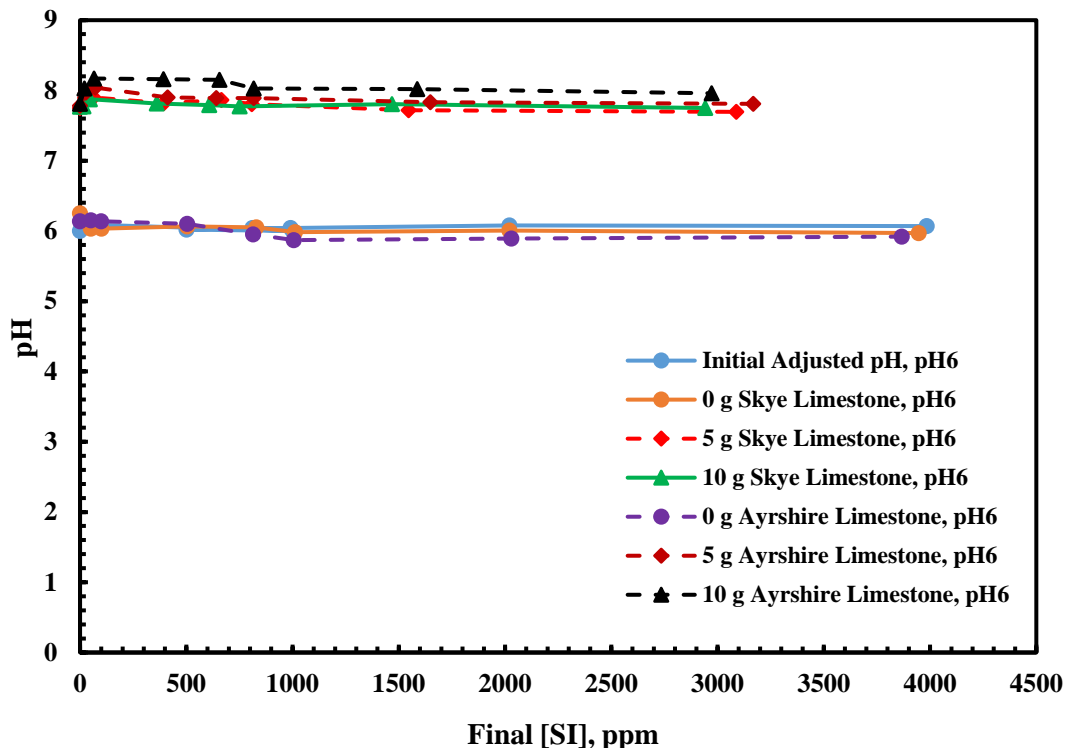
Figure 4.57. pH trend for different masses of Ayrshire limestone & Skye limestone (100-315 µm) versus final [PPCA] at pH_0 6; T=95°C

As shown in these figures, there are no significant changes in pH in the bulk compatibility tests (no limestone present); the constant lines at pH_0 4 & 6 are the solutions with no solid present, i.e. no reaction/adsorption. These compatibility results show that PPCA is compatible with NSSW without the limestone minerals in the solution. However, if limestone substrates are added into solution then at equilibrium, pH rises from its initial adjusted pH to ~8 due to dissolution of limestone substrates and the reaction of the scale inhibitor with divalent cations which was generated in situ, as described above. As [SI] increases, for the initial pH_0 6 case, the final pH tends to flatten out around pH 8 which is due to the limestone. However, at initial adjusted pH 4, the final pH reduced to pH ~7 which can be ascribed to more precipitation of PPCA/M^{2+} complex. This explains why more M-PPCA complex was produced at pH_0 4 than at pH_0 6. However, to prove that this explanation is correct, we must measure changes in the divalent ion levels particularly [Ca^{2+}] before and after the apparent adsorption experiments in the mixture of SI and NSSW solution. Figure 4.58 & Figure 4.59 show the differences in the normalised [Ca^{2+}] for both compatibility and adsorption tests at initial pH_0 4 and pH_0 6.
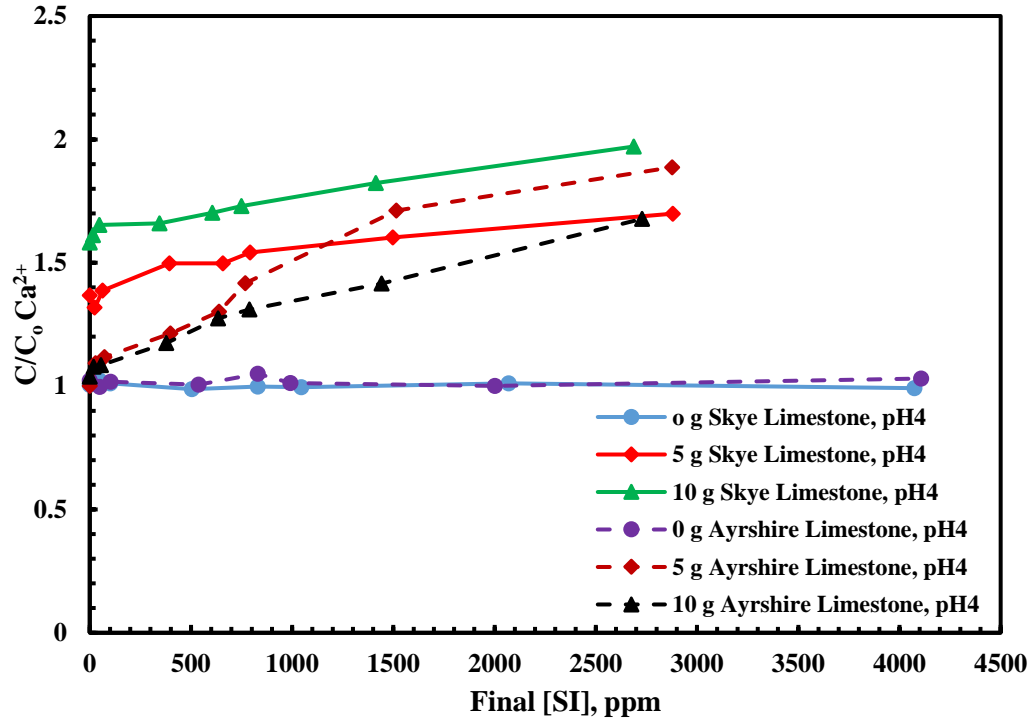
Figure 4.58. Comparison of C/C$_0$ of [Ca^{2+}] trends for PPCA/Ayrshire Limestone & PPCA/Skye limestone systems in pH$_0$ 4; T = 95°C
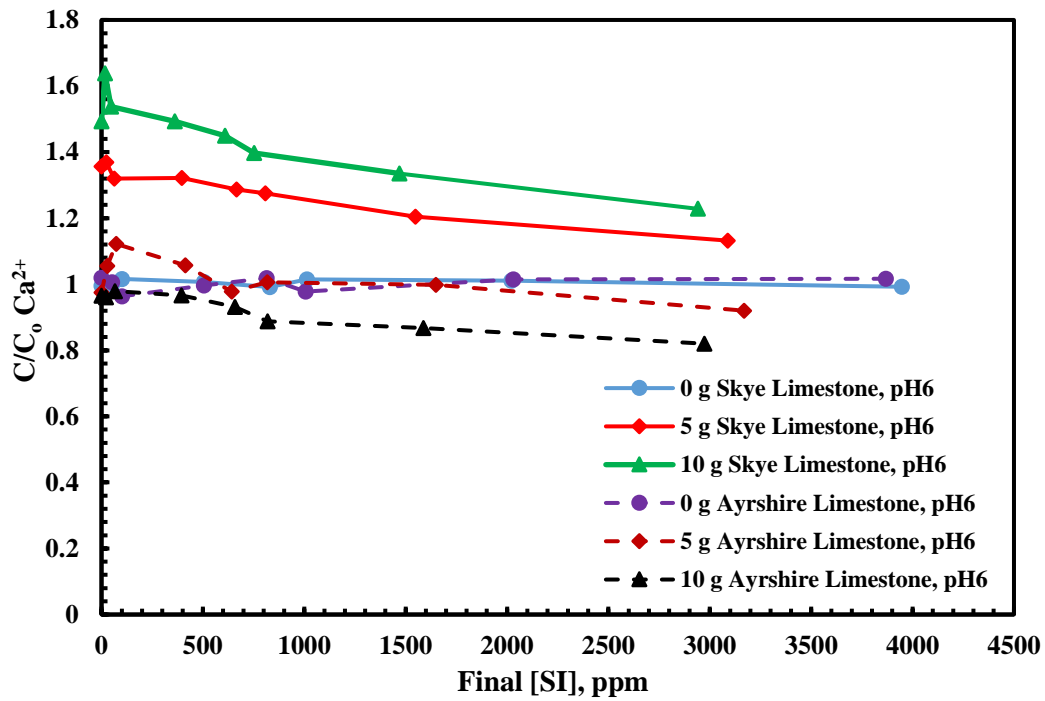
Figure 4.59. Comparison of C/C^0 of [Ca^{2+}] trends for PPCA/Ayrshire Limestone & PPCA/Skye limestone systems in pH$_0$ 6; T = 95°C

The [Ca^{2+}] results in Figure 4.58 & Figure 4.59 show quite clearly that there is no distinct change in [Ca^{2+}] in compatibility tests (no rock substrate) which means PPCA does not react with calcium and the scale inhibitor is completely compatible with NSSW. However, once limestone samples are added to the scale inhibitor solution, a considerable amount of additional [Ca^{2+}] is generated in situ due to rock dissolution, rising to ~2x and ~ 1.8x the pH_0 4 for Skye limestone and Ayrshire limestone respectively; note that these increases in [Ca^{2+}] are in spite of the loss of calcium from solution by precipitation of the SI/Ca complex. At pH_0 6, the calcium losses by complex precipitation and gains in solution by leaching from the Ayrshire limestone substrate are approximately balances (normalised levels of calcium remain at ~1). However, in PPCA/Skye limestone system at pH_0 6, the calcium generated in situ is used in complexation and reduces from ~x1.7 to ~x1.2 which is different than normalised calcium concentration in Ayrshire limestone/PPCA that this normalised concentration reaches to ~1.

Like the DETPMP/limestone systems, after filtration, all the filter papers containing limestone substrates and (in some cases) the precipitated complex for each of the PPCA concentrations tested were examined by ESEM-EDX analysis. In the PPCA case at initial pH value, pH_0 4, we could not see any traces of phosphorus on the limestone crystals themselves at the highest PPCA concentration (4000 ppm) although we observed precipitate on the filter paper. This lack of observed P (by EDX) might be attributed to the low content of this element in PPCA (~ 0.5 % phosphorus)[36].
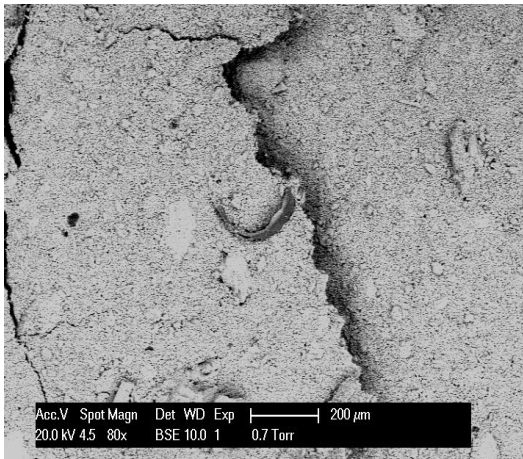
a) 4000 ppm, 100-315 µm Skye limestone, pH$_0$4
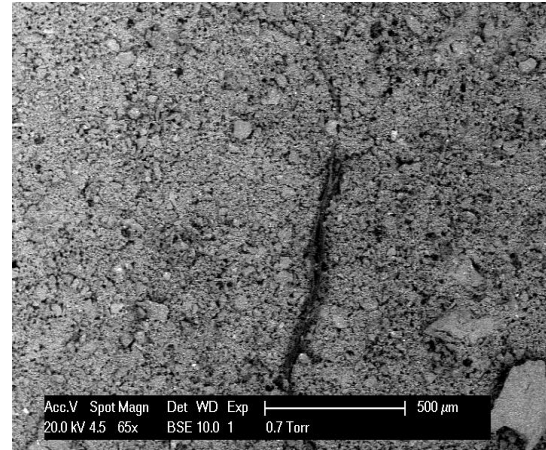
b) 4000 ppm, 100-315 µm Ayrshire limestone, pH$_0$4

Figure 4.60. Morphology of 4000 ppm PPCA Samples for 100-315 µm Ayrshire & Skye limestone at pH$_0$ 4 on ESEM photographed sample

Table 4.15. EDX signals on the 4000 ppm PPCA for 100-315 µm Skye and Ayrshire Limestone at pH$_0$ 4, T=95°C from ESEM

	Bulk Precipitate 4000 ppm (DETPMP/Skye Limestone		Bulk Precipitate 4000 ppm (DETPMP/Ayrshire Limestone)	
Element	% Weight	% Atomic	% Weight	% Atomic
C	8	9	21	22
O	66	74	67	60
Na	2	3	0.5	0.4
Mg	4	3	0.4	0.5
S	1	0.3	0.1	0.1
Cl	1	0.7	1	1
Ca	10	3	10	16
Fe	8	7	-	-

Results in Figure 4.60 and Table 4.15. show that phosphorous has not been detected at the highest concentration of PPCA (4000ppm), although we observe significant amounts of precipitate for this concentration, according to ICP results (and by visual observation, Figure 4.61). As discussed above, this is mainly because of the low content of phosphorus in PPCA[36].

208

a) 4000 ppm, 100-315 µm Ayrshire limestone, pH4   **b) 4000 ppm, 100-315 µm Skye limestone, pH4**
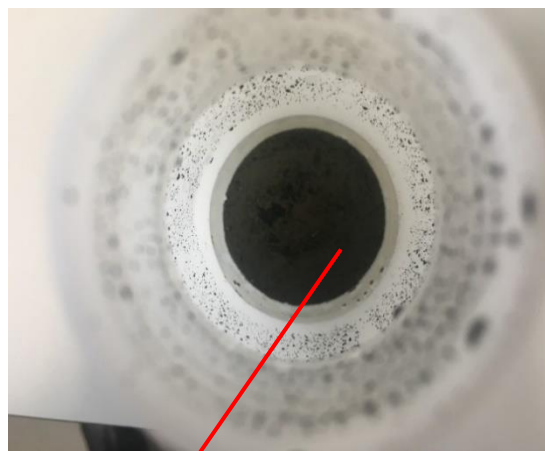
Precipitate formed and deposited on limestone grains

Figure 4.61. Visual observation of precipitate formed and deposited on Limestone grains at 4000 ppm PPCA& pH$_0$ 4

Thus, it was necessary to show the occurrence of precipitated PPCA/Ca complex by another analytical method such as Particle Size Analysis (PSA), and results for PSA are presented below. Particle size distributions (PSDs) have been measured for all of the Skye limestone experiments described above and this should detect any precipitate which has formed in these apparent adsorption experiments. We used a Particle Size Analyser (PSA) manufactured by the Malvern Company. Firstly, we measured particle size analysis for the larger pure Skye limestone mineral samples (100-315 µm) and, for this purpose, we used a 300 mm Lens (the largest one) to measure the PSD and the results are shown in Figure 4.62.
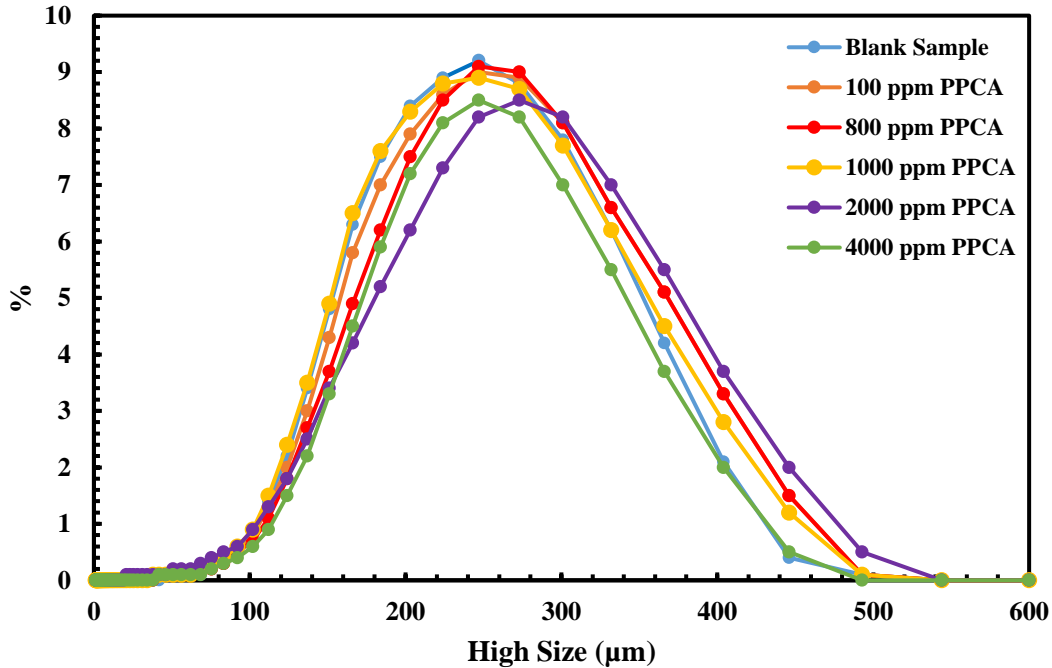
Figure 4.62. Particle Size Analysis for 100-315 µm Skye limestone residue in different concentrations and pH_0 4 with 300 mm lens

These PSD results in Figure 4.62 show that there is good consistency in the measurement of the limestone particle sizes with the largest 300mm lens for the experiments at pH_0 4. For these cases (pure limestone and 100ppm PPCA), we see that only large particle sizes are observed broadly in agreement with the limestone size range we expect. When these same sample cases (for example 100ppm PPCA) were examined by the smaller lens (45 mm lens) which can "see" much smaller particles (from ~1 – 20 µm), we see no fine particles of this size; see Figure 4.63– the "flat line" 100ppm case. However, we then examined cases using this smaller (45mm) lens for the experiments at increased PPCA concentrations where the system is going from a region of pure adsorption to coupled adsorption/precipitation. These cases are shown in Figure 4.63 and we now see peaks of PSD between ~1 – 10 µm. Clearly, these populations of smaller particles are the SI/Ca precipitated material which forms as this finer material; note that this is clearly distinguishable from the limestone grains (which are much bigger; see Figure 4.62).
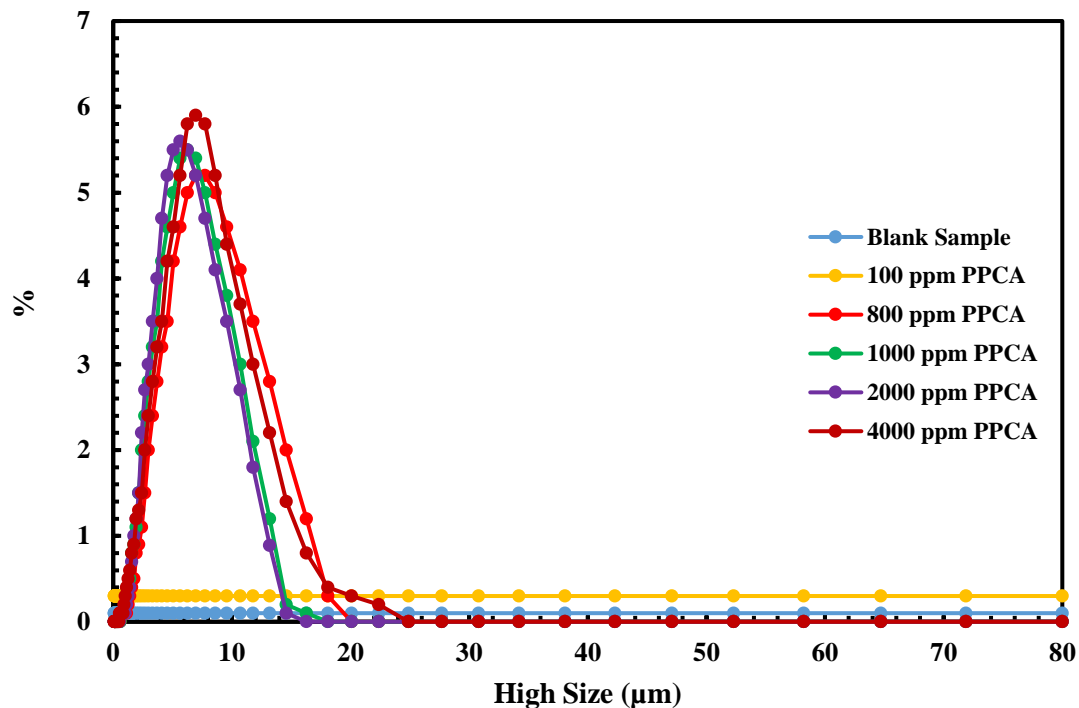
Figure 4.63. Particle Size Analysis for 100-315 µm precipitate deposited on filter paper in different concentrations and pH_0 4 with 45 mm lens

4.6.3. DETPMP & PPCA retention in Skye limestone substrate at T=80°C

In the next apparent adsorption experiments on DETPMP and PPCA, the effect of reducing the temperature was investigated. For this purpose, temperature was decreased from T = 95°C (Reservoir like temperature) to T = 80°C. Since these inhibitors were retained more on Skye limestone, this particular limestone was selected as adsorbent. For DETPMP, pH_0 6 was selected and for PPCA, pH_0 4 was chosen as these respective SIs were retained on the limestone substrates at their maximum levels.
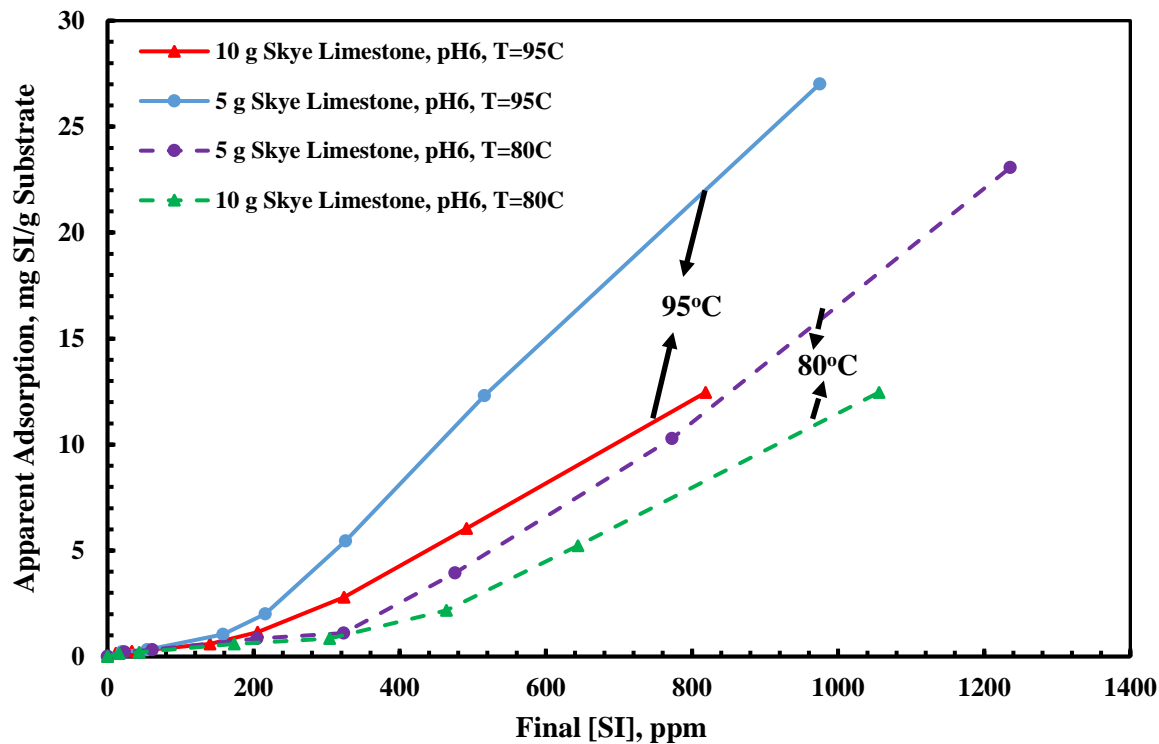
Figure 4.64. Comparison of apparent adsorption (Γ_{app} vs. C_f) for DETPMP onto 2 masses (m = 5g and 10g) of Skye limestone at two different temperatures (T = 95°C & 80°C); pH_0 6
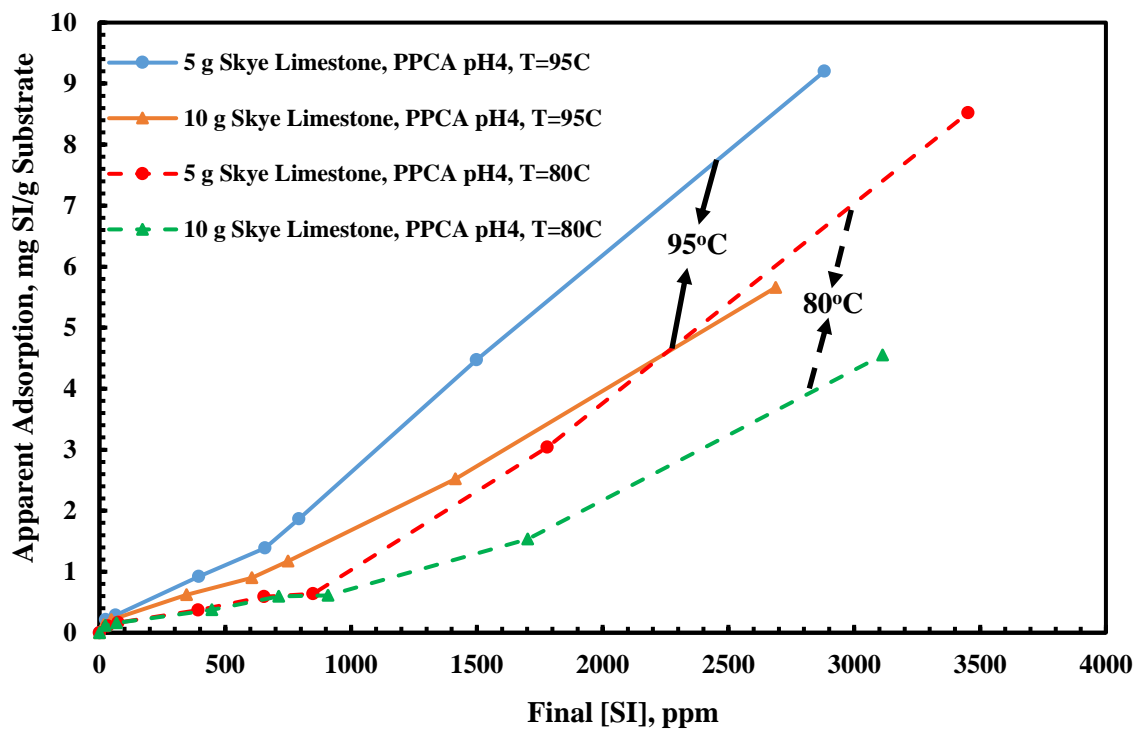
Figure 4.65. Comparison of Apparent adsorption (Γ_{app} vs. C_f) for PPCA onto 2 masses (m = 5g and 10g) of Skye Limestone at two different temperatures (T = 95°C & 80°C); pH_0 4

The first feature to note in Figure 4.64 is that, at both experimental temperatures (95°C & 80°C), regions of both pure adsorption and coupled adsorption/precipitation are observed. As shown in Figure 4.64, the region of pure adsorption at lower SI concentration is extended as temperature is reduced. At the higher temperature, the solubility of the SI-M^{2+}complex decreases resulting in more precipitation (higher apparent adsorption). The dominant retention mechanism of DETPMP on Skye limestone changes from coupled adsorption/precipitation to pure adsorption when temperature is decreased from T = 95°C to T = 80°C, respectively, although both mechanisms still occur. In fact, temperature affects the apparent adsorption of DETPMP on limestone substrate significantly, i.e. DETPMP is retained at higher levels (greater Γ_{app}) at higher temperature in limestone formations.

Figure 4.65 shows that the apparent adsorption of PPCA also decreases as temperature is reduced, as was observed for DETPMP. In addition, the range of pure adsorption retention mechanism of PPCA on limestone extends once temperature is decreased from 95°C to 80°C, although both mechanisms exist (~ 1000 ppm the retention mechanism changes to coupled adsorption/precipitation). In fact, the temperature decrease has affected apparent adsorption of PPCA on limestone substrate quite significantly. Thus, PPCA works more effectively at higher temperature in limestone formations in terms of the quantity of retention (as does DETPMP as observed in Figure 4.64).

Figure 4.66 & Figure 4.67 show the pH trends in solution as a function of final SI concentration for the corresponding apparent adsorption experiments in Figure 4.64 & Figure 4.65.
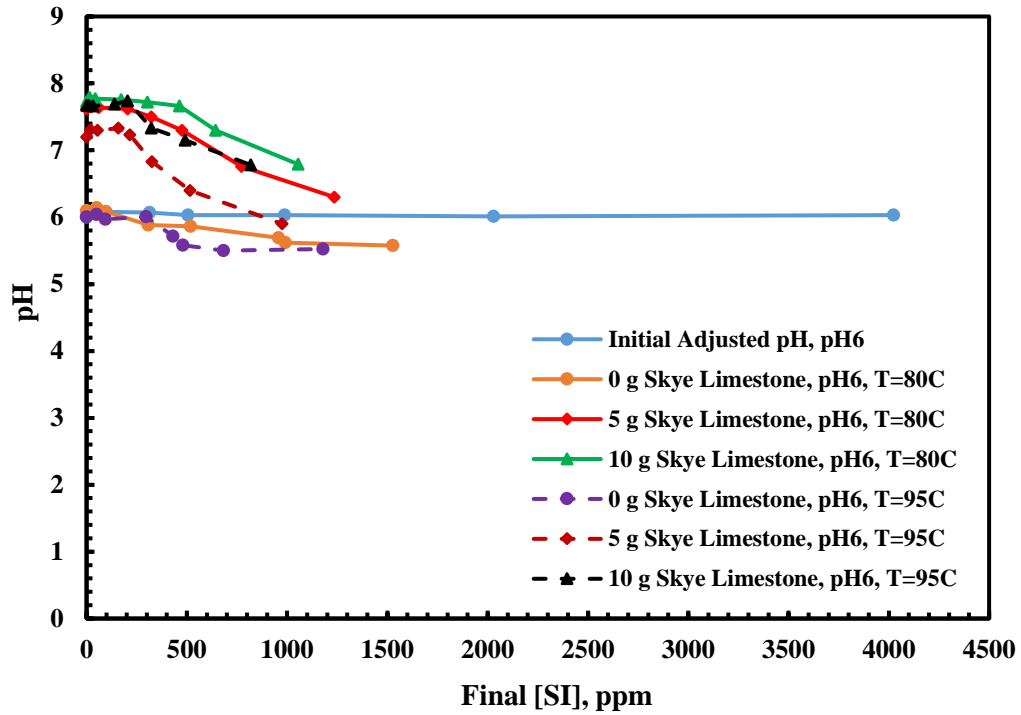
Figure 4.66. Comparison of pH trend for different masses of Skye limestone (100-315 µm) versus final [DETPMP] at pH_0 6; T = 95°C & 80°C
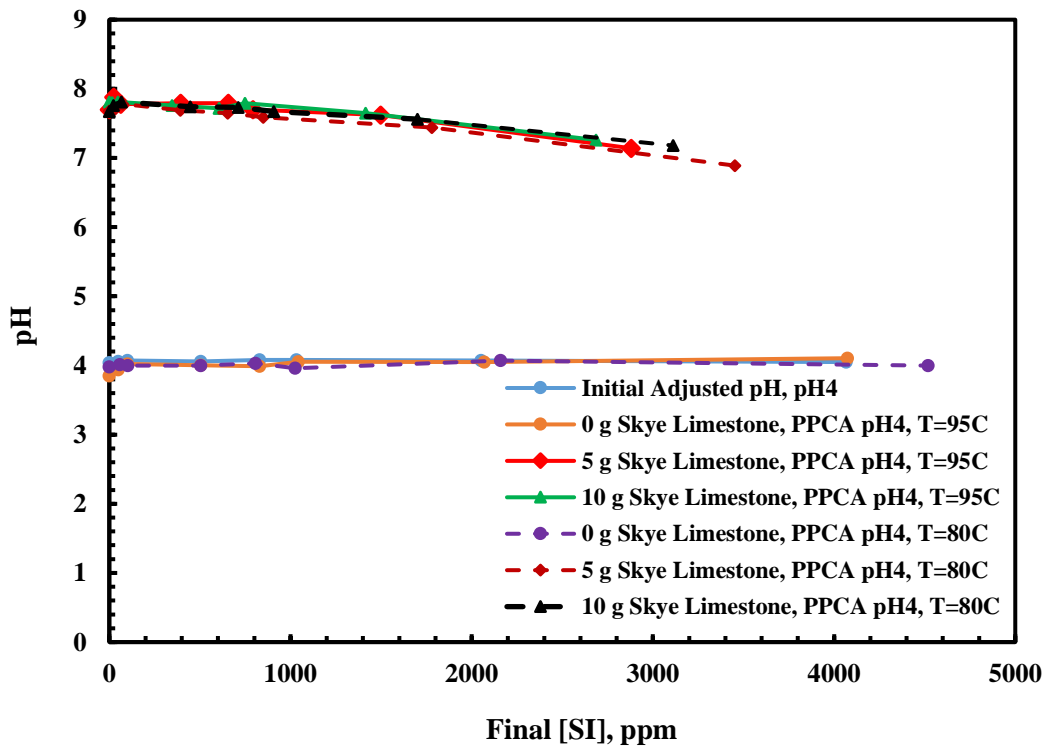
Figure 4.67. Comparison of pH trend for different masses of Skye limestone (100-315 µm) versus final [PPCA] at pH_0 4; T = 95°C & 80°C

Results in Figure 4.66 show that some precipitate is formed in the bulk compatibility experiment (no carbonate substrate present) and pH declines from the initial adjusted value (pH$_0$ 6) to pH ~5.75, although calcium concentration in NSSW is low. So, DETPMP is already incompatible with NSSW at pH$_0$ 6. After the addition of carbonate substrate to the SI solutions, pH increases because of limestone dissolution and divalent cations including Ca^{2+} and Fe^{2+} in solution also increase by dissolution of the carbonate substrate. In the region where the retention regime changes from pure adsorption to coupled adsorption/ precipitation, the pH then decreases due to chemical reaction between SI and divalent cations. Moreover, in the PPCA/Skye limestone case, as shown in Figure 4.67, there are no significant changes in pH in the bulk compatibility tests (no limestone present); the constant lines at pH$_0$ 4 are the solutions with no solid present, i.e. no reaction/adsorption. These compatibility results show that PPCA is compatible with NSSW without the limestone mineral in the solution. However, if limestone substrate is added to the solution then at equilibrium, pH rises from its initial adjusted pH to ~8 due to dissolution of carbonate substrates and the reaction of the scale inhibitor with the calcium which was generated in situ, as described above. As [SI] increases, the final pH reduced to pH ~7 & 7.2 in T=80°C & 95°C respectively which can be ascribed to more precipitation of PPCA/Ca complex in the PPCA/limestone system at 95°C than at 80°C.

To further establish the pure adsorption and coupled adsorption/ precipitation behaviour, changes in [Ca^{2+}] concentration were measured before and after the experiments in both adsorption and compatibility tests. Any decrease in the Ca^{2+} is due to precipitation of M^{2+}-DETPMP complex. Figure 4.68 & Figure 4.69 show the differences in normalised [Ca^{2+}] amount for both compatibility and adsorption tests for DETPMP at initial pH (pH$_0$ 6) and PPCA at initial pH (pH$_0$ 4) studied, respectively. Note that there are mechanisms for both increasing the final Ca^{2+} level (dissolution of the rock) and decreasing the Ca^{2+} level (precipitation of the SI – Ca^{2+} complex). The balance between these effects is clearly different in these figures and this must be explained by a successful model of this process.
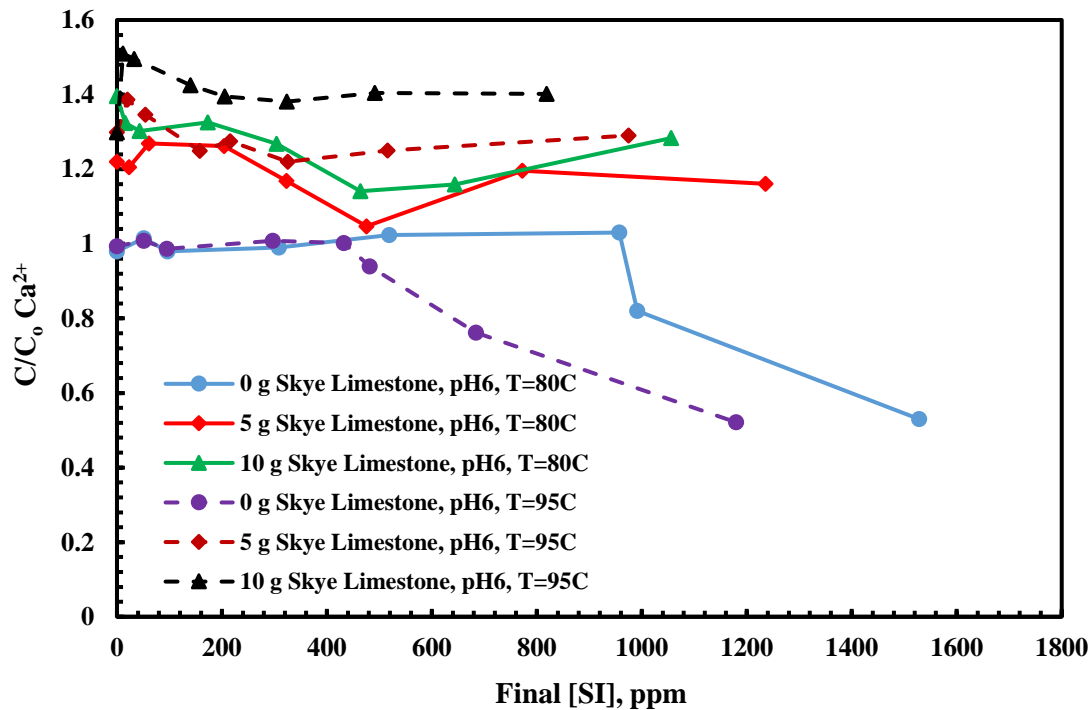
Figure 4.68. Comparison of changes in normalized C/C_0 of $[Ca^{2+}]$ for Skye limestone bed vs final [DETPMP] at pH_0 6; T = 95°C & 80°C
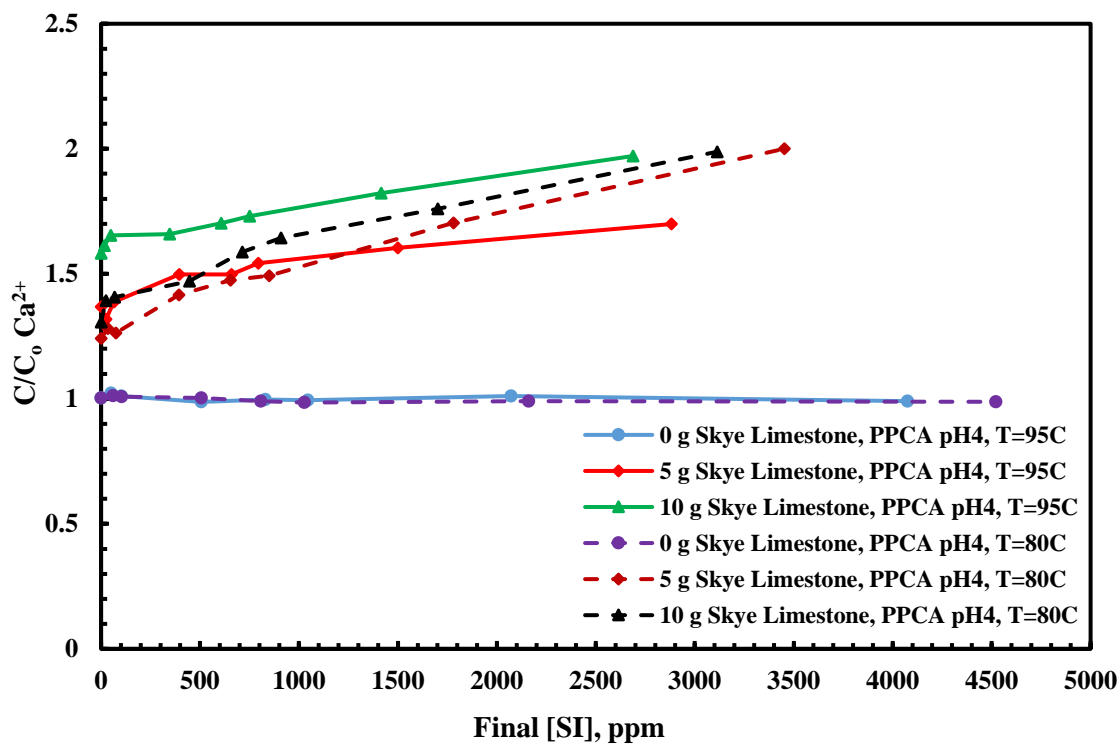
Figure 4.69. Comparison of changes in normalized C/C_0 of $[Ca^{2+}]$ for Skye limestone bed vs final [PPCA] at pH_0 4; T = 95°C & 80°C

As indicated Figure 4.68 , the value of C/C_o for calcium in the compatibility tests decreases due to chemical reaction between SI and calcium from the solution which confirms DETPMP is incompatible with NSSW at pH_0 6. In addition, the normalised calcium concentration decreased as temperature was reduced which means the remaining calcium concentration in solution at T = 80°C is higher than that at T = 95°C. In other words, calcium is less involved in the complexation process at lower temperature, which confirms the corresponding apparent adsorption results (lower apparent adsorption at the lower temperature).

In the PPCA/Skye limestone system, the $[Ca^{2+}]$ results in Figure 4.69 indicate quite clearly that there is no distinct change in $[Ca^{2+}]$ in compatibility tests (no rock substrate) which means that PPCA may bind with calcium to some degree but the complex is soluble and the scale inhibitor is completely compatible with NSSW at pH_0 4. However, once limestone is added to the scale inhibitor solution, a considerable amount of additional $[Ca^{2+}]$ is generated in situ due to rock dissolution, rising to ~2x the initial value for both temperatures; note that these increases in $[Ca^{2+}]$ are in spite of the loss of calcium from solution by precipitation of the SI/Ca complex. Moreover, normalised $[Ca^{2+}]$ increases continuously at pH_0 4 as rock is dissolved and M^{2+} is generated.

Finally, ESEM-EDX analysis was used to examine the surface of Skye limestone both before and after treatment in the apparent adsorption experiments. Therefore, after filtration, all the filter papers containing carbonate substrates and (in some cases) the precipitated complex for each of the DETPMP concentrations tested were dried and sent for ESEM-EDX analysis.
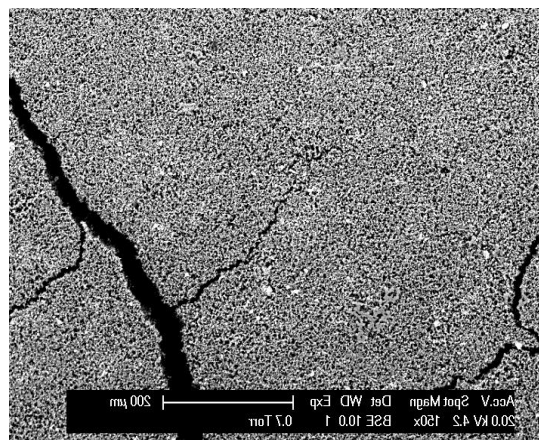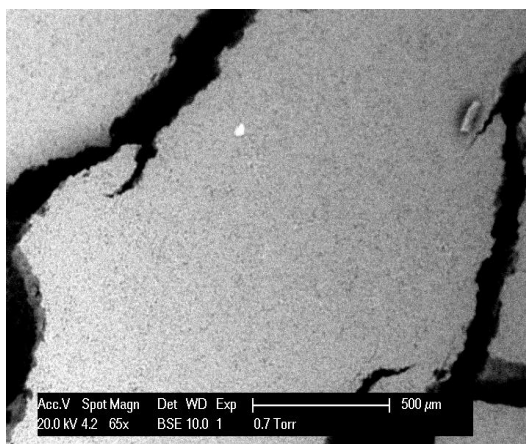
c) Compatibility test, 4000 ppm DETPMP, pH6, T=80ºC   **d) Bulk Precipitate, 4000 ppm DETPMP, pH6, T=80ºC**

Figure 4.70. Morphology of Bulk Precipitate at 4000 ppm DETPMP at pH_0 6, T=80ºC on ESEM photographed samples

Table 4.16. EDX signals on the 2000 & 4000 ppm DETPMP for 100-315 µm at pH_0 6, T=80ºC from ESEM

	Bulk Precipitate 4000 ppm (DETPMP/Skye Limestone)		Bulk Precipitate 4000 ppm (Compatibility test)	
Element	% Weight	% Atomic	% Weight	% Atomic
N	40	18	30	31
O	34	59	40	40
Na	2	2	3	4
Mg	4	4	6	7
P	11	10	14	12
S	-	-	-	-
Cl	3	2	2	4
Ca	5	3	5	4
Fe	1	2	-	-

As shown in Figure 4.70 and Table 4.16., significant levels of phosphorus are detected in all samples. These results are consistent with the corresponding apparent adsorption results. In addition, DETPMP is incompatible with NSSW and a bulk precipitate was formed in the absence of minerals in the solution at [DETPMP] = 4000 ppm. The quantities of phosphorus in compatibility experiment at 80ºC are ~ 14% wt for the 4000 ppm DETPMP case.

218

For the PPCA/Skye limestone system, phosphorous has not been detected by EDX analysis at the highest concentration of PPCA (4000ppm), although we observe significant amounts of precipitate for this concentration, according to ICP results (and by visual observation). As discussed above, this is mainly because of the low content of phosphorus in PPCA[36]. Thus, we have to show the occurrence of precipitated PPCA/Ca complex by another analytical method such as Particle Size Analysis (PSA), and results for PSA are presented below.
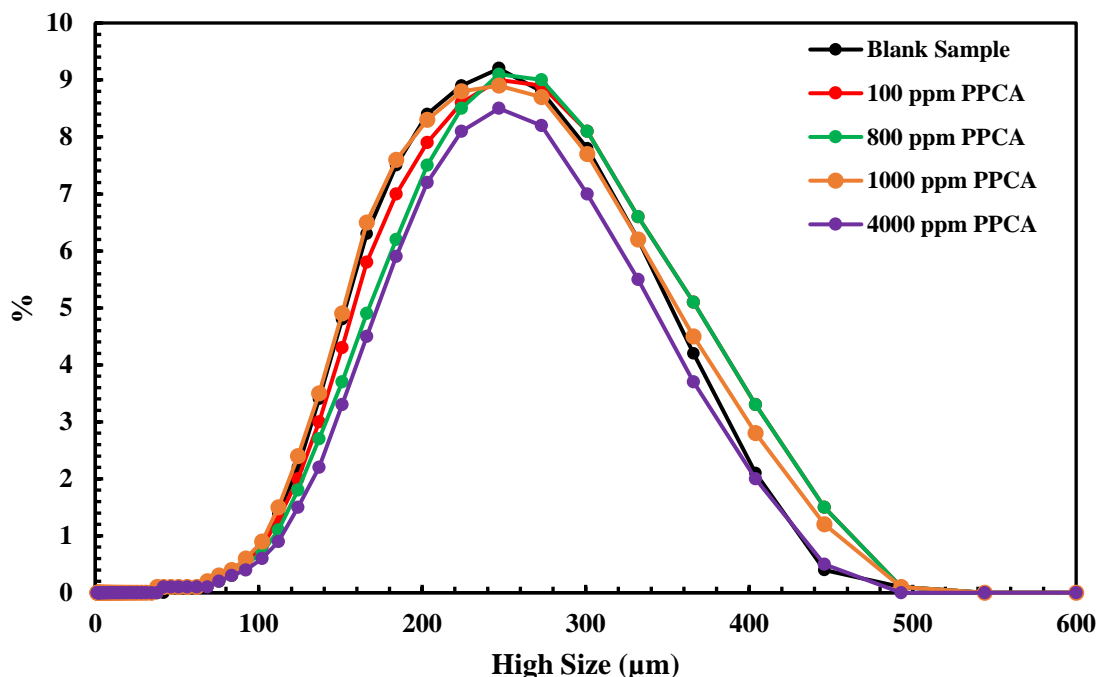
Figure 4.71. Particle Size Analysis for 100-315 µm Skye limestone residue in different concentrations and pH$_0$ 4 with 300 mm lens

These PSD results in Figure 4.71 show that there is good consistency in the measurement of the limestone particle sizes with the largest 300mm lens for the experiments at pH$_0$ 4. For these cases (pure limestone and 100ppm PPCA), we see that only large particle sizes are observed broadly in agreement with the limestone size range we expect. When these same sample cases (for example 100ppm PPCA) were examined by the smaller lens (45 mm lens) which can "see" much smaller particles (from ~1 – 20 µm), no fine particles of this size are observed; see Figure 4.72 and note the "flat line" 100ppm case. However, we then examined cases using this smaller (45mm) lens for the experiments at increased PPCA concentrations where the system is going from a region of pure adsorption to coupled adsorption/precipitation. These cases are shown in Figure 4.72 and we now see peaks of PSD between ~1 – 10 µm. Clearly, these populations of smaller particles are

the SI/Ca precipitated material which forms as this finer material; note that this is clearly distinguishable from the limestone grains (which are much bigger; see Figure 4.71).
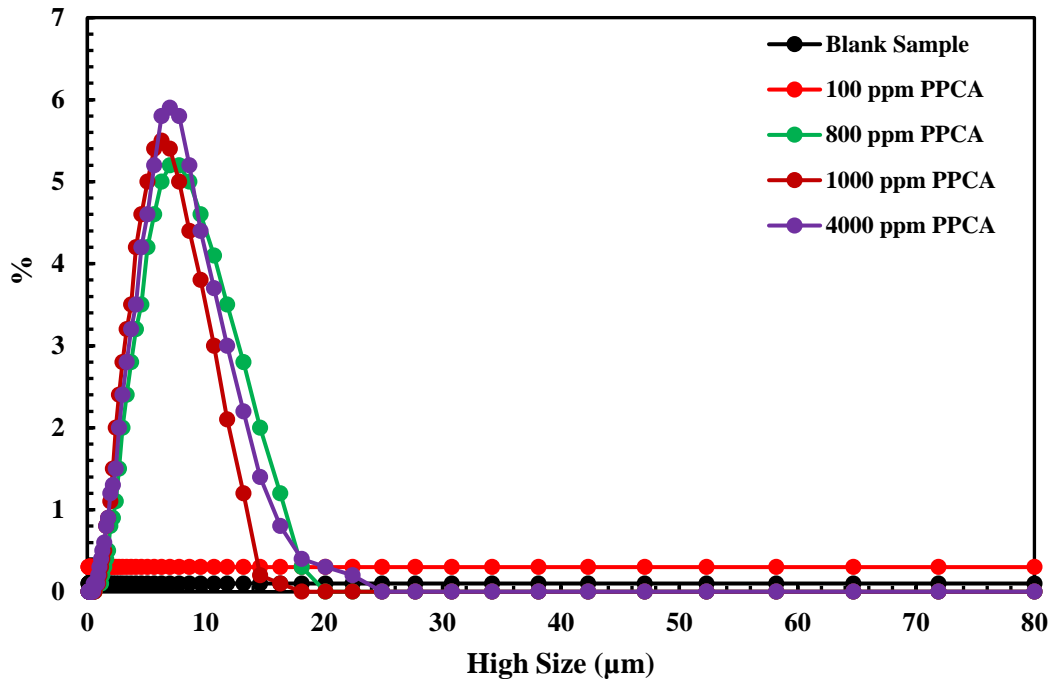
Figure 4.72. Particle Size Analysis for 100-315 µm precipitate deposited on filter paper in different concentrations and pH_0 4 with 45 mm lens

The specific conclusions from the work presented in this section, are as follows:

1. Both pure adsorption (Γ) and coupled adsorption precipitation (Γ/Π) regions are clearly observed for DETPMP and PPCA SIs on limestone substrates at pH_0 4 & pH_0 6 and T=95°C & T= 80°C. However, the region of pure adsorption is more extended to higher concentrations for DETPMP & PPCA/carbonate as temperature reduced.

2. The amount of apparent adsorption of DETPMP and PPCA on limestone decreases as temperature is reduced. At lower temperatures, the solubility of the SI-M^{2+} complex increases resulting in less precipitation and hence a lower "apparent adsorption".

3. For the DETPMP/Carbonate system, the quantity of apparent adsorption increases as the solution pH increases, contrary to the corresponding results for PPCA. This may be ascribed to two competing parameters, i.e. (a) the effect of pH where increasing pH gives a more dissociated SI (as it is a weak poly acid, H_nA), and (b) the level of solution calcium ion concentration, $[Ca^{2+}]$,

220

where a higher level of $[Ca^{2+}]$ tends to increase the amount of precipitate. For the phosphonate SI (DETPM), it is the solution pH (pH increase ➜ more dissociation) which is the more dominant effect controlling the system. However, for the polymeric SI, PPCA, it is the level of solution calcium, $[Ca^{2+}]$, which contributes more to the degree of precipitation of the PPCA_Ca complex.

4. For the PPCA/carbonate system, the amount of apparent adsorption increases as pH decreases, since at low pH more carbonate substrate is dissolved, and accordingly more divalent cations are generated in situ. At the lower initial pH_0 4, we still expect the PPCA to be *less* dissociated and hence form less precipitate. However, the combined effect of this higher calcium dissolution along with the increase in pH caused by the carbonate rock dissolution process itself leads to more PPCA/Ca precipitate.

5. Mineralogy has an important role on the retention of these SIs in carbonate systems since the retention behaviour of the various carbonates is significantly different between calcite and limestone systems (calcite system discussed earlier in the chapter). The retention of both SIs DETPMP and PPCA was greater for the limestone sample containing iron, as Fe^{2+} enhances the precipitate of $SI\text{-}M^{2+}$.

6. Our results appear to indicate that, as phosphonate functional group exists in the SI chemical structure, the reactivity of SI with Ca^{2+} increases resulting in more precipitate being formed and a corresponding increase in the apparent adsorption level. This is the reason why DETPMP is retained more on carbonates than PPCA, which has mostly carboxylic acid functional group.

7. Results from the ESEM/EDX and Particle Size Analysis (PSA) generally confirm, and are very consistent with, the static apparent adsorption results. EDX detected P (phosphorus) concentrations are seen in the deposit where clear coupled Γ/Π has occurred and the EDX level are higher as Γ_{app} (precipitation) increases. A little P is also detected directly on the carbonate grain surfaces but this is generally very minor compared with the high P levels in the finer bulk precipitate. When the 45mm lens is used in the PSA, then this much finer SI/Ca precipitate can be observed directly which has formed mainly from the bulk solution (only in the Γ_{app} regime). This finer precipitate is shown to have high levels of P by EDX. In addition, the amount of phosphorus (P) detected is higher at 95°C than at 80°C which is exactly in line with the corresponding apparent adsorption results.

Note: In this Chapter, the various parts of the work were carried out as indicated in the structure laid out in the Introduction (Section 4.1). The conclusions from each of these parts of the apparent adsorption research were presented at the end of each of these sections. A full overview and summary of all of this work, including the overall conclusions and findings of this research, are presented in the Chapter 5 below.

5. CHAPTER 5: SUMMARY of EXPERIMENTAL RESULTS and DISCUSSION

This chapter presents and discusses the results from the experimental study of the retention mechanisms of generically different scale inhibitors (SI) in carbonate systems. A wide range of "apparent adsorption" experiments were performed and the apparent adsorption, Γ_{app}, vs. C_f, the final SI concentration were plotted for various values of (m/V) ratio. As explained previously, this allowed us to easily identify concentration regions when pure adsorption (Γ) and where coupled adsorption/precipitation (Γ/Π) occurred. Supplementary data on the final solution Ca^{2+} (and Mg^{2+}) and pH were also collected for every apparent adsorption point. All of the SI/calcium precipitates were also analysed using Environmental Scanning Electron Microscope / Energy-Dispersive X-Ray Spectroscopy (ESEM/EDX) and Particle Size Analysis (PSA). These techniques give us direct information on the morphology of any precipitates formed, e.g., whether they were formed as free crystalline (or amorphous) precipitates or whether they formed as "coated structures" on the surface of the carbonate grains. The EDX measurements also gave us an approximate chemical composition of the precipitates; for example, it was able to establish if the precipitates contained P (from the SI) and Ca and in what approximate atomic ratios.

Here, we present typical results of the impact of pH, mineralogy and temperature on the bulk "apparent adsorption" behaviour of these common commercially available scale inhibitors (SI) on carbonate mineral substrates (calcite, dolomite and limestone). Table 5.1. presents a summary of all the experimental conditions examined and presented in this thesis.

Table 5.1. Experimental conditions examined to study scale inhibitor retention mechanisms on carbonate substrates

Scale Inhibitor	Experimental Temperature (°C)	Calcite (Adjusted pH)			Dolomite (Adjusted pH)			Limestone (Adjusted pH)		
		pH_0 2	pH_0 4	pH_0 6	pH_0 2	pH_0 4	pH_0 6	pH_0 2	pH_0 4	pH_0 6
DETPMP	95°C	✓	✓	✓	✓	✓	✓	-	✓	✓+80°C
PPCA	95°C	✓	✓	✓	✓	✓	✓	-	✓+ 80°C	✓
PFC	95°C	✓	✓	✓	✓	✓	✓	-	-	-
PAPE	80°C	-	✓	✓+60°C	-	✓	✓+60°C	-	-	-
VS-Co	95°C	-	✓	-	-	✓	✓	-	-	-

5.1.   Summary of Apparent Adsorption Results

All systems and conditions studied are shown in Table 5.1., but not all of the results are presented here. Instead, two "end-member" examples are shown for DETPMP (Figure 5.1) and PPCA (Figure 5.2). Figure 5.1and Figure 5.2 summarise a large amount of data and they are organized as follows: For each scale inhibitor (SI = DETPMP and PPCA), results are presented for three minerals in turn, viz. SI/Calcite, SI/Dolomite and SI/Limestone. Under each SI/mineral system, three corresponding sets of results are shown from left to right for all experiments – the apparent adsorption vs. the final SI concentration (Γ_{app} vs. C_f), the final pH for all cases and the final normalized $[Ca^{2+}]$ (normalized to its initial value in seawater, $[Ca^{2+}]_0 = 428$ppm). The final SI concentration range is dependent on the reactions that occurred, so the range can vary significantly, as shown in the following plots.

In the discussion below, we will first describe the results in Figure 5.1 and Figure 5.2 and then go on to explain them qualitatively. In simple terms, the amount of precipitation in the SI/carbonate system (i.e. the higher levels of Γ_{app}) depends on the pH and the solution equilibrium $[Ca^{2+}]$.   At higher pH, the SI is more dissociated and hence can chelate more Ca^{2+} and more precipitate may be formed[96,103]. At lower pH, SI interacts with the carbonate then additional Ca^{2+} dissolves which in turn causes additional precipitation. However, this entire system - SI dissociation ↔ carbonate mineral ↔ solution pH ↔ solution Ca^{2+} - is an equilibrium (and kinetic) system. The balance of SI dissociation and the solution Ca^{2+} and pH determines the overall behaviour and this "balance" is different for DETPMP and PPCA as we first show experimentally and then explain theoretically below.

(a) DETPMP/Dolomite

Apparent Adsorption, Γ_{app} (mg/g)

Legend:
- 5 g Dolomite, pH4
- 10 g Dolomite, pH4
- 5 g Dolomite, pH6
- 10 g Dolomite, pH6

Final pH

Legend:
- Initial Adjusted pH, pH4
- 0 g Dolomite, pH4
- 5 g Dolomite, pH4
- 10 g Dolomite, pH4
- Initial Adjusted pH, pH6
- 0 g Dolomite, pH6
- 5 g Dolomite, pH6
- 10 g Dolomite, pH6

Final Normalised [Ca^{2+}]; C/C$_o$

Legend:
- 0 g Dolomite, pH4
- 5 g Dolomite, pH4
- 10 g Dolomite, pH6
- 0 g Dolomite, pH6
- 5 g Dolomite, pH6
- 10 g Dolomite, pH6

(b) DETPMP/Calcite

Apparent Adsorption, Γ_{app} (mg/g)

Legend:
- 5 g Moroccan Calcite, pH4
- 10 g Moroccan Calcite, pH4
- 5 g Moroccan Calcite, pH6
- 10 g Moroccan Calcite, pH6

Final pH

Legend:
- Initial Adjusted pH, pH4
- 0 g Moroccan Calcite, pH4
- 5 g Moroccan Calcite, pH4
- 10 g Moroccan Calcite, pH4
- Initial Adjusted pH, pH6
- 0 g Moroccan Calcite, pH6
- 5 g Moroccan Calcite, pH6
- 10 g Moroccan Calcite, pH6

Final Normalised [Ca^{2+}]; C/C$_o$

Legend:
- 0 g Moroccan Calcite, pH4
- 5 g Moroccan Calcite, pH4
- 10 g Moroccan calcite, pH4
- 0 g Moroccan Calcite, pH6
- 5 g Moroccan calcite, pH6
- 10 g Moroccan Calcite, pH6

c) DETPMP/Limestone

Apparent Adsorption, Γ_{app} (mg/g)

Final pH

Final Normalised [Ca^{2+}]; C/C_o

Figure 5.1. Apparent adsorption, final pH and normalized Ca^{2+} results for DETPMP at two masses (m= 5 & 10 g) of carbonate, two initial pH (pH_0 4 & 6); (a) DETPMP/Dolomite (b) DETPMP/Calcite and (c) DETPMP/Limestone

(a) PPCA/Dolomite

Apparent Adsorption, Γ_{app} (mg/g)

Final pH

Final Normalised [Ca^{2+}]; C/C_o
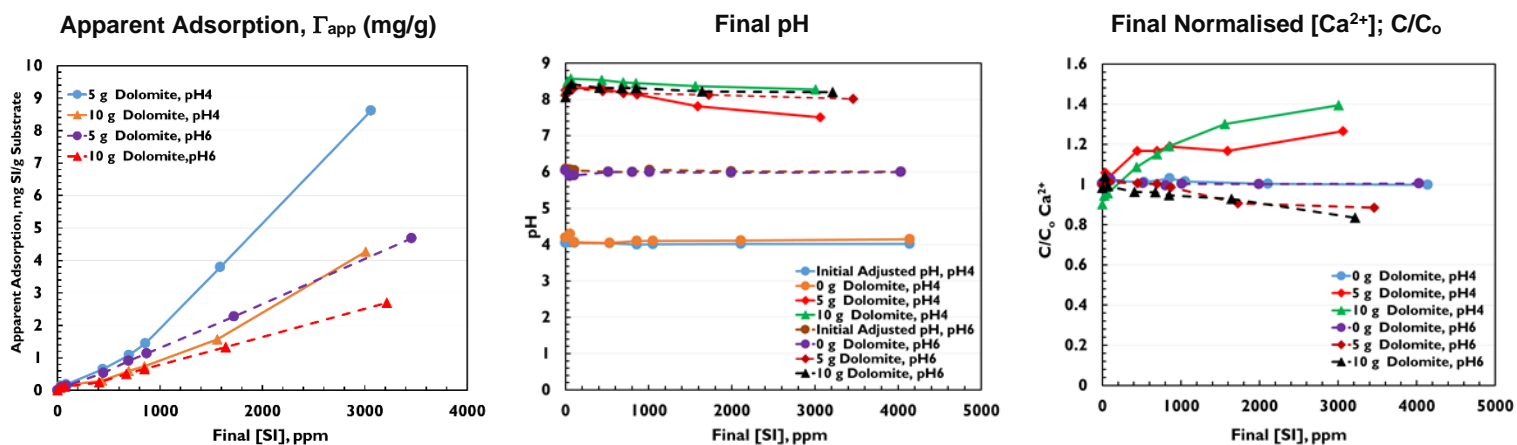
(b) PPCA/Calcite

(c) PPCA/Limestone
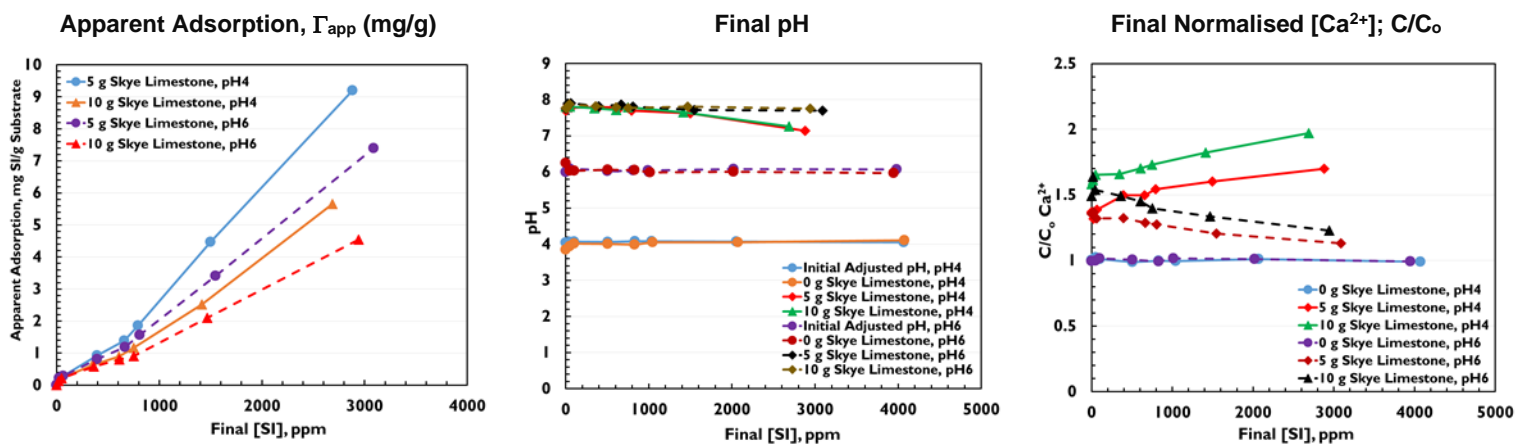
Figure 5.2. Apparent adsorption, final pH and normalized Ca^{2+} results for PPCA at two masses (m= 5 & 10 g) of carbonate, two initial pH (pH_0 4 & 6): (a) PPCA/Dolomite (b) PPCA/Calcite and (c) PPCA/Limestone

Figure 5.1 shows the results for apparent adsorption of DETPMP as a function of the final SI concentration (Γ_{app}, vs. C_f) for 2 masses of carbonate substrates (m = 5g and 10g). The results in Figure 5.1 clearly indicate that both pure adsorption (Γ) and coupled adsorption/precipitation (Γ/Π) occur for both initial pH values (pH_0 4 or 6), for all 3 minerals (calcite, dolomite and limestone). Pure adsorption is observed for [SI] up to ~100ppm, before the different (m/V) curves start to deviate, indicating that coupled adsorption/precipitation behaviour is occurring,

above this 100ppm DETPMP level. In addition, we note that for DETPMP, as pH increases, the amount of apparent adsorption (precipitation) increases. This is due to the higher dissociation of DETPMP at pH_0 6; i.e. the SI (DETPMP) is much more likely to complex with Ca^{2+} to form a SI/Ca complex in its dissociated form (i.e. at higher pH values) and less likely to form complexes at lower pH values[103]. Also, the amount of apparent adsorption of DETPMP on dolomite is greater ($\Gamma_{app} \sim 25$ mg/g) than on calcite ($\Gamma_{app} \sim 20$ mg/g) This result is counterintuitive since it is well known that calcite is much more reactive than dolomite and should give a higher solution Ca^{2+} (which indeed it does). Dolomite is less reactive than calcite chemically, and the calcium content which DETPMP needs for precipitation in the dolomite case is lower than for calcite (see the final normalized $[Ca^{2+}]$). However, the final solution pH is also shown in Figure 5.1, and it is seen that the final pH for DETPMP/dolomite is higher in comparison with the DETPMP/calcite system. Thus, the DETPMP becomes more dissociated, and more functional groups become available for complexation. Thus, for DETPMP it is the pH effect rather than the final $[Ca^{2+}]$ which leads to the higher apparent adsorption (mainly precipitation, Π) for the dolomite. It is shown below that the pH/Ca "balance" is the other way round for PPCA.

Figure 5.2 shows the Γ_{app} vs. C_f results for PPCA and the same three minerals (calcite, dolomite and limestone). Again, we observe the same pure adsorption region (Γ only) at lower PPCA concentrations (again, up to [PPCA] ~100ppm) for all carbonates. At concentrations [PPCA] >100ppm, the two apparent adsorption curves for different (m/V) ratios diverge showing that coupled adsorption/precipitation (Γ/Π) is occurring at these higher PPCA levels as was also seen for DETPMP. However, the apparent adsorption levels of PPCA are overall less than were observed for DETPMP, which is related to the DETPMP phosphonate functional groups that are susceptible to pH change and become dissociated at higher pH. PPCA mainly has carboxylic acid groups (phosphorus in the middle of backbone) which have less affinity to chelate calcium from the solution[36]. As shown in Figure 5.2, apparent adsorption of PPCA increases when pH decreases. At pH_0 4, the PPCA solution is more acidic and can dissolve more carbonate and accordingly more calcium (Ca^{2+}) will be generated *in situ*. So, the dissociated PPCA will interact with the increased calcium leached out of the system leading to more precipitation (i.e. an observed higher apparent adsorption). At pH_0 6, the PPCA would be somewhat more dissociated (more A^- in solution) as described above, but the amount of Ca^{2+} dissolved into solution would

be much less. The net effect here is that at the lower pH (initial pH_0 4), a higher $[Ca^{2+}]$ is dissolved in solution and the pH is increased (by the carbonate dissolution). Thus, the effect is an increased level of precipitation (i.e. a higher apparent adsorption) at this lower pH level. This adsorption behaviour is different when compared to the DETPMP/carbonate systems. Furthermore, PPCA is retained more in calcite (Γ_{app} ~ 10 mg/g), than in limestone (Γ_{app} ~ 9.5 mg/g) and finally in dolomite (Γ_{app} ~ 8.5 mg/g) due to the lower content of calcium in the dolomite substrate than in calcite and limestone. This observation is in contrast to the DETPMP retention in carbonates described above. Therefore, these results show that the level of solution $[Ca^{2+}]$ is more important than pH for PPCA, when considering the pH/Ca "balance".

Table 5.2. gives a summary of these observations alongside associated qualitative data, for all the SI types investigated.

Table 5.2. A summary of observations and qualitative data for the apparent adsorption results (Γ_{app}), for all SI types investigated, on various carbonate substrates

Scale Inhibitor	Calcite	Dolomite	Limestone
DETPMP	lowest Γ_{app} $\Gamma_{app} \sim 20mg/g$ @ highest [SI] pH6 Coupled Γ/Π dominant at 95°C; Γ_{app} at pH2 $\approx$ pH4 < pH6; pH contributes more than [Ca^{2+}]	highest Γ_{app} $\Gamma_{app} \sim 25mg/g$ @ highest [SI] pH6 Coupled Γ/Π dominant at 95°C; Γ_{app} at pH2 $\approx$ pH4 < pH6; pH contributes more than [Ca^{2+}]	$\Gamma_{calcite} < \Gamma_{limestone} \leq \Gamma_{dolomite}$ $\Gamma_{app} \sim 25mg/g$ @ highest [SI] pH6 Coupled Γ/Π dominant at 95°C; Extended Γ at 80°C; Γ_{app} at pH4 $\approx$ pH6 ; pH contributes more than [Ca^{2+}]
PPCA	highest Γ_{app} $\Gamma_{app} \sim 11mg/g$ @ highest [SI] pH2 Coupled Γ/Π dominant at 95°C; Γ_{app} at pH2 > pH4 > pH6; [Ca^{2+}] contributes more than pH in retention	lowest Γ_{app} $\Gamma_{app} \sim 10mg/g$ @ highest [SI] pH2 Coupled Γ/Π dominant at 95°C; Γ_{app} at pH2 > pH4 > pH6; [Ca^{2+}] contributes more than pH in retention	$\Gamma_{dolomite} < \Gamma_{limestone} \leq \Gamma_{calcite}$ $\Gamma_{app} \sim 9mg/g$ @ highest [SI] pH4 Coupled Γ/Π dominant at 95°C; Extended Γ at 80°C; Γ_{app} at pH4 > pH6; [Ca^{2+}] contributes more than pH in retention
PFC	lowest Γ_{app} $\Gamma_{app} \sim 9mg/g$ @ highest [SI] pH6 Coupled Γ/Π dominant for Ph$_0$= 4, 6; Γ dominant for pH$_0$= 2 at 95°C; Γ_{app} at pH2 < pH4 $\approx$ pH6; pH contributes more than [Ca^{2+}] in retention	highest Γ_{app} $\Gamma_{app} \sim 13mg/g$ @ highest [SI] pH2 Coupled Γ/Π dominant at 95°C; Γ_{app} at pH2 > pH4 $\approx$ pH6; pH contributes more than [Ca^{2+}] in retention	-
PAPE	lowest Γ_{app}	highest Γ_{app}	-

	$\Gamma_{app} \sim$ 6mg/g @ highest [SI] pH6	$\Gamma_{app} \sim$ 12mg/g @ highest [SI] pH6	
	Coupled Γ/Π dominant, 80°C , pH= 6; Pure Adsorption Γ, pH0= 4 Extended Γ at 60°C, pH0= 6; Γ_{app} at pH4 < pH 6;	Coupled Γ/Π dominant; at 80°C, pH = 4 & 6 at 60°C, pH= 6; Γ_{app} at pH4 ≈ pH 6;	
	Final pH contributes more than [Ca^{2+}] in retention	Final pH contributes more than [Ca^{2+}] in retention	
VS-Co	highest Γ_{app} $\Gamma_{app} \sim$ 4.5mg/g @ highest [SI] pH4	lowest Γ_{app} $\Gamma_{app} \sim$ 1.2mg/g @ highest [SI] pH4	-
	Coupled Γ/Π at > 3000ppm [VS-Co]; Γ to [VS-Co] =2500 ppm; Γ dominant at 95°C;	Some Coupled Γ/Π observed at pH4; Γ to [VS-Co] = 5000 ppm at pH4; Γ_{app} at pH4 > pH6; Γ dominant at 95°C;	
	[Ca^{2+}] contributes more than pH in retention	[Ca^{2+}] contributes more than pH in retention	

The scale inhibitor VS-Co exhibits the most "adsorption like" behaviour of all the SIs studied in our work (although we would expect Poly Vinyl Sulphonate (PVS) inhibitor to show almost pure adsorption behaviour). Figure 5.3 shows the apparent adsorption, Γ_{app}, vs. C_f for VS-Co on dolomite for two masses of substrate, m = 5g and 10g, at 95°C. The 100-315μm size fraction of dolomite was used and two initial pH values, pH0 4 and 6 were investigated.
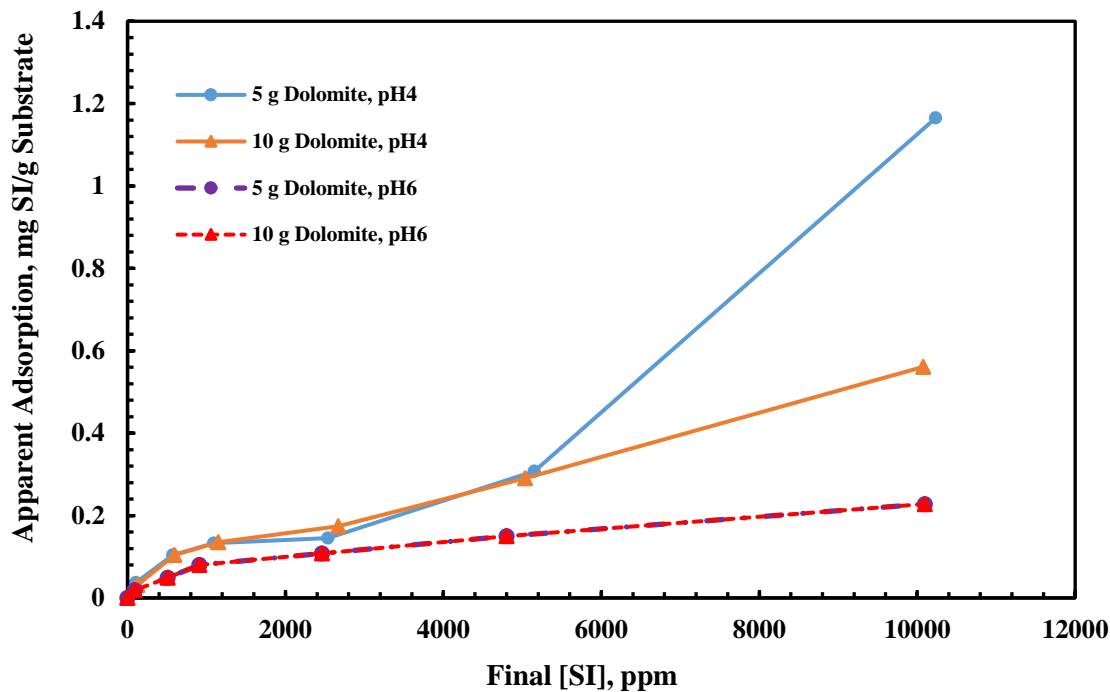
Figure 5.3. Comparison of apparent adsorption for VS-Co onto 2 masses (m = 5g and 10g) of dolomite at 95°C & pH$_0$ 4, 6

The Γ_{app} vs. C_f results in Figure 5.3, clearly show that only pure adsorption (Γ) is observed for the VS-Co /dolomite system at initial pH$_0$ 6, but that some coupled adsorption-precipitation (Γ/Π) is seen at higher concentrations for the pH$_0$ 4 case. It is also noted that, even when this precipitation behaviour is observed, the levels are very low (Γ_{app} ~ 1.2 mg/g), compared for example to DETPMP (Γ_{app} ~ 25 mg/g; see Figure 5.1(a)). The very low Γ_{app} levels in Figure 5.3 could be taken as being only pure adsorption. However, in our examination of the system using ESEM/EDAX and PSA we can directly observe small levels of precipitation for the Vs-Co/dolomite system at pH$_0$ 4 (see Figure 5.7, Figure 5.8 & Figure 5.9). Thus, the conclusion for the Vs-Co system is that it is pure adsorption however at lower initial pH levels, for higher SI concentrations, a small amount of precipitation can occur and this is directly observable. This is in contrast to other SIs such as DETPMP and PPCA (Figure 5.1 and Figure 5.2) where the precipitation region dominates for all carbonate minerals at initial pH$_0$ 4 and 6.

For these two VS-Co/dolomite systems, the final pH values have also been measured and these are shown in Figure 5.4, plotted against C_f, the final [VS-Co].
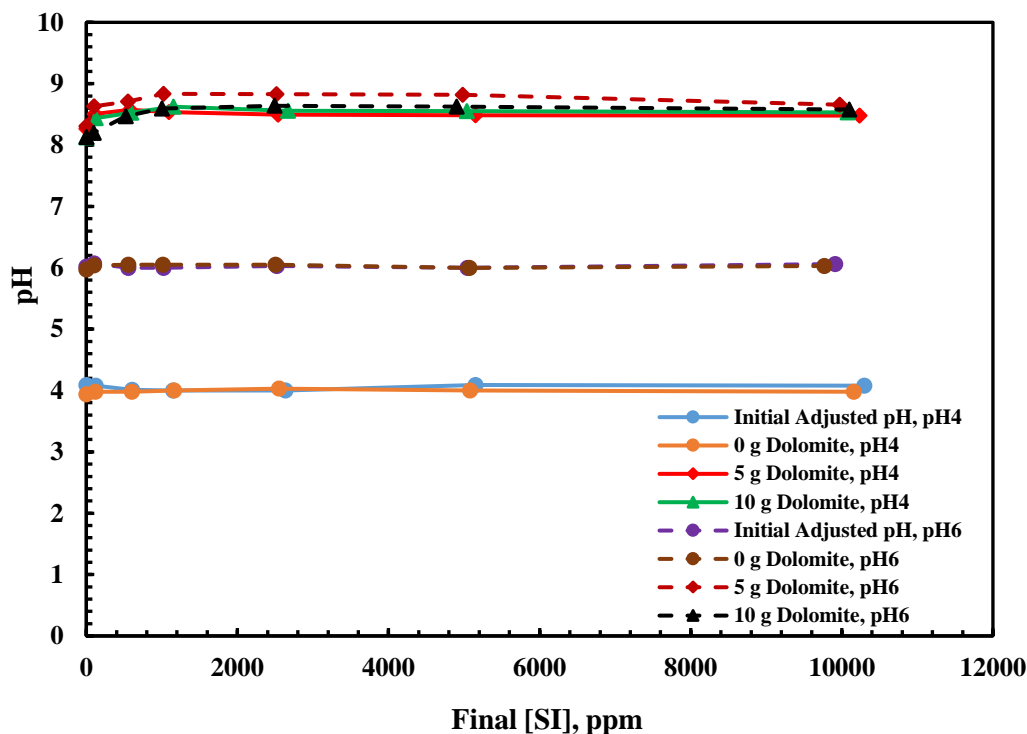
Figure 5.4. Comparison of final pH trend for different masses of Skye dolomite (100-315µm) versus final [VS-Co] at 95°C & pH_0 4, 6

The results in Figure 5.4 for the VS-Co dolomite system show that the pH rises from its initial value (pH_0 4or 6; initially adjusted pH) to pH ~ 8 due to dissolution of the dolomite substrate. Figure 5.5 shows that calcium (and magnesium – not shown) are leached out of the dolomite substrate. However, there is no significant reaction between VS-Co and M^{2+} in solution and the retention regime is mainly pure adsorption.

Figure 5.5 shows a steadily rising level of normalised $[Ca^{2+}]$ up to ~1.4 for the VS-Co dolomite system at pH_0 4, however at pH_0 6 the calcium loss, by complex precipitation and gains in solution by leaching from the dolomite substrate, are approximately balanced (normalised levels of calcium remain at ~1). For the VS-Co/dolomite system, this implies that increasing the [VS-Co] does indeed leach more Ca^{2+} from the dolomite into solution but this is not all precipitated.
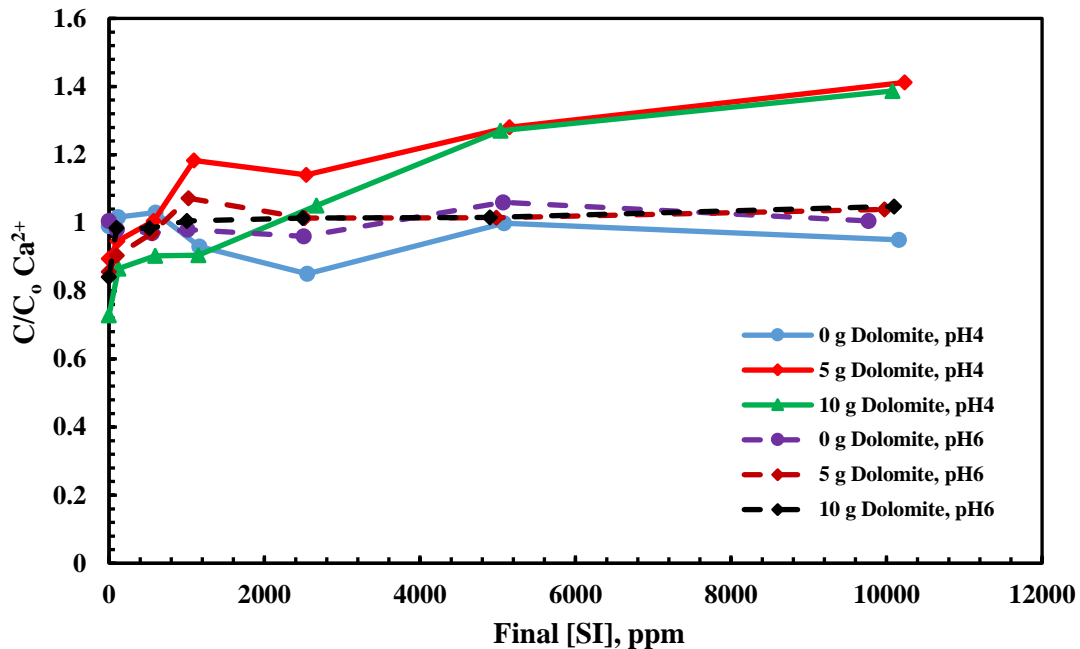
Figure 5.5. Comparison of C/Co of [Ca^{2+}] trends for VS-Co/Skye Dolomite at 95°C & pH_0 4, 6

It is well known that the sulphonate groups (have a low pKa; acidic) in the VS-Co structure are very tolerant to high levels of divalent ions such as Ca^{2+}; i.e., they have low binding constants to these divalent ions. In contrast, the phosphonate groups in other scale inhibitors bind more strongly to Ca^{2+} and the complex formed has a lower solubility.

Any precipitates generated or grains of carbonate mineral collected were studied in detail using Environmental Scanning Electron Microscopy/Energy Dispersive X-Ray (ESEM/EDX) and Particle Size Analysis (PSA). ESEM-EDX analysis was used to examine the surface of the carbonates both before and after treatment in the apparent adsorption experiments. This technique is usually utilized for SIs which have phosphorus, to confirm the corresponding apparent adsorption results and to observe whether the SI-M^{2+} complex is formed as a separate phase or if it forms as an integral coating around the grains. Here we present some examples of how to use these surface chemistry techniques in the context of SI/carbonate interactions. These measurements confirmed that, when precipitation occurred, it was mainly in the bulk solution and much less on the rock surface.
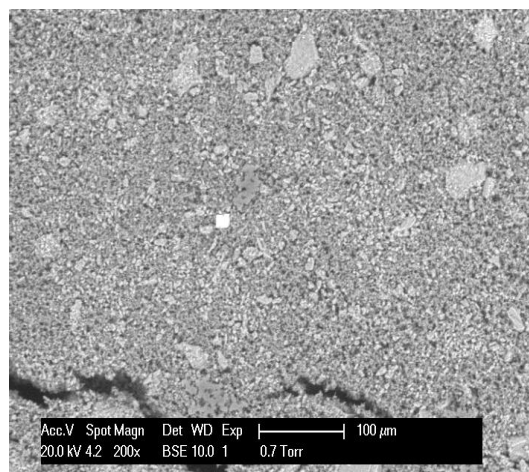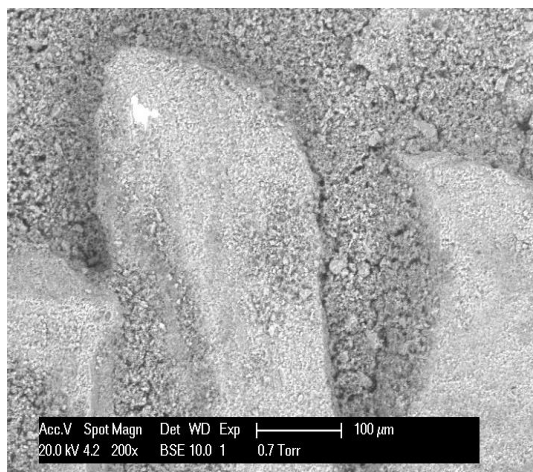
a) Limestone grain, 4000ppm DETPMP, pH$_0$6, 95°C   b) Precipitate, 4000ppm DETPMP, Limestone, pH$_0$6, 95°C

Figure 5.6. Morphology of limestone grains and bulk precipitation at 4,000ppm DETPMP at pH$_0$ 6, 95°C on ESEM photographed samples

Table 5.3. EDX analysis of 4,000ppm DETPMP for 100-315µm limestone at pH$_0$ 6

Element	Limestone grain 4000 ppm (pH=6)		Bulk precipitate 4000 ppm (pH=6)	
	% Weight	% Atomic	% Weight	% Atomic
C	16	23	-	-
Na	1	1	2	3
Mg	2	1	5	5
P	4	2	13	10
S	0.3	0.1	0.5	0.4
Cl	1	1	4	3
K	0.7	0.9	0.5	0.6
Ca	18	8	34	21
O	57	63	41	57

As shown in Figure 5.6 and Table 5.3., phosphorous is clearly detected at a higher level (~13% by weight) in the finer precipitate which forms in the bulk and is retained on the filter paper. However, there is a detectable amount (~ 4% by weight) on the limestone grains themselves. This amount is possibly some of the bulk SI/Ca precipitate adhering to the limestone surface or is part of the adsorbed SI on the limestone surface. However, no "surface coating" of the precipitated SI/Ca complex around the limestone grains was observed in these experiments.

Thus, we see no evidence for the hypothesis of "surface poisoning" by the Ca-DETPMP complex.

For the VS-Co/Ca complex case, these techniques can be used, as sulphur can be used to detect the VS-Co as it is a sulphonated copolymer SI. However, to make sure the VS-Co/M^{2+} complex has been formed in the solution and it is not the sulphur from the seawater sulphate content being measured, we need to use PSA as an alternative analytical method to confirm the apparent adsorption results.
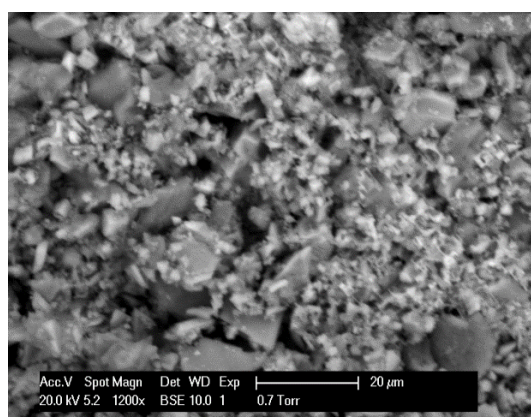
a) 10,000ppm VS-Co, 100-315µm dolomite, pH$_0$4 **b) Precipitate, 10,000ppm VS-Co, dolomite, pH$_0$4**
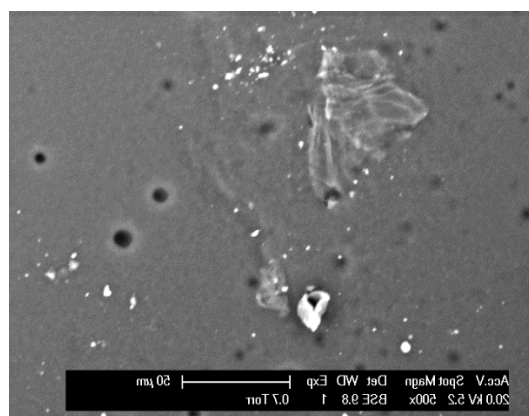
Figure 5.7. Morphology of 10,000ppm VS-Co samples for 100-315µm dolomite & bulk precipitate at pH$_0$ 4 on an ESEM photographed sample

Table 5.4. EDX analysis of 10,000ppm VS-Co for 100-315µm dolomite at pH$_0$ 4

Element	Dolomite grain 10000 ppm (pH=4)		Bulk precipitate 10000 ppm (pH=4)	
	% Weight	% Atomic	% Weight	% Atomic
C	-	-	12	18
O	61	76	54	61
Na	0.7	0.7	2	1.5
Mg	16	13	12	9
S	0.3	0.3	1	0.5
Cl	2	1	3	2
Ca	19	9	17	8

As indicated in Figure 5.7 and Table 5.4., only a trace amount of sulphur can be detected on the dolomite grain but we cannot say with certainty whether it is related to VS-Co since there are two sources of sulphur, seawater and VS-Co. Thus, we utilised the PSA method to confirm the results. PSA with the largest lens (300mm lens) was performed first and results for all particulates are shown in Figure 5.8. This figure shows the measurement of the carbonate grain size distribution and hence highlighted no significant particle size change occurred. Using the smaller (45mm) lens, much smaller particles can be detected, if they are present, as shown in Figure 5.9. Note that smaller particles in the size range 1 – 20µm are only detected for the highest concentration VS-Co (10,000ppm) case. These could be identified visually in the ESEM micrographs, Figure 5.7. No such particulates were observed in the pure adsorption region, as expected.
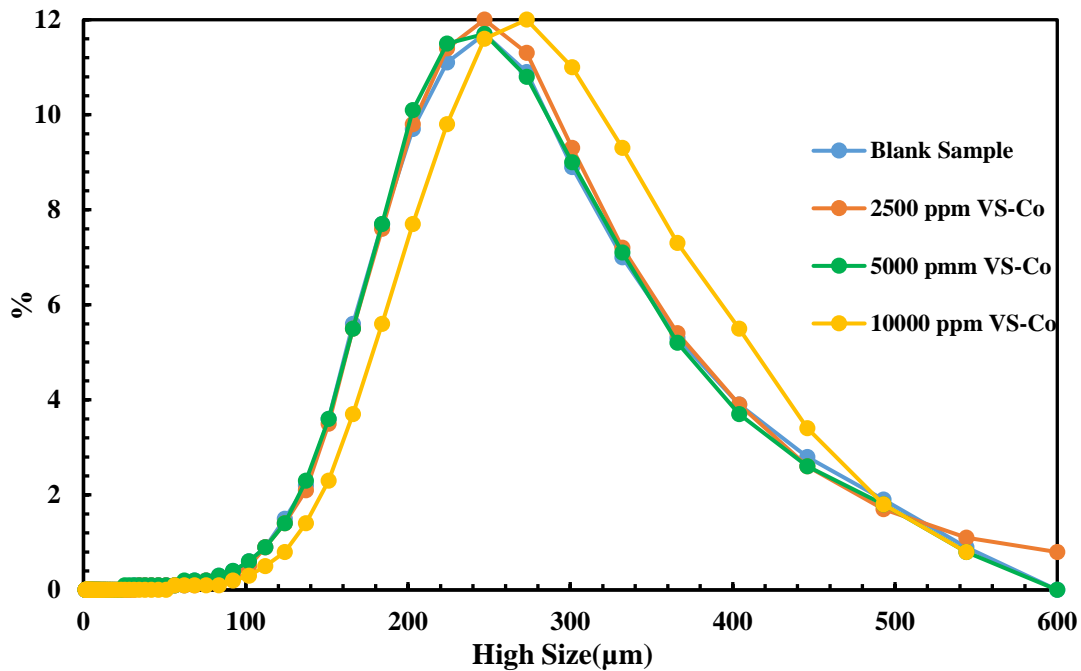
Figure 5.8. Particle Size Analysis for 100-315µm dolomite residue at different SI concentrations
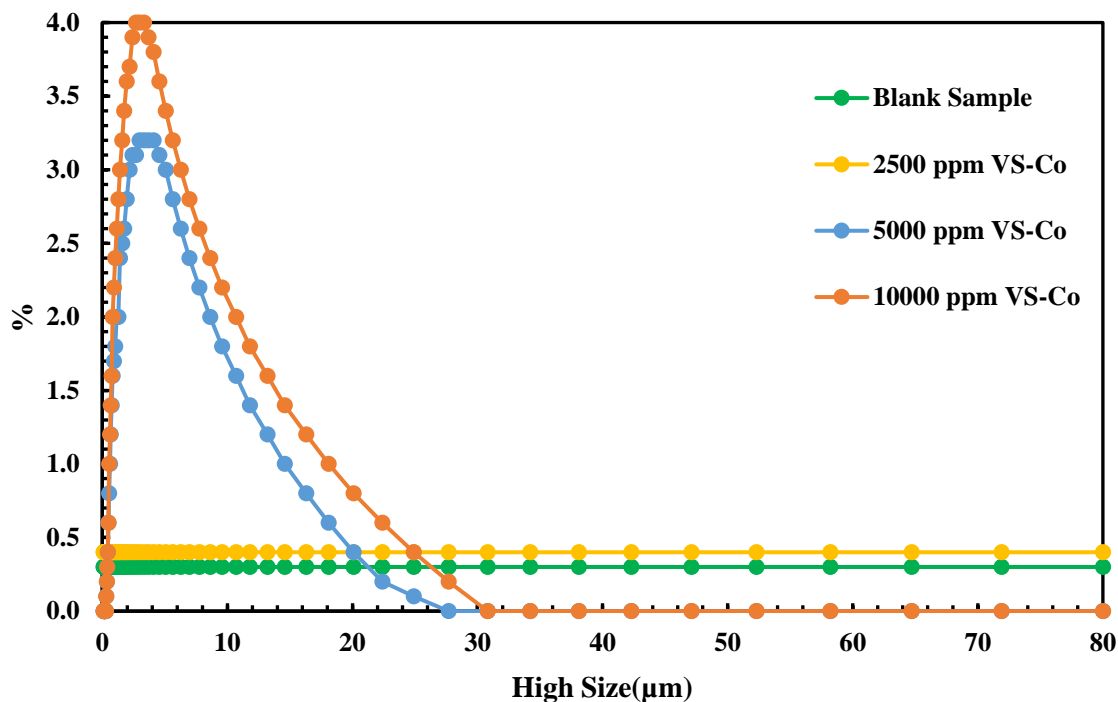
Figure 5.9. Particle Size Analysis for 100-315µm dolomite residue at different SI concentrations

5.2.   Summary and Conclusions

The bulk "apparent adsorption" behaviour (Γ_{app} vs. C_f,) of five commercially available scale inhibitors (SI = DETPMP, PPCA, PFC, PAPE and VS-Co) on three carbonate mineral substrates (calcite, dolomite and limestone) have been studied. In this research work, example results were presented for three of these SIs whilst the results for the others are presented elsewhere[10,42,44]. These carbonate systems are much more chemically reactive than sandstone minerals (e.g. quartz and clays) which have been studied previously. A systematic study has been carried out on the SI/Ca precipitates formed, by applying both ESEM/EDX and particle size analysis (PSA).

The main conclusions from this work are as follows:

1. For all SIs, regions of both pure adsorption (Γ) at lower [SI] and coupled adsorption/precipitation (Γ/Π) retention mechanisms at higher [SI] were observed, with the dominant mechanism depending on SI chemistry, temperature and mineralogy. For most SIs, precipitation was by far the dominant component of the "apparent adsorption", Γ_{app}, in the

carbonate system, except for VS-Co where adsorption was much more prominent and very low (but observable) levels of precipitation were observed at an initial low pH value. The highest retention was observed for the phosphonate followed by the phosphate ester and polymeric SIs, for all substrates, due to the phosphonates higher phosphorus content, which are more reactive with Ca^{2+}, causing greater precipitation.

2. The precipitation region was determined by the SI type and the levels of Ca^{2+} and pH resulting from the equilibrium coupled SI/carbonate/pH /solution Ca^{2+} system. These two factors (final $[Ca^{2+}]$ and pH) determined the amount of precipitate for a given SI type since pH governs the state of dissociation of the SI (more dissociation at higher pH values leads to more Ca^{2+} chelation and more precipitate) and the actual $[Ca^{2+}]$ in solution. Taking the DETPMP and PPCA "end members" as examples then, on balance, the phosphonate SI (DETPMP) is more sensitive to the final pH whereas the PPCA was more sensitive to the level of Ca^{2+} in solution. This was concluded after finding that the highest polymeric SIs retention was observed at low pH for all substrates due to the increase in divalent cations (Ca^{2+}, Mg^{2+} and Fe^{2+}) available from rock dissolution for SI-M^{2+} precipitation. For phosphonate and phosphate ester SIs, the retention was greatest at high pH, as the SI functional groups were more dissociated (available) for complexation with M^{2+} ions.

3. The conclusion in (2) above was further emphasised by the following observations: (i) for polymeric inhibitors such as PPCA, their retention was highest on calcite (highest relative calcium content), followed by limestone and then dolomite. This confirms that calcium accessibility contributes more to the polymer inhibitor retention in carbonate reservoirs in comparison to pH. (ii) the phosphonate and phosphate ester SIs were retained most on dolomite (higher final solution pH and more SI dissociated), followed by limestone and calcite. This means it is solution pH that affected the level of dissociated SI and thus is more important in determining the phosphonate SI retention (precipitation).

4. Results from the ESEM/EDX and Particle Size Analysis (PSA) generally confirm and are very consistent with the static adsorption results. EDX-detected P (phosphorus) concentrations were observed in the deposit where coupled Γ/Π has clearly occurred and the P levels are higher as Γ_{app} (precipitation) increases. A small amount of P is also detected directly on the carbonate grain surfaces but this is generally minor compared with the high P levels in the finer bulk

precipitate. When the 45mm lens is used in the PSA, then much finer SI/Ca precipitate, formed mainly in the bulk solution (only in the Γ_{app} regime), can be observed directly. This finer precipitate is shown to have high levels of P by EDX, hence indicating the P containing scale inhibitor involvement.

5.3. FUTURE WORK SUGGESTIONS

This research work has considered the important parameters governing the retention in carbonate rocks for various scale inhibitors widely applied in the oilfield (phosphonate, polymeric and phosphate ester scale inhibitors). Carbonate substrates with different mineralogy compositions (calcite, dolomite and limestone) have been studied with regard to the operational conditions (pH of scale inhibitors injected and reservoir temperature) in static conditions to understand the fundamental of scale inhibitor retention. However, rarely in research is the last word spoken on a particular topic, and this work is no exception. There are several areas of research within the topic of "scale inhibitor retention in carbonates", that would certainly merit further detailed study, and some of these are listed below:

(1) **The Full Modelling of the SI/Carbonate System:** To the best of our knowledge, there is no equilibrium model which can describe the system used in this work correctly. The system to be modelled here is the SI treated as a weak polyacid (H_nA), with Ca/Mg binding to form sparingly soluble complexes, coupled to the aqueous carbonate system. Some attempts have been made in this work to develop a preliminary model as presented in Appendix 2.1 and in work published by Silva et al.[94] Solutions of these equations agree qualitatively with our results and certainly support our mechanistic understanding of the system. However, a full quantitative description of our experimental results has eluded us to date. I would suggest that developing this quantitative agreement between the results of this thesis and a full model would be a priority for a new PhD entering this area of research. Such a complete model, when incorporated into a transport model, would greatly enhance our ability to simulate scale inhibitor squeeze treatments in both laboratory and in the field.

(2) **Dynamic SI Retention Experiments in Carbonate Packs/Cores:** The "apparent adsorption" experiments in this thesis have been *equilibrium* bulk experiments. However, to apply the results in field SI squeeze treatments then an understating the dynamics of scale inhibitor flow through porous media is required. This can be achieved by studying the flow of

the various SI species used in this work through carbonate packs or through carbonate cores. This will introduce the kinetic or dynamic aspects of the processes (which are already extremely complex). In addition, this will yield information on any potential formation damage resulting from scale inhibitor interaction with carbonates in the near well formation. Also, the information from such dynamic floods can be used to improve our simulations of squeeze treatments and also to compare the performance of various scale inhibitors in terms of their dynamic retention and return behaviour. In particular, this work is highly recommended for the scale inhibitor/dolomite systems as this has not been done previously and there is no experimental data in the literature on this matter. This work will also help us to make the correct choice of scale inhibitor for squeeze treatments in the various types of carbonate system (dolomites, limestones, chalks etc.). When the dynamic adsorption tests are performed, these can be combined with the equilibrium static apparent adsorption experimental results to give a more comprehensive understanding of this important and complex SI/brine/carbonate system.

Another potential research area is how to increase scale inhibitor adsorption capacity. As a general rule, all carbonate samples which were used in this research were water-wet. However, in reality most of carbonate reservoirs are oil-wet. So, the efficiency of scale inhibitor retention reduces due to poor adsorption/ precipitation of inhibitors near wellbore (the adhered oil on the reservoir rock hinders adsorption of scale inhibitor on the reservoir rock and also decrease the reactivity of scale inhibitor with carbonate rock). Therefore, there is a great potential of research work on fabrication of proper chemical formulations such as surfactants or mutual solvents to change the wetting state of carbonate rocks near wellbore and consequently increase the adsorption capacity of the rocks. On the other hand, a potential of wettability alteration by scale inhibitor can be also investigated to minimize the oil production reduction from the scale inhibitor squeezed results from trapping water around wellbore and does not let oil flow come out due to a big capillary resistance against the oil flow from reservoir into the well.

(3) **SI Treatments in Fractured Carbonates:** Finally, scale inhibitor squeeze treatment design in fracture carbonate reservoir would be a very important and technically challenging potential research topic. This topic has not been extensively studied and would be new in inorganic scale management research. The main concern of scale inhibitor deployment in fractured carbonate reservoir is that the injected scale inhibitor may predominantly flow into the fracture spaces

rather than into the rock matrix, and hence mass transfer of scale inhibitor chemical into the matrix may not occur or be very low. Consequently, after a main SI treatment on back-production of the well, most of the scale inhibitor may be quickly returned to the well and very short squeeze lifetimes would be obtained. To investigate and model scale inhibitor squeeze treatments in fracture reservoirs, both modelling and experiments in fractured carbonate cores could be performed; this work could study the impact of fracture presence and also fracture orientation on the efficiency of scale inhibitor squeeze treatments in carbonate reservoirs. There are several challenges in obtaining and preparing representative fractured carbonate rock samples for laboratory flow experiments. Indeed, this is largely why there are also no lab studies of this. However, given the importance of scale management in fractured carbonate reservoirs, this topic cannot be neglected by the scale research community for much longer.

6. APPENDIX: GENERAL EQUIPMENT AND APPARATUS

6.1. General Laboratory Procedure of ESEM/EDX Analysis

Materials to remember to take to the machine:

1. Upon arrival at the machine, check that the equipment is ready to use and if any settings have been changed to those appropriate for your specific sample use;

    a. Machine should always have been left in 'hivac' mode => Vent first before going to H_2O custom

    b. If already in 'hivac' mode, Vent first and then set up for low vac conditions by => H_2O custom, No PCA -> pump. Custom = 1 vent, pump – 0.4 pump, purge = 5 time and the stage goes to the middle X 0 Y 0 coordinates. Beam should be ~ 20-30μk. If > 40-60 then filament is starting to fail

2. Press the High Tension (HT) button next to the computer to turn the HT on (the button will illuminate when switched on). The Vacuum button should always be on when the machine is not being used.
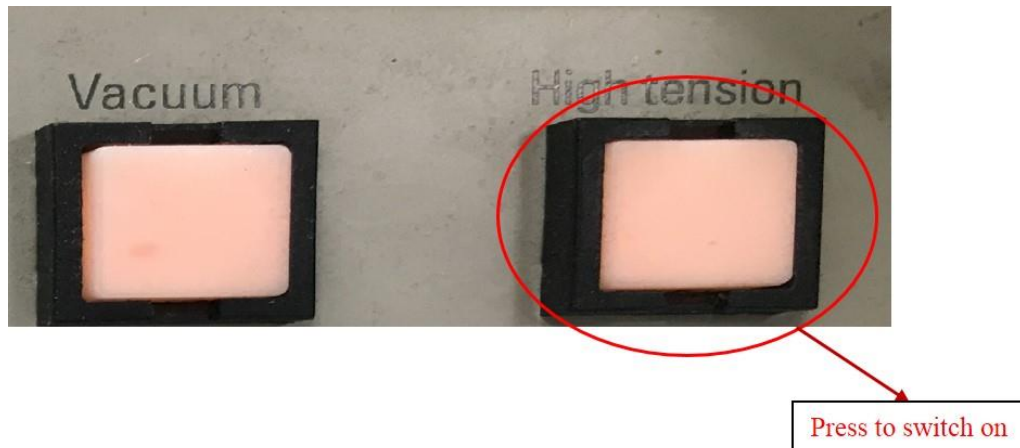

Figure 6.1. Photograph of the vacuum and high tension control buttons on the ESEM instrument. These are located on the left-hand side of the desk

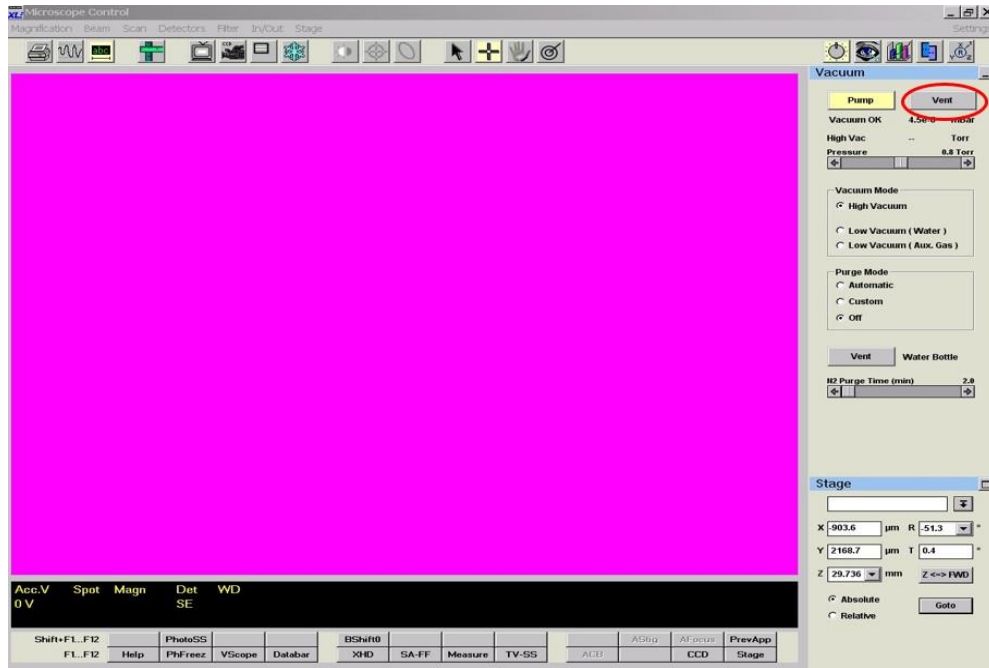3. Release the vacuum by clicking the Vent button on the computer screen once (Figure 6.2)

243

Figure 6.2. Screen-grab of ESEM control software screen showing the location of the "Vent" button on the "Vacuum tab.

4. The vent process may not start immediately after clicking the Vent button, however do not click the Vent button repeatedly as this may cause the software to crash. The venting process is accompanied by a characteristic noise of air being released and if this is not heard within 30 seconds of clicking the button, then attempt again

5. There is no obvious sign that the vent process is complete. To establish whether or not the vacuum is in effect, *gently* attempt to slide open the door of the vacuum chamber with your fingers. If the vacuum is still intact then this will not work, if it is released, then the door will open easily. Use minimal effort to open door. Forcing the door open when it is not ready will destroy the EDX window, resulting in costly replacement and several months to repair!

6. Use blunt point forceps to place a sample on the stage inside the chamber. If a filter paper with sample on it is being investigated then place copper weights, for example 3 x 1 p coins on the edges of sample to avoid the paper and sample being blown about or there is a copper ring of an appropriate size available. If looking at loose material, then shake off excess material, otherwise this will be spread throughout the chamber during pump-down. Close the chamber door gently (otherwise the EDX window will break), also check that the sample is not going to hit the BSE detector, Figure 6.3, as the door is closed.
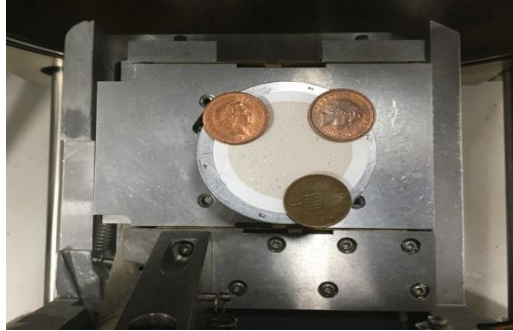
7. Using the controls on the screen, move the stage as far as possible to the bottom back right of the chamber. Furthermore, the EDX must be moved out and away from the sample chamber. These steps must be followed every time the vacuum is pumped or vented, to prevent particulates from entering the system and causing damage to the equipment and detector.

8. Expand the Vacuum bar and then click Low Vacuum (Water). Click 'ok' for 'no PLA'
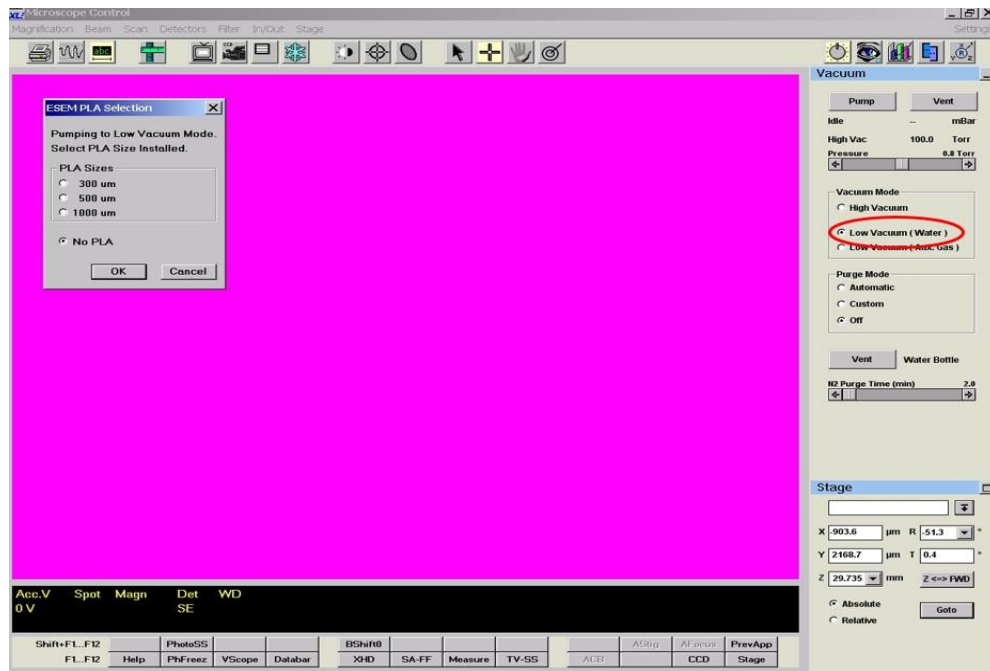
9. Go to Purge Mode bar and click on "Custom" check box. In custom purge setup, the following information should appear (Upper Pressure: 1.00 Torr; Lower Pressure: 0.4 Torr; Cycles: 5), having checked the information, click on OK. The pressure normally sits around 0.7 Torr
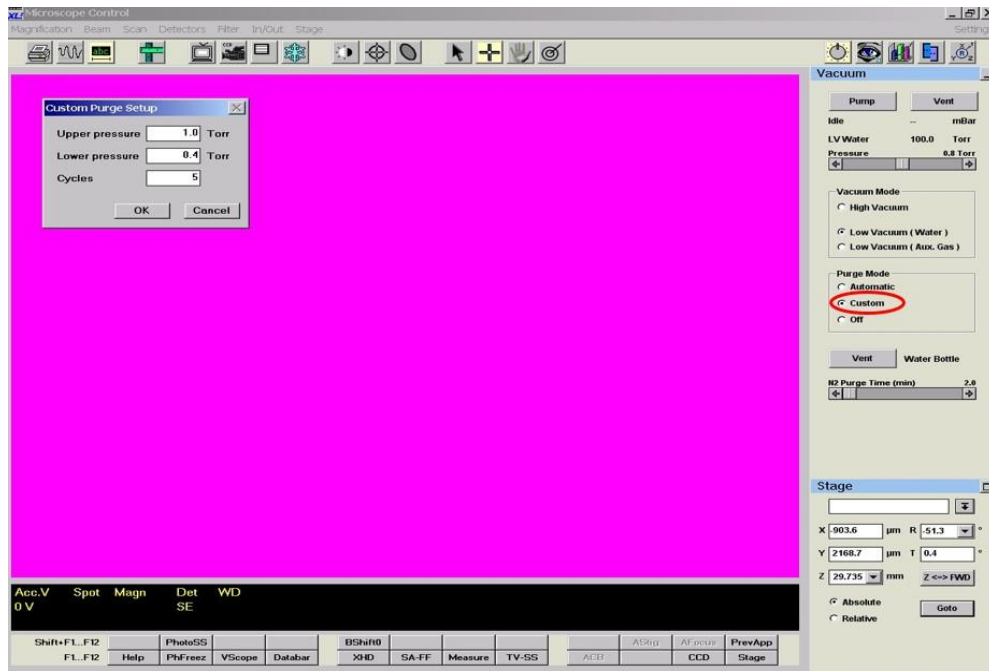
10. Now the machine is ready to be vacuumed by clicking on PUMP and then OK
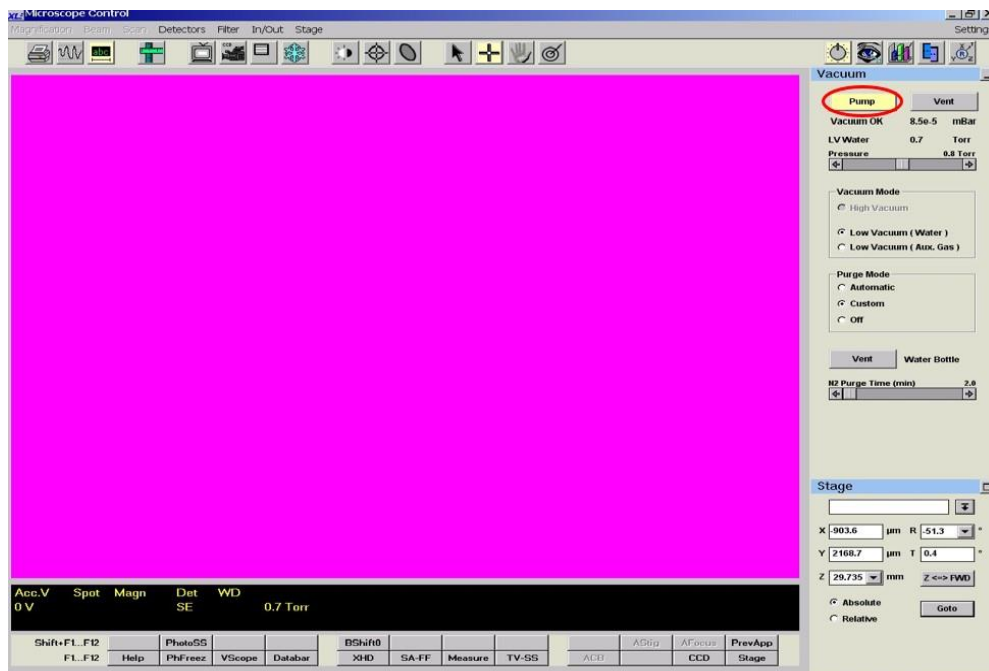
11. The sample stage should now be seen on the computer screen. If not, go to Detectors at top of screen and click CCD to see the stage on the computer screen.
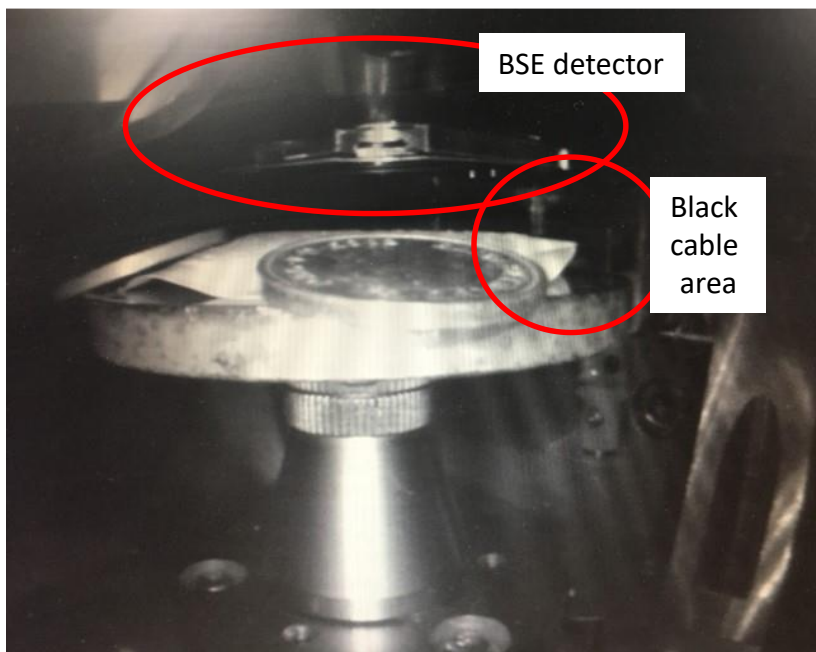
Figure 6.3. CCD image of stage with filter paper in place, weighted with three 1p coins.

12. Do not raise the stage while the machine is being vacuumed.

13. When the vacuum status reads "Vacuum OK", it is then safe to adjust the stage. First move it from the 'safe zone area' using X 0 and Y 0 and by rotating the Z-direction black knob clockwise for up (vertical alignment, Figure 6.4) on the machine. As a guide, after adjustment, the stage is approximately level with the black cable on the back wall of the chamber, Figure 6.3. Check the focus on the backscatter detection screen (BSE/detector tab) where an image is viewed – step 19.

14. Once this has been initially performed for the first sample of the session, to move forward from the safe zone next time, use X 0, Y 0 and Z 10 (or move the stage Z alignment using Z knob until the screen reading is close to 10mm for Z – then image should still be in focus). Prior to moving or pressing anything to move, go to the BSE screen and be ready to cancel the stage movement, by hovering the curser over the pop-up window cancel button.
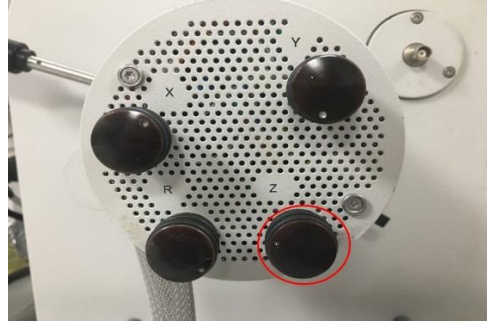
Figure 6.4. Photo of the outside of the chamber door, highlighting the Z-direction control for vertical alignment.

15. Minimize Vacuum tab and expand Beam tab. Click on 20.0 kV button to switch on the electron source (Figure 6.5). It may take a few seconds for the beam to stabilise, which is confirmed when the Emission Current (µA) reaches a stable reading. This is not always the same reading between analyses therefore one must use a stable number as indication.
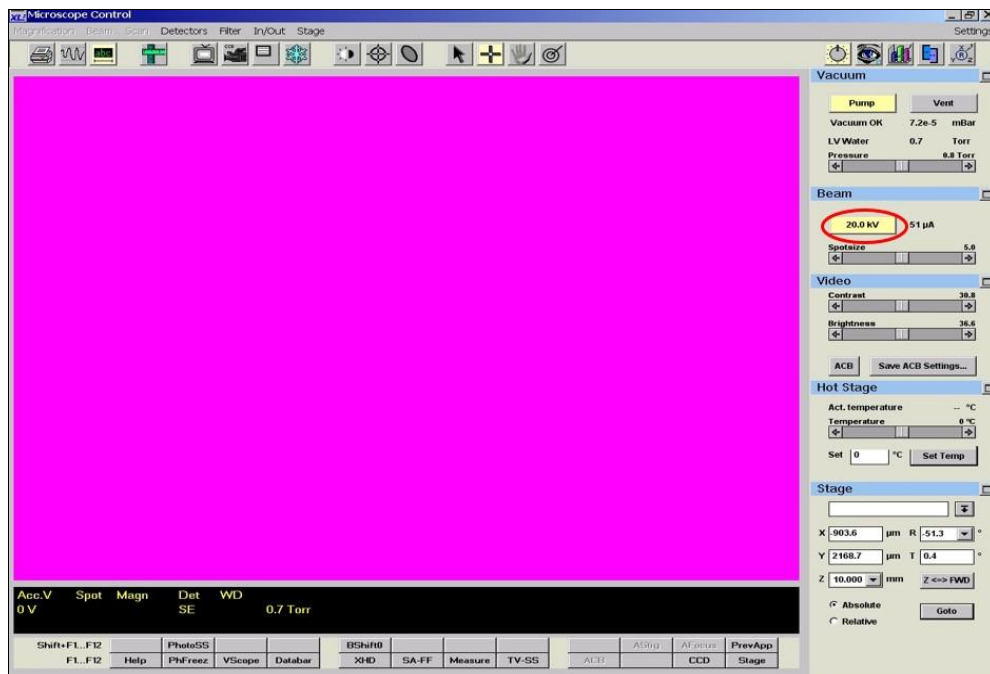
Figure 6.5. Screen grab showing the location of the 20.0 kV button in the Beam tab

16. The machine has now been set up and is ready to take images by following the next steps

17. Now, the sample appears in microscopic scale and a pop-up box will appear asking to link the working distance (WD) to the Z direction. Read but do not click OK on this box until the focus instructions have been followed and focus has been established in the next few steps.

248

18. To obtain an ESEM image, click on the **Detectors** drop-down menu and then select **BSE** (Figure 6.6).
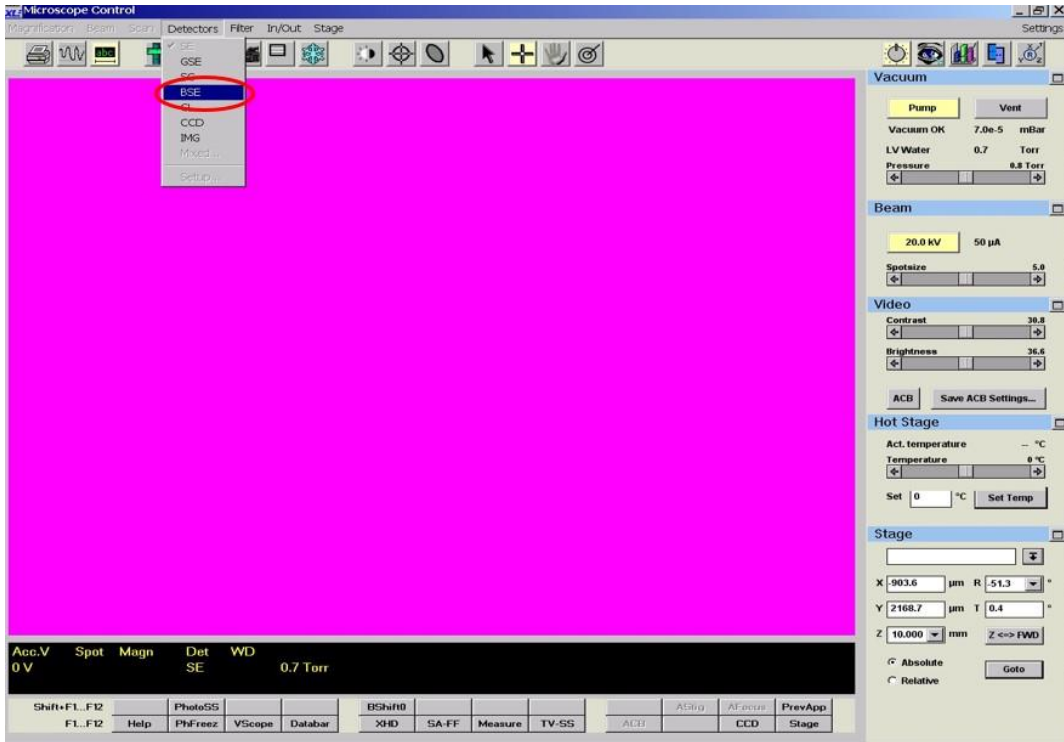
Figure 6.6. Screen grab showing the location of the BSE detector option within the Detectors drop-down menu.

19. To zoom in or zoom out, (+) and (-) buttons on the keyboard are used, respectively. Right click the mouse (changes to a double headed arrow) and hold to be able to focus and drag right or left to improve the resolution of the image. The mouse does both automatically. If manually adjusting the focus using the manual user interface board – do course initially and then fine adjustment – use stigmator X only/no Y and do not use the shift X and Y. Can also use the image contrast/brightness, magnification +/- and focus – course/fine buttons.

20. Once the focus is correct, click OK on the WD to Z direction box which will link the two distances. Then in the Stage tab, click on the Z drop down menu and select 10.000 µm

21. To double check beam alignment, click on the Crossover check-box in the Beam tab. If the beam does not appear centrally then left click and hold in Gun Tilt, then drag until the beam is centralized. After adjusting the beam, remove tick mark from the Crossover box if image still

looks too bright/dark then click on the auto contrast brightness icon ▣ situated left of the beam target icon.

22. After focusing and identifying which area is of interest for an image, click Scan tab on top bar and choose Slow Scan 2: 13.4 ms, 484 lines or Slow Scan 3 for better resolution. If image is still shimmering, check 'scan mode', make sure it's Slow Scan 1.
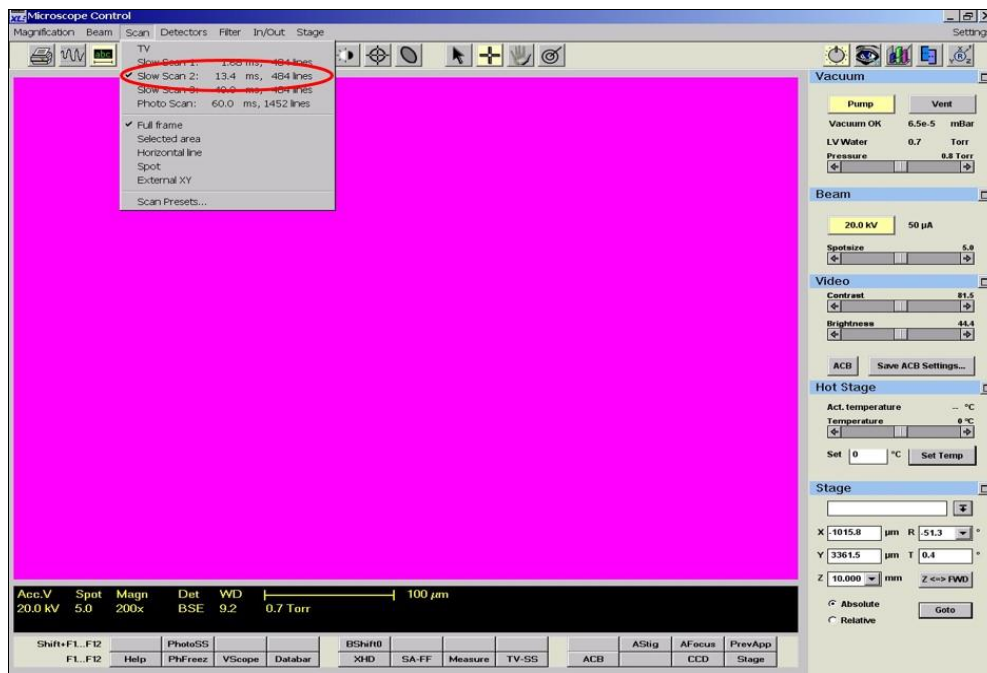
23. A horizontal scan line will appear at the top of the image and slowly descend as the image resolution improves with the slower scan speed. Once the scan line has reached the bottom of the image, click the Freeze box (a blue snowflake on the top bar) to freeze ESEM image.
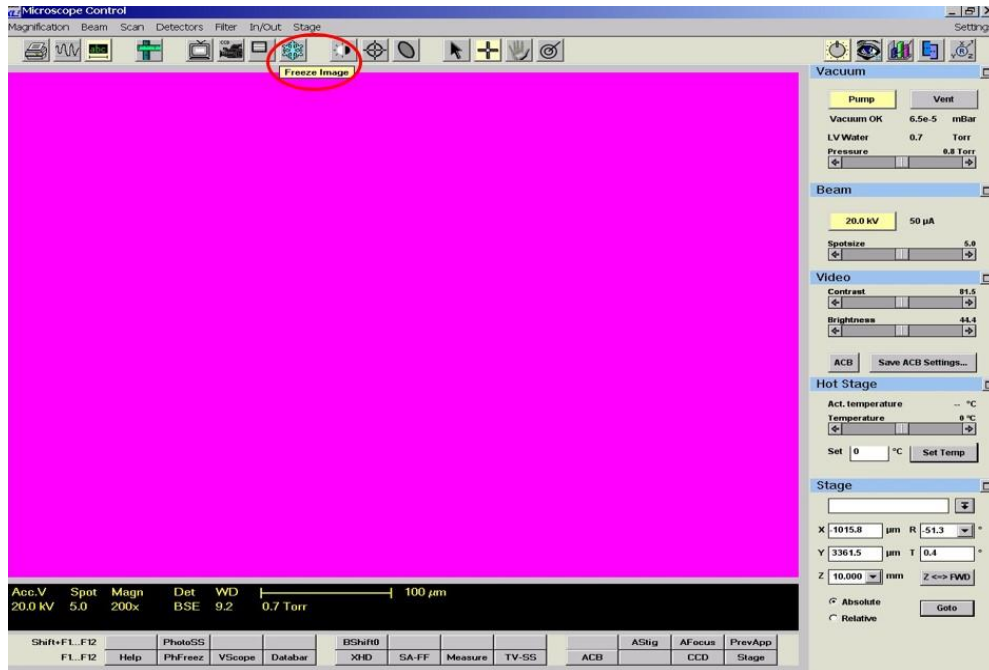
24. Finally, go to In/Out tab on the top bar and Select Image… from the drop down menu. Choose an appropriate file name (no more than 7 characters) and click save.
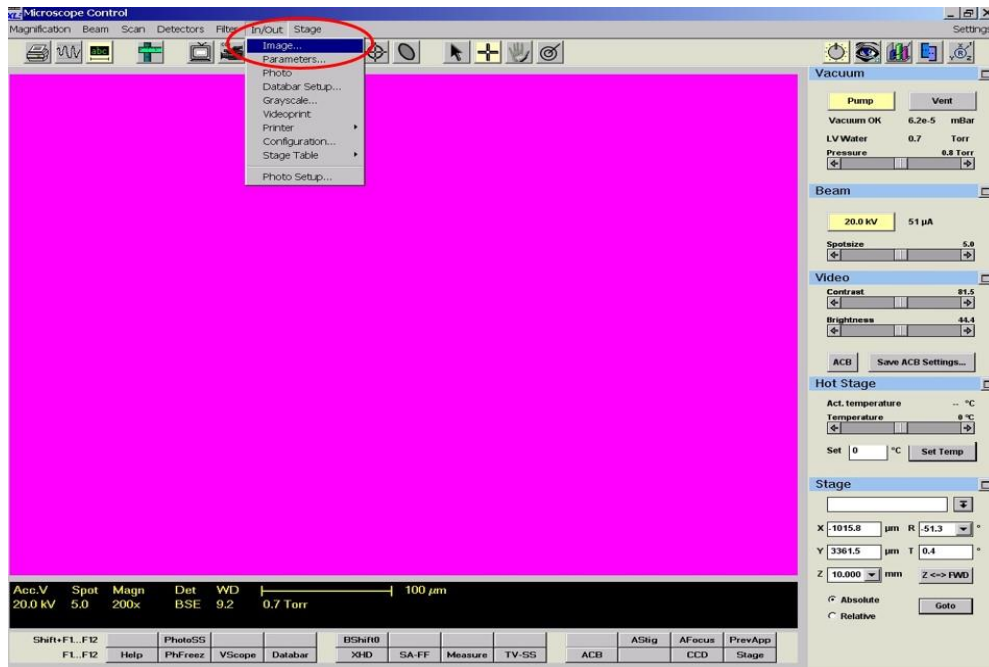
25. Having obtained the ESEM image, it is time to run EDX analysis, if required. The project and folders should already have been set up. If using the EDX, move the EDX beam in now. To get the pop up window for the EDX move the mouse cursor to the farthest left hand computer screen. Go to INCA Analyser, go to Options tab, go to detector control and go to slide. Move the EDX beam IN.

26. Click SAMPLE (in the left-hand flow chart diagram) and enter a Sample Name. Copy and paste this sample name into Sample ID.
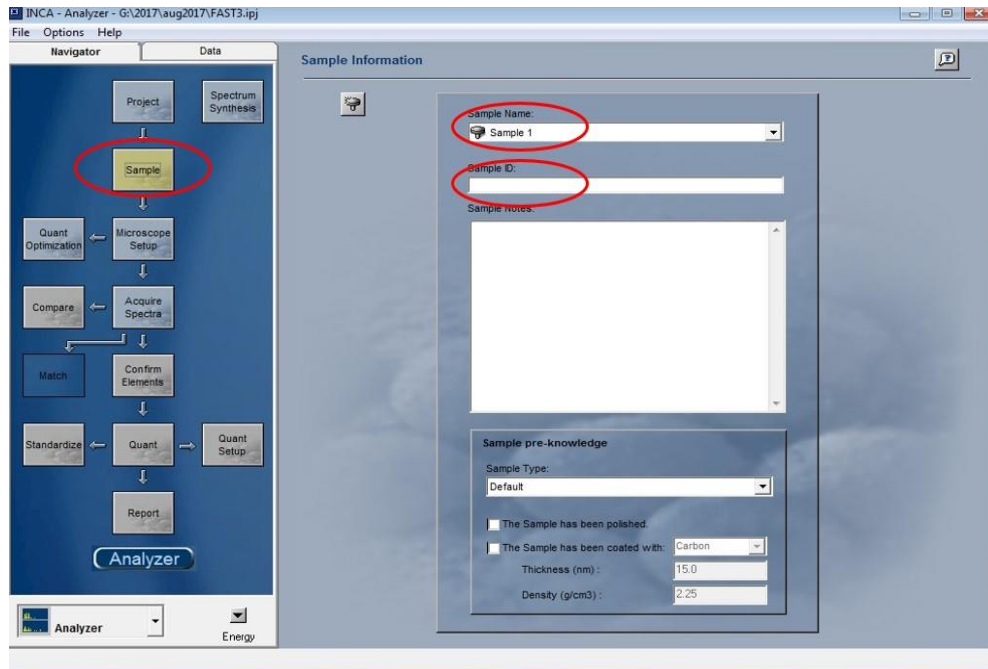
27. Click Acquire Spectra; paste the sample name into the Site box and then click the green circle button to start the spectrum acquisition. Right click -> noise peak -> remove. If elements shown are 'not real', click on confirm element and unselect from periodic table
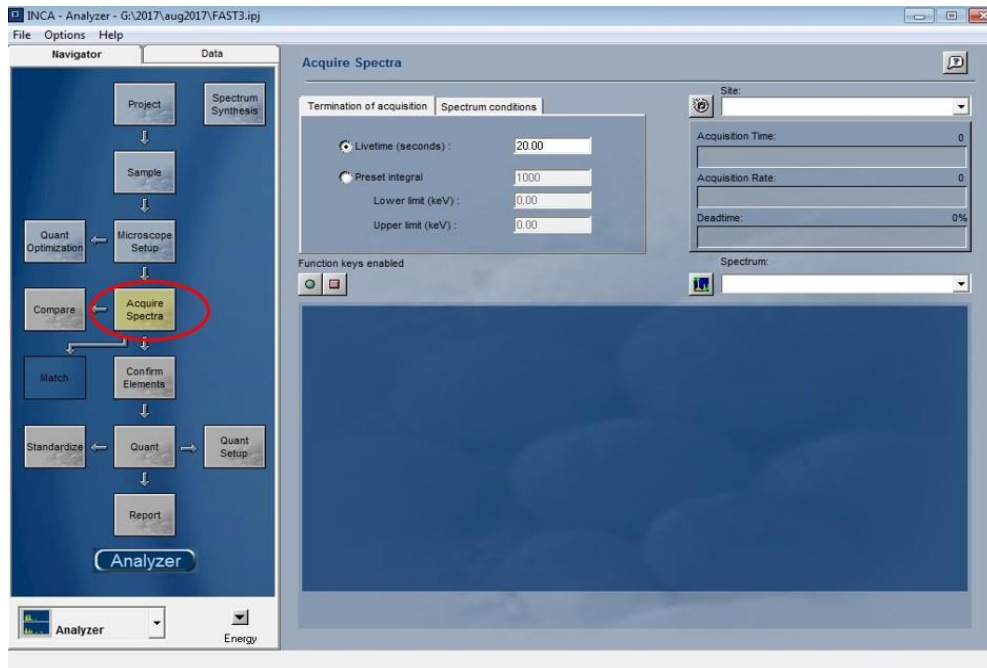
28. Right click on spectrum image and choose full screen option to enlarge the spectrum. This gives a better image for a paper or poster.
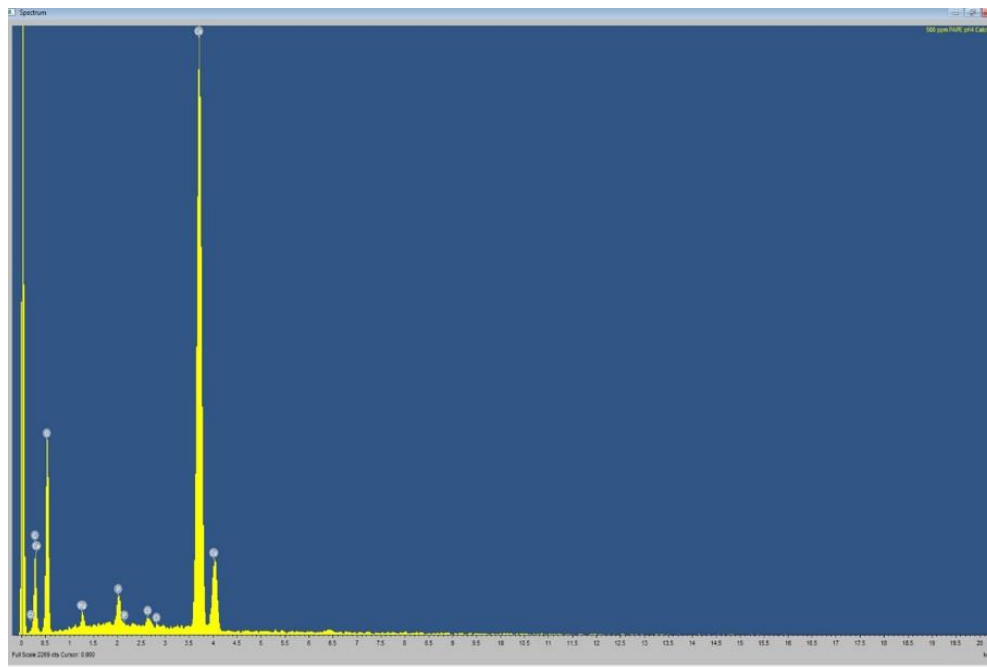
29. To save the spectrum, right click again and choose firstly Export, Metafile and click Save at the end

30. Click on Quant and then select the Full Results tab. Use columns AFGH in a report, as a table
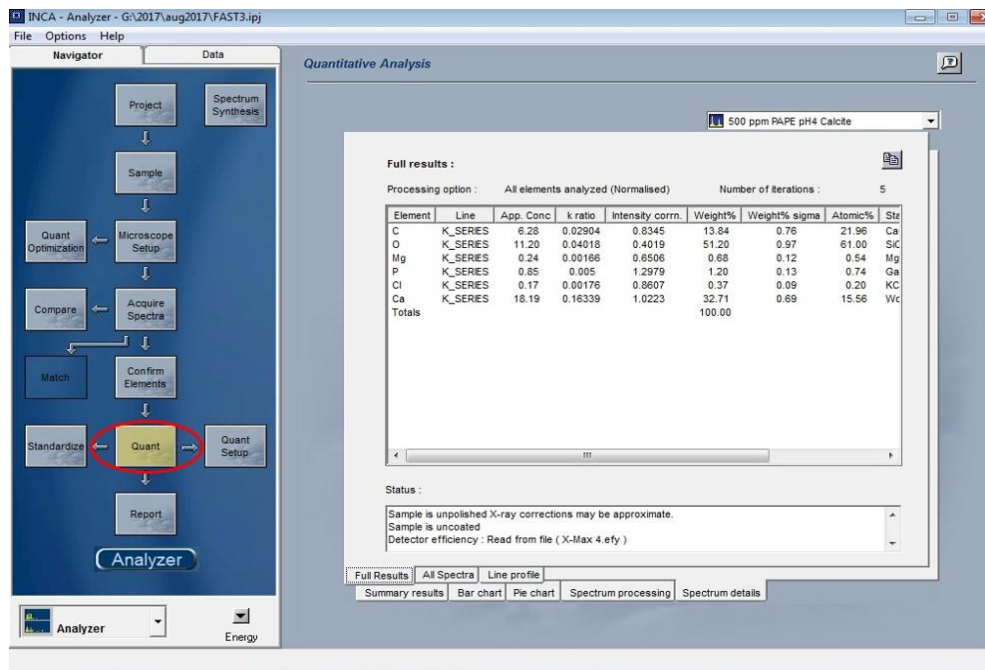
31. Click on the box at the top, right-hand side of this dialogue box (looks like two sheets of paper overlaid – clipboard icon). This will copy the table of results. An Excel spreadsheet will have already been created into which the EDX results can be pasted in, with appropriate labelling. Save both the Excel data file and the Project data file

32. Having finished with the EDX beam now. Go to INCA Analyser, go to Options tab, go to detector control and go to slide. Move the EDX beam OUT.

33. At this stage, the ESEM/EDX analysis of this section of the sample is complete. It is at this point that the analyst can decide whether to:

- Continue to analyse other areas of the sample; (defreeze the image by pressing the Freeze box (Snowflake) as mentioned in one of the procedural steps above and go to Slow Scan1 for ease of focusing, change the area by clicking on the image and repeat the image collecting procedural steps, whilst moving the EDX beam IN/OUT as appropriate.

- Change sample entirely; (vent the system as described in step 4 and the important notes in red at the beginning of the document – Safe Zone area and EDX IN/OUT and then repeat the procedural steps 4 – 32 or;

- Shut down the instrument having completed all analysis, step 34.

34. The ESEM/EDX analysis has been completed for the samples so it is time to exit from the corresponding software and the machine. Perform these items before leaving the ESEM machine.

- On the ESEM software (right hand computer screen) click on Detector and then CCD boxes
- Double click on the safe zone area to move the stage away
- Vent the system as described in step 4/5 and important red notes
- Remove the sample from the chamber and then close the vacuum chamber door
- In the Vacuum tab, select High Vacuum and Purge mode "Off"
- Click on the Pump button to establish the vacuum on the chamber and press the High Tension button on the left to switch this off
- The instrument can now be left and the session is finished. He will provide the data in due course

6.2. General Laboratory Procedure of Particle Size Analyser

The Operation Procedure of Particle Size Distribution Analysis is as follows:

a. Turn on the instrument. The switch is located on the back-left hand side. The laser must also be switched on by turning the key adjacent to the switch.

b. Attach the appropriate lens to the flow cell. The following lens will analyse these size ranges

Lens	Size Range
300 mm	1.2 - 600 μm
100 mm	0.5 - 180 μm
45 mm	0.1 - 80 μm

c. Allow the instrument to warm up for 30 minutes.

d. Switch on the PC and select Malvern Mastersizer option (F1).

e. At the instrument parameters page type "easy" to select the "Easy" measurement mode.

f. Press F10 - Set Parameters.

g. Press the END key to change the following parameters

Presentation - "Std"

Focal Length - Input the lens to be used

Beam Length - "2.2nm" is standard

Data Storage - Facility does not work

Kill Data - "0" always set as this

h. Press F2 (Sample details) and input sample details.

i. Introduce mobile phase into sample cell and start stirrer (set to 1/3 of max speed) so that fluid flows through the flow cell.

j. Press "a" to align the laser.

k. Press F3 (Set Zero). This sets the background level for the analysis. The mobile phase should be flowing through the cell at this point.

l. Dropwise, add dispersion to be analysed to mobile phase.

m. Press F4 (Check Sample Concentration) to assess the sample concentration and obstruction level (This value must be between 0.1 and 0.3). If below add more of the dispersion until range is reached.

n. Press F5 to measure particle size distribution.

o. The results obtained are printed out as the table detailed overleaf.

Note:

Normally, an initial first pass measurement is made using the 300mm lens to roughly ascertain the samples distribution. Following this, an approximate particle size estimate can be made and the appropriate lens can then be used.

Following a change in lens, the flow cell must be emptied, rinsed clean and the mobile phase is introduced to the cell. The complete procedure (from step 6 to step 15) must then be performed.

Figure 6.7. Particle Size Analyser - Malvern MS-20

7. References

1. Kelland, M. A. Production chemicals for the oil and gas industry. (CRC press, 2014).

2. Delon Jimenez, P. Improving squeeze scale inhibitor adsorption and flow back characteristics with surfactants. (University of Stavanger, Norway, 2014).

3. Fevang, S. Synthesizing and Testing for New Biodegradable Scale Inhibitors. (University of Stavanger, Norway, 2017).

4. Erany, R. A study of scale and scaling potential during high salinity and low salinity waterflooding. (University of Stavanger, Norway, 2016).

5. Ibrahim, J. M. B. M. Establishing scale inhibitor retention mechanisms in pure adsorption and coupled adsorption/precipitation treatments. (PhD thesis, Heriot-Watt University, 2012).

6. Hajirezaie, S. Scale formation in porous media and its impact on oil recovery. (University of Oklahoma, 2016).

7. Boyle, M. J. & Mitchell, R. W. Scale inhibition problems associated with North Sea oil production. in Offshore Europe (Society of Petroleum Engineers, 1979).

8. Vetter, O. J. G. How barium sulfate is formed: an interpretation. J. Pet. Technol. **27**, 1–515 (1975).

9. Johnson, K. S. Water Scaling Problem in the Oil Production Industry. Chem. Oil Ind. 140–151 (1983).

10. Kahrwad, M., Sorbie, K. S. & Boak, L. S. Coupled adsorption/precipitation of scale inhibitors: experimental results and modeling. SPE Prod. Oper. **24**, 481–491 (2009).

11. Crabtree, M. et al. Fighting scale—removal and prevention. Oilf. Rev. **11**, 30–45 (1999).

12. Liu, D. Research on performance evaluation and anti-scaling mechanism of green scale inhibitors by static and dynamic methods. (Arts et Métiers ParisTech (Arts et Métiers - Paris Campus - HESAM University), 2011).

13. Boak, L. S. Factors that impact scale inhibitor mechanisms. (PhD thesis, Heriot-Watt University, 2013).

14. Sastri, V. S. Corrosion inhibitors: principles and applications. (Wiley New York, 1998).

15. Kleinitz, W., Dietzsch, G. & Köhler, M. Halite scale formation in gas-producing wells. Chem. Eng. Res. Des. **81**, 352–358 (2003).

16. Kleinitz, W., Koehler, M. & Dietzsch, G. The precipitation of salt in gas producing wells. in SPE European formation damage conference (Society of Petroleum Engineers, 2001).

17. Smith, K. & Przybylinski, J. L. The Effect of Common Brine Constituents on the Efficacy of Halite Precipitation Inhibitors. in CORROSION 2006 (NACE International, 2006).

18. Wylde, J. J. & Slayer, J. L. Halite scale formation mechanisms, removal and control: a global overview of mechanical, process, and chemical strategies. in SPE International Symposium on Oilfield Chemistry (Society of Petroleum Engineers, 2013).

19. Moghadasi, J., Jamialahmadi, M., Müller-Steinhagen, H. & Sharif, A. Formation damage due to scale formation in porous media resulting from water injection. in SPE international symposium and exhibition on formation damage control (Society of Petroleum Engineers, 2004).

20.   Sorbie, K. S. & Mackay, E. J. Mixing of injected, connate and aquifer brines in waterflooding and its relevance to oilfield scaling. J. Pet. Sci. Eng. **27**, 85–106 (2000).

21.   Todd, A. C. & Yuan, M. D. Barium and strontium sulfate solid-solution scale formation at elevated temperatures. SPE Prod. Eng. **7**, 85–92 (1992).

22.   Jordan, M. M., Collins, I. R. & Mackay, E. J. Low sulfate seawater injection for barium sulfate scale control: A life-of-field solution to a complex challenge. SPE Prod. Oper. **23**, 192–209 (2008).

23.   Liu, W. J., Hui, F., Lédion, J. & Wu, X. W. Inhibition of scaling of water by the electrostatic treatment. Water Resour. Manag. **23**, 1291–1300 (2009).

24.   Puntervold, T. & Austad, T. Injection of seawater and mixtures with produced water into North Sea chalk formation: Impact on wettability, scale formation and rock mechanics caused by fluid-rock interaction. in SPE/EAGE Reservoir Characterization and Simulation Conference (Society of Petroleum Engineers, 2007).

25.   Olajire, A. A. A review of oilfield scale management technology for oil and gas production. J. Pet. Sci. Eng. **135**, 723–737 (2015).

26.   Moghadasi, J., Müller-Steinhagen, H., Jamialahmadi, M. & Sharif, A. scale Deposits in Porous Media and their Removal By eDta injection. (2007).

27.   Zhang, P., Shen, D., Kan, A. T. & Tomson, M. B. Phosphino-polycarboxylic acid modified inhibitor nanomaterial for oilfield scale control: transport and inhibitor return in formation media. RSC Adv. **6**, 59195–59205 (2016).

28.   Vetter, O. J., Kandarpa, V. & Harouaka, A. Prediction of scale problems due to injection of incompatible waters. J. Pet. Technol. **34**, 273–284 (1982).

29.   Graham, G. M., Dyer, S. J., Shone, P., Mackay, E. J. & Juhasz, A. High temperature core flooding experiments for the selection of appropriate scale inhibitor products for potential application as downhole squeeze treatments in high temperature reservoir environments. in International Symposium on Oilfield Scale (Society of Petroleum Engineers, 2001).

30.   Gill, J. S. & Varsanik, R. G. Computer modeling of the specific matching between scale inhibitors and crystal structure of scale forming minerals. J. Cryst. Growth **76**, 57–62 (1986).

31.   Hong, S. A. & Shuler, P. J. A mathematical model for the scale inhibitor squeeze process. in SPE International Symposium on Oilfield Chemistry (Society of Petroleum Engineers, 1987).

32.   Boak, L. S. Investigation of the Adsorption and Barium Sulpahte Inhibition Efficiency Properties of Novel Polyethylene Imines With More Conventional Scale Inhibitors. M. Phil, Dep. Pet. Eng. Heriot Watt Univ. (1996).

33.   Graham, G. M., Boak, L. S. & Sorbie, K. S. The influence of formation calcium and magnesium on the effectiveness of generically different barium sulphate oilfield scale inhibitors. SPE Prod. Facil. **18**, 28–44 (2003).

34.   Shaw, S. S. & Sorbie, K. Synergistic properties of phosphonate and polymeric scale-inhibitor blends for barium sulfate scale inhibition. SPE Prod. Oper. **30**, 16–25 (2015).

35.   Van der Leeden, M. C. & Van Rosmalen, G. M. Development of inhibitors for barium sulphate deposition. in 3rd International Symposium on Chemicals in the Oil Industry 65–85 (1988).

36.   Shaw, S. S. Investigation into the mechanisms of formation and prevention of barium sulphate

oilfield scale. (PhD thesis, Heriot-Watt University, 2012).

37.   Van der Leeden, M. C. & Van Rosmalen, G. M. Inhibition of barium sulfate deposition by polycarboxylates of various molecular structures. SPE Prod. Eng. **5**, 70–76 (1990).

38.   Popov, K. I., Kovaleva, N. E., Rudakova, G. Y., Kombarova, S. P. & Larchenko, V. E. Recent state-of-the-art of biodegradable scale inhibitors for cooling-water treatment applications. Therm. Eng. **63**, 122–129 (2016).

39.   Fink, J. Petroleum engineer's guide to oil field chemicals and fluids. (Gulf Professional Publishing, 2015).

40.   Shaw, S. S., Sorbie, K. & Boak, L. S. The effects of barium sulfate saturation ratio, calcium, and magnesium on the inhibition efficiency: Part II polymeric scale inhibitors. SPE Prod. Oper. **27**, 390–403 (2012).

41.   Sorbie, K. S. & Laing, N. How scale inhibitors work: mechanisms of selected barium sulphate scale inhibitors across a wide temperature range. in SPE International Symposium on Oilfield Scale (Society of Petroleum Engineers, 2004).

42.   Jarrahian, K., Sorbie, K. S., Singleton, M. A., Boak, L. S. & Graham, A. J. The Effect of pH and Mineralogy on the Retention of Polymeric Scale Inhibitors on Carbonate Rocks for Application in Squeeze Treatments. SPE Prod. Oper. **34**, 344–360 (2019).

43.   Valiakhmetova, A., Sorbie, K. S., Jordan, M. M. & Boak, L. S. Novel Studies on Precipitated Phosphate Ester Scale Inhibitors for Precipitation Squeeze Application. in SPE International Conference on Oilfield Chemistry (Society of Petroleum Engineers, 2017).

44.   Jarrahian, K., Boak, L. S., Graham, A. J., Singleton, M. A. & Sorbie, K. S. Experimental Investigation of the interaction between a phosphate ester scale inhibitor and carbonate rocks for application in squeeze treatments. Energy & Fuels **33**, 4089–4103 (2019).

45.   Kan, A. T., Fu, G., Tomson, M. B., Al-Thubaiti, M. & Xiao, A. J. Factors affecting scale inhibitor retention in carbonate-rich formation during squeeze treatment. Spe J. **9**, 280–289 (2004).

46.   Mohammed, G. & Galadima, A. The chemistry of chemical scale inhibitors and the mechanism of interactions with carbonate reservoir rock. Int. J. Pet. Sci. Technol. **5**, 33–46 (2011).

47.   Iler, R. K. The colloid chemistry of silica and silicates. (Cornell University Press, 1955).

48.   Meyers, K. O., Skillman, H. L. & Herring, G. D. Control of formation damage at Prudhoe Bay, Alaska, by inhibitor squeeze treatment. J. Pet. Technol. **37**, 1–19 (1985).

49.   Sorbie, K. S. et al. The effect of pH, calcium, and temperature on the adsorption of phosphonate inhibitor onto consolidated and crushed sandstone. in SPE Annual Technical Conference and Exhibition (Society of Petroleum Engineers, 1993).

50.   Jordan, M. M. et al. The effect of clay minerals, pH, calcium and temperature on the adsorption of phosphonate scale inhibitor onto reservoir core and mineral separates. in (NACE International, Houston, TX (United States), 1994).

51.   Kan, A., Yan, L., Bedient, P. B., Oddo, J. E., & Tomson, M. B. Sorption and fate of phosphonate scale inhibitors in the sandstone reservoir: studied by laboratory apparatus with core material. in SPE Production Operations Symposium (Society of Petroleum Engineers, 1991).

52.   Pokrovsky, O. S., Golubev, S. V., & Schott, J. Dissolution kinetics of calcite, dolomite and magnesite at 25 C and 0 to 50 atm pCO_2. Chem. Geol. **217**, 239–255 (2005).

53. Pierre, A., Lamarche, J. M., Mercier, R., Foissy, A. & Persello, J. Calcium as potential determining ion in aqueous calcite suspensions. J. Dispers. Sci. ANDTECHNOLOGY **11**, 611–635 (1990).

54. Somasundaran, P. & Agar, G. E. The zero point of charge of calcite. J. Colloid Interface Sci. **24**, 433–440 (1967).

55. Strand, S., Høgnesen, E. J. & Austad, T. Wettability alteration of carbonates—Effects of potential determining ions (Ca2+ and SO42−) and temperature. Colloids Surfaces A Physicochem. Eng. Asp. **275**, 1–10 (2006).

56. Miles, L. New well treatment inhibits scale. Oil Gas J 96–99 (1970).

57. Shuler, P. J & Jenkins, W. H. Prevention of downhole scale deposition in the Ninian Field. SPE Prod. Eng. **6**, 221–226 (1991).

58. Olson, J. B. & Moore, D. C. A temperature activated extended lifetime scale inhibitor squeeze system. J. B. Olson, D. C. Moore, N. Holland-Jones, Pap. (1992).

59. Hardy, J. A., Barthorpe, R. T. & Rhudy, J. S. Scale control in the south brae field. SPE Prod. Facil. **9**, 127–131 (1994).

60. Plummer, M. A. Preventing plugging by insoluble salts in a hydrocarbon-bearing formation and associated production wells. (1988).

61. Pardue, J. E. A new inhibitor for scale squeeze applications. in SPE International Symposium on Oilfield Chemistry (Society of Petroleum Engineers, 1991).

62. Pardue, J. E. Results of field tests with a new extended squeeze life scale inhibitor. J. E. Pardue, Pap. (1992).

63. Farooqui, N. M. A detailed study of the scale inhibitor phase envelope of PPCA in the context of precipitation squeeze treatments. (PhD thesis, Heriot-Watt University, 2016).

64. Carlberg, B. L. Precipitation squeeze can control scale in high-volume wells. Oil Gas J.;(United States) **81**, (1983).

65. Browning, F. H. & Fogler, H. S. Precipitation and dissolution of calcium-phosphonates for the enhancement of squeeze lifetimes. SPE Prod. Facil. **10**, 144–150 (1995).

66. Wat, R. M. S., Montgomery, H. T. R., Maclean, A. F. & Bland, I. D. Squeeze Application Using a Polymer Scale Inhibitor-A Case History. in 4th International Oilfield Chemical Symposium, Geilo, Norway 18–21 (1993).

67. Sorbie, K. S. A Simple Model of Precipitation Squeeze Treatments. in SPE International Conference on Oilfield Scale (Society of Petroleum Engineers, 2012).

68. Malandrino, A., Yuan, M. D., Sorbie, K. S. & Jordan, M. M. Mechanistic study and modelling of precipitation scale inhibitor squeeze processes. in SPE International Symposium on Oilfield Chemistry (Society of Petroleum Engineers, 1995).

69. Poetker, R. H. & Stone, J. D. Squeezing Inhibitor into Formation. Pet. Engr., 28, No. 5. (1956).

70. Smith, C. F., Nolan III, T. J. & Crenshaw, P. L. Removal and inhibition of calcium sulfate scale in waterflood projects. J. Pet. Technol. **20**, 1–249 (1968).

71. Kerver, J. K. & Heilhecker, J. K. Scale inhibition by the squeeze technique. J. Can. Pet. Technol. **8**, 15–23 (1969).

72.   Kerver, J. K. & Morgan III, F. A. Corrosion inhibitor squeeze technique: laboratory adsorption-desorption studies. Mater. Prot.;(United States) **4**, (1965).

73.   Durham, D. K. Equations for Prediction of Scale Inhibitor Return After Squeeze Treatment. in SPE California Regional Meeting (Society of Petroleum Engineers, 1983).

74.   King, G. E. & Warden, S. L. Introductory Work in Scale Inhibitor Squeeze Performance: Core Tests and Field Results. in SPE International Symposium on Oilfield Chemistry (Society of Petroleum Engineers, 1989).

75.   Przybylinski, J. L. Adsorption and desorption characteristics of mineral scale inhibitors as related to the design of squeeze treatments. in SPE International Symposium on Oilfield Chemistry (Society of Petroleum Engineers, 1989).

76.   Sorbie, K. S., Todd, A. C., Thornton, A. R. & Wat, R. M. S. Interpretation and theoretical modelling of inhibitor/tracer corefloods. in 1990 SPE Annual Technical Conference and Exhibition 697–709 (1990).

77.   Sorbie, K. S., Yuan, M. D., Todd, A. C. & Wat, R. M. S. The modelling and design of scale inhibitor squeeze treatments in complex reservoirs. in SPE International Symposium on Oilfield Chemistry (Society of Petroleum Engineers, 1991).

78.   Tantayakom, V., Fogler, H. S., Charoensirithavorn, P. & Chavadej, S. Kinetic study of scale inhibitor precipitation in squeeze treatment. Cryst. Growth Des. **5**, 329–335 (2005).

79.   Ibrahim, J. M., Sorbie, K. & Boak, L. S. Coupled adsorption/precipitation experiments: 1. Static results. in SPE International Conference on Oilfield Scale (Society of Petroleum Engineers, 2012).

80.   Yan, F., Zhang, F., Bhandari, N., Wang, L., Dai, Z., Zhang, Z., Liu, Y., Ruan, G., Kan, A. & Tomson, M. Adsorption and precipitation of scale inhibitors on shale formations. J. Pet. Sci. Eng. **136**, 32–40 (2015).

81.   Jordana, R., Howe, R. F. & Guan, H. Retention and release of scale inhibitor in different clay minerals. in SPE International Conference and Exhibition on Oilfield Scale 2012 617–626 (2012).

82.   Funkhouser, G. P. & Gdanski, R. D. Improved Adsorption-Isotherm Modelling for Phosphonate Scale Inhibitors. in Proc (2001).

83.   Gdanski, R. D. & Funkhouser, G. P. Mineralogy driven scale inhibitor squeeze designs. in SPE European Formation Damage Conference (Society of Petroleum Engineers, 2005).

84.   Gdanski, R. D. & Funkhouser, G. P. Successful model of the kinetic release of a phosphonate scale inhibitor. in NIF International Oilfield Chemistry Symposium, Geilo, Norway 1–4 (2001).

85.   Rogers, L. A. et al. Use of inhibitors for scale control in brine-producing gas and oil wells. SPE Prod. Eng. **5**, 77–82 (1990).

86.   Baraka-Lokmane, S. & Sorbie, K. S. Effect of pH and scale inhibitor concentration on phosphonate–carbonate interaction. J. Pet. Sci. Eng. **70**, 10–27 (2010).

87.   Tomson, M. B. et al. Mechanistic understanding of rock/phosphonate interactions and effect of metal ions on inhibitor retention. SPE J. **13**, 325–336 (2008).

88.   Thomas, W. S., Sorbie, K. S. & Singleton, M. A. Coupled adsorption/precipitation tests with a phosphonate inhibitor and carbonate substrate. in SPE International Oilfield Scale Conference and Exhibition (Society of Petroleum Engineers, 2014).

89. Atkinson, G., Raju, K. & Howell, R. D. The thermodynamics of scale prediction. in SPE International Symposium on Oilfield Chemistry (Society of Petroleum Engineers, 1991).

90. Kan, A. T., Cao, X., Yan, X., Oddo, J. E. & Tomson, M. B. The Transport of Chemical Scale Inhibitors and Its Importance to the Squeeze Procedure. in Paper No 33 Presented at the NACE Annual Conf and Corrosion Show, Nashville, TN (1992).

91. Brod, M. Performance of Scale Inhibitors in Squeeze Application. in SPE International Symposium on Oilfield Chemistry (Society of Petroleum Engineers, 1991).

92. Chen, P. Inhibitor adsorption study and the effect of inhibitor on kinetics of BaSO4 crystal growth. (1995).

93. Jarrahian, K., Sorbie, K., Singleton, M., Boak, L. & Graham, A. Building a Fundamental Understanding of Scale-Inhibitor Retention in Carbonate Formations. SPE Prod. Oper. (2019).

94. D. Silva, Kh. Jarrahian, K. S. S. & E. J. M. Thermodynamic Modelling of the Precipitation Chemistry of Scale Inhibitors and Divalent Cations (Ca and Mg). in Chemistry in the Oil Industry XVI: "New Chemistries for Old Problems (2019).

95. Boak, L. S. & Sorbie, K. S. New Developments on the Analysis of Scale Inhibitors. in SPE International Conference on Oilfield Scale (Society of Petroleum Engineers, 2010).

96. Shaw, S. S. & Sorbie, K. S. Structure, Stoichiometry, and Modeling of Calcium Phosphonate Scale-Inhibitor Complexes for Application in Precipitation-Squeeze Processes. SPE Prod. Oper. **29**, 139–151 (2014).

97. Jarrahian, K., Singleton, M., Boak, L. & Sorbie, K. S. Surface Chemistry of Phosphonate Scale Inhibitor Retention Mechanisms in Carbonate Reservoirs. Cryst. Growth Des. **20**, 5356–5372 (2020).

98. Valiakhmetova, A., Sorbie, K. S., Boak, L. S. & Shaw, S. S. Solubility and Inhibition Efficiency of Phosphonate Scale Inhibitor_Calcium_Magnesium Complexes for Application in Precipitation Squeeze Treatment. in SPE International Conference and Exhibition on Formation Damage Control (Society of Petroleum Engineers, 2016).

99. Shaw, S., Welton, T. D., & Sorbie, K. S. The Relation Between Barite Inhibition by Phosphonate Scale Inhibitors and the Structures of Phosphonate-Metal Complexes. in SPE International Conference on Oilfield Scale. Society of Petroleum Engineers (Society of Petroleum Engineers, 2012). doi:https://doi.org/10.2118/155114-MS.

100. Kirby, A. J., & Younas, M. The reactivity of phosphate esters. Diester hydrolysis. J. Chem. Soc. B Phys. Org. 510–513 (1970) doi:10.1039/J29700000510.

101. Alkattan, M., Oelkers, E. H., Dandurand, J.-L. & Schott, J. An experimental study of calcite and limestone dissolution rates as a function of pH from− 1 to 3 and temperature from 25 to 80 C. Chem. Geol. **151**, 199–214 (1998).

102. Jordan, M. M., Kemp, S., Sorhaug, E., Sjursaether, K., & Freer, B. Effective management of scaling from and within carbonate oil reservoirs, North Sea Basin. Chem. Eng. Res. Des. **81**, 359– 372 (2003).

103. Valiakhmetova, A., Sorbie, K. S., Boak, L. S., & Shaw, S. S. Solubility and inhibition efficiency of phosphonate scale inhibitor_calcium_magnesium complexes for application in a precipitation-squeeze treatment. SPE Prod. Oper. **32**, 343–350 (2017).

104. Jarrahian, K. & Sorbie, K. S. Mechanistic Investigation of Adsorption Behaviour of Two Scale Inhibitors on Carbonate Formations for Application in Squeeze Treatments. Energy & Fuels (2020).